OPEN ACCESS
OPUS AUGSBURG

Universität Augsburg
Universitätsbibliothek

Super-localized orthogonal decomposition for deterministic and stochastic homogenization problems

Hannah Mohr

Angaben zur Veröffentlichung / Publication details:

Mohr, Hannah. 2026. “Super-localized orthogonal decomposition for deterministic and stochastic homogenization problems.” Augsburg: Universität Augsburg.

Nutzungsbedingungen / Terms of use: **CC BY-NC-ND 4.0**

Dieses Dokument wird unter folgenden Bedingungen zur Verfügung gestellt: / This document is made available under these conditions:
CC-BY-NC-ND 4.0: Creative Commons: Namensnennung - Nicht kommerziell - Keine Bearbeitung
Weitere Informationen finden Sie unter: / For more information see:
https://creativecommons.org/licenses/by-nc-nd/4.0/deed.de

Super-Localized Orthogonal Decomposition for deterministic and stochastic homogenization problems

Dissertation

zur Erlangung des akademischen Grades

Dr. rer. nat.

eingereicht an der

Mathematisch-Naturwissenschaftlich-Technischen Fakultät

der Universität Augsburg

von

Hannah Mohr

Augsburg, Juli 2025

Erstgutachter: Prof. Dr. Daniel Peterseim
Zweitgutachter: Prof. Dr. Axel Målqvist

Tag der mündlichen Prüfung: 13.10.2025

Abstract

Many physical phenomena in science and engineering, ranging from groundwater flow in porous media to the mechanical behavior of composite materials, are governed by partial differential equations (PDEs) with highly heterogeneous coefficients that vary across multiple spatial scales. Accurately simulating such multiscale problems poses significant computational challenges. Classical numerical methods, such as the finite element method (FEM), require resolving the finest scales, leading to excessively large systems. While analytical homogenization offers effective macroscopic models under idealized assumptions (e.g., periodicity or scale separation), such assumptions are rarely valid in practical applications.

This thesis is devoted to the numerical homogenization of elliptic diffusion problems with highly heterogeneous coefficients, both deterministic and stochastic. We focus on advancing the Super-Localized Orthogonal Decomposition (SLOD) method, which enables accurate coarse-scale approximations without relying on restrictive structural assumptions. SLOD builds upon the classical Localized Orthogonal Decomposition (LOD) method by constructing basis functions with super-exponential decay, achieved via carefully designed local source terms. We analyze the approximation properties of SLOD and propose practical stabilization strategies to ensure numerical robustness.

Building on this foundation, we develop a multilevel extension termed Hierarchical SLOD (HSLOD). This method constructs quasi-orthogonal hierarchical basis functions, enabling a multiresolution decomposition of the solution space. The hierarchical structure yields improved conditioning of the resulting linear systems and facilitates efficient, parallelizable solvers. Furthermore, the hierarchical approach allows existing SLOD approximations to be improved incrementally by adding further discretization levels.

In the stochastic setting, we extend both SLOD and HSLOD into a collocation-type framework for numerical stochastic homogenization. The proposed methods efficiently compute expected solutions to PDEs with random coefficients by exploiting the super-exponential decay of the localized basis functions and the simplicity of the collocation-type approach, which avoids assembling global stiffness matrices. We derive rigorous error estimates by linking the methods to results from quantitative stochastic homogenization theory. All of our theoretical results are supported by comprehensive numerical experiments that demonstrate the effectiveness of the proposed methods.

Acknowledgments

First and foremost, I would like to express my sincere gratitude to Daniel Peterseim for offering me the opportunity to join his research group and for his guidance, support, and encouragement throughout the past years. I am also grateful to Axel Målqvist for kindly agreeing to serve as the co-examiner of this dissertation. Many thanks go to my co-authors José C. Garay, Moritz Hauck, and Christoph Zimmer for the productive and enjoyable collaboration over the last three years. A significant part of the results presented in this thesis grew out of our joint work. I would also like to thank Camilla Belponer, Matthias Deiml, Martin Hermann, and Fabian Kröpfl for carefully proofreading this dissertation and for their helpful comments and suggestions, which have greatly improved the final version. Moreover, I am thankful to all current and former colleagues at the Chair for Computational Mathematics, the Research Unit for Applied Analysis, the Research Unit for High-Performance Scientific Computing, and the Chair for Inverse Problems at the University of Augsburg. The collegial and friendly atmosphere in these groups has made my time here especially enjoyable. I will always look back fondly on the many inspiring discussions, the collaborative spirit, the delicious Muffin Monday breaks, and the occasional game of table soccer. I gratefully acknowledge financial support from the European Research Council (ERC) through the Horizon 2020 research and innovation programme of the European Union (Grant agreement No. 865751 — RandomMultiScales). Last but not least, I would like to thank my family and friends for their continuous support and encouragement throughout this journey.

Augsburg, Juli 2025 *Hannah Mohr*

Contents

List of Figures

1. Introduction

1.1. Motivation

Many physical systems in science and engineering are governed by partial differential equations (PDEs) whose coefficients vary on multiple spatial scales. These variations may arise from material inhomogeneities, geometric complexity, or randomness in the medium and are frequently observed in fields such as geophysics, material science, hydrology, and biological tissue modeling. For instance, modeling groundwater flow through porous rock formations requires capturing the fine-scale pore geometry caused by variations in soil type, microscopic inclusions, or heterogeneous subsurface structures; see [Hel97]. These fine features can span several orders of magnitude smaller than the overall geological domain and need to be resolved by numerical methods in order to get accurate macroscopic approximation on the kilometer scale (c.f. [NH06]). Another example of multiscale phenomena is the elastic behavior of paper, where macroscopic mechanical properties depend on the microscopic arrangement of cellulose fibers [KMM$^+$18]. Similarly, in composite materials, such as fiber-reinforced concrete or polymers, the microscopic structure of short reinforcing fibers significantly improves the tensile strength and overall performance of the material, see for example [FL96, BS07, LPR$^+$21].

Numerical simulation of such systems poses a fundamental challenge: fully resolving all scales involved is often computationally infeasible due to the resulting high-dimensional discretization. Standard discretization techniques such as finite element methods (FEMs) lose their efficiency when the mesh must resolve the finest scale variations, leading to intractable memory and runtime requirements. In many practical applications, however, the goal is not to resolve every fine-scale feature but rather to capture the effective or macroscopic behavior of the PDE solution. Therefore, one may try to average the coefficients at a coarser scale. However, naive averaging often leads to macroscopic models whose effective properties differ significantly from those of the original fine-scale system, see, e.g., [MP20, Chapter 2].

To address this issue, homogenization theory offers a powerful analytical framework. In its classical form, homogenization seeks to replace a highly oscillatory PDE with an effective, or homogenized, equation that captures the large-scale behavior of the solution. Under idealized assumptions such as periodicity, scale separation, and statistical stationarity, this approach yields rigorous asymptotic approximations and effective coefficients that can be computed through auxil-

iary cell problems (see, for example, [JKO94, Tar09, BLB23]). However, these assumptions are often violated in practical applications. Natural systems rarely exhibit perfect periodicity or clear scale separation, as illustrated by the example of groundwater flow through heterogeneous geological formations. Although many manufactured composites often exhibit a clear separation of scales, e.g., between the size of the fibers and the size of the workpiece, and may even possess a periodic microstructure, these idealized conditions are frequently violated in practice. Material imperfections, random perturbations, or defects introduced during manufacturing can disrupt periodicity and scale separation. Furthermore, in many real-world scenarios, only partial or noisy data is available, obtained through numerical simulations or experimental measurements rather than explicit analytical models.

In such settings, numerical homogenization has emerged as a computational counterpart to classical analytical homogenization. Instead of seeking explicit formulas, these methods construct effective models or approximation spaces directly from the problem data by identifying low-dimensional spaces that can accurately approximate the solution. Typically, this is achieved by enriching standard finite element spaces with fine-scale information extracted through localized computations or solution operators associated with the governing PDE. The resulting methods aim to solve the original multiscale problem on a coarse computational grid without resolving all microscopic features explicitly, while retaining high accuracy. Compared to classical FEMs, numerical homogenization incurs only moderate computational overhead, such as basis functions with slightly larger support or an increased number of basis functions per mesh entity. Crucially, these methods are inherently non-asymptotic and do not rely on assumptions of scale separation or periodicity, which makes them especially appealing for real-world applications characterized by structural complexity or data-driven models. An overview on the history of numerical homogenization methods is given in the next section.

1.2. Literature review

The field of numerical homogenization has a long and distinguished history, rooted in early efforts to design multiscale methods capable of addressing problems lacking clear scale separation. A seminal contribution in this direction was the development of generalized FEMs that incorporated fine-scale information directly into the discrete solution space for one-dimensional problems [BO83]. This approach was later extended to two-dimensional problems in [BCO94], thereby laying the foundation for many modern multiscale techniques. A major shift occurred in the mid-1990s with the emergence of a diverse class of numerical homogenization methods. In what follows, we review key developments in this area, following the classification and structure outlined in [AHP21], which also provides a more comprehensive overview.

Homogenization-based approaches

One prominent class of numerical multiscale methods is based on analytical homogenization theory. A notable example is the Two-Scale Finite Element Method introduced in [MS02]. This method draws inspiration from the theory of two-scale convergence [Ngu89, All92] and constructs coarse-scale basis functions that mimic the structure of test functions used in this analytical framework. By design, the method is restricted to periodic microstructures. It was later extended in [HS05] by incorporating the more general concept of multiscale convergence [AB96], enabling the method to address a broader class of problems. Further generalizations and developments can be found in [Hoa08, HS11, XH14, CH18, TH19, TH20].

Another widely used method grounded in classical homogenization is the Heterogeneous Multiscale Method (HMM), proposed in [EE03]. HMM seeks to compute a macroscopic finite element approximation of the homogenized PDE by capturing fine-scale information locally in small representative cells. The success of HMM relies heavily on the assumption of scale separation and the availability of representative cells, which is often the case in engineering applications. Since these cells are much smaller than the coarse elements and cover only a small fraction of the global domain, the method is highly efficient. The first rigorous error analyses of HMM were established in [Abd05, Ohl05], and a comprehensive overview of the method, its theory, and extensions can be found in [AEEVE12].

Variational approaches

One influential direction in numerical homogenization has been the development of variational approaches. A seminal contribution in this area was the Variational Multiscale Method (VMM), proposed in [Hug95]. This method aimed to stabilize standard FEMs for multiscale problems by using local Green's functions to incorporate unresolved fine-scale effects into a coarse-scale variational formulation. This early version of the method relied on the assumption that fine-scale features were strongly localized within each coarse mesh element, allowing local correctors to be computed independently. While this assumption is generally unrealistic, the conceptual framework laid the groundwork for many modern multiscale methods.

The initial limitation was overcome in [HFMQ98], where global corrector Green's functions were constructed from fine-scale residuals, and the solution space was decomposed into a coarse finite element space and a fine-scale complement. This decomposition was further formalized in [HS07] through the use of projection operators, with the coarse and fine-scale spaces chosen as the image and kernel of a projection, respectively. This led to an operator-based representation of the global correctors, which in turn enabled the correction of standard basis functions to incorporate fine-scale information. Although these corrected basis functions are inherently global, numerical investigations

in [Mål05, LM05, HS07, Mål11] revealed that they exhibit exponential decay away from their coarse support. This observation justified their localization to element patches for practical computations. Moreover, a posteriori error estimates supporting this approach were developed in [LM05, LM07, NPP08, LM09].

A rigorous proof of exponential decay for elliptic multiscale problems was first provided in [MP14], leading to the formal introduction of the Localized Orthogonal Decomposition (LOD) method. Subsequent work refined the localization strategy in [HP13] and extended the framework in [HM14, HMP15, Pet16] to accommodate a broader class of finite element spaces, boundary conditions and non-symmetric and inf-sup stable problems. An alternative perspective on LOD as an additive Schwarz method was presented in [KY16, KPY18], offering another proof for the localization properties. The transition from conforming to non-conforming spaces was addressed in [EGMP13] within the context of discontinuous Galerkin methods, and further generalized in [Mai20]. Higher-order extensions of LOD were proposed in [Mai21] and refined in [DHM23].

A related line of work is the development of Rough Polyharmonic Splines in [OZB14], which also feature exponentially decaying basis functions and similar computational complexity to LOD. These ideas were extended to hierarchical information games in [Owh15], giving rise to multiresolution numerical homogenization techniques in [Owh17, OS19]. A multiresolution version of LOD was then introduced in [FP20] and further refined in [HP22a]. For a comprehensive overview of LOD, we refer the reader to the textbook [MP20] and the review article [AHP21].

A recent advancement of the LOD method is the introduction of the Super-Localized Orthogonal Decomposition (SLOD) in [HP22b] in the context of elliptic diffusion problems. In contrast to the classical LOD, the SLOD enforces localization more directly by minimizing the conormal derivative of the basis functions on the boundaries of their local patches. This stabilization yields super-exponentially decaying basis functions in practice. As a result, for a given coarse mesh size H, an accuracy of $\mathcal{O}(H)$ can be achieved using basis functions supported on patches of diameter $\mathcal{O}(H|\log H|^{(d-1)/d})$, where d is the spatial dimension. In comparison, the classical LOD requires support of diameter $\mathcal{O}(H|\log H|)$ to reach the same accuracy. The SLOD approach has since been generalized and extended in [FHKP23, BFP24, BHP24, FHP24, PWZ24].

Another influential direction in the development of numerical multiscale methods which is rooted in the variational multiscale formulation of [Hug95], originates from the concept of residual-free bubbles, introduced in [BFHR97]. Residual-free bubbles are smooth functions that vanish on the boundary of individual grid elements and are constructed by integrating local Green's functions. These bubbles can also be used to stabilize standard Galerkin methods in the presence of multiscale features. A closely related approach is the Multiscale Finite Element Method (MsFEM), proposed in [HW97]. MsFEM can be viewed as a homogenization-based reinterpretation of residual-free bubbles. Its core idea is to solve local versions of the target PDE within each coarse mesh element, using the solutions

as basis functions of the method. A key challenge in MsFEM lies in the choice of boundary conditions for these local problems: mismatches between the coarse mesh and the underlying microstructure can lead to large so-called resonance errors. To mitigate this issue, oversampling strategies can be employed, whereby the local PDEs are solved on patches that extend beyond the original coarse elements. A rigorous error analysis of MsFEM in periodic homogenization settings with scale separation was established in [HWC99, EHW00, HWZ04, EH09, BLT14]. In non-periodic settings, important asymptotic convergence results were derived in [Glo06, Glo08, Glo12]. A posteriori error estimators tailored to MsFEM were developed in [HOS14, CL18, LRLBH22]. Moreover, an exponentially convergent variant of the method was proposed in [CHW24]. For a comprehensive overview of MsFEM, we refer to [CEH23].

Spectral approaches

Another important class of numerical homogenization methods are spectral approaches, which aim to capture the relevant fine-scale information by solving (local) spectral problems. A prominent example is the Multiscale Spectral Generalized Finite Element Method (MS-GFEM), which goes back to [BL11]. The central idea is to partition the global computational domain into small subdomains and define, on each subdomain, a suitable local compact operator that accounts for the fine-scale features of the problem. By solving spectral problems associated with these local operators, finite-dimensional approximation spaces are constructed on each subdomain. These local spaces are then made globally conforming by multiplying with a partition of unity. The resulting basis can be used within a standard Galerkin framework. In contrast to variational approaches such as LOD, the convergence of MS-GFEM is established in the number of local basis functions and not in the diameter of the subdomains. The method has been further developed in, among others, [BLSS20, MSD22, MAS23, MM24, AMS25]. For a comprehensive overview of MS-GFEM, we refer to [Ma25].

A combination of MsFEM and MS-GFEM led to the development of the Generalized Multiscale Finite Element Method (GMsFEM), introduced in [EGH13]. The main idea is to enhance the accuracy of the multiscale space obtained from residual-free bubbles computed with homogeneous Dirichlet boundary conditions on the boundaries of coarse grid elements. To achieve this, additional bubbles with boundary conditions induced by fine-scale nodal basis functions are computed. From this typically large snapshot space, a small number of relevant basis functions are selected by solving local spectral problems. Further developments of GMsFEM can be found, for example, in [CEGL16, CEL19, CCE+20].

Stochastic homogenization approaches

Several numerical methods have been developed to solve PDEs with random coefficients, including the stochastic FEM and the stochastic collocation method; see

the review article [GWZ14] and references therein. These methods are effective when the dimension of the stochastic input is low. However, their performance deteriorates significantly in high-dimensional settings due to the so-called curse of dimensionality, which remains a central challenge in uncertainty quantification. To address this, stochastic homogenization has emerged as an alternative. Analogous to analytical homogenization, it aims to derive an effective deterministic model that captures the macroscopic behavior of materials with microscopically random properties, thereby circumventing the need to fully resolve fine-scale uncertainties. The qualitative theory of stochastic homogenization for PDEs with random coefficients dates back to the foundational works [Koz79, PV79, Yur86]. To go beyond mere qualitative results, researchers began to rigorously quantify the error between the heterogeneous and homogenized models, leading to the development of quantitative stochastic homogenization. This theory has yielded optimal-order convergence rates for linear elliptic PDEs with random coefficients, as established in [GO11, GO12, AKM17]. For nonlinear problems, (non-optimal) convergence rates have been derived in [ACS14, AC18, AFK20]. Further important developments in this area include [GNO14, AS16, GO17, GNO20, DGO20, HMS21]. A comprehensive overview of the quantitative theory of stochastic homogenization can be found in [AKM19]. In parallel, various numerical approaches have been proposed for the computation of effective coefficients in the stochastic setting, including [BP04, CELS15, BLBL16, LBLM16, Mou18, KKO20].

Several computational methods in stochastic homogenization that go beyond the computation of homogenized coefficients have been developed, including [ZCH15, HMZ19, AHKM21, LOW24]. In addition, several of the presented classical multiscale frameworks such as HMM, VMM, MsFEM, and GMsFEM have been adapted to the stochastic setting. Representative contributions include [EMZ05] (HMM), [BJ11] (HMM and MsFEM), [CS08, GMP10, BLT14], and the comprehensive review in [ACB+11] (MsFEM), as well as [JMSDO14] (VMM) and [CEGL16, CELZ18] (GMsFEM). A notable development in this direction is the combination of quantitative stochastic homogenization with the LOD, as proposed and analyzed in [GP19, FGP21]. Specifically, using a reformulation of the LOD based on a quasi-local discrete integral operator introduced in [GP17], one can derive an effective deterministic model by taking expectations. This model yields a coarse-scale approximation to the expected value of the solution. Further applications of LOD in the context of numerical stochastic homogenization are discussed, for example, in [FP20, MV22, KV25].

1.3. Outline and contribution

The goal of this thesis is to present and analyze recent advancements of the SLOD, originally introduced in [HP22b]. These developments are carried out in the context of elliptic diffusion problems with highly heterogeneous diffusion coefficients, where classical discretization approaches, such as the FEM, often

fail to efficiently resolve the multiscale nature of the solution.

The thesis is structured as follows. Chapter 2 motivates the need for multiscale methods by illustrating the limitations of classical FEMs in the presence of fine-scale features induced by highly heterogeneous coefficients. Moreover, we introduce the concept of prototypical multiscale approximation spaces, which are obtained by applying the global solution operator of the elliptic diffusion problem to classical finite element spaces (e.g., piecewise constants). Although these spaces yield ideal approximation properties, they are infeasible in practice due to their globally supported basis functions. As a possible solution to this issue, we present a short introduction of the LOD method. LOD turns the ideal approach into a practical numerical scheme by introducing localization techniques, which lead to basis functions that exhibit exponential decay away from their associated coarse elements.

Chapter 3 introduces the SLOD method, an improvement over the classical LOD. The key advancement lies in the super-exponential decay of the localized basis functions observed in practice, which is achieved through a novel localization strategy. This strategy identifies local source terms whose responses under the local solution operator exhibit minimal conormal derivatives on patch boundaries. We rigorously prove the super-exponential decay in the special case of a constant diffusion coefficient. Furthermore, we discuss the challenges associated with ensuring stability of the resulting basis, since stability is not guaranteed a priori. We therefore propose and investigate several stabilization techniques to ensure robustness in practical computations.

Building on the SLOD framework, Chapter 4 presents the Hierarchical SLOD (HSLOD), an extension to multilevel settings. We construct a hierarchical basis of the approximate solution space, consisting of superlocalized basis functions that are quasi-orthogonal across hierarchy levels with respect to the energy inner product. This hierarchical construction induces both a sparse compression of the solution space and an orthogonal multiresolution decomposition of the approximate solution operator. This decomposition effectively decouples different scales and solution components. Consequently, the original PDE can be reduced to a set of independent linear systems, one per level, which can be solved in parallel, leading to significant computational efficiency. The condition numbers for these systems are mesh-independent except for the first level.

In the second part of this thesis, we address random diffusion coefficients, extending the SLOD methodology to a stochastic setting in Chapter 5. By leveraging the SLOD localization strategy, we develop a novel collocation-type stochastic homogenization method. This approach benefits from the super-exponential decay of basis functions relative to the coarse mesh, enabling substantial computational savings during the sampling phase. The method is particularly well-suited for parallel computing environments due to its simple and communication-efficient structure: basis functions are computed locally with minimal inter-patch communication. Additionally, we provide an error analysis that links the proposed numerical method to the quantitative theory of stochas-

tic homogenization, demonstrating both theoretical and practical convergence properties.

Finally, in Chapter 6, we synthesize the ideas developed in the preceding chapters to construct a hierarchical stochastic numerical homogenization method. The collocation-type formulation is retained to preserve simplicity and computational efficiency, while the hierarchical structure improves the conditioning of the system matrices associated with the local hierarchical source terms. We provide an accompanying error analysis grounded in the quantitative theory of stochastic homogenization and demonstrate the method's convergence through numerical experiments.

The work presented in this thesis emerged from a collaborative effort within the project Computational Random Multiscale Problems, funded by the European Research Council. Many of the results included here were developed jointly with other project members and initially disseminated as preprints or journal articles.

In particular, the stochastic SLOD method described in Chapter 5 was developed in collaboration with Moritz Hauck and Daniel Peterseim and published in *Multiscale Modeling & Simulation* [HMP25]. Likewise, the HSLOD method presented in Chapter 4 is a revised and extended version of the preprint [GMPZ24], which resulted from a collaboration with José C. Garay, Christoph Zimmer, and Daniel Peterseim. However, specific parts of the latter work were originally developed and proven by José C. Garay. These include Theorem 4.3.2, the results in Section 4.4 concerning additional compression stages, and the condition number estimate in Theorem 4.5.3, along with the two preceding lemmas. Their presentation here has been adapted slightly for consistency with the overall style of the thesis.

In contrast, certain parts of this thesis represent original contributions that have not been previously published. These include the illustrative proof of the super-exponential decay of the SLOD basis functions in the special case $A \equiv 1$ (Section 3.3.1) and a novel stabilization technique for SLOD basis functions (Section 3.4.3), both presented in Chapter 3, as well as the entirety of Chapter 6.

The numerical experiments presented in this thesis were performed in `MATLAB`, based on preliminary code developed at the Chair of Computational Mathematics at the University of Augsburg.

Notation. Throughout this work, we adopt the following notational conventions. We write $C > 0$ to denote a generic constant that is independent of the mesh sizes h and H, the oversampling parameter m, and the microscopic scale ε. Such constants may, however, depend on the dimension d, the domain D, and the uniform bounds on the diffusion coefficient. We emphasize that the value of C may vary from one estimate to another. To simplify notation, we use the symbol $a \lesssim b$ (or equivalently $b \gtrsim a$) to indicate that $a \leq Cb$ for some constant $C > 0$ as described above. If both $a \lesssim b$ and $a \gtrsim b$ hold, we write $a \approx b$.

Part I.

Deterministic coefficients

2. Localized Orthogonal Decomposition

Classical FEMs are widely used for solving PDEs. However, these methods face significant challenges when applied to problems with highly heterogeneous coefficients, particularly when these coefficients exhibit fine-scale variations. In such cases, FEM often requires a mesh that is fine enough to resolve these small-scale features, leading to high computational costs. Moreover, the convergence of the FEM solution can be arbitrarily slow, especially when the solution exhibits low regularity; cf. [BO00].

One possible approach to overcome these limitations is the LOD method, originally introduced in [MP14] and later refined in [HP13], within the context of elliptic model problems (see also [MP20]). The main objective of the LOD method is to deliver effective approximations of solutions to PDEs on a coarse scale, particularly when the problem involves complex, heterogeneous coefficients that vary on small scales. To this end, the LOD method constructs a problem-adapted solution space. This is achieved by decomposing the given solution space into an infinite-dimensional fine-scale space representing the unresolved small-scale features and its finite-dimensional coarse complement in a problem-adapted fashion. The coarse space captures essential fine-scale information, enabling an accurate approximation of the solution. The final LOD approximation is then obtained via, for example, a Galerkin projection using a localized version of the coarse complementary space. This approach ensures reliable approximations on arbitrarily coarse meshes, provided that the diameter of the patches, where the basis functions of the localized complement space are computed, is increased logarithmically with the desired accuracy.

Various LOD variants have been developed in relatively general settings (see, e.g., the review articles [Pet16, AHP21] and the dissertation [Mai20]). In this work, however, we limit ourselves to an overview of the lowest-order LOD method from [Mai21, HP22a], tailored to elliptic diffusion problems. Our introduction to the LOD is intentionally brief, as comprehensive expositions are already available; cf. the textbook [MP20] and the review article [AHP21]. Before presenting the LOD approach, we first introduce the classical FEM, highlight its limitations, and discuss a prototypical operator-dependent method. The presentation in this chapter is inspired by [AHP21, Hau23].

2.1. Model problem

We consider the prototypical elliptic diffusion problem

$$-\operatorname{div}(A\nabla u) = f \tag{2.1}$$

subject to homogeneous Dirichlet boundary conditions on a polygonal Lipschitz domain $D \in \mathbb{R}^d$ with $d \in \{1, 2, 3\}$. Without loss of generality, we assume that D is scaled to unit size. The diffusion coefficient $A \in L^\infty(D, \mathbb{R}^{d\times d})$ is a matrix-valued function which is supposed to be symmetric and positive definite almost everywhere. More precisely, we assume that there exist constants $0 < \alpha \leq \beta < \infty$ such that

$$\alpha\|\eta\|_2^2 \leq (A(x)\eta)\cdot\eta \leq \beta\|\eta\|_2^2 \tag{2.2}$$

holds for all $\eta \in \mathbb{R}^d$ and for almost all $x \in D$.

We assume $f \in L^2(D)$, the space of square-integrable functions on D. For any subdomain $S \subseteq D$, we denote the L^2-norm and inner product restricted to S by $\|\cdot\|_{L^2(S)}$ and $(\cdot,\cdot)_{L^2(S)}$, respectively. Furthermore, we denote by $H^k(D)$ with $k \in \mathbb{N}_0$, the Sobolev space of functions in $L^2(D)$ that have square-integrable weak derivatives up to order k. The H^k-norm restricted to $S \subseteq D$ is denoted by $\|\cdot\|_{H^k(S)}$. Notably, $H^0(D) = L^2(D)$ and $\|\cdot\|_{H^0(S)} = \|\cdot\|_{L^2(S)}$.

The solution space of the weak formulation of the elliptic diffusion problem (2.1) is the Sobolev space $\mathcal{V} \coloneqq H_0^1(D)$ which is a closed subspace of $H^1(D)$ that accounts for the homogeneous Dirichlet boundary conditions. The bilinear form $a : \mathcal{V}\times\mathcal{V} \to \mathbb{R}$ associated with the model problem is given, for any $u, v, \in \mathcal{V}$, by

$$a(u, v) \coloneqq \int_D (A\nabla u)\cdot\nabla v \,\mathrm{d}x.$$

Under the given assumptions on the diffusion coefficient A, the bilinear form $a(\cdot,\cdot)$ defines an inner product on $\mathcal{V}$, inducing the energy norm $\|\cdot\|_a \coloneqq \sqrt{a(\cdot,\cdot)}$.

The weak formulation of (2.1) seeks $u \in \mathcal{V}$ such that

$$a(u, v) = (f, v)_{L^2(D)} \tag{2.3}$$

holds for all $v \in \mathcal{V}$. Due to the coercivity of $a(\cdot,\cdot)$, the Lax–Milgram theorem establishes the well-posedness of the model problem (2.3) and ensures the existence of a unique solution $u \in \mathcal{V}$. Moreover, applying Friedrichs' inequality (see e.g. [Beb03]), yields the estimate

$$\|\nabla u\|_{L^2(D)} \leq \alpha^{-1}\frac{\operatorname{diam}(D)}{\pi}\|f\|_{L^2(D)}.$$

We denote the solution operator of the problem by $\mathcal{A}^{-1} : L^2(D) \to \mathcal{V}$, mapping $f \in L^2(D)$ to the unique solution $u \in \mathcal{V}$ of (2.3).

2.2. Finite element method

The Galerkin FEM is the most widely used approach for computing numerical solutions to second-order elliptic PDEs in variational form, such as (2.3). The method seeks the best approximation of the solution within a finite-dimensional subspace of $\mathcal{V}$. The discretization is based on a sequence of meshes $\{\mathcal{T}_H\}_{H>0}$, where each mesh is a finite subdivision of D into closed, convex and shape regular elements (in the sense of [EG04, Definition 1.107]), with mesh size parameter H. Although various types of meshes are possible, we focus on conforming Cartesian meshes, where the mesh elements are d-rectangles. More precisely, any $(d-1)$-dimensional face of an element $K \in \mathcal{T}_H$ is either a subset of the boundary ∂D, or a face of another element, see also [EG04, Definition 1.55]. In particular, we assume that the domain D allows a decomposition into such elements. Additionally, we assume that the sequence of meshes is quasi-uniform (see [EG04, Definition 1.140]), meaning there exists a constant $C_{\mathrm{qu}} > 0$ such that

$$H \coloneqq \max_{K \in \mathcal{T}_H} H_K \leq C_{\mathrm{qu}} \min_{K \in \mathcal{T}_H} H_K,$$

holds for all meshes, where H_K denotes the diameter of the element K.

On these meshes, we define the finite element space of first-order polynomials as

$$\mathcal{V}_H^{\mathrm{fem}} \coloneqq \{v \in \mathcal{V} : \forall K \in \mathcal{T}_H : \, v|_K \text{ is a polynomial of coordinate degree } \leq 1\}.$$

The $\mathbb{P}^1$-FEM seeks the Galerkin approximation $u_H^{\mathrm{fem}} \in \mathcal{V}_H^{\mathrm{fem}}$ such that

$$a(u_H^{\mathrm{fem}}, v) = (f, v)_{L^2(D)}$$

holds for all $v \in \mathcal{V}_H^{\mathrm{fem}}$. The unique existence of $u_H^{\mathrm{fem}} \in \mathcal{V}_H^{\mathrm{fem}}$ is guaranteed by the coercivity of the bilinear form $a(\cdot, \cdot)$. Céa's Lemma (see, e.g., [Cia78, Theorem 2.4]) establishes the quasi-optimality of the finite element approximation in $\mathcal{V}_H^{\mathrm{fem}}$. Furthermore, under additional regularity assumptions on the domain D and on the derivatives of the diffusion coefficient, the unique solution of (2.3) satisfies $u \in H^2(D)$. By applying classical interpolation results (see, e.g., [EG17, Theorem 6.4]), we obtain the error estimate

$$\|u - u_H^{\mathrm{fem}}\|_{\mathcal{V}} \lesssim H \|D^2 u\|_{L^2(D)},$$

which indicates optimal first-order convergence. Note however, that if the solution exhibits lower regularity, the convergence rate correspondingly decreases. Moreover, when dealing with a highly heterogeneous diffusion coefficient A_ε, that varies on some fine-scale ε, the H^2-seminorm of the true solution may also depend on ε. This is illustrated in [MP20, Chapter 2], where a one-dimensional diffusion problem on $D = (0, 1)$ with homogeneous Dirichlet boundary conditions is analyzed for a smooth but rapidly oscillating coefficient A_ε. In this setting,

the true solution $u_\varepsilon \in H^2(D)$ satisfies $\|D^2 u_\varepsilon\|_{L^2(D)} \approx \varepsilon^{-1}$. Consequently, the mesh size must resolve the microscopic scale, i.e., $H \lesssim \varepsilon$, to ensure a meaningful error bound. Notably, in the pre-asymptotic regime, where the mesh does not resolve the oscillations of the coefficient, neither the macroscopic behavior of the solution nor its microscopic features are well approximated. In fact, classical FEMs can perform arbitrarily poorly for PDEs with rough coefficients, as shown in [BO00].

2.3. Prototypical operator-dependent method

The goal of this section is to construct a coarse-scale space with superior approximation properties compared to the previously introduced standard finite element space. This improvement is achieved by incorporating problem-dependent shape functions that encode fine-scale information a priori. Notably, we are not restricted to a particular choice of the underlying space for the coarse space, nor do we require it to be a subspace of $H^1(D)$. To keep the construction simple, we choose the space of piecewise constant functions on the coarse mesh $\mathcal{T}_H$, defined as

$$\mathbb{P}^0(\mathcal{T}_H) \coloneqq \{\mathbb{1}_K : K \in \mathcal{T}_H\},$$

where $\mathbb{1}_K$ denotes the characteristic function of an element $K \in \mathcal{T}_H$. The coarse-scale shape functions are then obtained by applying the solution operator $\mathcal{A}^{-1}$ to $\mathbb{P}^0(\mathcal{T}_H)$. Hence, a natural definition of a prototypical problem-specific ansatz space is given by

$$\mathcal{V}_H^a \coloneqq \operatorname{span}\{\mathcal{A}^{-1}\mathbb{1}_K : K \in \mathcal{T}_H\}. \tag{2.4}$$

Using this space, the prototypical Galerkin method seeks a discrete approximation $u_H \in \mathcal{V}_H^a$ such that

$$a(u_H, v) = (f, v)_{L^2(D)} \tag{2.5}$$

holds for all $v \in \mathcal{V}_H^a$. The approximation error of this method satisfies the bound

$$\|\nabla(u - u_H)\|_{L^2(D)} \lesssim H^{1+s}\|f\|_{H^s(D)}$$

for any $f \in H^s(D)$ with $s \in \{0, 1\}$, see, e.g., [AHP21, Example 3.10]. Notably, this method is exact when the right-hand side satisfies $f \in \mathbb{P}^0(\mathcal{T}_H)$.

Despite its strong approximation properties, the canonical basis functions $\{\mathcal{A}^{-1}\mathbb{1}_K : K \in \mathcal{T}_H\}$ of $\mathcal{V}_H^a$ are inherently non-local. This is illustrated in Figure 2.1 for the one-dimensional setup. Due to their global support, these functions are impractical for computations. Consequently, we refer to (2.5) as the ideal method, which serves as a theoretical benchmark rather than a feasible numerical scheme. The construction of an approximately local basis of the problem-specific ansatz space $\mathcal{V}_H^a$ is the true challenge of numerical homogenization. Various strategies to accomplish this will be discussed in the following.

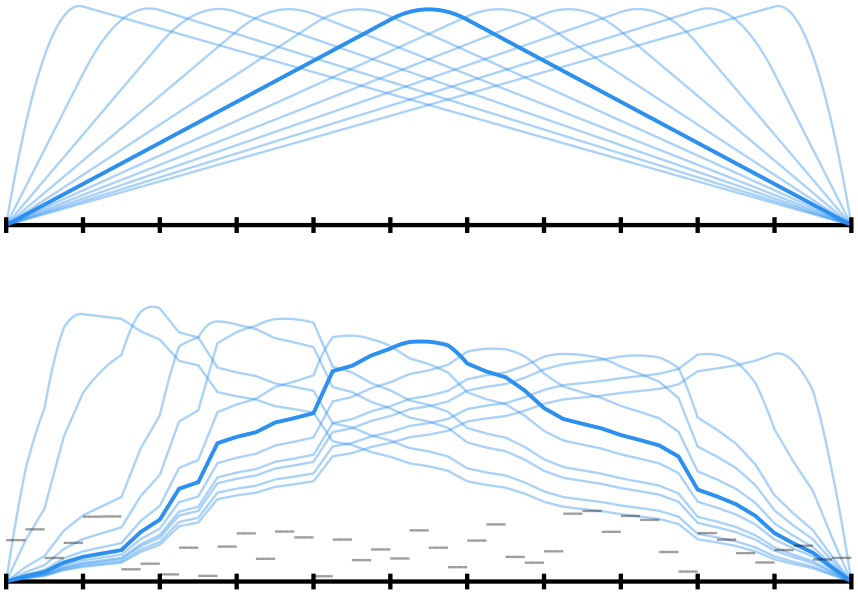

Figure 2.1.: Globally supported prototypical basis functions for the model problem (2.3) in one spatial dimension, for $A \equiv 1$ (top) and a piecewise constant coefficient illustrated in gray (bottom).

2.4. Orthogonal decomposition

Before constructing a more practical basis for $\mathcal{V}_H^a$ that can be well-approximated by local functions, we first introduce the L^2-orthogonal projection onto the space of piecewise constants which is denoted by $\Pi_H : L^2(D) \to \mathbb{P}^0(\mathcal{T}_H)$. For all $K \in \mathcal{T}_H$, the projection satisfies the local stability property

$$\|\Pi_H v\|_{L^2(K)} \leq \|v\|_{L^2(K)}, \tag{2.6}$$

for all $v \in L^2(K)$, as well as the local approximation property

$$\|v - \Pi_H v\|_{L^2(K)} \leq \pi^{-1} H \|\nabla v\|_{L^2(K)}, \tag{2.7}$$

for all $v \in H^1(K)$, see, e.g., [PW60, Beb03]. Given this projection, we introduce the infinite-dimensional fine-scale space

$$\mathcal{W} \coloneqq \{w \in \mathcal{V} : \Pi_H w = 0\},$$

which consists of microscopic functions that are not resolved by the coarse-scale space $\mathcal{V}_H^a$. Together, these two spaces form an a-orthogonal decomposition of $\mathcal{V}$, meaning that

$$\mathcal{V} = \mathcal{V}_H^a \oplus \mathcal{W}$$

with the orthogonality property

$$a(\mathcal{V}_H^a, \mathcal{W}) = 0,$$

see, e.g., [AHP21, Theorem 3.5].

To incorporate fine-scale information into the coarse approximation space, the LOD utilizes correction operators. The ideal correction operator $\mathcal{C} : \mathcal{V} \to \mathcal{W}$ is defined by

$$a(\mathcal{C}v, w) = a(v, w) \tag{2.8}$$

for all $v \in \mathcal{V}$ and $w \in \mathcal{W}$. The well-posedness of (2.8) follows from the Lax–Milgram theorem, since $\mathcal{W}$ is a closed subspace of $\mathcal{V}$. A crucial observation is that the correction operator can be decomposed into element-wise correctors. More precisely, we can write

$$\mathcal{C} = \sum_{K \in \mathcal{T}_H} \mathcal{C}_K \tag{2.9}$$

where each element corrector $\mathcal{C}_K : \mathcal{V} \to \mathcal{W}$ satisfies

$$a(\mathcal{C}_K v, w) = a_K(v, w) \coloneqq \int_K (A\nabla v) \cdot \nabla w \,\mathrm{d}x \tag{2.10}$$

for all $v \in \mathcal{V}$ and $w \in \mathcal{W}$. A key property of the element correctors, first rigorously established in [MP14], is their exponential decay away from the associated mesh elements. This decay motivates their localization, which is discussed in the next section.

An alternative characterization of the problem-specific ansatz space $\mathcal{V}_H^a$ can be obtained using the correction operator $\mathcal{C}$ together with bubble functions associated with coarse mesh elements. More precisely, for each element $K \in \mathcal{T}_H$, we choose non-negative bubbles $b_K \in H_0^1(K)$ with $\Pi_H b_K = \mathbb{1}_K$ such that

$$\|b_K\|_{L^2(K)} \lesssim H\|\nabla b_K\|_{L^2(K)} \lesssim \|\mathbb{1}_K\|_{L^2(K)}, \tag{2.11}$$

see, e.g. [AHP21, Example 3.11] for an explicit construction of these functions; however, their exact representation is not important. The space of bubble functions is then defined as

$$B_H \coloneqq \operatorname{span}\{b_K : K \in \mathcal{T}_H\}.$$

Using this notation, the problem-specific approximation space $\mathcal{V}_H^a$ can be reformulated as

$$\mathcal{V}_H^a = (1 - \mathcal{C})B_H, \tag{2.12}$$

which is shown for example in [AHP21, Lemma 3.12]. This relation motivates the definition of the ideal LOD basis functions as

$$\varphi_K^{\mathrm{lod}} = (1 - \mathcal{C})b_K \tag{2.13}$$

for $K \in \mathcal{T}_H$. Although these functions are globally supported, they inherit the exponential decay property of the element correctors.

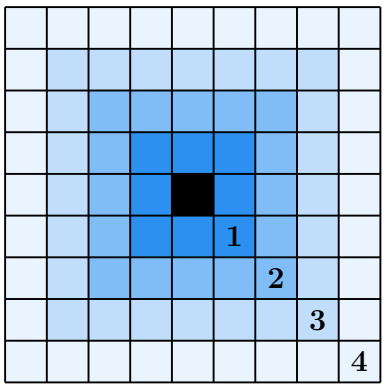

Figure 2.2.: Illustration of the m-th order patch $\mathsf{N}^m(K)$ for an element $K \in \mathcal{T}_H$, shown in black. Varying shades of blue represent different patch orders, ranging from $m = 1, \dots, 4$.

2.5. Localization strategy

The localization of the element correctors, and consequently the localization of the LOD basis functions, is motivated by their exponential decay. The localization approach relies on the concept of local patches in the coarse mesh $\mathcal{T}_H$, which are constructed based on neighborhood relations between elements. Given a union of elements $S \subset D$, we define the first order element patch $\mathsf{N}^1(S)$ of S by

$$\mathsf{N}^1(S) \coloneqq \bigcup \{T \in \mathcal{T}_H : T \cap S \neq \emptyset\}.$$

For any $m = 2, 3, 4, \dots$, the m-th order patch $\mathsf{N}^m(K)$ of the element $K \in \mathcal{T}_H$ is then recursively given by

$$\mathsf{N}^m(K) \coloneqq \mathsf{N}^1(\mathsf{N}^{m-1}(K)); \tag{2.14}$$

see Figure 2.2 for an schematic illustration using a Cartesian mesh.

The submesh of $\mathcal{T}_H$ restricted to the patch $\mathsf{N}^m(K)$ is given by

$$\mathcal{T}_{H,\mathsf{N}^m(K)} \coloneqq \{T \in \mathcal{T}_H : T \subset \mathsf{N}^m(K)\}.$$

The restriction of the L^2-orthogonal projection to this patch is denoted by $\Pi_{H,\mathsf{N}^m(K)} : L^2(\mathsf{N}^m(K)) \to \mathbb{P}^0(\mathcal{T}_{H,\mathsf{N}^m(K)})$. Note that in the remainder of this thesis, we do not distinguish between locally defined L^2- or H^1_0-functions and their extensions by zero to the whole domain.

To approximate correctors locally, we define the localized fine-scale subspaces for each element $K \in \mathcal{T}_H$ and oversampling parameter $m \in \mathbb{N}$ as

$$\mathcal{W}_{K,m} \coloneqq \{w \in H^1_0(\mathsf{N}^m(K)) : \Pi_{H,\mathsf{N}^m(K)} w = 0\}. \tag{2.15}$$

The localized element correctors $\widehat{\mathcal{C}}_{K,m}$ are then defined by solving

$$a(\widehat{\mathcal{C}}_{K,m} v, w) = a_K(v, w)$$

for all $v \in \mathcal{V}$ and $w \in \mathcal{W}_{K,m}$. This equation is identical to the original element corrector definition (2.10) but now constrained to the localized fine-scale space $\mathcal{W}_{K,m}$. Relation (2.9) motivates defining the localized corrector $\widehat{\mathcal{C}}_m$ as the sum of these localized element correctors $\widehat{\mathcal{C}}_{K,m}$, i.e.,

$$\widehat{\mathcal{C}}_m \coloneqq \sum_{K \in \mathcal{T}_H} \widehat{\mathcal{C}}_{K,m}.$$

Due to the exponential decay of the element correctors $\widehat{\mathcal{C}}_{K,m}$, the localized corrector $\widehat{\mathcal{C}}_m$ provides an exponentially accurate approximation of the full corrector $\mathcal{C}$. More precisely, the localization error satisfies

$$\|\nabla(\mathcal{C} - \widehat{\mathcal{C}}_m)v\|_{L^2(D)} \lesssim m^{d/2} \exp(-Cm)\|\nabla v\|_{L^2(D)},$$

for all $v \in \mathcal{V}$, where $C > 0$ is a constant independent of H and m. The proof builds on classical LOD techniques and follows the arguments in [MP20, Theorem 4.3] and [HP22a, Lemma 5.4]. A formulation adapted to the present context can also be found in [DHM23, Lemma 5.2].

2.6. Practical multiscale method

Using the localization strategy from the previous section, we introduce localized versions of the ideal LOD basis functions defined in (2.13), thereby transforming the ideal numerical homogenization method (2.5) into a computationally feasible scheme. However, instead of merely replacing the correctors with their localized counterparts, we additionally employ a $\mathcal{V}$-stable projection operator $\mathcal{P}_H$, first introduced in [AHP21, Equation (3.13)]. This operator cures numerical pollution effects at the cost of slightly increasing the support of the LOD basis functions; see [HP22a, DHM23]. The construction of $\mathcal{P}_H$ is based on the quasi-interpolation operator $\mathcal{I}_H$ from which it inherits the $\mathcal{V}$-stability. The quasi-interpolation is defined as $\mathcal{I}_H \coloneqq \mathcal{E}_H \circ \Pi_H$, where $\mathcal{E}_H$ denotes an averaging operator that maps piecewise constants to the space of continuous piecewise linear functions. For interior nodes z, it is defined as

$$(\mathcal{E}_H v)(z) \coloneqq \frac{1}{\#\{K \in \mathcal{T}_H : z \in K\}} \sum_{K \in \mathcal{T}_H : z \in K} v|_K(z),$$

while for nodes on the Dirichlet boundary, we set $(\mathcal{E}_H v)(z) \coloneqq 0$. The operator $\mathcal{E}_H$ is well known from the theory of domain decomposition methods; see, e.g., [Osw93, Bre94]. Since $\mathcal{P}_H$ should satisfy $\ker \mathcal{P}_H = \ker \Pi_H$, we need to correct $\mathcal{I}_H v$ such that the element-wise averages of v on $\mathcal{T}_H$ are preserved. This leads to the definition

$$\mathcal{P}_H v \coloneqq \mathcal{I}_H v + \sum_{K \in \mathcal{T}_H} b_K \fint_K (v - \mathcal{I}_H v)\,\mathrm{d}x.$$

Since the operator $\mathcal{I}_H$ is quasi-local in the sense that it extends the support of a function by only one layer of elements, the same property also holds for $\mathcal{P}_H$.

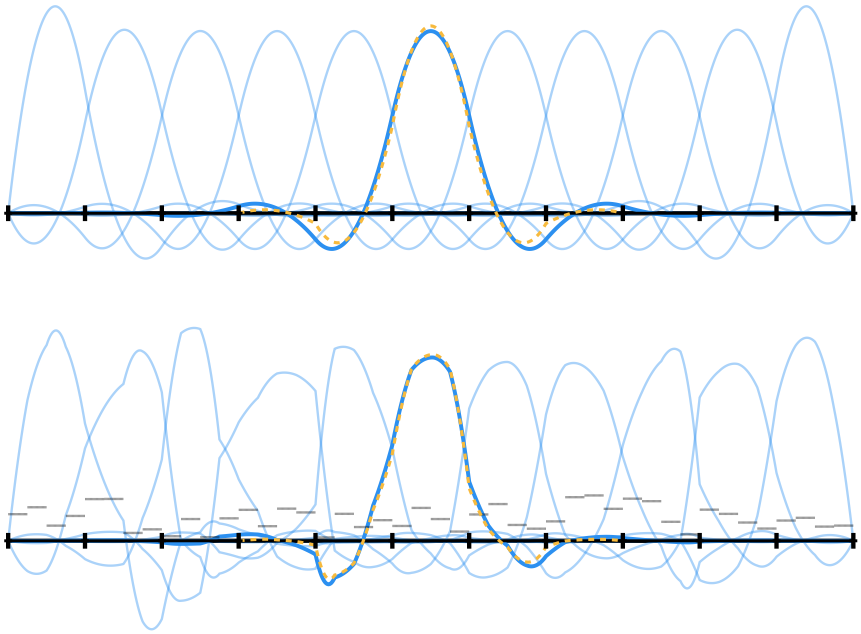

Figure 2.3.: Ideal LOD basis for the model problem (2.3) in one spatial dimension, for $A \equiv 1$ (top) and a piecewise constant coefficient illustrated in gray (bottom). The localized counterparts with $m = 1$ for the central basis functions are depicted in yellow.

Building on the ideal coarse space formulation from (2.12), we introduce the localized, problem-adapted ansatz space $\mathcal{V}_{H,m}^{\mathrm{lod}}$ of the LOD method for a given oversampling parameter $m \in \mathbb{N}$, incorporating the projection operator $\mathcal{P}_H$, as

$$\mathcal{V}_{H,m}^{\mathrm{lod}} \coloneqq (1 - \widehat{\mathcal{C}}_m)\mathcal{P}_H B_H.$$

The associated localized LOD basis functions for $K \in \mathcal{T}_H$ are defined by

$$\hat{\varphi}_{K,m}^{\mathrm{lod}} = (1 - \widehat{\mathcal{C}}_m)\mathcal{P}_H b_K.$$

An illustration comparing ideal and localized LOD basis functions is provided in Figure 2.3. The classical LOD then computes a Galerkin approximation in the localized ansatz space; that is, it seeks $u_{H,m}^{\mathrm{lod}} \in \mathcal{V}_{H,m}^{\mathrm{lod}}$ such that

$$a(u_{H,m}^{\mathrm{lod}}, v) = (f, v)_{L^2(D)}$$

holds for all $v \in \mathcal{V}_{H,m}^{\mathrm{lod}}$. Using standard LOD techniques (see, e.g., [MP20, Theorem 5.2]), we obtain, for $f \in H^s(D)$ with $s \in \{0, 1\}$, the error estimate

$$\|\nabla(u - u_{H,m}^{\mathrm{lod}})\|_{L^2(D)} \lesssim H^{1+s}\|f\|_{H^s(D)} + m^{d/2}\exp(-Cm)\|f\|_{L^2(D)},$$

where the constant $C > 0$ is independent of H and m. For a proof adapted to the present context, we refer to [DHM23, Theorem 6.2]. This estimate implies that choosing $m \gtrsim |\log(H)|$ recovers the convergence rate of the ideal method.

3. Super-Localized Orthogonal Decomposition

In this chapter, we introduce an enhanced localization technique within the LOD framework, building on the concepts presented in the previous chapter. This refined approach, known as the Super-Localized Orthogonal Decomposition (SLOD), was first introduced in [HP22b] for an elliptic diffusion problem. We refer to [Hau23] for a more general setting. The key idea behind SLOD is to identify local finite element source terms for all patches, ensuring that their responses decay rapidly under the local solution operators. This decay is enforced by minimizing the conormal derivatives of the responses at the patch boundaries. The resulting local responses are taken as the SLOD basis functions.

A crucial advantage of SLOD is that, in practice, the localization error decays super-exponentially as the patch size increases. Consequently, local basis functions supported on patches of diameter $\mathcal{O}(H|\log H|^{(d-1)/d})$, where d denotes the spatial dimension, are sufficient to maintain optimal algebraic convergence rates in H without pre-asymptotic effects. In contrast, the standard LOD framework requires basis functions supported on patches of diameter $\mathcal{O}(H|\log H|)$ to achieve similar accuracy. Despite these empirical benefits, a rigorous proof of the super-exponential decay of SLOD basis functions remains an open problem. However, in the special case of a constant diffusion coefficient, we establish this decay through an analysis based on Steklov eigenfunctions. Moreover, even in the general heterogeneous setting, classical LOD techniques can be used to show that the localization error of the SLOD basis functions decays at least exponentially.

In the classical LOD, equivalently to solving local sub-scale correction problems, the basis functions can also be obtained by solving local constrained energy minimization problems, where the constraints impose a Kronecker delta condition with respect to element averages, ensuring the stability of the LOD basis functions, see [OS19,Mai21]. In contrast, for the SLOD this constraint is removed to enforce the decay of the basis functions in a more direct way. As a result, the stability of the basis is not inherently guaranteed. To address this limitation, we explore various stabilization techniques to ensure robustness while preserving the benefits of the improved localization strategy.

The results in this chapter are largely drawn from [HP22b], whose presentation we follow closely. In particular, Section 3.1 builds on [HP22b, Section 4], while Sections 3.2 and 3.3.2 are based on [HP22b, Sections 5–6]. Furthermore, Section 3.4.1 and Section 3.5.1 are adapted from [HP22b, Appendix B]. In addition,

the stabilization technique presented in Section 3.4.2 and the first part of Section 3.5.2 are based on [BFP24, Section 7]. The stabilization approach discussed in Section 3.4.4 and the second part of Section 3.5.2 follow [GMPZ24, Section 3.1]. In contrast, the results presented in Sections 3.3.1 and 3.4.3 are novel contributions.

3.1. Localization strategy

As for the LOD, the SLOD localization strategy is based on local patches as defined in (2.14). To simplify notation, we fix an element $K \in \mathcal{T}_H$, an oversampling parameter $m \in \mathbb{N}$ and define the m-th order patch of K as $D_K := \mathsf{N}^m(K)$, assuming that D_K does not coincides with the whole domain D. The submesh $\mathcal{T}_{H,D_K}$ consists of elements in the patch, and the $L^2(D_K)$-orthogonal projection onto piecewise constants is denoted by $\Pi_{H,D_K} \colon L^2(D_K) \to \mathbb{P}^0(\mathcal{T}_{H,D_K})$.

The ideal SLOD basis function $\varphi^{\mathrm{slod}}_{K,m} \in \mathcal{V}^a_H$, where $\mathcal{V}^a_H$ denotes the prototypical problem-specific ansatz space defined in (2.4), is given by

$$\varphi^{\mathrm{slod}}_{K,m} = \mathcal{A}^{-1} g^{\mathrm{slod}}_{K,m}, \quad \text{with} \quad g^{\mathrm{slod}}_{K,m} := \sum_{T \in \mathcal{T}_{H,D_K}} c_T \mathbb{1}_T, \tag{3.1}$$

where the coefficients $(c_T)_{T \in \mathcal{T}_{H,D_K}}$ are to be determined. The localized approximation $\hat{\varphi}^{\mathrm{slod}}_{K,m} \in H^1_0(D_K)$ is the Galerkin projection of $\varphi^{\mathrm{slod}}_{K,m}$ onto $H^1_0(D_K)$, satisfying

$$a_{D_K}(\hat{\varphi}^{\mathrm{slod}}_{K,m}, v) := \int_{D_K} (A \nabla \hat{\varphi}^{\mathrm{slod}}_{K,m}) \cdot \nabla v \,\mathrm{d}x = (g^{\mathrm{slod}}_{K,m}, v)_{L^2(D_K)}, \tag{3.2}$$

for all $v \in H^1_0(D_K)$.

Since the local function $\hat{\varphi}^{\mathrm{slod}}_{K,m}$ is generally a poor approximation of $\varphi^{\mathrm{slod}}_{K,m}$, an appropriate choice of $g^{\mathrm{slod}}_{K,m}$ is crucial for accuracy in the energy norm. To analyze this choice, we define the trace operator restricted to the closed subspace $\mathcal{V}_{D_K} := \{v|_{D_K} : v \in \mathcal{V}\} \subset \mathcal{V}$, consisting of functions with trace zero on the boundary segment $\partial D_K \cap \partial D$, by

$$\mathrm{tr} = \mathrm{tr}_{D_K} \colon \mathcal{V}_{D_K} \to X := \operatorname{range} \mathrm{tr} \subset H^{1/2}(\partial D_K). \tag{3.3}$$

We refer to [LM72] for details. The space X is equipped with the norm

$$\|w\|_X := \inf\{\|v\|_{H^1(D_K)} : v \in \mathcal{V}_{D_K}, \mathrm{tr}\, v = w\}. \tag{3.4}$$

Hence, the continuity of the trace operator follows regardless of the patch geometry. Additionally, we define the A-harmonic extension tr^{-1} as a continuous right-inverse of tr. Given $w \in X$, it satisfies $\mathrm{tr}\, \mathrm{tr}^{-1} w = w$ and

$$a_{D_K}(\mathrm{tr}^{-1} w, v) = 0, \tag{3.5}$$

for all $v \in H_0^1(D_K)$.

The conormal derivative of $u \in H^1(D_K)$ with $\mathrm{div} A\nabla u \in L^2(D_K)$ is defined as the functional $\gamma_{\partial_n} u = A\nabla u \cdot n \in X'$, where n is the outward normal to D_K, satisfying

$$\langle \gamma_{\partial_n} u, \mathrm{tr}\, v\rangle_{X'\times X} = (\mathrm{div} A\nabla u, v)_{L^2(D_K)} + a(u,v) \tag{3.6}$$

for all $v \in H^1(D_K)$. Using the definition of the conormal derivative, we can know characterize the localization error.

Lemma 3.1.1 (Localization error of SLOD basis functions)**.** *The localization error of the SLOD basis function satisfies*

$$a(\varphi_{K,m}^{\mathrm{slod}} - \hat{\varphi}_{K,m}^{\mathrm{slod}}, v) = -\langle \gamma_{\partial_n} \hat{\varphi}_{K,m}^{\mathrm{slod}}, \mathrm{tr}\, v\rangle_{X'\times X} = (g_{K,m}^{\mathrm{slod}}, \mathrm{tr}^{-1}\mathrm{tr}\, v)_{L^2(D_K)},$$

for all $v \in \mathcal{V}$.

Proof. Let $v \in \mathcal{V}$. From (3.5), and using that $v - \mathrm{tr}^{-1}\mathrm{tr}\, v \in H_0^1(D_K)$ for all $v \in \mathcal{V}$, we obtain that

$$a(\hat{\varphi}_{K,m}^{\mathrm{slod}}, v) = a_{D_K}(\hat{\varphi}_{K,m}^{\mathrm{slod}}, v - \mathrm{tr}^{-1}\mathrm{tr}\, v) = (g_{K,m}^{\mathrm{slod}}, v - \mathrm{tr}^{-1}\mathrm{tr}\, v)_{L^2(D_K)}.$$

The combination with the weak formulation of (3.1), yields the assertion. □

Thus, the localization error is controlled by the quasi-orthogonality of $g_{K,m}^{\mathrm{slod}}$ to

$$Y \coloneqq \mathrm{tr}^{-1} X \subset \mathcal{V}_{D_K}, \tag{3.7}$$

the space of A-harmonic functions in D_K. Equivalently, a small localization error corresponds to a small X'-norm of the conormal derivative of $\hat{\varphi}_{K,m}^{\mathrm{slod}}$. An optimal choice for $g_{K,m}^{\mathrm{slod}}$ follows from the singular value decomposition (SVD) of $\Pi_{H,D_K}|_Y$, which has rank at most $N = \#\mathcal{T}_{H,D_K}$. The SVD is given by

$$\Pi_{H,D_K}|_Y\, v = \sum_{k=1}^{N} \sigma_k (v, w_k)_{H^1(D_K)} g_k,$$

where $\sigma_1 \geq \cdots \geq \sigma_N \geq 0$ are singular values, $g_1, \ldots, g_N$ are $L^2(D_K)$-orthonormal left singular vectors, and $w_1, \ldots, w_N$ are $H^1(D_K)$-orthonormal right singular vectors. The left singular vector g_N corresponding to the smallest singular value σ_N is an optimal choice for $g_{K,m}^{\mathrm{slod}}$ in the sense that

$$g_N \in \operatorname*{arg\,min}_{g\in\mathbb{P}^0(\mathcal{T}_{H,D_K})\colon \|g\|_{L^2(D_K)}=1} \sup_{v\in Y\colon \|v\|_{H^1(D_K)}=1} (g,v)_{L^2(D_K)}. \tag{3.8}$$

Thus, we define

$$\sigma_K = \sigma_K(H,m) \coloneqq \sigma_N = \sup_{v\in Y\colon \|v\|_{H^1(D_K)}=1} (g_N\,,\, v)_{L^2(D_K)}, \tag{3.9}$$

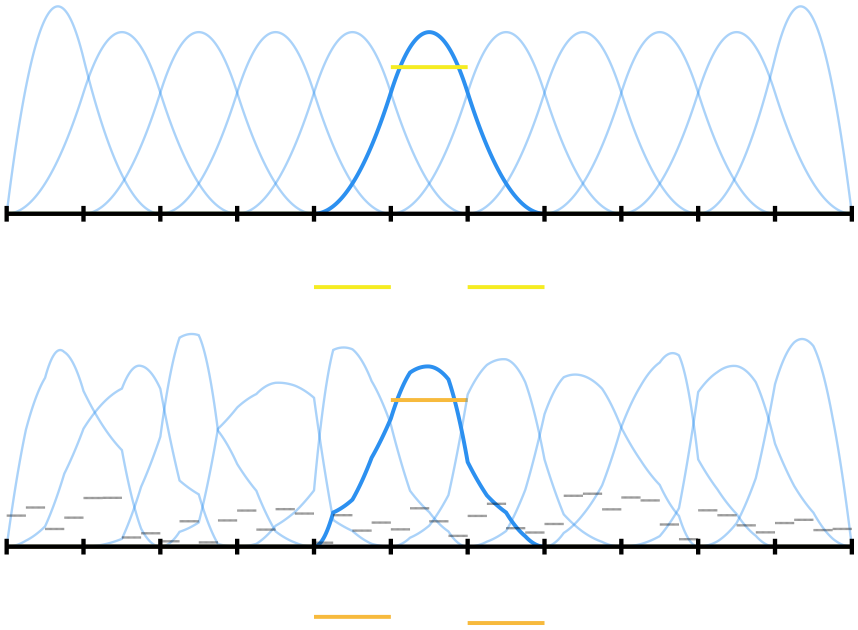

Figure 3.1.: Truly local SLOD basis functions for the model problem (2.3) in one spatial dimension, for $A \equiv 1$ (top) and a piecewise constant coefficient illustrated in gray (bottom). The L^2-normalize right-hand sides corresponding to the central basis functions are depicted in different shades of yellow.

which quantifies the quasi-orthogonality between $g_{K,m}^{\mathrm{slod}}$ and Y. Moreover, it provides a direct estimate of the X'-norm of the conormal derivative of $\hat{\varphi}_{K,m}^{\mathrm{slod}}$, up to a constant depending on the patch geometry.

In one spatial dimension, both the trace space and Y have at most two dimensions. Consequently, for $m = 1$, we can select an L^2-normalized local source term $g_{K,m}^{\mathrm{slod}} \in \mathbb{P}^0(\mathcal{T}_{H,D_K})$ that is L^2-orthogonal to Y, resulting in a local basis. This means that $\varphi_{K,m}^{\mathrm{slod}}$ coincides with its localized counterpart $\hat{\varphi}_{K,m}^{\mathrm{slod}}$. For the Poisson problem, this basis corresponds to quadratic B-splines; see [PT95, Chapter 2]. Figure 3.1 illustrates this case, along with an example of truly local SLOD basis functions in one dimension for a piecewise constant diffusion coefficient A. Whether a truly local basis for $\mathcal{V}_H^a$ exists in higher dimensions remains an open question. Figure 3.2 illustrates localized SLOD basis functions along with their L^2-normalized local source terms for the model problem (2.3) in two dimensions with a constant coefficient $A \equiv 1$.

The potential non-uniqueness of the smallest singular value is evident in the one-dimensional case, where for $m \geq 2$, multiple optimal choices for the local source term exist by a simple counting argument. In higher dimensions, clusters of small singular values may arise for certain patch geometries near the boundary of the domain D. Numerical strategies to ensure stability of $\{g_{K,m}^{\mathrm{slod}} : K \in \mathcal{T}_H\}$

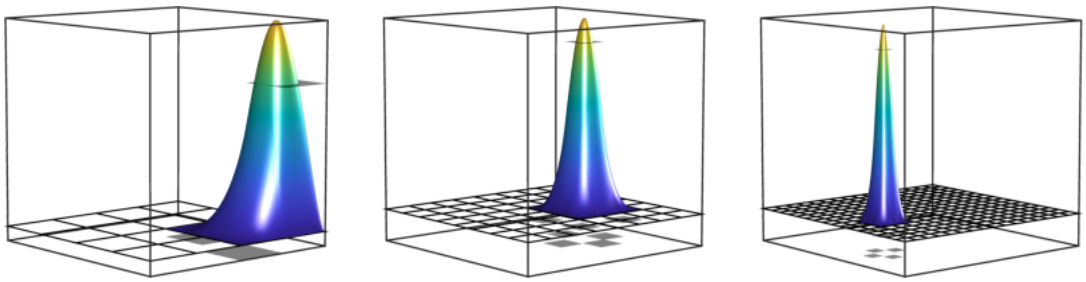

Figure 3.2.: SLOD basis functions for the model problem (2.3) with $A \equiv 1$ in two spatial dimensions, shown for different coarse mesh sizes. The oversampling parameter is set to $m = 1$ and the corresponding L^2-normalized right-hand sides are depicted in gray.

are discussed in Section 3.4. For the subsequent numerical analysis, we impose the following assumption.

Assumption 3.1.2 (Riesz stability)**.** The set $\{g_{K,m}^{\mathrm{slod}} : K \in \mathcal{T}_H\}$ is a Riesz basis of $\mathbb{P}^0(\mathcal{T}_H)$, i.e., there exists a constant $C_{\mathrm{rb}} = C_{\mathrm{rb}}(H, m) > 0$ such that for all possible choices of $(c_K)_{K\in\mathcal{T}_H}$ it holds that

$$C_{\mathrm{rb}}^{-1} \sum_{K\in\mathcal{T}_H} c_K^2 \leq \Big\| \sum_{K\in\mathcal{T}_H} c_K g_{K,m}^{\mathrm{slod}} \Big\|_{L^2(D)}^2,$$

where C_{rb} depends polynomially on H^{-1} and m.

3.2. Practical multiscale method

Applying the SLOD localization strategy, we define a localized version of the prototypical problem-specific ansatz space (2.4) as the span of the localized basis functions $\hat{\varphi}_{K,m}^{\mathrm{slod}}$ from (3.2). Given a fixed oversampling parameter m, we set

$$\mathcal{V}_{H,m}^{\mathrm{slod}} := \mathrm{span}\{\hat{\varphi}_{K,m}^{\mathrm{slod}} : K \in \mathcal{T}_H\} \subset \mathcal{V}.$$

The localized method then seeks the Galerkin approximation $u_{H,m}^{\mathrm{slod}} \in \mathcal{V}_{H,m}^{\mathrm{slod}}$ satisfying

$$a(u_{H,m}^{\mathrm{slod}}, v) = (f\,,\, v)_{L^2(D)}, \tag{3.10}$$

for all $v \in \mathcal{V}_{H,m}^{\mathrm{slod}}$.

Alternatively, we define a collocation-type SLOD approximation $u_{H,m}^{\mathrm{slod,c}} \in \mathcal{V}_{H,m}^{\mathrm{slod}}$ as

$$u_{H,m}^{\mathrm{slod,c}} = \sum_{K\in\mathcal{T}_H} c_K\, \hat{\varphi}_{K,m}^{\mathrm{slod}}, \tag{3.11}$$

where the coefficients $(c_K)_{K\in\mathcal{T}_H}$ correspond to the expansion of $\Pi_H f$ in terms of the local source terms $g_{K,m}^{\mathrm{slod}}$. This approach resembles collocation, as it ensures

that the PDE holds on average within each element of $\mathcal{T}_H$, up to localization errors. Like the Galerkin method, it requires solving only a coarse-scale linear system, but with the advantage that assembling the system matrix depends solely on the coarse functions $g_{K,m}^{\mathrm{slod}}$, avoiding the computation of inner products between the SLOD basis functions $\hat{\varphi}_{K,m}^{\mathrm{slod}}$. However, this reduction in computational cost comes at the expense of losing the best-approximation property of the Galerkin solution in $\mathcal{V}_{H,m}^{\mathrm{slod}}$ with respect to the energy norm.

In the following, we derive an a posteriori error estimate for the two methods introduced above, closely following [HP22b, Theorem 6.1]. The estimate involves the quantity

$$\sigma = \sigma(H,m) \coloneqq \max_{K\in\mathcal{T}_H} \sigma_K(H,m), \tag{3.12}$$

which represents the maximal localization error over the coarse mesh; see (3.9). It also depends on the Riesz stability constant C_{rb} from Theorem 3.1.2, which measures the linear independence of the local source terms $\{g_{K,m}^{\mathrm{slod}} : K \in \mathcal{T}_H\}$. Both constants can be computed a posteriori, as outlined in Section 3.5.1. Furthermore, we provide a priori upper bounds for σ in the next section.

Theorem 3.2.1 (A posteriori error estimate)**.** *Let $\{g_{K,m}^{\mathrm{slod}} : K \in \mathcal{T}_H\}$ be stable in the sense of Assumption 3.1.2. Then, for any $f \in H^s(D)$ with $s \in \{0,1\}$, the SLOD Galerkin and collocation-type approximations $u_{H,m}^{\mathrm{slod}}$ and $u_{H,m}^{\mathrm{slod,c}}$, defined in* (3.10) *and* (3.11)*, respectively, satisfy*

$$\begin{aligned}
\|u - u_{H,m}^{\mathrm{slod}}\|_a &\leq \|u - u_{H,m}^{\mathrm{slod,c}}\|_a \\
&\lesssim H\|f - \Pi_H f\|_{L^2(D)} + C_{\mathrm{rb}}^{1/2}\, m^{d/2}\sigma\|f\|_{L^2(D)} \\
&\lesssim \left(H^{1+s} + C_{\mathrm{rb}}^{1/2}\, m^{d/2}\sigma\right)\|f\|_{H^s(D)}
\end{aligned}$$

with $C_{\mathrm{rb}}(H,m)$ from Assumption 3.1.2. This result implies that both approximations converge to the exact solution at an algebraic rate in H, up to an additional error due to localization.

Proof. The first inequality follows directly from Céa's Lemma (see, e.g., [Cia78]), which implies that the SLOD Galerkin approximation $u_{H,m}^{\mathrm{slod}}$ is the best approximation of u in $\mathcal{V}_{H,m}^{\mathrm{slod}}$ with respect to the energy norm. Using the triangle inequality, we obtain

$$\|u - u_{H,m}^{\mathrm{slod}}\|_a \leq \|u - u_{H,m}^{\mathrm{slod,c}}\|_a \leq \|u - \tilde{u}\|_a + \|\tilde{u} - u_{H,m}^{\mathrm{slod,c}}\|_a.$$

The particular choice $\tilde{u} = \mathcal{A}^{-1}\Pi_H f$, yields for the first term

$$\begin{aligned}
\|u - \tilde{u}\|_a^2 &= (f - \Pi_H f, u - \tilde{u})_{L^2(D)} \\
&\lesssim H\|f - \Pi_H f\|_{L^2(D)}\|u - \tilde{u}\|_a \\
&\lesssim H^{1+s}\|f\|_{H^s(D)}\|u - \tilde{u}\|_a,
\end{aligned} \tag{3.13}$$

where we used the approximation property (2.7) of Π_H for the last two inequalities.

For the second term, we use the fact that the prototypical method (2.5) is exact for $\Pi_H f$. This allows us to represent $\tilde{u}$ in terms of the ideal basis functions $\varphi_{K,m}^{\mathrm{slod}}$, namely

$$\tilde{u} = \sum_{K \in \mathcal{T}_H} c_K \, \varphi_{K,m}^{\mathrm{slod}},$$

where $(c_K)_{K \in \mathcal{T}_H}$ denote the coefficients of the expansion of $\Pi_H f$ in terms of the basis functions $g_{K,m}^{\mathrm{slod}}$. Defining $e \coloneqq \tilde{u} - u_{H,m}^{\mathrm{slod,c}}$, we obtain

$$\|e\|_a^2 = \sum_{K \in \mathcal{T}_H} c_K \, a(\varphi_{K,m}^{\mathrm{slod}} - \hat{\varphi}_{K,m}^{\mathrm{slod}}, e). \tag{3.14}$$

Using Theorem 3.1.1 and the definitions of $\sigma_K(H,m)$ and $\sigma(H,m)$ in (3.9) and (3.12), respectively, we get

$$\begin{aligned} a(\varphi_{K,m}^{\mathrm{slod}} - \hat{\varphi}_{K,m}^{\mathrm{slod}}, e) &= (g_{K,m}^{\mathrm{slod}}, \mathrm{tr}^{-1}\mathrm{tr}\, e)_{L^2(\mathsf{N}^m(K))} \\ &\leq \sigma \, \|\mathrm{tr}^{-1}\mathrm{tr}\, e\|_{H^1(\mathsf{N}^m(K))} \\ &\lesssim \sigma \, \|e\|_{H^1(\mathsf{N}^m(K))}, \end{aligned} \tag{3.15}$$

where tr and tr^{-1} denote the trace and A-harmonic extension operators on $\mathsf{N}^m(K)$, respectively. To prove the last inequality, we decompose $\mathrm{tr}^{-1}\mathrm{tr}\, e = e + e_0$, where $e_0 \in H_0^1(\mathsf{N}^m(K))$ satisfies $a(e_0, v) = -a(e, v)$ for all $v \in H_0^1(\mathsf{N}^m(K))$. The inequality then follows from

$$\begin{aligned} \|e_0\|_{H^1(\mathsf{N}^m(K))}^2 &= \|\nabla e_0\|_{L^2(\mathsf{N}^m(K))}^2 + \|e_0\|_{L^2(\mathsf{N}^m(K))}^2 \\ &\lesssim a(e_0, e_0) \leq |a(e, e_0)| \\ &\lesssim \|e\|_{H^1(\mathsf{N}^m(K))} \|e_0\|_{H^1(\mathsf{N}^m(K))}, \end{aligned}$$

where we employed Friedrichs' inequality and that D is of unit size.

Combining (3.14), (3.15), the discrete Cauchy–Schwarz inequality, Theorem 3.1.2, and the finite overlap of the patches, we derive

$$\begin{aligned} \|e\|_a^2 &= \sum_{K \in \mathcal{T}_H} c_K \, a(\varphi_{K,m}^{\mathrm{slod}} - \hat{\varphi}_{K,m}^{\mathrm{slod}}, e) \\ &\lesssim \sigma \sum_{K \in \mathcal{T}_H} c_K \|e\|_{H^1(\mathsf{N}^m(K))} \\ &\leq \sigma \sqrt{\sum_{K \in \mathcal{T}_H} c_K^2} \sqrt{\sum_{K \in \mathcal{T}_H} \|e\|_{H^1(\mathsf{N}^m(K))}^2} \\ &\lesssim C_{\mathrm{rb}}^{1/2} \, m^{d/2} \sigma \, \|e\|_a \|f\|_{L^2(D)}, \end{aligned}$$

where we used Friedrichs' inequality in the last step. In combination with (3.13), the assertion directly follows.

□

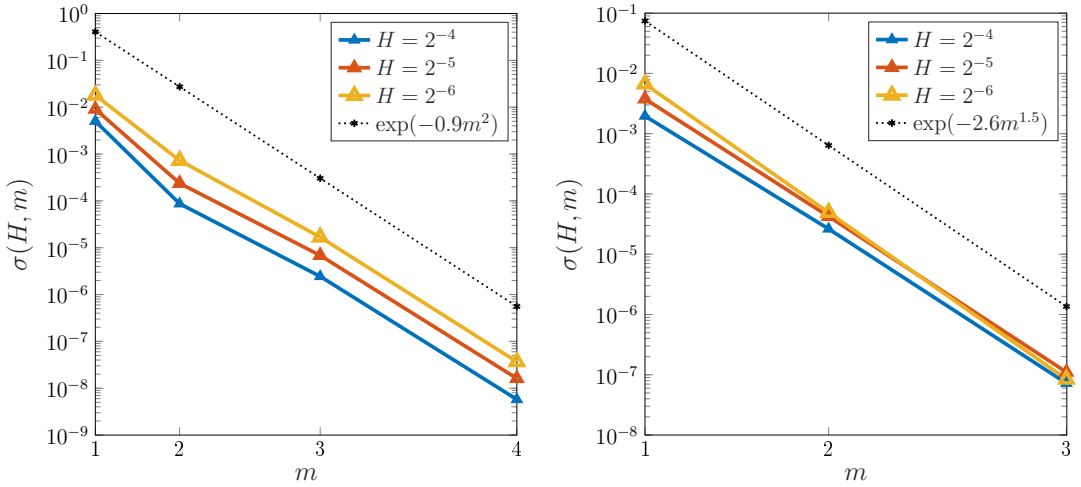

Figure 3.3.: Decay of $\sigma(H, m)$ as a function of the oversampling parameter m for different values of the coarse mesh size H for the 2d experiment (left) and the 3d experiment (right).

3.3. Decay of localization error

In the following, we analyze the behavior of the parameter σ defined in (3.12) and, consequently, the decay of the localization error in the SLOD method. Numerical experiments demonstrate that σ exhibits super-exponential decay as m increases. Specifically, the results suggest that

$$\sigma(H, m) \leq C_d(H, m) \exp\Big(- Cm^{\frac{d}{d-1}}\Big),$$

where $C_d(H, m) > 0$ depends at most polynomially on H^{-1} and m, while $C > 0$ is independent of both H and m. This behavior is illustrated in Figure 3.3, which displays results for a two-dimensional example with a piecewise constant diffusion coefficient and a three-dimensional case with a periodic coefficient. In both settings, the diffusion coefficient A assumes values between $\alpha = 0.1$ and $\beta = 1$. Further details on the numerical setup can be found in Section 3.6.

However, no existing theoretical results confirm this observed behavior. For the elliptic model problem in (2.3) with constant coefficient $A \equiv 1$, we rigorously establish the super-exponential decay of σ using Steklov eigenfunctions, thereby closing this theoretical gap. Additionally, we present the pessimistic exponential decay bound for σ derived in [HP22b], which applies to more general settings and can be proven using LOD techniques.

3.3.1. Super-exponential decay

We consider the elliptic model problem (2.3) with a constant coefficient $A \equiv 1$ and prove that the localization error of the SLOD decays super-exponentially. This result is obtained by leveraging the super-exponential decay of Steklov

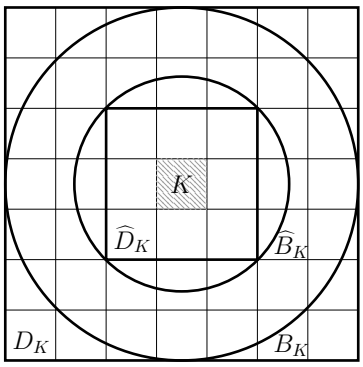

Figure 3.4.: Visualization of the patches $D_K = \mathsf{N}^m(K)$ and $\widehat{D}_K = \mathsf{N}^{\lfloor m/2 \rfloor}(K)$, along with the balls B_K and $\widehat{B}_K$ centered around K. The oversampling parameter is chosen as $m = 3$.

eigenfunctions on a d-dimensional ball and builds on the arguments from [HP22b, Section 7], where a mathematical motivation for the super-exponential decay of σ is provided beyond the case $A \equiv 1$. Since the SLOD basis functions are truly local in the one-dimensional case, we restrict our analysis to $d \in \{2, 3\}$.

To this end, we fix an oversampling parameter $m \in \mathbb{N}$ and extend the domain $D = (0, 1)^d$ by m-layers of coarse mesh elements. For each $K \in \mathcal{T}_H$ we define the extended patch $D_K \coloneqq \mathsf{N}^m_{\text{ext}}(K)$, where the patches are constructed as described in (2.14), but using an extension of the coarse mesh $\mathcal{T}_H$ to the extended domain D^m. On these patches, we solve the SLOD patch problems (3.2) with $A \equiv 1$, ignoring global Dirichlet boundary conditions. By correcting the resulting functions $\hat{\varphi}^{\text{ext}}_{K,m}$ corresponding to boundary patches, we obtain the SLOD basis functions, which satisfies global Dirichlet boundary conditions on the original domain D. In Section 3.4.3 this ansatz is explained in more detail. In the following, we derive the super-exponential decay of the localization error $\sigma^{\text{ext}}(H, m)$ corresponding to the SLOD functions $\hat{\varphi}^{\text{ext}}_{K,m}$ on the extended domain. The super-exponential decay of the SLOD basis follows as a consequence, since σ is bounded by (a multiple of) σ^{ext}.

For each $K \in \mathcal{T}_H$, we define B_K as the largest ball centered around K that is fully contained within the extended patch $D_K = \mathsf{N}^m_{\text{ext}}(K)$. Additionally, we introduce $\widehat{D}_K \coloneqq \mathsf{N}^{\lfloor m/2 \rfloor}_{\text{ext}}(K)$, with $\mathsf{N}^0_{\text{ext}}(K) \coloneqq K$, and define $\widehat{B}_K$ as the smallest ball centered around K such that the relation $\widehat{D}_K \subset \widehat{B}_K$ holds. An illustration using a Cartesian mesh is provided in Figure 3.4. While the following analysis is not limited to Cartesian meshes, the relation $\widehat{D}_K \subset \widehat{B}_K \subsetneq B_K \subset D_K$ must hold for all $K \in \mathcal{T}_H$.

The Steklov eigenfunctions on the ball B_K are solutions to the eigenvalue problem

$$\Delta \psi = 0 \text{ in } B_K, \quad \text{with} \quad \nabla \psi \cdot n = \lambda \psi \text{ on } \partial B_K,$$

where n denotes the outer normal unit vector. The eigenvalues $\{\lambda_j : j \in \mathbb{N}_0\}$ are non-negative and ordered such that $0 = \lambda_0 \leq \lambda_1 \leq \dots$. The corresponding

eigenfunctions form a basis of the Steklov spectrum and, in this specific case, are given explicitly (see also [SAK23, Example 2.1]) by

$$\psi_j(r,\theta_1,\dots,\theta_{d-1}) = r_B^{-\frac{d-1}{2}} \left(\frac{r}{r_B}\right)^{C_{\mathrm{se}}(j,d)} H_j(\theta_1,\dots,\theta_{d-1}), \tag{3.16}$$

where the exponent $C_{\mathrm{se}}(j,d)$ is defined as

$$C_{\mathrm{se}}(j,d) = \begin{cases} \lfloor j/2 \rfloor, & \text{if } d=2, \\ \lfloor \sqrt{j} \rfloor, & \text{if } d=3. \end{cases}$$

Here, r_B is the radius of B_K and $\{H_j(\theta_1,\dots,\theta_{d-1}) : j \in \mathbb{N}_0\}$ is an arbitrary orthonormal basis (with increasing degree in j) of the vector space of all d-dimensional spherical harmonics. We refer to [AH12, Section 2.1] for further details on spherical harmonics.

The next lemma states the super-exponential decay of the Steklov eigenfunctions in the interior of the Ball B_K.

Lemma 3.3.1 (Decay of Steklov eigenfunctions)**.** *The Steklov eigenfunctions $\{\psi_j : j \in \mathbb{N}_0\}$ defined on the ball $B_K \subset \mathsf{N}^m_{\mathrm{ext}}(K)$ satisfy for all $j \in \mathbb{N}_0$ and all $K \in \mathcal{T}_H$ that*

$$\|\psi_j\|_{L^2(\mathsf{N}^{\lfloor m/2 \rfloor}_{\mathrm{ext}}(K))} \leq C_{\mathrm{sd}}(H,m)\exp(-Cj^{\frac{1}{d-1}}),$$

where $C>0$ is a constant independent of H and m, while C_{sd} depends polynomially on H and m.

Proof. For a fixed $K \in \mathcal{T}_H$, we consider the smallest ball $\widehat{B}_K$ of radius $r_{\widehat{B}}$ centered at K, such that $\widehat{D}_K \subset \widehat{B}_K \subsetneq B_K$. Using (2.6) and the fact that $\{H_j : j \in \mathbb{N}_0\}$ form an orthonormal basis with respect to $L^2(\mathbb{S}^{d-1})$, we obtain, for the case $d=2$, that

$$\begin{aligned} \|\psi_j\|_{L^2(\mathsf{N}^{\lfloor m/2 \rfloor}_{\mathrm{ext}}(K))} \leq \|\psi_j\|_{L^2(\widehat{B}_K)} &= \left(\int_0^{r_{\widehat{B}}} \int_{\mathbb{S}^1} |\psi_j(r,\theta)|^2 r \,\mathrm{d}S\mathrm{d}r\right)^{1/2} \\ &\leq \left(\int_0^{r_{\widehat{B}}} \left(\frac{r}{r_B}\right)^j \mathrm{d}r\right)^{1/2} \\ &\leq C_{\mathrm{sd}}(H,m)\exp(-Cj), \end{aligned}$$

with $C = -\log\left(\sqrt{\frac{r_{\widehat{B}}}{r_B}}\right) > 0$. The case $d=3$ follows analogously, where the constant C satisfies $C = -\log\left(\frac{r_{\widehat{B}}}{r_B}\right) > 0$. □

Let Y_B denote the space of A-harmonic functions on B_K. The Steklov spectrum spanned by the $L^2(\partial B_K)$-orthonormal and a-orthogonal set of Steklov eigenfunctions $\{\psi_j : j \in \mathbb{N}_0\}$ is a complete subspace of Y_B, see [Auc05]. Arbitrary functions in Y_B can be expanded as

$$v = \sum_{j=0}^{\infty} (u,\psi_j)_{L^2(\partial B_K)} \psi_j, \tag{3.17}$$

where the sum converges in the $H^1(B_K)$-norm.

The next theorem, following the arguments of [HP22b, Theorem 7.3], states the super-exponential decay of σ^{ext} for the considered case $A \equiv 1$. For the proof, we use the fact that every function in the space Y of A-harmonic functions on D_K is, restricted to B_K, also an element of the space Y_B.

Theorem 3.3.2 (Super-exponential decay)**.** *Let $M \in \mathbb{N}$ be the largest number such that, for all $m \leq M$, no extended patch includes the whole domain D. Then, there exist a constant $C > 0$ independent of H and m, such that, for all $m \leq M$, the localization error of the SLOD functions on the extended patches satisfies*

$$\sigma^{\mathrm{ext}}(H,m) \lesssim C_{\mathrm{sd}}(H,m)\, m^{d-\frac{d}{d-1}} \exp(-Cm^{\frac{d}{d-1}})$$

with $C_{\mathrm{sd}}(H,m)$ from Theorem 3.3.1.

Proof. For $K \in \mathcal{T}_H$ we define $\widehat{D}_K \coloneqq \mathsf{N}_{\mathrm{ext}}^{\lfloor m/2 \rfloor}(K)$ and let $\widehat{N} = \#\mathcal{T}_{H,\widehat{D}_K}$ denote the number of elements in $\widehat{D}_K$. Let $\{\psi_j : j \in \mathbb{N}_0\}$ be the set of Steklov eigenfunctions, as defined in (3.16), on $B_K \subset D_K$.

We estimate σ_K^{ext} by choosing a (possibly) suboptimal local source term for the SLOD basis function. This choice is the L^2-normalized $g \in \mathbb{P}^0(\mathcal{T}_{H,\widehat{D}_K})$ such that it is L^2-orthogonal to the first $\widehat{N}-1$ Steklov eigenfunctions, i.e.,

$$g \perp_{L^2(\widehat{D}_K)} \{\psi_0, \dots, \psi_{\widehat{N}-2}\}.$$

If this choice is non-unique, one may require L^2-orthogonality to even more Steklov eigenfunctions until g is uniquely determined. This choice may not coincide with the optimal one in (3.8) but suffices to derive an upper bound for σ_K^{ext}.

By (3.17) and Theorem 3.3.1, this choice yields, for all $v \in Y_B$, that

$$\begin{aligned}
(g\,,\,v)_{L^2(\widehat{D}_K)} &= \Big(g\,,\,\sum_{j=\widehat{N}-1}^{\infty} (v\,,\,\psi_j)_{L^2(\partial B_K)}\psi_j\Big)_{L^2(\widehat{D}_K)} \\
&\leq \Big\|\sum_{j=\widehat{N}-1}^{\infty} (v\,,\,\psi_j)_{L^2(\partial B_K)}\psi_j\Big\|_{L^2(\widehat{D}_K)} \\
&\leq \|v\|_{L^2(\partial B_K)} \sum_{j=\widehat{N}-1}^{\infty} \|\psi_j\|_{L^2(\widehat{D}_K)} \\
&\lesssim C_{\mathrm{sd}}(H,m)\,\|v\|_{H^1(B_K)} \sum_{j=\widehat{N}-1}^{\infty} \exp(-Cj^{\frac{1}{d-1}}),
\end{aligned}$$

where we used the trace inequality (see, e.g., [BS08, Chapter 1.6]) in the last step. Rewriting the last sum as a (generalized) geometric sum with the base $\theta \coloneqq \exp(-C) < 1$ and estimating the sum against an integral, we get

$$\sum_{j=\widehat{N}-1}^{\infty} \exp(-Cj^{\frac{1}{d-1}}) = \sum_{j=\widehat{N}-1}^{\infty} \theta^{j^{\frac{1}{d-1}}} \lesssim \int_{\widehat{N}-1}^{\infty} \theta^{x^{\frac{1}{d-1}}}\,\mathrm{d}x.$$

Using a change of variables and integrating by parts such that the term x^{d-2} in the product $x^{d-2}\theta^x$ also vanishes for the case $d = 3$ yields

$$\int_{\widehat{N}-1}^{\infty} \theta^{x^{\frac{1}{d-1}}} \,\mathrm{d}x = (d-1) \int_{(\widehat{N}-1)^{\frac{1}{d-1}}}^{\infty} x^{d-2}\theta^x \,\mathrm{d}x \lesssim (\widehat{N}-1)^{\frac{d-2}{d-1}} \theta^{(\widehat{N}-1)^{\frac{1}{d-1}}}.$$

With the definition of θ and $\widehat{N} - 1 \approx m^d$, we obtain

$$\begin{aligned}
\sigma_K^{\mathrm{ext}}(H,m) &\leq \sup_{v \in Y\colon \|v\|_{H^1(D_K)}=1} |(g\,,\,v)_{L^2(\widehat{D}_K)}| \\
&\leq \sup_{v \in Y_B\colon \|v\|_{H^1(B_K)}=1} |(g\,,\,v)_{L^2(\widehat{D}_K)}| \\
&\lesssim C_{\mathrm{sd}}(H,m)\, m^{d-\frac{d}{d-1}} \exp(-C' m^{\frac{d}{d-1}}),
\end{aligned}$$

introducing $C' > 0$ that only differs from C by a constant factor. Taking the maximum over all mesh elements $K \in \mathcal{T}_H$ yields the assertion □

Remark 3.3.3 (Theorem 3.3.2 in 1d)**.** Interpreting $\frac{d}{d-1}$ as infinity for $d = 1$, Theorem 3.3.2 is consistent with the earlier result that the SLOD basis is local in one dimension.

3.3.2. Pessimistic exponential decay

A rigorous bound on the exponential decay of σ was first established in [HP22b]. In what follows, we outline the key ideas of the proof. To this end, we analyze a non-stabilized version of the local LOD basis functions introduced in Section 2.6, which are defined by

$$\hat{\varphi}_{K,m}^{\mathrm{lod}} \coloneqq (1 - \widehat{\mathcal{C}}_m) b_K \tag{3.18}$$

for $K \in \mathcal{T}_H$. Each such LOD basis function possesses locally in $D_K = \mathsf{N}^m(K)$ a $\mathcal{T}_H$-piecewise constant right-hand side $g_{K,m}^{\mathrm{lod}} \in \mathbb{P}^0(\mathcal{T}_{H,D_K})$. This result was shown in [HP22b, Lemma A.2] using the saddle-point formulation from [OS19, Mai20], which seeks $\hat{\varphi}_{K,m}^{\mathrm{lod}}$ along with a Lagrange multiplier $\lambda \in \mathbb{P}^0(\mathcal{T}_{H,D_K})$ such that

$$\begin{pmatrix} \mathcal{A}_{D_K} & \mathcal{P}_{D_K}^T \\ \mathcal{P}_{D_K} & 0 \end{pmatrix} \begin{pmatrix} \hat{\varphi}_{K,m}^{\mathrm{lod}} \\ \lambda \end{pmatrix} = \begin{pmatrix} 0 \\ \mathbb{1}_K \end{pmatrix},$$

where the patch-local operators are defined as follows. The restricted solution operator $\mathcal{A}_{D_K}\colon H_0^1(D_K) \to H^{-1}(D_K)$ is given by $\mathcal{A}_{D_K} u = a_{D_K}(u, \cdot)$, where a_{D_K} denotes the restriction of a to D_K. The operator $\mathcal{P}_{D_K}\colon H_0^1(D_K) \to \mathbb{P}^0(\mathcal{T}_{H,D_K})$ is defined by $\mathcal{P}_{D_K} u = \Pi_{H,D_K} u$. Its transpose, $\mathcal{P}_{D_K}^T\colon \mathbb{P}^0(\mathcal{T}_{H,D_K}) \to H^{-1}(D_K)$, satisfies

$$\langle \mathcal{P}_{D_K}^T p, v \rangle_{H^{-1}(D_K)\times H_0^1(D_K)} \coloneqq (p\,,\,v)_{L^2(D_K)}$$

for all $p \in \mathbb{P}^0(\mathcal{T}_{H,D_K})$ and $v \in H_0^1(D_K)$. The LOD right-hand sides are then given by

$$g_{K,m}^{\mathrm{lod}} = \mathcal{S}_{D_K}^{-1} \mathbb{1}_K \in \mathbb{P}^0(\mathcal{T}_{H,D_K})$$

where $\mathcal{S}_{D_K}$ denotes the Schur complement, defined as

$$\mathcal{S}_{D_K} \colon \mathbb{P}^0(\mathcal{T}_{H,D_K}) \to \mathbb{P}^0(\mathcal{T}_{H,D_K}), \quad p \mapsto (\mathcal{P}_{D_K} \mathcal{A}_{D_K}^{-1} \mathcal{P}_{D_K}^T) p.$$

The following lemma, established in [HP22b, Lemma 6.4], proves the exponential decay of σ using this choice of basis. Moreover, it confirms that the corresponding local source terms $g_{K,m}^{\mathrm{lod}}$ satisfy Theorem 3.1.2. A full proof of the lemma is given in [HP22b, Appendix A], and a more detailed discussion can be found in [Hau23, Theorem 5.4.3].

Lemma 3.3.4 (Stability and exponential decay of classical LOD basis)**.** *Suppose that m is chosen at least proportional to $|\log H|$. Then, the local source terms of the LOD basis functions satisfy*

$$H^4 \sum_{K \in \mathcal{T}_H} c_K^2 \lesssim \Big\| \sum_{K \in \mathcal{T}_H} c_K \frac{g_{K,m}^{\mathrm{lod}}}{\|g_{K,m}^{\mathrm{lod}}\|_{L^2(D)}} \Big\|_{L^2(D)}^2 \tag{3.19}$$

for all $(c_K)_{K \in \mathcal{T}_H}$. Furthermore, inserting the normalized versions of $g_{K,m}^{\mathrm{lod}}$ in (3.9) *yields*

$$\sigma(H, m) \lesssim H^{-1} \exp(-Cm) \tag{3.20}$$

with $C > 0$ independent of H and m.

Combining Theorem 3.2.1 and Theorem 3.3.4 yields an a priori error estimate with convergence rates matching those of the classical LOD based on piecewise constant finite elements; see Section 2.6.

3.4. Stable basis computation

An efficient implementation of the SLOD basis functions requires that the set $\{g_{K,m}^{\mathrm{slod}} : K \in \mathcal{T}_H\}$ is a stable basis of $\mathbb{P}^0(\mathcal{T}_H)$ in the sense of Theorem 3.1.2 and that the local source terms can be computed with minimal communication between the patches. As first discussed in [HP22b, Appendix B], stability issues can arise whenever there are nested groups of patches near the boundary of the domain D. Figure 3.5 illustrates such a scenario, considering $D = (0,1)^2$ with a Cartesian mesh and $m = 2$. The patches corresponding to the elements at positions[1] $(1,1)$, $(1,2)$, and $(2,1)$ are all contained within the patch of element $(2,2)$. This nesting results in an unfavorable selection of basis functions, as the functions associated with the smallest singular values across the different patches are nearly identical. In particular, they almost coincide with the basis function expected for the patch of element $(1,1)$, leading to instability in the basis representation. In the following subsections, we explore various solutions to

[1] Here, the position is a vector in $\{1, \dots, H^{-1}\}^2$ where the first and second components determine the location in the x- and y-directions, respectively. The numbering is chosen such that $(1,1)$ corresponds to the bottom-left element.

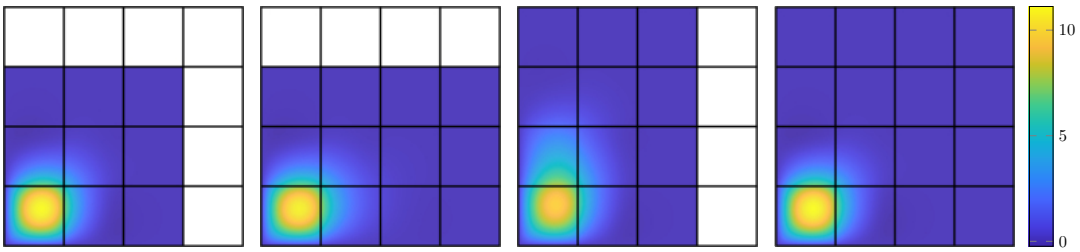

Figure 3.5.: Solutions of the patch problems (3.2) for right-hand sides corresponding to the smallest singular values on the patches associated with elements $(1,1)$, $(2,1)$, $(1,2)$ and $(2,2)$ (from left to right), for the case $A \equiv 1$.

these stability issue and present efficient methods for computing the SLOD basis functions. For simplicity, we henceforward consider D to be the unit hypercube in d dimensions with $d \geq 2$ discretized using a Cartesian mesh $\mathcal{T}_H$.

As outlined in Section 3.1, there are two general approaches to compute the SLOD basis functions: minimizing the conormal derivative of the basis function or selecting a local source term corresponding to the smallest singular value of the operator $\Pi_{H,D_K}|_Y$. Practical implementation details for both methods are provided in Section 3.5. While the stabilization technique in Section 3.4.4 focuses on minimizing the conormal derivative, all other stabilization approaches are formulated in the SVD setting but can be adapted to conormal derivative minimization. A comparison of the different approaches based on numerical experiments is provided in Section 3.6.

3.4.1. Representative patches

One possible approach to addressing the stability issues in the example above is to consider only the largest patch, in this case, the patch of element $(2,2)$, and to compute the functions corresponding to the four smallest singular values. A visualization of these functions is provided in Figure 3.6. The resulting functions are linearly independent and form a basis for a space that includes the functions naturally expected for the four elements.

This stabilization procedure was introduced in [HP22b, Appendix B] and can be easily generalized. The key idea is to identify groups of patches for which the basis functions are computed simultaneously. To achieve this, all patches $\mathsf{N}^m(K)$ where K has a distance of at least m layers to the boundary of D are treated independently. In contrast, patches where K has exactly a distance of $m-1$ layers to ∂D serve as representatives for corresponding groups of patches. Every remaining patch $\mathsf{N}^m(K)$, meaning those where K has a distance of less than $m-1$ layers to ∂D, is uniquely assigned to that group, where the representative patch of the group is a superset of the patch $\mathsf{N}^m(K)$. The basis functions are then computed on the representative patch of each group and correspond to the

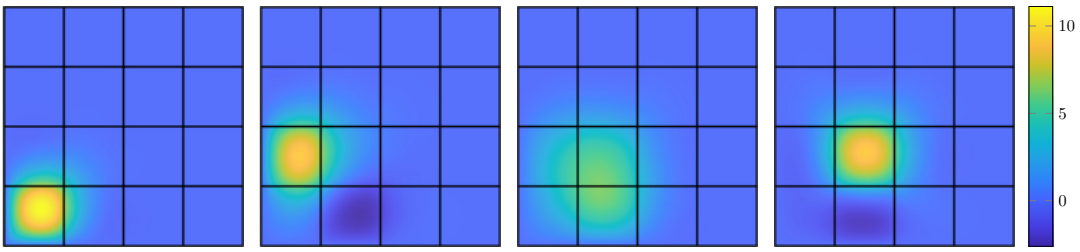

Figure 3.6.: Functions obtained by solving the patch problem (3.2) for the right-hand sides corresponding to the four smallest singular values on the patch of element $(2, 2)$, for the case $A \equiv 1$.

functions associated with the k smallest singular values, where k denotes the number of patches within the group.

3.4.2. Weighted L^2-norm

The here presented stabilization technique achieves stability by an additional optimization step and was first introduced in [BFP24, Section 7] for convection-dominated diffusion problems. Instead of choosing $g_{K,m}^{\text{slod}}$ as in (3.8), we consider local source terms associated with a certain range of the lowermost singular value.

Given the singular values $\sigma_1 \geq \sigma_2 \geq \cdots \geq \sigma_N \geq 0$ associated with the patch D_K, we consider all indices $1 \leq i \leq N$ such that

$$\frac{\sigma_i}{\sigma_1} \leq \max\left\{\left(\frac{\sigma_N}{\sigma_1}\right)^{1/p}, 10^{-10}\right\}$$

and denote the resulting set of indices by $\mathcal{I}$. Each index in the set $\mathcal{I}$ corresponds to a potential candidate for a local source term. For the choice $p = 1$ only the smallest singular value is considered. Since this optimization problem is meaningful whenever multiple functions are considered, we restrict ourselves to the choices $p > 1$.

Among these candidate functions, we choose the one that minimizes a weighted $L^2(D_K)$-norm under the unit mass constraint. The weighted $L^2(D_K)$-norm is defined using a piecewise constant weighting function that is zero in the central element T and grows polynomially as the distance from the center increases. This enforces a concentration of mass in the reference element K, resulting in linearly independent local source terms $\{g_{K,m}^{\text{slod}} : K \in \mathcal{T}_H\}$ in practice. More specifically, we introduce the distance function $\text{dist}(K, T)$ between the elements $K, T \in \mathcal{T}_H$ as

$$\text{dist}(K, T) \coloneqq H^{-1}|M_K - M_T| \in \mathbb{N}^d,$$

where $M_K, M_T \in \mathbb{R}^d$ are the midpoints of the elements K and T, respectively. The weighting function is then defined for each element $T \in \mathcal{T}_{H,D_K}$ as

$$w_K(T) \coloneqq \left|\text{dist}(K, T)\right|_\infty^r$$

64	64	64	64	64
64	1	1	1	64
64	1	0	1	64
64	1	1	1	64
64	64	64	64	64

Figure 3.7.: Piecewise constant weighting function w_K for an interior element $K \in \mathcal{T}_H$ with $m = 2$ in two spatial dimensions.

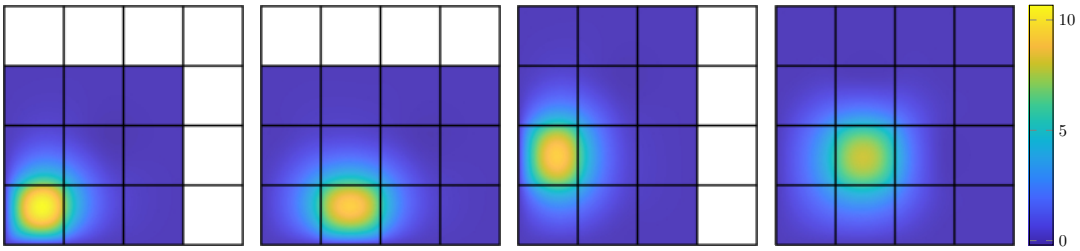

Figure 3.8.: Functions obtained by solving the patch problem (3.2) for the right-hand sides corresponding to small singular values, while minimizing a weighted L^2-norm on the associated patch, for the case $A \equiv 1$.

for a parameter $r \geq 1$, where $|\cdot|_\infty$ denotes the infinity norm on $\mathbb{R}^d$. Figure 3.7 provides an illustration of this weighting function in two spatial dimensions for the choice $r = 6$.

Figure 3.8 shows the SLOD basis functions computed using this weighting function and $p = 2$, corresponding to the problematic functions in the exemplary case. Notably, this stabilization technique yields basis functions that align with intuitive expectations. However, the optimal choice of the parameters r and p may vary depending on the specific problem.

3.4.3. Domain extension

In this section, we introduce a new stabilization technique for handling homogeneous Dirichlet boundary conditions. Unlike the approach proposed in Section 3.4.1, this method produces basis functions that align with intuitive expectations and is applicable to the stochastic setting discussed in Chapter 5. Furthermore, the new stabilization technique does not introduce any additional parameters. For simplicity, we focus on the computation of a stable SLOD basis using Cartesian meshes, where we denote the side length of the elements by H instead of their diameter. However, the proposed stabilization technique can be extended to other types of meshes.

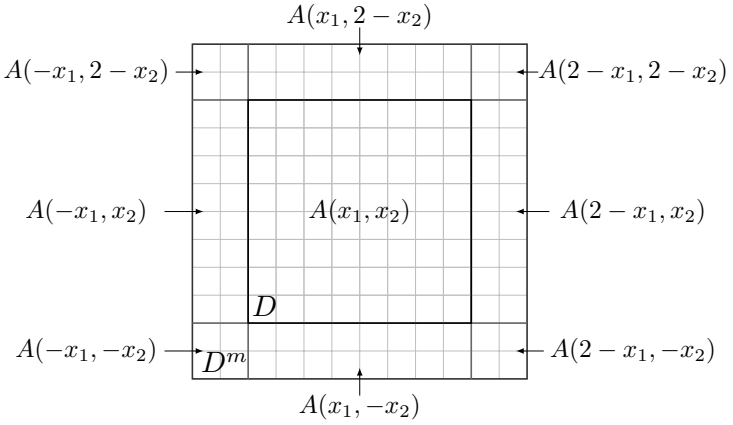

Figure 3.9.: Extension of the domain $D = (0, 1)^2$ with the extended coarse mesh $\mathcal{T}_H^m$ and $m = 2$. Additionally the extension of the diffusion coefficient A is displayed.

We extend the domain $D = (0, 1)^d$ by m-layers of coarse mesh elements. More precisely, we have

$$D^m := \{x \in \mathbb{R}^d : \ |x - D|_\infty < mH\}.$$

By $\mathcal{T}_H^m$ we denote the extension of the Cartesian coarse mesh $\mathcal{T}_H$ to D^m. The diffusion coefficient A is extended to the overlapping domain $\overline{D^m}$ by 'mirroring' it at the boundaries of D. See Figure 3.9 for an illustration in two dimensions. For each $K \in \mathcal{T}_H$ we define the patch $D_K^{\text{ext}} := \mathsf{N}_{\text{ext}}^m(K)$, where the patches are constructed as described in (2.14), but using the extended coarse mesh $\mathcal{T}_H^m$ instead of $\mathcal{T}_H$. The SLOD patch problems (3.2) are then solved for all patches with right-hand sides corresponding to the respectively smallest singular value, ignoring global Dirichlet boundary conditions but including the extended diffusion coefficient. We denote the resulting functions by $\hat{\varphi}_{K,m}^{\text{ext}} \in H_0^1(D_K^{\text{ext}})$ and the corresponding local source terms by $g_{K,m}^{\text{ext}} \in \mathbb{P}^0(\mathcal{T}_{H,D_K^{\text{ext}}}^m)$.

To account for the global Dirichlet boundary conditions, we need to correct all functions corresponding to boundary patches. Therefore, we consider $K \in \mathcal{T}_H$ with $\partial D \cap \operatorname{int}(D_K^{\text{ext}}) \neq \emptyset$ and extend $\hat{\varphi}^{\text{ext}} = \hat{\varphi}_{K,m}^{\text{ext}}$ by zero to $\mathbb{R}^d$. The corrected localized SLOD basis function $\hat{\varphi}_{K,m}^{\text{slod}} \in H_0^1(D)$ for $d = 2$, which satisfies global Dirichlet boundary conditions, is defined as

$$\begin{aligned}\hat{\varphi}_{K,m}^{\text{slod}}(x_1, x_2) = \hat{\varphi}^{\text{ext}}(x_1, x_2) &- \hat{\varphi}^{\text{ext}}(-x_1, x_2) - \hat{\varphi}^{\text{ext}}(x_1, -x_2) \\ &- \hat{\varphi}^{\text{ext}}(2 - x_1, x_2) - \hat{\varphi}^{\text{ext}}(x_1, 2 - x_2) + \hat{\varphi}^{\text{ext}}(-x_1, -x_2) \\ &+ \hat{\varphi}^{\text{ext}}(2 - x_1, -x_2) + \hat{\varphi}^{\text{ext}}(2 - x_1, 2 - x_2) + \hat{\varphi}^{\text{ext}}(-x_1, 2 - x_2),\end{aligned}$$

for $(x_1, x_2) \in D$. The corresponding local source term $g_{K,m}^{\text{slod}} \in \mathbb{P}^0(\mathcal{T}_H)$ can be computed by correcting $g_{K,m}^{\text{ext}}$ in the same way. In three dimensions, the corrected

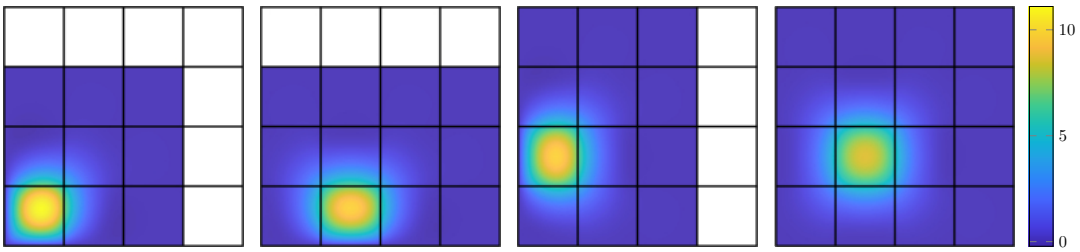

Figure 3.10.: SLOD basis functions obtained by correcting the solutions of the patch problems (3.2) for right-hand sides corresponding to the smallest singular values on the extended patches associated with the elements $(1,1),(2,1),(1,2)$ and $(2,2)$ (from left to right), for the case $A \equiv 1$.

SLOD basis function and its corresponding local source term can be obtained analogously by taking into account all correction terms corresponding to faces, edges, and corners of the domain D. The global Dirichlet boundary conditions of $\hat{\varphi}_{K,m}^{\mathrm{slod}}$ can be easily checked by noting that $\hat{\varphi}_{K,m}^{\mathrm{ext}}(x) = 0$ for all $x \in \mathbb{R}^d \setminus D^m$. The smallness of the conormal derivative of $\hat{\varphi}_{K,m}^{\mathrm{slod}}$ on $\partial D_K \setminus \partial D$ follows from the smallness of the conormal derivative of $\hat{\varphi}_{K,m}^{\mathrm{ext}}$ on $\partial D_K^{\mathrm{ext}}$.

Figure 3.10 illustrates the SLOD basis functions for the problematic patches associated with elements in the left corner of $D = (0,1)^2$, computed using this new stabilization technique.

3.4.4. Correction of LOD functions

In the following, we present a stabilization technique which leads to a practically stable SLOD basis by correcting local LOD basis functions. This stabilization technique was proposed in [GMPZ24, Section 3] in the context of the hierarchical SLOD.

Given $D_K \coloneqq \mathsf{N}^m(K)$, the local LOD basis function $\hat{\varphi}_{K,m}^{\mathrm{lod}}$ defined in (3.18) satisfies

$$\hat{\varphi}_{K,m}^{\mathrm{lod}} = \mathcal{A}_{D_K}^{-1} g_{K,m}^{\mathrm{lod}}, \quad \text{with} \quad g_{K,m}^{\mathrm{lod}} = \mathcal{S}_{D_K}^{-1} \mathbb{1}_K, \tag{3.21}$$

where the patch-local operators $\mathcal{A}_{D_K}$ and $\mathcal{S}_{D_K}$ are defined in Section 3.3.2. For $T \in \mathcal{T}_{H,D_K} \setminus \{K\}$, we define

$$\hat{\varphi}_{T,m}^{(K)} := \mathcal{A}_{D_K}^{-1} g_{T,m}, \quad \text{with} \quad g_{T,m} = \mathcal{S}_{D_K}^{-1} \mathbb{1}_T. \tag{3.22}$$

By construction, the SLOD basis function is in the span of these LOD functions and can be computed using a linear combination of them. More precisely, we define

$$\hat{\varphi}_{K,m}^{\mathrm{slod}} := \hat{\varphi}_{K,m}^{\mathrm{lod}} + \sum_{T \in \mathcal{T}_{H,D_K} \setminus \{K\}} c_T \hat{\varphi}_{T,m}^{(K)}, \tag{3.23}$$

where the coefficients $(c_T)_{T \in \mathcal{T}_{H,D_K} \setminus \{K\}}$ are chosen such that $\hat{\varphi}_{K,m}^{\mathrm{slod}}$ has minimal conormal derivative.

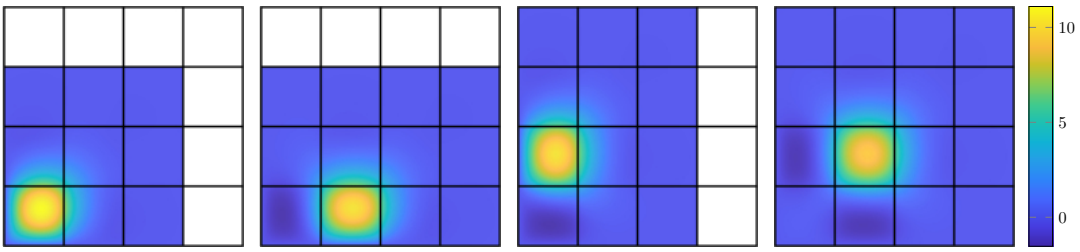

Figure 3.11.: SLOD basis functions obtained by correcting LOD basis functions for patches associated with the elements $(1,1),(2,1),(1,2)$ and $(2,2)$ (from left to right), for the case $A \equiv 1$.

Note that, to guarantee stability of the SLOD basis, we additionally choose the coefficients such that

$$\|z_K^{-1}\Pi_H\hat{\varphi}_{K,m}^{\mathrm{slod}} - \mathbb{1}_K\|_{L^\infty(D)} \leq \delta_s, \tag{3.24}$$

with

$$z_K = \fint_K \hat{\varphi}_{K,m}^{\mathrm{slod}}\,\mathrm{d}x$$

and $\delta_s \geq 0$ small. Condition (3.24) impels the support of $\hat{\varphi}_{K,m}^{\mathrm{slod}}$ to be reasonably concentrated around K, ensuring the linear independency and stability of the SLOD basis. In contrast, the stability of the local LOD basis is given a priori, as the LOD functions satisfy the Lagrange property

$$\Pi_H\hat{\varphi}_{K,m}^{\mathrm{lod}} = \mathbb{1}_K, \quad \text{and} \quad \Pi_H\hat{\varphi}_{T,m}^{(K)} = \mathbb{1}_T$$

for $T \in \mathcal{T}_{H,D_K} \setminus \{K\}$. Hence, setting $\delta_s = 0$ recovers the Riesz-stable standard LOD basis. However, this choice yields basis functions that exhibit only exponential decay. To retain stability while achieving super-localization, we aim to select δ_s small enough to ensure Riesz stability, yet large enough to preserve the desired super-exponential decay properties. In practice, we have found that choosing $\delta_s = 0.5$ strikes a good balance and satisfies these two requirements.

An illustration of the stabilized SLOD basis functions, computed using this technique and associated with the problematic patches from the introductory example, is given in Figure 3.11.

3.5. Practical implementation

In this section, we discuss the practical implementation of computing the SLOD basis functions introduced in Section 3.1 with the two possible approaches mentioned there. The first approach involves random sampling to approximate the space Y from (3.7), followed by computing the SVD of the operator $\Pi_{H,D_K}|_Y$, while the second approach is based on minimizing the conormal derivative of the local SLOD basis functions.

For a given oversampling parameter m, we consider a (possibly extended) patch D_K and denote the number of coarse elements within this patch by $N \coloneqq \#\mathcal{T}_{H,D_K}$. In practical implementations, all local infinite-dimensional problems arising in the derivation of the basis functions must be approximated in a finite-dimensional setting. To achieve this, we discretize the domain using the $\mathbb{P}^1$-finite element method on a fine mesh $\mathcal{T}_{h,D_K}$, obtained by uniformly refining $\mathcal{T}_{H,D_K}$. We denote the nodes of the fine mesh $\mathcal{T}_{h,D_K}$ by z_j for $j \in \mathcal{N} \coloneqq \{1,\dots,n\}$. The corresponding hat functions, denoted by $\{\Lambda_j : j \in \mathcal{N}\}$, satisfy the nodal property $\Lambda_j(z_i) = \delta_{ij}$ for all $i,j \in \mathcal{N}$.

3.5.1. Random sampling and Singular Value Decomposition

The random sampling approach to approximate the space Y that we explain in the following was introduced in [HP22b, Appendix B] and is similar to [BS18, CLLW20]. Approximating the space Y by harmonic polynomials [BL11] or Steklov eigenfunctions [MSD22] would also be possible.

We assume that the nodes of the fine mesh $\mathcal{T}_h$ are numbered in a manner that enables the decomposition of the index set $\mathcal{N}$ into three disjoint subsets, corresponding to $\Gamma_1 \coloneqq \partial D_K \setminus \partial D$, $\Gamma_2 \coloneqq \partial D_K \cap \partial D$, and the interior $D_K \setminus \partial D_K$. Specifically, we write $\mathcal{N} = \mathcal{N}_1 \cup \mathcal{N}_2 \cup \mathcal{N}_0$, with

$$\mathcal{N}_1 \coloneqq \{1,\dots,n_1\}, \quad \mathcal{N}_2 \coloneqq \{n_1+1,\dots,n_1+n_2\}, \quad \mathcal{N}_0 \coloneqq \{n_1+n_2+1,\dots,n\}.$$

To approximate the space Y from (3.7), we compute discrete A-harmonic extensions of random sample boundary data prescribed on Γ_1. Denoting with $M \in \mathbb{N}$ the number of samples, we define $\mathbf{S}_1 \in \mathbb{R}^{n_1 \times M}$ to be the matrix having sample vectors of length n_1 as columns. The entries in each column correspond to the nodal values of sample finite element boundary functions on Γ_1. We use independent and uniformly distributed nodal values within the interval $[-1,1]$. For the numerical experiments in Section 3.6, we set the number of samples to $M = 5N$.

Let $\mathbf{S}^{n\times M}$ be the matrix whose columns are coordinate vectors of the discrete A-harmonic extensions of the columns of $\mathbf{S}_1$. We can calculate the matrix $\mathbf{S}$ as

$$\mathbf{S} = \begin{pmatrix} \mathbf{S}_1 \\ \mathbf{0} \\ \mathbf{S}_0 \end{pmatrix} \quad \text{with} \quad \mathbf{S}_0 \coloneqq -\mathbf{A}_0^{-1}\mathbf{A}_1\mathbf{S}_1,$$

$\mathbf{A}_0 \coloneqq (a_{D_K}(\Lambda_j,\Lambda_i))_{i,j\in\mathcal{N}_0}$, $\mathbf{A}_1 \coloneqq (a_{D_K}(\Lambda_j,\Lambda_i))_{i\in\mathcal{N}_1,j\in\mathcal{N}_0}$ and $\mathbf{0}$ denoting the $n_2 \times M$ zero matrix. Next, the SVD of the matrix $\mathbf{X} \coloneqq \mathbf{P}(\mathbf{S}^T\mathbf{K}\mathbf{S})^{-1/2} \in \mathbb{R}^{N\times M}$ is computed, where $\mathbf{P} \in \mathbb{R}^{N\times M}$ is the column-wise application of the L^2-projection onto the characteristic functions $\{\mathbb{1}_T : T \in \mathcal{T}_{H,D_K}\}$ to $\mathbf{S}$. The matrix $\mathbf{K} \in \mathbb{R}^{n\times n}$ is the sum of the stiffness matrix and the mass matrix with respect to $\mathcal{T}_{h,D_K}$. It shall be noted that the term $(\mathbf{S}^T\mathbf{K}\mathbf{S})^{-1/2}$ guarantees that the right singular

vectors of $\mathbf{X}$ represent a set of $H^1(D_K)$-orthonormal functions. However, in practice it seems reasonable to apply the SVD directly to $\mathbf{P}$, i.e., $(\mathbf{S}^T\mathbf{K}\mathbf{S})^{-1/2}$ does not need to be computed, since numerical experiments show no noticeable difference in the choice of basis and the resulting errors.

The reduced SVD of $\mathbf{X}$ reads

$$\mathbf{X} = \mathbf{G}\mathbf{\Sigma}\mathbf{H}^T$$

with $\mathbf{G} \in \mathbb{R}^{N\times N}$, $\mathbf{\Sigma} \in \mathbb{R}^{N\times M}$, and $\mathbf{H} \in \mathbb{R}^{M\times M}$. The last column of $\mathbf{G}$ is the coordinate vector with respect to the basis $\{\mathbb{1}_T : T \in \mathcal{T}_{H,D_K}\}$ of the local source term corresponding to the smallest singular value of the (possibly extended) patch D_K.

Depending on the stabilization technique, different modifications may be necessary. The last several columns of $\mathbf{G}$ may be considered in the case of representative patches from Section 3.4.1. Alternatively, an additional optimization step may be introduced by incorporating a weighted L^2-norm (Section 3.4.2). In the case of domain extension, the correction from Section 3.4.3 must be applied for boundary patches. Once the right-hand side $g^{\mathrm{slod}}_{K,m}$ is determined, the fully discretized counterpart of $\hat{\varphi}^{\mathrm{slod}}_{K,m}$ can be obtained by solving a discretized version of (3.2).

Remark 3.5.1 (Computation of the Riesz stability constant)**.** Given the local source terms $\{g^{\mathrm{slod}}_{K_i,m} : i = 1, \dots, \#\mathcal{T}_H\}$, the Riesz stability constant C_{rb} appearing in Theorem 3.2.1 equals the reciprocal of the smallest eigenvalue of the matrix $\mathbf{R} \in \mathbb{R}^{\#\mathcal{T}_H\times\#\mathcal{T}_H}$ with entries given by $\mathbf{R}_{ij} = (g^{\mathrm{slod}}_{K_i,m}, g^{\mathrm{slod}}_{K_j,m})_{L^2(D)}$.

3.5.2. Minimization of the conormal derivative

Given an oversampling parameter $m \in \mathbb{N}$, we consider an element $K \in \mathcal{T}_H$ and its corresponding (possibly extended) patch D_K. To compute the SLOD basis function $\hat{\varphi}^{\mathrm{slod}}_{K,m}$, we first determine the local responses of the solution operator. Specifically, for each element $T \in \mathcal{T}_{H,D_K}$ within the patch, we compute the response of the restricted solution operator $\mathcal{A}^{-1}_{D_K}$ to its characteristic function $\mathbb{1}_T$. By construction, $\hat{\varphi}^{\mathrm{slod}}_{K,m}$ lies in the span of these local responses $\mathcal{A}^{-1}_{D_K}\mathbb{1}_T$.

Next, we select $\hat{\varphi}^{\mathrm{slod}}_{K,m}$ from this low-dimensional space by minimizing the conormal derivatives under a unit mass constraint. This minimization is realized by computing the smallest generalized eigenvalue of the symmetric, positive (semi-) definite matrices

$$\Big(\int_{\partial D_K} \gamma_{\partial_n}(\mathcal{A}^{-1}_{D_K}\mathbb{1}_\tau)\gamma_{\partial_n}(\mathcal{A}^{-1}_{D_K}\mathbb{1}_T)\,\mathrm{d}s\Big)_{\tau,T\in\mathcal{T}_{H,D_K}}$$

and

$$\Big(\int_{D_K} (\mathcal{A}^{-1}_{D_K}\mathbb{1}_\tau)(\mathcal{A}^{-1}_{D_K}\mathbb{1}_T)\,\mathrm{d}x\Big)_{\tau,T\in\mathcal{T}_{H,D_K}}.$$

The corresponding generalized eigenvector provides the coordinate representation of a possible right-hand side for $\hat{\varphi}_{K,m}^{\mathrm{slod}}$ with respect to the basis $\{\mathbb{1}_T : T \in \mathcal{T}_H\}$.

As in the previous subsection, depending on the stabilization technique, multiple smallest eigenvalues may be considered, or for boundary patches, the additional correction must be applied. Once the right-hand side $g_{K,m}^{\mathrm{slod}}$ is determined, its coordinate vector provides the coefficients for expanding $\hat{\varphi}_{K,m}^{\mathrm{slod}}$ in terms of the local responses of the restricted solution operator. Alternatively, the fully discretized counterpart $\hat{\varphi}_{K,m}^{\mathrm{slod}}$ can be computed by solving a discretized version of (3.2).

For the stabilization technique introduced in Section 3.4.4 which corrects LOD basis functions, we choose an alternative approach to minimize the conormal derivative. Let $\Gamma := \partial D_K \setminus \partial D$, and denote by $I_\Gamma := \{i \in \mathbb{N} : z_i \in \Gamma\}$ the set of indices corresponding to the nodes of the fine mesh $\mathcal{T}_h$ that lie on Γ. We then define the matrix

$$\mathbf{B} \coloneqq \Big(a(\mathcal{A}_{D_K}^{-1}\mathbb{1}_T, \Lambda_i) - (\mathbb{1}_T, \Lambda_i)_{L^2(D_T)}\Big)_{T\in\mathcal{T}_{H,D_K}, i\in I_\Gamma}.$$

For the right-hand side $g_{K,m}^{\mathrm{lod}}$ of the local LOD basis function given in (3.21), we denote by $\mathbf{g}_K$ its coefficient vector with respect to the basis $\{\mathbb{1}_T : T \in \mathcal{T}_{H,D_K}\}$. Similarly, we collect the coefficient vectors of the local source terms $g_{T,m}$ for $T \in \mathcal{T}_{H,D_K} \setminus \{K\}$, given in (3.22), as columns of the matrix $\mathbf{G} \in \mathbb{R}^{N\times(N-1)}$. The coefficient vector $\mathbf{c} = (c_T)_{T\in\mathcal{T}_{H,D_K}\setminus\{K\}}$ which minimizes the conormal derivative in (3.23) is obtained as the least-squares solution of

$$\mathbf{BGc} = -\mathbf{Bg}_K,$$

i.e.,

$$\mathbf{c} = -\Big((\mathbf{BG})^T\mathbf{BG}\Big)^{-1}(\mathbf{BG})^T\mathbf{Bg}_K. \tag{3.25}$$

To additionally satisfy the stability condition in (3.24), we express $(\mathbf{BG})^T\mathbf{BG}$ in terms of its SVD, given by

$$(\mathbf{BG})^T\mathbf{BG} = \sum_{i=1}^{r} \sigma_i u_i v_i^T,$$

where σ_i is the i-th singular value, with $\sigma_1 \geq \ldots \geq \sigma_r$, and u_i and v_i are the corresponding left and right singular vectors, respectively. Here, r denotes the rank of $(\mathbf{BG})^T\mathbf{BG}$. The coefficient vector ensuring a stable SLOD basis in (3.23) is then computed as

$$\mathbf{c} = -\Big(\sum_{i=1}^{r_K} \sigma_i^{-1} v_i u_i^T\Big)(\mathbf{BG})^T\mathbf{Bg}_K, \tag{3.26}$$

where $r_K \leq r$ is chosen iteratively to guarantee that condition (3.24) is satisfied.

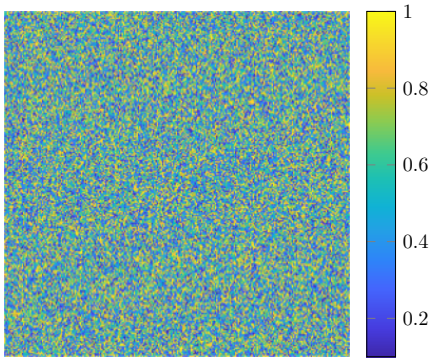

Figure 3.12.: Visualization of the piecewise constant coefficient A on a mesh with mesh size 2^{-8}. The lower bound of the coefficient is set to $\alpha = 0.1$.

3.6. Numerical experiments

In this section, we present numerical experiments assessing the different variants of computing the SLOD basis functions introduced in this chapter. We consider the domain $D = (0,1)^d$, with $d \in \{2,3\}$, discretized by uniform Cartesian meshes $\mathcal{T}_H$, where the mesh size H denotes the side length of the elements rather than their diameter. For the practical implementation, all infinite-dimensional problems arising in the local patch computations are approximated by their $\mathbb{P}^1$-finite element discretizations on a fine mesh with mesh size 2^{-10}, obtained through successive uniform refinements of the coarse mesh $\mathcal{T}_{H,D_K}$ on the respective patches. Based on the extensive numerical analysis of fine-scale discretizations for the classical LOD, cf. [MP20, AHP21], we expect that the theoretical results remain valid in the present setting.

For the numerical experiments in two dimensions, we choose A to be a realization of a coefficient that is piecewise constant with respect to a mesh of size 2^{-8}. The element-wise values are independent and identically distributed random variables taking values between α and $\beta = 1$, with different choices of α. An illustration of the coefficient with $\alpha = 0.1$ is provided in Figure 3.12. As right-hand side, we consider

$$f(x_1, x_2) = 2\pi^2 \sin(x_1) \sin(x_2).$$

Figure 3.13 presents the relative energy errors of the fully discrete numerical approximations obtained by the Galerkin method (3.10), measured with respect to the reference solution u_h. The reference solution is computed using the $\mathbb{P}^1$-FEM on the global fine mesh with mesh size $h = 2^{-10}$. The figure compares the approximation errors for the different practical variants of the SLOD method introduced in this chapter. Specifically, it displays the errors resulting from the various stabilization techniques discussed in Section 3.4, applied using either the approach based on random sampling and the SVD or the approach based on the minimization of the conormal derivative. Note that we only consider combinations of H and m for which all patch-problems (3.2) are non-global.

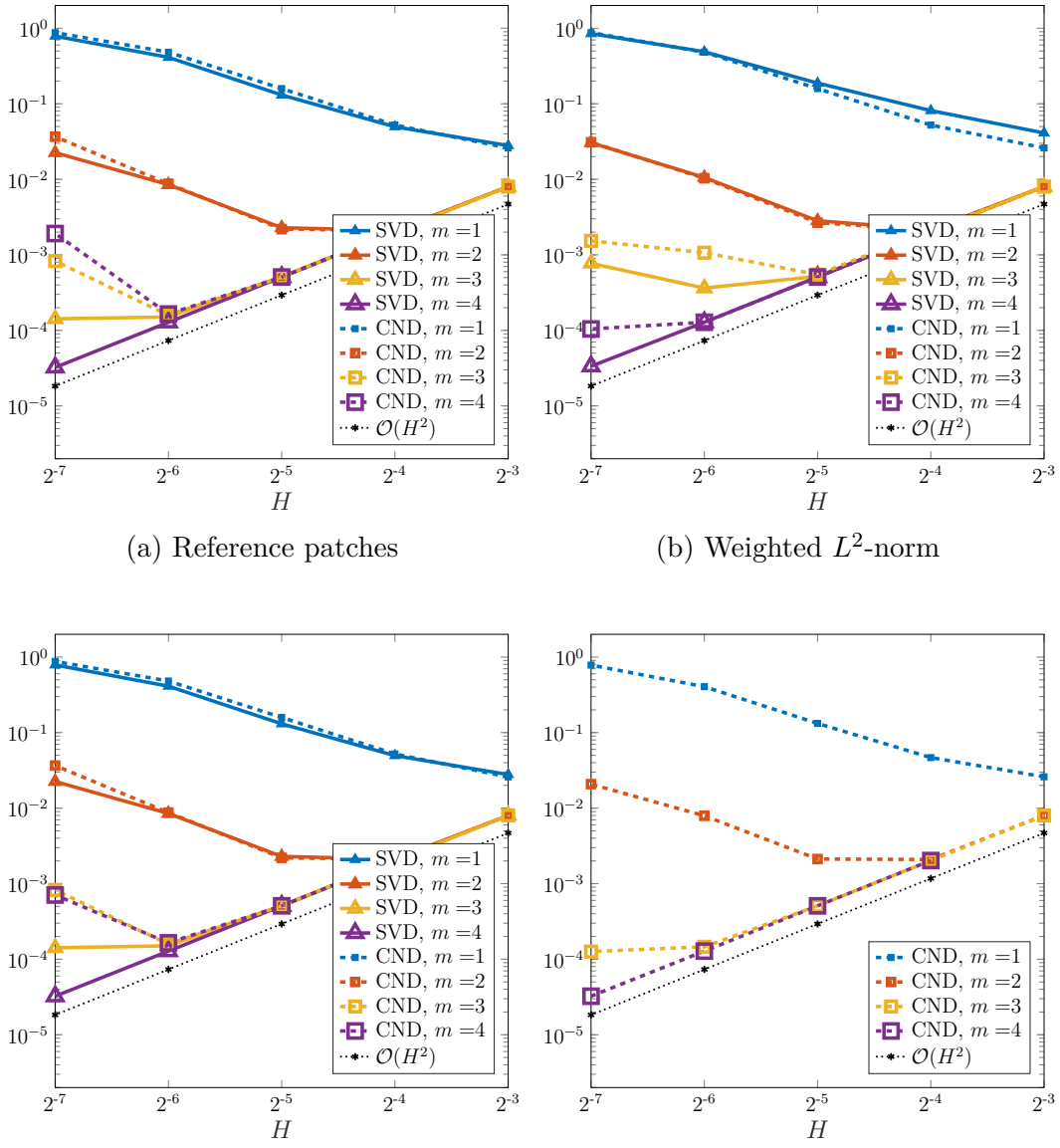

(a) Reference patches

(b) Weighted L^2-norm

(c) Domain extension

(d) Correction of LOD functions

Figure 3.13.: Relative energy errors of the SLOD Galerkin approximations as a function of the coarse mesh size H for the different stabilization techniques described in Section 3.4. The errors are shown for the two approaches, based on either the Singular Value Decomposition (SVD) or the minimization of the conormal derivative (CND), in the 2d setting for various oversampling parameters m. The lower bound on the diffusion coefficient is set to $\alpha = 0.1$.

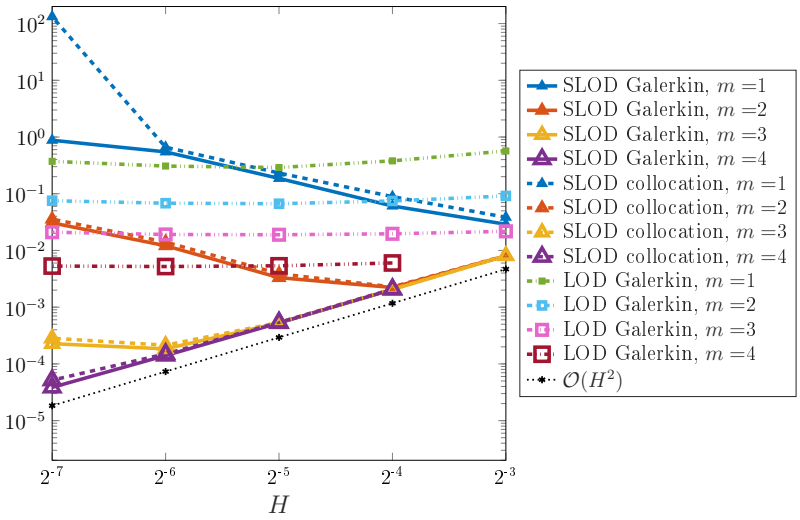

Figure 3.14.: Relative energy errors of the SLOD Galerkin, the SLOD collocation and the LOD Galerkin approximations as a function of the coarse mesh size H for the 2d experiment. The lower bound on the diffusion coefficient is set to $\alpha = 10^{-5}$.

All investigated variants exhibit similar relative energy errors, with the expected convergence rate for a smooth right-hand side $f \in H^1(D)$. In general, the approach of minimizing the conormal derivative shows slightly larger errors for small coarse mesh sizes compared to the SVD-based approach. Among the stabilization techniques, the weighted L^2-norm approach (see Section 3.4.2) exhibits the largest deviations, being highly sensitive to parameter choices; in this case, we used $r = 6$ and $p = 2$. No significant differences are observed between the SVD-based method combined with stabilization techniques using reference patches (see Section 3.4.1) or domain extension (see Section 3.4.3), and the correction of the LOD basis functions via conormal derivative minimization (see Section 3.4.4).

Figure 3.14 illustrates the relative energy errors of the SLOD Galerkin approximation defined (3.10) and the SLOD collocation approximation from (3.11), both computed using the SVD combined with the domain extension stabilization technique, for a high-contrast piecewise constant coefficient A with $\alpha = 10^{-5}$. Compared to the low-contrast case, the differences in the errors are marginal. For reference, the relative energy errors of the stabilized LOD approximation from Section 2.6 are also shown.

In Figure 3.15, the relative energy errors of the two SLOD approximations with respect to the online computing time are illustrated for oversampling parameters $m = 3, 4$. The markers indicate the considered coarse mesh sizes, ranging from 2^{-4} to 2^{-7}. The online computing time includes only the representation of the approximate solution and the right-hand side in terms of the basis functions, as well as the solution of the coarse-scale linear system. When also accounting

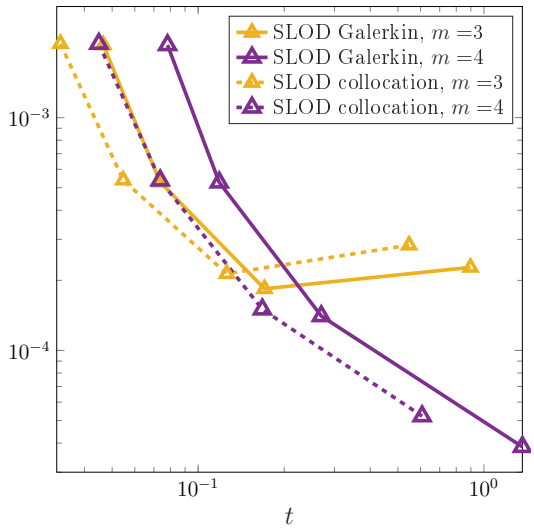

Figure 3.15.: Relative energy errors of the SLOD Galerkin and the SLOD collocation approximations as a function of the online computing time t in second for the 2d experiment. The lower bound on the diffusion coefficient is set to $\alpha = 10^{-5}$. The markers indicate the considered coarse mesh sizes, ranging from 2^{-4} to 2^{-7}.

for the time required to assemble the system matrix, the computational savings of the collocation variant compared to the Galerkin method become even more apparent.

Remark 3.6.1 (Numerical setup in 3d)**.** For the three-dimensional experiment in Section 3.3, we use the simpler periodic coefficient

$$A(x_1, x_2, x_3) = \frac{1}{10} + \frac{9}{20}\Big(\prod_{i=1}^{3} \sin(2^8 \pi x_i) + 1\Big)$$

and a fine mesh with mesh size 2^{-8} for the $\mathbb{P}^1$-finite element discretization. The periodicity of the diffusion coefficient on a mesh with mesh size 2^{-7} is exploited in the numerical implementation to reduce computational costs: the basis functions need to be computed only for $\mathcal{O}(m^d)$ reference patches. The remaining basis functions can then be obtained by translation; see [GP15].

4. Hierarchical Super-Localized Orthogonal Decomposition

The SLOD introduced in the previous chapter provides a powerful framework for constructing highly localized basis functions. In this chapter, we extend these ideas by introducing a hierarchical variant of the SLOD, referred to as HSLOD, which enables the efficient computation of approximate solutions to the elliptic model problem.

The HSLOD is built upon a sequence of nested meshes and their associated function spaces. The hierarchical basis spans the finest-level function space while incorporating basis functions from all coarser levels. This hierarchical structure is particularly advantageous in the presence of multiple scales within the diffusion matrix A. A key property of the hierarchical method is that its basis functions are (quasi-)orthogonal across levels with respect to the bilinear form a. As a result, the associated stiffness matrix exhibits a block-diagonal structure, where each diagonal block corresponds to a different level of the hierarchy. This decomposition effectively decouples contributions from different levels, allowing them to be computed independently and in parallel. Moreover, given a SLOD or HSLOD approximate solution, it provides the flexibility to incrementally refine the approximation by adding additional discretization levels, thereby improving accuracy in a systematic manner.

The construction of hierarchical basis functions that induce an orthogonal multiresolution decomposition of the solution operator was first introduced in the framework of gamblets, see [Owh15, Owh17, OS19]. This concept was later connected with the LOD framework in [FP20], leading to the development of a hierarchical LOD. A stabilized multiresolution LOD, which is not limited to elliptic problems, was subsequently introduced in [HP22a]. We combine the concepts of hierarchical a-orthogonal basis functions with the localization strategy of the SLOD, leading to super-exponentially decaying basis functions in practice, as the size of the patches on which the functions are defined is increased. The proposed HSLOD method achieves greater sparsity in the compressed representation of the solution space compared to gamblets-based and hierarchical LOD methods. This leads to a higher sparsity in the block-diagonal stiffness matrix, reducing both memory consumption and computational cost while maintaining accuracy.

Furthermore, we use the new stabilization strategy introduced in Section 3.4.4 for computing SLOD basis functions. The hierarchical basis is then constructed as a linear combination of these stabilized functions. This approach ensures that

the hierarchical stiffness matrix remains well-conditioned (up to the contrast). Beyond improving numerical robustness, the stabilization also enhances the overall quality and efficiency of the method, enabling the reliable treatment of challenging scenarios, such as high-contrast channels in the diffusion coefficient.

While the presentation has been slightly adapted for consistency and completeness, the content of this chapter is primarily based on the preprint article

[GMPZ24] J. C. Garay, H. Mohr, D. Peterseim, and C. Zimmer. Hierarchical Super-Localized Orthogonal Decomposition Method. *arXiv preprint 2407.18671*, 2024.

4.1. Construction of the hierarchical basis

In this section, we focus on the construction of an a-orthogonal hierarchical basis corresponding to the elliptic model problem (2.3). Therefore, we need to adapt some definitions to the multilevel setting. Let $\mathcal{T}_1$ denote a Cartesian mesh of D with mesh size H_1, and consider a sequence of successively refined meshes $\{\mathcal{T}_\ell\}_{\ell\in\{1,\dots,L\}}$, where $L \in \mathbb{N}$ and each refinement satisfies $H_{\ell+1} = H_\ell/2$ for $\ell \leq L-1$. We denote by $\Pi_\ell : L^2(D) \to \mathbb{P}^0(\mathcal{T}_\ell)$ the L^2-orthogonal projection onto the space of piecewise constant functions with respect to the mesh $\mathcal{T}_\ell$.

The prototypical operator-adapted ansatz space $\mathcal{V}_\ell^a$ on level ℓ is given by applying the solution operator $\mathcal{A}^{-1}$ to $\mathbb{P}^0(\mathcal{T}_\ell)$, i.e.,

$$\mathcal{V}_\ell^a \coloneqq \operatorname{span}\{\mathcal{A}^{-1}\mathbb{1}_K : K \in \mathcal{T}_\ell\}.$$

In the following, we derive a hierarchical basis of $\mathcal{V}_L^a$, which includes basis functions from all coarser levels. Therefore, we first outline a procedure to generate a hierarchical basis, ensuring that the basis functions are a-orthogonal across levels, regardless of their support. We then consider localization strategies using the SLOD method to develop a basis suitable for practical applications.

4.1.1. Strict a-orthogonal basis

In this subsection, we construct globally supported hierarchical basis functions that are fully a-orthogonal across levels, leading to a block-diagonal hierarchical stiffness matrix. Therefore, we define $N_\ell \coloneqq \#\mathcal{T}_\ell$ as the number of elements in the mesh $\mathcal{T}_\ell$. The number of hierarchical basis functions corresponding to level ℓ is then denoted by N_ℓ^b, given by

$$N_\ell^b \coloneqq \begin{cases} N_1, & \text{if } \ell = 1, \\ (2^d - 1)N_{\ell-1}, & \text{if } \ell > 1. \end{cases}$$

Thus, at each level, we must determine N_ℓ^b linearly independent basis functions that are a-orthogonal to all basis functions associated with coarser levels.

To achieve this, we define each basis function $\psi^a_{\ell,i} \in \mathcal{V}^a_L$ by

$$\psi^a_{\ell,i} = \mathcal{A}^{-1} \sum_{K \in \mathcal{T}_\ell} c_K^{(\ell,i)} \mathbb{1}_K, \tag{4.1}$$

for any level $1 \leq \ell \leq L$ and $i \in \{1, \dots, N^b_\ell\}$. The non-trivial coefficients $c_K^{(\ell,i)}$ are chosen such that $\{c_K^{(1,i)} \mathbb{1}_K\}_{i \in \{1,\dots,N_1\}}$ forms a basis of $\mathbb{P}^0(\mathcal{T}_1)$. For levels $\ell > 1$, the coefficients are constructed to enforce the a-orthogonality condition across different levels, i.e.,

$$a(\psi^a_{\ell,i}, \psi^a_{p,j}) = 0 \quad \text{for all} \;\; 1 \leq p < \ell \tag{4.2}$$

Investigating this condition, we observe that

$$a(\psi^a_{\ell,i}, \psi^a_{p,j}) = \Big(\sum_{K \in \mathcal{T}_p} c_K^{(p,j)} \mathbb{1}_K, \psi^a_{\ell,i} \Big)_{L^2(D)} = \sum_{K \in \mathcal{T}_p} c_K^{(p,j)} \int_K \psi^a_{\ell,i} \, \mathrm{d}x = 0.$$

Therefore, the a-orthogonality condition (4.2) is satisfied if

$$\int_K \psi^a_{\ell,i} \, \mathrm{d}x = 0 \quad \text{for all} \;\; K \in \mathcal{T}_{\ell-1}, \tag{4.3}$$

since any element of $\mathcal{T}_p$ with $p < \ell$ is a union of elements from $\mathcal{T}_{\ell-1}$.

By defining $\alpha_{K,T} := \int_K \mathcal{A}^{-1} \mathbb{1}_T \, \mathrm{d}x$ and using the definition of $\psi^a_{\ell,i}$ from (4.1), we can rewrite condition (4.3) as

$$\sum_{T \in \mathcal{T}_\ell} c_T^{(\ell,i)} \alpha_{K,T} = 0 \quad \text{for all} \;\; K \in \mathcal{T}_{\ell-1}.$$

Let $\mathbf{D}^{(\ell)} \in \mathbb{R}^{N_{\ell-1} \times N_\ell}$ such that $\mathbf{D}^{(\ell)}_{n,m} = \alpha_{K_n,T_m}$ and $\mathbf{c}^{(\ell,i)} = (c_{T_m}^{(\ell,i)})_{m \in \{1,\dots N_\ell\}}$, with $K_n \in \mathcal{T}_{\ell-1}$, $T_m \in \mathcal{T}_\ell$. Hence, the a-orthogonality condition is satisfied for any level $\ell > 1$ if

$$\mathbf{D}^{(\ell)} \mathbf{c}^{(\ell,i)} = 0 \quad \text{for all} \;\; i \in \{1, \dots, N^b_\ell\}, \tag{4.4}$$

which implies that $\mathbf{c}^{(\ell,i)} \in \ker(\mathbf{D}^{(\ell)})$. Note that $\operatorname{rank}(\mathbf{D}^{(\ell)}) \leq N_{\ell-1}$. Consequently, $\dim(\ker(\mathbf{D}^{(\ell)})) \geq N_\ell - N_{\ell-1} = N^b_\ell$. Hence, there exists infinity many choice of coefficient vectors that satisfy condition (4.2). In principle, any set of N^b_ℓ linearly independent vectors from $\ker(\mathbf{D}^{(\ell)})$ can be chosen to form a basis for $\mathcal{V}^a_L$ at level $\ell > 1$, while any basis of $\mathbb{P}^0(\mathcal{T}_1)$ can be used for the coarsest level. However, the resulting basis functions $\psi^a_{\ell,i}$ are generally globally supported, leading to a (block-diagonal) stiffness matrix that lacks sparsity. Therefore, an ideal choice would be a set of coefficient vectors for which the associated hierarchical basis functions are locally supported. We study the feasibility of such an option in the following.

4.1.2. Localization strategy

To construct locally supported functions that satisfy the a-orthogonality condition, we adopt the localization strategy associated with the SLOD introduced in Chapter 3. Accordingly, the corresponding piecewise-constant right-hand sides of the hierarchical basis functions must also undergo localization. However, it is generally not feasible to achieve both strict a-orthogonality and full localization simultaneously. To preserve locality, the a-orthogonality condition may need to be partially relaxed. A practical compromise thus balances adherence to orthogonality and locality against computational cost, permitting minor deviations to enable an efficient scheme based on purely local computations. For computing the local HSLOD basis using the SLOD localization strategy, various approaches can be explored. One option is to define local variants of the matrices $\mathbf{D}^{(\ell)}$ from (4.4) based on the concept of patches, and then determine coefficient vectors within the corresponding kernels such that the associated HSLOD basis functions have a minimal conormal derivative. This approach, however, introduces potential stability issues.

Our ansatz employs linear combinations of SLOD basis functions defined in (3.2) to approximately satisfy both localization and a-orthogonality. To extend this concept to the multilevel case, we generalize the definition of patches. In accordance with (2.14), we recursively define the m-th order patch on level ℓ for an element $K \in \mathcal{T}_\ell$ as

$$\mathsf{N}_\ell^m(K) \coloneqq \mathsf{N}_\ell^1(\mathsf{N}_\ell^{m-1}(K)) \quad \text{with} \quad \mathsf{N}_\ell^1(K) \coloneqq \bigcup\{T \in \mathcal{T}_\ell : \, T \cap K \neq \emptyset\}. \tag{4.5}$$

For the hierarchical basis functions on level $\ell = 1$, we use local SLOD functions defined on $\mathcal{T}_1$. In the following we give an Ansatz for the HSLOD basis derivation for $\ell > 1$. Those HSLOD functions are defined on patches corresponding to elements $T \in \mathcal{T}_{\ell-1}$ of the coarser level. On each such patch, $2^d - 1$ hierarchical basis functions need to be defined. To formalize this, we introduce the quantity

$$J_i \coloneqq \left\lfloor \frac{i-1}{2^d - 1} \right\rfloor + 1, \tag{4.6}$$

which indicates the reference element $T_{J_i} \in \mathcal{T}_{\ell-1}$ and, consequently, the patch. For convenience, we fix the oversampling parameter $m \in \mathbb{N}$ and refer to the m-th order patch of $T_{J_i} \in \mathcal{T}_{\ell-1}$ on level $\ell - 1$ simply as $D_{J_i}^{(\ell-1)} \coloneqq \mathsf{N}_{\ell-1}^m(T_{J_i})$.

On level $\ell > 1$, we define the local HSLOD basis functions $\hat{\psi}_{\ell,i,m}^{\mathrm{hslod}} \in H_0^1(D_{J_i}^{(\ell-1)})$ for each $i \in \{1, \dots, N_\ell^b\}$ as a linear combination of local SLOD functions. These SLOD functions are defined on the mesh $\mathcal{T}_\ell$ and are supported strictly within the patch $D_{J_i}^{(\ell-1)}$. In contrast to HSLOD functions, the patches associated with SLOD basis functions at level ℓ are constructed as unions of elements from $\mathcal{T}_\ell$. We denote by $D_K^{(\ell)}$ the patch $\mathsf{N}_\ell^m(K)$ on which the SLOD function $\hat{\varphi}_{\ell,K,m}^{\mathrm{slod}}$, corresponding to $K \in \mathcal{T}_\ell$, is supported. Furthermore, for each element $T_{J_i} \in \mathcal{T}_{\ell-1}$, we define the set

$$S_{J_i}^{(\ell)} \coloneqq \{K \in \mathcal{T}_\ell : \, \mathrm{supp}(\hat{\varphi}_{\ell,K,m}^{\mathrm{slod}}) \subset D_{J_i}^{(\ell-1)}\}.$$

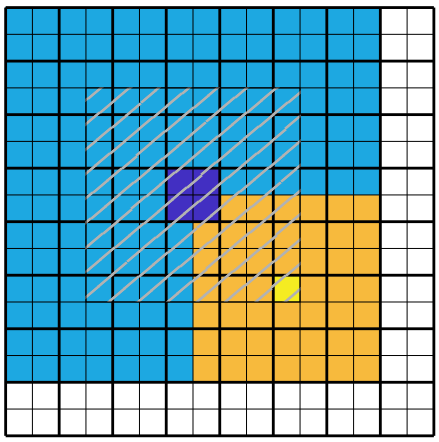

Figure 4.1.: Illustration of the various patches in the HSLOD context on the mesh $\mathcal{T}_\ell$, with the coarser mesh $\mathcal{T}_{\ell-1}$ represented using bold lines. Specifically, it shows the patch $D_{J_i}^{(\ell-1)}$ (●) corresponding to a hierarchical basis function associated with the reference element $T_{J_i} \in \mathcal{T}_{\ell-1}$ (●) . Additionally, it depicts the patch $D_K^{(\ell)}$ (●) surrounding $K \in S_{J_i}^{(\ell)}$ (●). The set $S_{J_i}^{(\ell)}$ (⊘) corresponding to the patch $D_{J_i}^{(\ell-1)}$ is also highlighted.

An illustration of the different patches introduced in this section, along with the set $S_{J_i}^{(\ell)}$, is provided in Figure 4.1.

We define the HSLOD basis function $\hat{\psi}_{\ell,i,m}^{\text{hslod}} \in H_0^1(D_{J_i}^{(\ell-1)})$ as

$$\hat{\psi}_{\ell,i,m}^{\text{hslod}} = \sum_{K \in S_{J_i}^{(\ell)}} d_K^{(\ell,i)} \hat{\varphi}_{\ell,K,m}^{\text{slod}}, \tag{4.7}$$

where the non-trivial coefficients $(d_K^{(\ell,i)})_{K \in S_{J_i}^{(\ell)}}$ are chosen such that

$$\Pi_{\ell-1} \hat{\psi}_{\ell,i,m}^{\text{hslod}} = 0. \tag{4.8}$$

This condition is locally equivalent to (4.3) and ensures that the a-orthogonality condition is satisfied to some extent. Specifically, it guarantees a-orthogonality when the support of a basis function on a finer mesh is fully contained within the support of a basis function on a coarser mesh; see also Theorem 4.1.1 below.

Although $\#S_{J_i}^{(\ell)} > \#\mathcal{T}_{\ell-1,D_{J_i}^{(\ell-1)}}$ implies that there are infinitely many choices of non-trivial coefficients that satisfy (4.8), not all such choices yield a stable HSLOD basis. To ensure stability, specifically, the linear independence of the $2^d - 1$ hierarchical basis functions associated with the patch, we select functions whose masses are centered within the reference coarse element $T_{J_i} \in \mathcal{T}_{\ell-1}$, but are concentrated in different elements of the refined mesh $\mathcal{T}_\ell$. First, we define the set of descendants of an element $T \in \mathcal{T}_{\ell-1}$ as

$$\text{des}(T) \coloneqq \{K \in \mathcal{T}_\ell : \ K \subset T\}.$$

Let $\widetilde{\mathrm{des}}(T)$ be any subset of $\mathrm{des}(T)$ such that $\#\widetilde{\mathrm{des}}(T) = 2^d - 1$. Additionally, we define a subset of descendants of the patch $D_{J_i}^{(\ell-1)}$ as

$$\widetilde{\mathrm{des}}(D_{J_i}^{(\ell-1)}) := \{K \in \widetilde{\mathrm{des}}(T) : T \in \mathcal{T}_{\ell-1, D_{J_i}^{(\ell-1)}}\},$$

and take $\widetilde{\Pi}_\ell : H_0^1(D_{J_i}^{(\ell-1)}) \to \mathbb{P}^0(\widetilde{\mathrm{des}}(D_{J_i}^{(\ell-1)}))$ as the $L^2(\widetilde{\mathrm{des}}(D_{J_i}^{(\ell-1)}))$-orthogonal projection onto piecewise constants.

To construct a stable HSLOD basis, we choose the coefficients in (4.7) such that, in addition to satisfying (4.8), $\hat{\psi}_{\ell,i,m}^{\mathrm{hslod}}$ fulfills

$$\widetilde{\Pi}_\ell \hat{\psi}_{\ell,i,m}^{\mathrm{hslod}} = \mathbb{1}_{K_i}, \tag{4.9}$$

where $K_i \in \mathcal{T}_\ell$ is a descendent of the reference element T_{J_i} with $K_i \in \widetilde{\mathrm{des}}(T_{J_i})$. After enforcing condition (4.8), we are left with at most

$$\#S_{J_i}^{(\ell)} - \#\mathcal{T}_{\ell-1, D_{J_i}^{(\ell-1)}} \leq \#\widetilde{\mathrm{des}}(D_{J_i}^{(\ell-1)})$$

degrees of freedom. Consequently, condition (4.9) cannot, in general, be satisfied exactly, except in the one-dimensional case. Instead, we determine the non-trivial coefficients such that the algebraic form of this condition is satisfied in the least-squares sense.

This construction ensures that the HSLOD basis functions supported on the same patch are linearly independent. In addition, it drives the coefficients $d_K^{(\ell,i)}$ to be small for elements that are near the boundary of the patch. As a consequence, the conormal derivative of $\hat{\psi}_{\ell,i,m}^{\mathrm{hslod}}$ on the interior patch boundary $\Sigma_{J_i} \coloneqq \partial D_{J_i}^{(\ell-1)} \setminus \partial D$ is small, since each SLOD basis function $\hat{\varphi}_{\ell,K,m}^{\mathrm{slod}}$ with $K \in S_{J_i}^{(\ell)}$ has a small conormal derivative on Σ_{J_i}.

4.1.3. Practical hierarchical basis

To handle the case $\ell = 1$ consistently with all other levels, we extend the definition of the quantity J_i in (4.6) by setting $J_i = i$ for $\ell = 1$, and use the generalized formulation

$$J_i := \left\lfloor \frac{i-1}{(2^d-1)^{\min(\ell-1,0)}} \right\rfloor + 1. \tag{4.10}$$

Hence, the hierarchical basis functions $\hat{\psi}_{\ell,i,m}^{\mathrm{hslod}}$ are defined on patches $D_{J_i}^{(\ell-1)}$ which, at all levels, are associated with elements $T_{J_i} \in \mathcal{T}_{\max(\ell-1,1)}$. We define the normalized HSLOD function $\hat{\psi}_{\ell,i,m} \in H_0^1(D_{J_i}^{(\ell-1)})$ as

$$\hat{\psi}_{\ell,i,m} = \hat{\psi}_{\ell,i,m}^{\mathrm{hslod}} / \|\hat{\psi}_{\ell,i,m}^{\mathrm{hslod}}\|_a. \tag{4.11}$$

In addition, introducing the normalized coefficients

$$\hat{d}_K^{(\ell,i)} = d_K^{(\ell,i)} / \|\hat{\psi}_{\ell,i,m}^{\text{hslod}}\|_a, \tag{4.12}$$

the hierarchical basis function can be written as the linear combination

$$\hat{\psi}_{\ell,i,m} = \sum_{K \in S_{J_i}^{(\ell)}} \hat{d}_K^{(\ell,i)} \hat{\varphi}_{\ell,K,m}^{\text{slod}}. \tag{4.13}$$

In particular, for $\ell = 1$, we have $S_{J_i}^{(\ell)} = \{T_i\}$, so that the hierarchical basis function coincides with the (normalized) SLOD function associated with the element $T_i \in \mathcal{T}_1$.

Note that the localized hierarchical basis functions are, in general, not a basis for the prototypical ansatz space $\mathcal{V}_L^a$. However, by using the same coefficients $\hat{d}_K^{(\ell,i)}$ that define $\hat{\psi}_{\ell,i,m}$, a basis for $\mathcal{V}_L^a$ can be constructed using the global SLOD functions defined in (3.1), as

$$\psi_{\ell,i,m} = \sum_{K \in S_{J_i}^{(\ell)}} \hat{d}_K^{(\ell,i)} \varphi_{\ell,K,m}^{\text{slod}}. \tag{4.14}$$

The prolongation by zeros of the above coefficient vector defining the hierarchical basis functions to $\mathbb{R}^{N_\ell}$ is not necessarily an element of $\ker(\mathbf{D}^{(\ell)})$ as defined in Section 4.1.1. Consequently, the stiffness matrix associated with the global functions $\psi_{\ell,i,m}$ will, in general, not be block-diagonal.

Analogous to the construction of the hierarchical basis functions, a local source term associated to $\hat{\psi}_{\ell,i,m}$ and $\psi_{\ell,i,m}$ can be defined as

$$g_{\ell,i,m} = \sum_{K \in S_{J_i}^{(\ell)}} \hat{d}_K^{(\ell,i)} g_{\ell,K,m}^{\text{slod}} \in \mathbb{P}^0(\mathcal{T}_{\ell,D_{J_i}^{(\ell-1)}}), \tag{4.15}$$

where $g_{\ell,K,m}^{\text{slod}} \in \mathbb{P}^0(\mathcal{T}_{\ell,D_K^{(\ell)}})$ is the $L^2(D_K^{(\ell)})$-normalized local source term of $\hat{\varphi}_{\ell,K,m}^{\text{slod}}$.

An example of the hierarchical basis functions in one dimension is illustrated in Figure 4.2 for the model problem (2.3) with a constant diffusion coefficient $A \equiv 1$ along with an example for a piecewise constant coefficient. For visualization purposes, the HSLOD basis functions shown are not normalized with respect to the energy norm but are instead scaled to be of the same order. Different colors indicate the levels to which the basis functions are associated to. The considered mesh sizes range from $H_1 = 1$ to $H_4 = 2^{-3}$. Figure 4.3 shows the HSLOD basis functions associated to the fifth level in the hierarchy (with mesh size $H_5 = 2^{-4}$), as well as the corresponding hierarchical LOD (HLOD) functions for the same parameters. The comparison illustrates the smaller conormal derivatives of the HSLOD basis functions. In Figure 4.4, the hierarchical basis functions in two dimensions along with their corresponding L^2-normalized local source terms are displayed. The figure depicts HSLOD basis functions across three levels ($\ell = 1, \ldots, 3$) corresponding to mesh sizes $H_\ell = 2^{-2}, \ldots, 2^{-4}$.

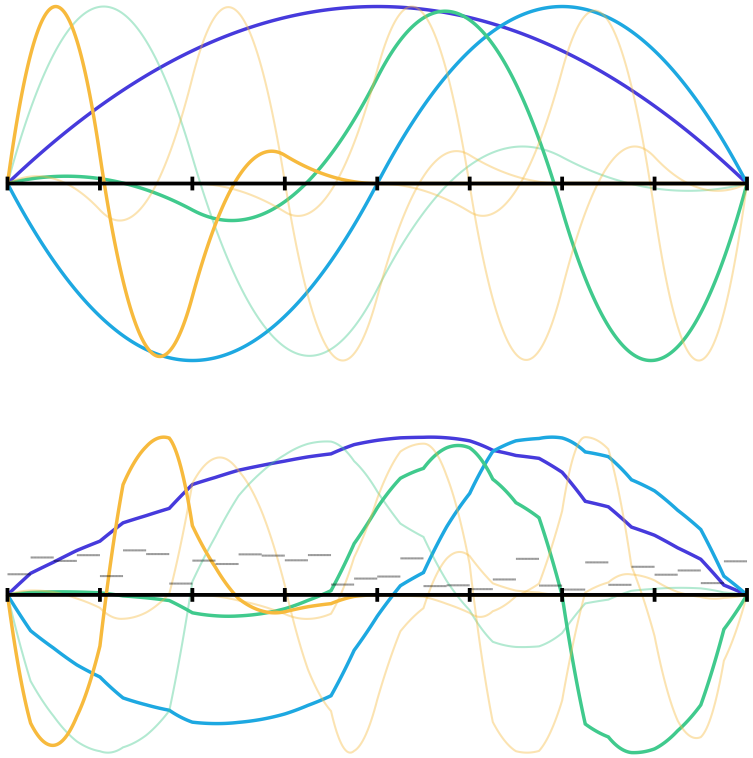

Figure 4.2.: Local (scaled) HSLOD basis functions for the model problem (2.3) in one spatial dimension, for $A \equiv 1$ (top) and a piecewise constant coefficient illustrated in gray (bottom), shown for levels $\ell = 1$ (●) up to $\ell = 4$ (●). The oversampling parameter is set to $m = 1$.

In the following, we analyze the quality of the local HSLOD basis with respect to a-orthogonality and localization error. To this end, we introduce the quantity

$$\zeta = \zeta(H_L, m) := \max_{\ell \in \{1,\dots,L\}} \max_{i \in \{1,\dots,N_\ell^b\}} \sqrt{\sum_{K \in S_{J_i}^{(\ell)}} |\hat{d}_K^{(\ell,i)}|^2}. \tag{4.16}$$

Furthermore, let $\sigma_{\ell,K}$ denote the localization error associated with the SLOD function $\hat{\varphi}_{\ell,K,m}^{\mathrm{slod}}$, as defined in (3.9). A global measure of the localization error of SLOD functions across levels is then given by

$$\sigma = \sigma(H_L, m) := \max_{\ell \in \{1,\dots,L\}} \max_{K \in \mathcal{T}_\ell} \sigma_{\ell,K}. \tag{4.17}$$

As shown in Section 3.3, σ can be expected to decay super-exponentially, and is shown to decay at least exponentially, see Theorem 3.3.4. More precisely, we have

$$\sigma \lesssim H_L^{-1} \exp(-Cm).$$

An upper bound on ζ will be provided in Section 4.5.

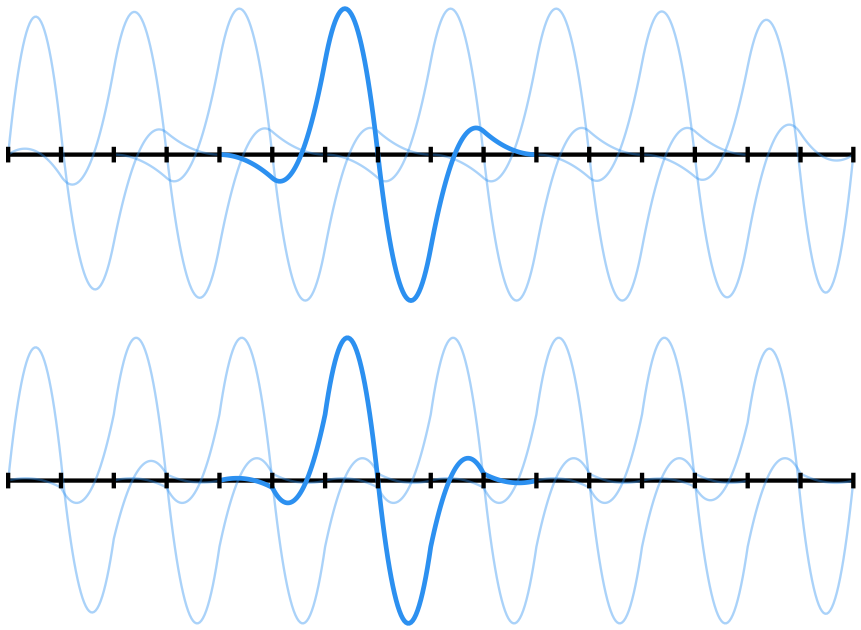

Figure 4.3.: Local HSLOD (top) and HLOD (bottom) basis functions for the model problem (2.3) with $A \equiv 1$ in one spatial dimension, associated to the level with mesh size 2^{-4}. The oversampling parameter is set to $m = 1$.

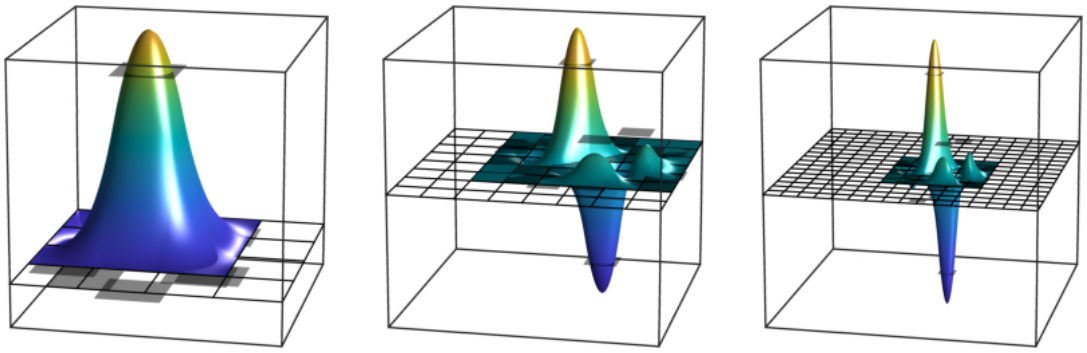

Figure 4.4.: HSLOD basis functions and their corresponding L^2-normalized local source terms for the model problem (2.3) with a constant coefficient $A \equiv 1$ in two spatial dimensions. Basis functions associated to levels $\ell = 1$ (left) up to $\ell = 3$ (right) are illustrated. The oversampling parameter is set to $m = 1$.

The next lemma investigates the a-orthogonality condition and gives an estimate of the off-block diagonal entries of the stiffness matrix associated with the HSLOD basis functions. Of course, the a-inner product of two basis functions can only be non-zero if the corresponding patches are at least partially overlapping.

Lemma 4.1.1 (Orthogonality condition of HSLOD functions)**.** *Let $\hat{\psi}_{\ell,i,m}$ and $\hat{\psi}_{p,j,m}$ be two hierarchical basis functions defined on levels $\ell < p$ with partially overlapping patches, i.e., $\mathsf{N}^m_{\ell-1}(T_{J_i}) \cap \mathsf{N}^m_{p-1}(T_{J_j}) \neq \emptyset$. Then, it holds that*

$$a(\hat{\psi}_{\ell,i,m}, \hat{\psi}_{p,j,m}) \begin{cases} = 0 & \text{if } \mathsf{N}^m_{p-1}(T_{J_j}) \subset \mathsf{N}^m_{\ell-1}(T_{J_i}), \\ \lesssim m^{d/2}\zeta\sigma & \text{otherwise}, \end{cases} \tag{4.18}$$

where ζ is given in (4.16) and σ is given in (4.17).

Proof. If the support of the finer-level basis function $\hat{\psi}_{p,j,m}$ is entirely contained within $\mathsf{N}^m_{\ell-1}(T_{J_i})$, i.e., $\hat{\psi}_{p,j,m} \in H^1_0(\mathsf{N}^m_{\ell-1}(T_{J_i}))$, then, since $g_{\ell,i,m} \in \mathbb{P}^0(\mathcal{T}_\ell)$, condition (4.8) implies

$$a(\hat{\psi}_{\ell,i,m}, \hat{\psi}_{p,j,m}) = (g_{\ell,i,m}, \hat{\psi}_{p,j,m})_{L^2(D)} = 0.$$

For the case where the supports of $\hat{\psi}_{\ell,i,m}$ and $\hat{\psi}_{p,j,m}$ partially overlap, we use the representation of $\hat{\psi}_{\ell,i,m}$ from (4.13) to obtain that

$$a(\hat{\psi}_{\ell,i,m}, \hat{\psi}_{p,j,m}) = \sum_{K \in S^{(\ell)}_{J_i}} \hat{d}^{(\ell,i)}_K a(\hat{\varphi}^{\mathrm{slod}}_{\ell,K,m}, \hat{\psi}_{p,j,m}).$$

By applying the definition of the conormal derivative from (3.6), along with (4.8) and (3.4), we can deduce for each term separately that

$$\begin{aligned} a(\hat{\varphi}^{\mathrm{slod}}_{\ell,K,m}, \hat{\psi}_{p,j,m}) &= \langle \gamma_{\partial n} \hat{\varphi}^{\mathrm{slod}}_{\ell,K,m}, \mathrm{tr}(\hat{\psi}_{p,j,m}|_{D^{(\ell)}_K}) \rangle_{X' \times X} + (g^{\mathrm{slod}}_{\ell,K,m}, \hat{\psi}_{p,j,m})_{L^2(D^{(\ell)}_K)} \\ &\leq \|\gamma_{\partial n} \hat{\varphi}^{\mathrm{slod}}_{\ell,K,m}\|_{X'} \|\mathrm{tr}(\hat{\psi}_{p,j,m}|_{D^{(\ell)}_K})\|_X \\ &\leq \|\gamma_{\partial n} \hat{\varphi}^{\mathrm{slod}}_{\ell,K,m}\|_{X'} \|\hat{\psi}_{p,j,m}\|_{H^1(D)} \\ &\lesssim \sigma, \end{aligned}$$

where we used the fact that the HSLOD basis functions are normalized to one, and that σ is a measure of the conormal derivative of $\hat{\varphi}^{\mathrm{slod}}_{\ell,K,m}$, see Section 3.1. Here, tr denotes the trace operator on $D^{(\ell)}_K$, the patch associated with $\hat{\varphi}^{\mathrm{slod}}_{\ell,K,m}$. In combination with the Cauchy–Schwarz inequality and (4.16), the claim follows as

$$a(\hat{\psi}_{\ell,i,m}, \hat{\psi}_{p,j,m}) \lesssim \sum_{K \in S^{(\ell)}_{J_i}} \hat{d}^{(\ell,i)}_K \sigma \leq \sqrt{|S^{(\ell)}_{J_i}|} \Big(\sum_{K \in S^{(\ell)}_{J_i}} |\hat{d}^{(\ell,i)}_K|^2 \Big)^{1/2} \sigma \lesssim m^{d/2} \zeta \sigma.$$

□

The next lemma quantifies the approximation quality of the localized basis by providing an upper bound on the localization error between the local HSLOD basis functions $\hat{\psi}_{\ell,i,m}$ and their global counterparts $\psi_{\ell,i,m}$ in the energy-norm.

Lemma 4.1.2 (Localization error of HSLOD functions)**.** *Let $\hat{\psi}_{\ell,i,m}$ and $\psi_{\ell,i,m}$ be hierarchical basis functions as defined in* (4.13) *and* (4.14)*. Then the following estimate holds*

$$\|\psi_{\ell,i,m} - \hat{\psi}_{\ell,i,m}\|_a \lesssim m^{d/2}\zeta\sigma,$$

where ζ is given in (4.16) and σ is given in (4.17).

Proof. From the definitions of the HSLOD basis functions (4.13) and (4.14), together with (3.15), Friedrichs' inequality, and the Cauchy–Schwarz inequality, it follows that

$$\begin{aligned}
\|\psi_{\ell,i,m} - \hat{\psi}_{\ell,i,m}\|_a &= \Big\| \sum_{K\in S^{(\ell)}_{J_i}} \hat{d}^{(\ell,i)}_K \left(\varphi^{\mathrm{slod}}_{\ell,K,m} - \hat{\varphi}^{\mathrm{slod}}_{\ell,K,m}\right) \Big\|_a \\
&\leq \max_{K\in S^{(\ell)}_{J_i}} \left\{ \left\|\varphi^{\mathrm{slod}}_{\ell,K,m} - \hat{\varphi}^{\mathrm{slod}}_{\ell,K,m}\right\|_a \right\} \sum_{K\in S^{(\ell)}_{J_i}} |\hat{d}^{(\ell,i)}_K| \\
&\lesssim m^{d/2}\zeta\sigma.
\end{aligned}$$

□

This implies that $m^{d/2}\zeta\sigma$ serves as a measure of the localization error of the HSLOD basis functions. Furthermore, Theorem 4.1.1 indicates that smaller localization errors correspond to near-complete a-orthogonality across levels.

4.2. Practical multiscale methods

Using the localized basis functions from the previous section, we now introduce two possible multiscale methods based on this hierarchical basis. Before introducing the methods, we first define, for $1 \leq \ell \leq L$,

$$\hat{\mathcal{V}}_{\ell,m} \coloneqq \mathrm{span}\{\hat{\psi}_{\ell,i,m} : \ i = 1, \ldots, N^b_\ell\},$$

which will serve as the level-wise ansatz spaces in the following. The overall ansatz space is then defined as

$$\hat{\mathcal{V}}^{\mathrm{ML}}_{L,m} \coloneqq \hat{\mathcal{V}}_{1,m} \oplus \cdots \oplus \hat{\mathcal{V}}_{L,m}.$$

For simplicity, we refer to the hierarchical basis functions of $\hat{\mathcal{V}}^{\mathrm{ML}}_L$ and $\mathcal{V}^a_L$ using their global indices. Thus, with

$$i = \begin{cases} j, & \text{if } \ell = 1, \\ \#\mathcal{T}_{\ell-1} + j, & \text{if } \ell > 1, \end{cases} \tag{4.19}$$

we have the relations

$$\hat{\psi}_{i,m} = \hat{\psi}_{\ell,j,m} \quad \text{and} \quad \psi_{i,m} = \psi_{\ell,j,m} \tag{4.20}$$

with corresponding local source terms $g_{i,m} = g_{\ell,j,m}$. Using global indices, we refer to the patches associated with the hierarchical basis functions as $D_i = D_{J_j}^{(\ell-1)}$. With this notation established, we are now ready to define the two multiscale methods.

Level-wise Galerkin method. In this hierarchical approach, we first seek, for each level, the sub-scale solution $u_{\ell,m} \in \hat{\mathcal{V}}_{\ell,m}$, which satisfies

$$a(u_{\ell,m}, v) = (f, v)_{L^2(D)}$$

for all $v \in \hat{\mathcal{V}}_{\ell,m}$. The approximate solution to the model problem (2.3) is then given by the sum of these Galerkin approximations, i.e.,

$$u_{L,m}^{\mathrm{ML}} = u_{1,m} + \cdots + u_{L,m}. \tag{4.21}$$

Hence, this approach leverages the nearly block-diagonal structure of the stiffness matrix associated with the HSLOD basis, effectively neglecting the off-block diagonal entries.

Collocation-type method. A collocation-type discrete approximation to (2.3) is given by

$$u_{L,m}^{\mathrm{col}} = \sum_{i=1}^{N_L} c_i \hat{\psi}_{i,m}, \tag{4.22}$$

where $(c_i)_{i\in\{1,\dots,N_L\}}$ are the coefficients of the expansion of $\Pi_L f$ in the basis functions $\{g_{i,m} : i = 1, \dots N_L\}$ of $\mathbb{P}^0(\mathcal{T}_L)$. Note that, unlike the level-wise Galerkin method, the collocation-type method does not exploit the a-orthogonality of the hierarchical basis. This is because the a-orthogonality of the HSLOD basis functions does not generally imply the L^2-orthogonality of the corresponding local source terms $g_{i,m}$. Therefore, it is not possible to improve an existing collocation-type approximation by solely considering an additional fine level in the hierarchy. This aspect is further examined in Section 4.6.

As in the case of the SLOD method, a minimal requirement for ensuring the stability and convergence of both hierarchical multiscale methods is that the set $\{g_{i,m} : i = 1, \dots, N_L\}$ spans $\mathbb{P}^0(\mathcal{T}_L)$ in a stable way. In practical implementations, this condition is enforced via (4.9). For the subsequent numerical analysis, we impose the following assumption for the hierarchical setting, in line with Theorem 3.1.2.

Assumption 4.2.1 (Riesz stability)**.** The set $\{g_{i,m} : i = 1, \dots, N_L\}$ is a Riesz basis of $\mathbb{P}^0(\mathcal{T}_L)$, i.e., there exists a constant $C_{\mathrm{rb}} = C_{\mathrm{rb}}(H_L, m) > 0$ such that for all possible choices of $(c_i)_{i\in\{1,\dots,N_L\}}$ it holds that

$$C_{\mathrm{rb}}^{-1} \sum_{i=1}^{N_L} c_i^2 \leq \left\| \sum_{i=1}^{N_L} c_i g_{i,m} \right\|_{L^2(D)}^2,$$

where C_{rb} depends polynomially on H_L^{-1} and m.

4.3. Error analysis

In this section, we present an error analysis of the previously introduced methods. We begin by establishing an error bound for the collocation-type variant and then use this result to derive the error analysis for the level-wise Galerkin method. In both cases, several HSLOD-specific quantities arise in an a posteriori manner, which will be further examined in Section 4.5.

Theorem 4.3.1 (Error bound of the collocation-type variant)**.** *Let the set $\{g_{i,m} : i = 1, \dots, N_L\}$ be stable in the sense of Theorem 4.2.1. Then, for any $f \in H^s(D)$ with $s \in \{0, 1\}$, the solution of the collocation-type method introduced in* (4.22) *satisfies*

$$\begin{aligned} \|u - u_{L,m}^{\mathrm{col}}\|_a &\lesssim H_L \|f - \Pi_L f\|_{L^2(D)} + C_{\mathrm{rb}}^{1/2} \sqrt{L} m^d \zeta \sigma \|f\|_{L^2(D)} \\ &\lesssim \left(H_L^{1+s} + C_{\mathrm{rb}}^{1/2} \sqrt{L} m^d \zeta \sigma \right) \|f\|_{H^s(D)} \end{aligned}$$

with C_{rb} from Theorem 4.2.1. This result implies that the collocation-type approximation converges to the exact solution at an algebraic rate in H_L, up to an additional error due to localization.

Proof. By using the triangle inequality with $\tilde{u} = \mathcal{A}^{-1}\Pi_L f$, we obtain that

$$\|u - u_{L,m}^{\mathrm{col}}\|_a \leq \|u - \tilde{u}\|_a + \|\tilde{u} - u_{L,m}^{\mathrm{col}}\|_a. \tag{4.23}$$

Using the same arguments as in Theorem 3.2.1, we can estimate the first term as

$$\|u - \tilde{u}\|_a \lesssim H \|f - \Pi_L f\|_{L^2(D)} \lesssim H^{1+s} \|f\|_{H^s(D)}. \tag{4.24}$$

For the second term of (4.23), we use the exactness of the prototypical method for $\Pi_L f$, see Section 2.3. Hence, we can represent $\tilde{u}$ using the global HSLOD basis functions as

$$\tilde{u} = \sum_{i=1}^{N_L} c_i \psi_{i,m},$$

where $(c_i)_{i\in\{1,\dots,N_L\}}$ are the coefficients of the expansion of $\Pi_L f$ in the basis functions $g_{i.m}$. With the definition of the collocation-type method in (4.22) we obtain

$$\|\tilde{u} - u_{L,m}^{\mathrm{col}}\|_a^2 = \sum_{i=1}^{N_L} c_i \, a(\psi_{i,m} - \hat{\psi}_{i,m}, \tilde{u} - u_{L,m}^{\mathrm{col}}). \tag{4.25}$$

Let $e \coloneqq \tilde{u} - u_{L,m}^{\mathrm{col}}$. Using the relations (4.20), the definitions of the HSLOD functions (4.13) and (4.14), (3.15) and the Cauchy–Schwarz inequality, it follows that

$$\begin{aligned} a(\psi_{i,m} - \hat{\psi}_{i,m}, e) &= a(\psi_{\ell,j,m} - \hat{\psi}_{\ell,j,m}, e) \\ &= \sum_{K \in S_{J_j}^{(\ell)}} \hat{d}_K^{(\ell,j)}\, a(\hat{\varphi}_{\ell,K,m}^{\mathrm{slod}} - \varphi_{\ell,K,m}^{\mathrm{slod}}, e) \\ &\lesssim \sigma \sum_{K \in S_{J_j}^{(\ell)}} \hat{d}_K^{(\ell,j)} \|e\|_{H^1(D_K^{(\ell)})} \\ &\leq \sigma \sqrt{\sum_{K \in S_{J_j}^{(\ell)}} |\hat{d}_K^{(\ell,j)}|^2} \sqrt{\sum_{K \in S_{J_j}^{(\ell)}} \|e\|_{H^1(D_K^{(\ell)})}^2} \\ &\lesssim m^{d/2} \zeta \sigma \|e\|_{H^1(D_{J_j}^{(\ell-1)})}, \end{aligned} \tag{4.26}$$

where $D_K^{(\ell)}$ is the associated patch to $\hat{\varphi}_{\ell,K,m}^{\mathrm{slod}}$ and $D_{J_j}^{(\ell-1)}$ is the one corresponding to $\hat{\psi}_{\ell,j,m}$. For the last step, we used (4.16), the fact that

$$D_K^{(\ell)} \subset D_{J_j}^{(\ell-1)} \quad \text{for} \quad K \in S_{J_j}^{(\ell)},$$

and the finite overlap of patches.

Referring back to the global indices of the basis functions yields the relation $D_i = D_{J_j}^{(\ell-1)}$. Combining this with (4.25) and (4.26) and applying the Cauchy–Schwarz inequality, we obtain

$$\begin{aligned} \|\tilde{u} - u_{L,m}^{\mathrm{col}}\|_a^2 &\lesssim m^{d/2} \zeta \sigma \sum_{i=1}^{N_L} c_i \|\tilde{u} - u_{L,m}^{\mathrm{col}}\|_{H^1(D_i)} \\ &\leq m^{d/2} \zeta \sigma \sqrt{\sum_{i=1}^{N_L} c_i^2} \sqrt{\sum_{i=1}^{N_L} \|\tilde{u} - u_{L,m}^{\mathrm{col}}\|_{H^1(D_i)}^2} \\ &\lesssim C_{\mathrm{rb}}^{1/2} \sqrt{L} m^d \zeta \sigma \|f\|_{L^2(D)} \|\tilde{u} - u_{L,m}^{\mathrm{col}}\|_a. \end{aligned}$$

For the last inequality we used Theorem 4.2.1, Friedrichs' inequality, and the finite overlap of patches per level. The combination of (4.23), (4.24) and the previous estimate yields the assertion. □

In contrast to the collocation-type variant, the level-wise Galerkin method (4.21) exploits the nearly blockwise structure of the stiffness matrix associated with the HSLOD basis functions $\hat{\psi}_{i,m}$ by disregarding the off-block diagonal entries. To evaluate the error introduced by this approximation, we first establish the following lemma, which quantifies the impact of neglecting the off-block diagonal entries in a matrix.

Lemma 4.3.2 (Disregarding off-block diagonal entries)**.** *Let $\mathbf{A} \in \mathbb{R}^{n\times n}$ a symmetric positive definite (SPD) matrix, and let $\bar{\mathbf{A}} \in \mathbb{R}^{n\times n}$ be the block-diagonal matrix whose diagonal blocks coincide with those of $\mathbf{A}$. Denote by $\mathcal{N}_b \in \mathbb{N}$ the number of diagonal blocks of $\bar{\mathbf{A}}$, and by $n_i \in \mathbb{N}$ the number of rows of its i-th diagonal block. Define $\Delta\mathbf{A} := \mathbf{A} - \bar{\mathbf{A}}$, and let $\Delta\mathbf{A}_i$ be the rectangular submatrix of $\Delta\mathbf{A}$ consisting of the rows of $\Delta\mathbf{A}$ corresponding to the indices of the i-th diagonal block of $\mathbf{A}$. Let $\mathbf{b} \in \mathbb{R}^n$ be arbitrary, $\mathbf{x} \in \mathbb{R}^n$ such that $\mathbf{A}\mathbf{x} = \mathbf{b}$, and $\bar{\mathbf{x}} \in \mathbb{R}^n$ such that $\bar{\mathbf{A}}\bar{\mathbf{x}} = \mathbf{b}$. Then, the error bound*

$$\|\mathbf{x} - \bar{\mathbf{x}}\|_2 \leq \Big(\sum_{i=1}^{\mathcal{N}_\mathbf{b}} \lambda_{\min}^{-2}\left(\mathbf{A}_{ii}\right) \|\Delta\mathbf{A}_i\|_2^2 \|\mathbf{x}\|_2^2 \Big)^{\frac{1}{2}}$$

holds, where $\mathbf{A}_{ii} \in \mathbb{R}^{n_i\times n_i}$ is the i-th diagonal block of $\bar{\mathbf{A}}$ and $\mathbf{A}$.

Proof. Let $\mathbf{x} = [\mathbf{x}_1^T, \ldots, \mathbf{x}_{\mathcal{N}_\mathbf{b}}^T]^T$, $\bar{\mathbf{x}} = [\bar{\mathbf{x}}_1^T, \ldots, \bar{\mathbf{x}}_{\mathcal{N}_\mathbf{b}}^T]^T$, and $\mathbf{b} = [\mathbf{b}_1^T, \ldots, \mathbf{b}_{\mathcal{N}_\mathbf{b}}^T]^T$, where $\mathbf{x}_i, \bar{\mathbf{x}}_i, \mathbf{b}_i \in \mathbb{R}^{n_i}$. Since the diagonal blocks of $\bar{\mathbf{A}}$ and $\mathbf{A}$ coincide, we have $\Delta\mathbf{A}_{ii} := \mathbf{A}_{ii} - \bar{\mathbf{A}}_{ii} = 0$. This implies that $\mathbf{b}_i = \mathbf{A}_{ii}\mathbf{x}_i + \Delta\mathbf{A}_i\mathbf{x}$. Since $\mathbf{b}_i = \mathbf{A}_{ii}\bar{\mathbf{x}}_i$, it follows that $\mathbf{A}_{ii}(\mathbf{x}_i - \bar{\mathbf{x}}_i) + \Delta\mathbf{A}_i\mathbf{x} = 0$, or equivalently $\mathbf{x}_i - \bar{\mathbf{x}}_i = -\mathbf{A}_{ii}^{-1}\Delta\mathbf{A}_i\mathbf{x}$. Taking norms, we get that

$$\|\mathbf{x}_i - \bar{\mathbf{x}}_i\|_2 \leq \|\mathbf{A}_{ii}^{-1}\|_2 \|\Delta\mathbf{A}_i\|_2 \|\mathbf{x}\|_2 = \lambda_{\min}^{-1}\Big(\mathbf{A}_{ii}\Big) \|\Delta\mathbf{A}_i\|_2 \|\mathbf{x}\|_2.$$

Thus, the assertion follows by noticing that $\|\mathbf{x} - \bar{\mathbf{x}}\|_2^2 = \sum_{i=1}^{\mathcal{N}_\mathbf{b}} \|\mathbf{x}_i - \bar{\mathbf{x}}_i\|_2^2$. □

The next lemma provides a result that will be useful for bounding the Euclidean norm of the coefficient vectors of basis functions in subsequent error estimates. This result follows from the Rayleigh quotient bounds of the Gram matrix of a basis and is closely related to Theorem 4.2.1.

Lemma 4.3.3 (Rayleigh quotient bounds of the Gram matrix)**.** *Let $\mathcal{V}$ be an inner product space with norm $\|\cdot\|_\mathcal{V}$ induced by the inner product $(\cdot,\cdot)_\mathcal{V}$. Let $\{b_i : i = 1, \ldots, n\}$ be a basis of $\mathcal{V}$. Then, for any finite sequence of real numbers $(c_i)_{i\in\{1,\ldots,n\}}$, it holds that*

$$\lambda_{\min}(\mathbf{B}) \sum_{i=1}^n |c_i|^2 \leq \left\| \sum_{i=1}^n c_i b_i \right\|_\mathcal{V}^2 \leq \lambda_{\max}(\mathbf{B}) \sum_{i=1}^n |c_i|^2,$$

where $\mathbf{B} \in \mathbb{R}^{n\times n}$ is the Gram matrix with $\mathbf{B}_{ij} = (b_i, b_j)_\mathcal{V}$.

Proof. Let $v = \sum_{i=1}^n c_i b_i \in \mathcal{V}$ be arbitrary. Then, we have that

$$\|v\|_\mathcal{V}^2 = (v, v)_\mathcal{V} = \sum_{i=1}^n c_i \sum_{j=1}^n c_j (b_i, b_j)_\mathcal{V} = \mathbf{c}^T\mathbf{B}\mathbf{c}$$

with $\mathbf{c} = [c_1, \ldots, c_n]^T \in \mathbb{R}^n$. Since $\mathbf{B}$ is symmetric, and $\{b_i : i = 1, \ldots, n\}$ forms a basis of $\mathcal{V}$, it follows that $\mathbf{c}^T\mathbf{B}\mathbf{c} = \|v\|_\mathcal{V}^2 > 0$ for any $\mathbf{c} \in \mathbb{R}^n \setminus \{0\}$. Thus, $\mathbf{B}$ is an SPD matrix. Consequently, the associated Rayleigh quotient is bounded by

$$\lambda_{\min}(\mathbf{B}) \leq \frac{\mathbf{c}^T\mathbf{B}\mathbf{c}}{\mathbf{c}^T\mathbf{c}} \leq \lambda_{\max}(\mathbf{b}),$$

where $\lambda_{\min}(\mathbf{B})$ and $\lambda_{\max}(\mathbf{B})$ are the smallest and largest eigenvalues of $\mathbf{B}$, respectively, satisfying $0 < \lambda_{\min}(\mathbf{B}) \leq \lambda_{\max}(\mathbf{B})$. This directly yields the assertion. □

Let $\mathbf{A}_L \in \mathbb{R}^{N_L \times N_L}$ be the full stiffness matrix associated with the HSLOD basis functions with $(\mathbf{A}_L)_{ij} = a(\hat{\psi}_{i,m}, \hat{\psi}_{j,m})$. Let $\mathbf{A}_L^{\mathrm{ML}} \in \mathbb{R}^{N_L \times N_L}$ be the corresponding block-diagonal stiffness matrix with

$$(\mathbf{A}_L^{\mathrm{ML}})_{ij} = \begin{cases} a(\hat{\psi}_{i,m}, \hat{\psi}_{j,m}) & \text{if level}(\hat{\psi}_{i,m}) = \text{level}(\hat{\psi}_{j,m}), \\ 0 & \text{otherwise.} \end{cases}$$

The a posteriori error bound of the level-wise Galerkin method is then given by the following theorem.

Theorem 4.3.4 (Error bound of level-wise Galerkin method)**.** *Let the set $\{g_{i,m} : i = 1, \dots, N_L\}$ be stable in the sense of Theorem 4.2.1. Then, for any $f \in H^s(D)$ with $s \in \{0, 1\}$, the solution of the level-wise Galerkin method introduced in* (4.21) *satisfies*

$$\begin{aligned} \|u - u_{L,m}^{\mathrm{ML}}\|_a \lesssim\ & H_L^{1+s} \|f\|_{H^s(D)} \\ & + C_{\mathrm{rb}}^{1/2} \sqrt{L} m^d \zeta \sigma \|f\|_{L^2(D)} \\ & + \left(\frac{1 + H_L^{-d} \zeta \sigma}{\lambda_{\min}(\mathbf{A}_L)} \right)^{1/2} H_L^{-d} \lambda_{\min}^{-1}\left(\mathbf{A}_L^{\mathrm{ML}}\right) \sqrt{L} m^d \zeta \sigma \|f\|_{L^2(D)} \end{aligned}$$

with C_{rb} from Theorem 4.2.1. This result implies that the level-wise Galerkin approximation converges to the exact solution at an algebraic rate in H_L, up to additional errors due to localization and the truncation of off-block diagonal entries in the hierarchical stiffness matrix.

Proof. Let $\hat{u}$ be the Galerkin approximation in the space $\hat{\mathcal{V}}_{L,m}^{\mathrm{ML}}$, i.e., for all $v \in \hat{\mathcal{V}}_{L,m}^{\mathrm{ML}}$ it holds that

$$a(\hat{u}, v) = (f, v)_{L^2(D)}.$$

Hence, $\hat{u}$ is the approximate solution associated with the full stiffness matrix $\mathbf{A}_L \in \mathbb{R}^{N_L \times N_L}$. Using the triangle inequality, we get that

$$\|u - u_{L,m}^{\mathrm{ML}}\|_a \leq \|u - \hat{u}\|_a + \|\hat{u} - u_{L,m}^{\mathrm{ML}}\|_a. \tag{4.27}$$

By applying Céa's Lemma and Theorem 4.3.1, we obtain for the first term that

$$\|u - \hat{u}\|_a \leq \|u - u_{L,m}^{\mathrm{col}}\|_a \lesssim H_L^{1+s} \|f\|_{H^s(D)} + C_{\mathrm{rb}}^{1/2} \sqrt{L} m^d \zeta \sigma \|f\|_{L^2(D)}. \tag{4.28}$$

To approximate the second term in (4.27), we express both $\hat{u} \in \hat{\mathcal{V}}_L^{\mathrm{ML}}$ and $u_{L,m}^{\mathrm{ML}} \in \hat{\mathcal{V}}_L^{\mathrm{ML}}$ using the HSLOD basis functions. Therefore, we define the right-hand side vector $\mathbf{f} \coloneqq [(f, \hat{\psi}_{1,m})_{L^2(D)}, \cdots, (f, \hat{\psi}_{N_L,m})_{L^2(D)}]^T$. Then, the Galerkin solutions admit the representations

$$\hat{u} = \sum_{i=1}^{N_L} \hat{c}_i \hat{\psi}_{i,m} \quad \text{and} \quad u_{L,m}^{\mathrm{ML}} = \sum_{i=1}^{N_L} c_i^{\mathrm{ML}} \hat{\psi}_{i,m},$$

where $[\hat{c}_1, \dots, \hat{c}_{N_L}]^T = \hat{\mathbf{c}} = \mathbf{A}_L^{-1}\mathbf{f}$ and $[c_1^{\mathrm{ML}}, \dots, c_{N_L}^{\mathrm{ML}}]^T = \mathbf{c}^{\mathrm{ML}} = (\mathbf{A}_L^{\mathrm{ML}})^{-1}\mathbf{f}$. We define the coefficient difference by $\mathbf{c}_d = \hat{\mathbf{c}} - \mathbf{c}^{\mathrm{ML}}$.

Let $\Delta_L^{\mathrm{ML}} := \mathbf{A}_L - \mathbf{A}_L^{\mathrm{ML}}$ denote the matrix of discarded off-block entries. For each level ℓ, let Δ_ℓ be the rectangular submatrix of Δ_L^{ML} consisting of the rows corresponding to those in the ℓ-th diagonal block of $\mathbf{A}_L^{\mathrm{ML}}$. Moreover, let $\mathbf{A}_{\ell\ell}^{(L)}$ be the ℓ-th diagonal block of $\mathbf{A}_L^{\mathrm{ML}}$ and $\mathbf{A}_L$. From Theorem 4.3.2, Theorem 4.3.3, and Friedrichs' inequality, it follows that

$$\begin{aligned}
\|\hat{u} - u_{L,m}^{\mathrm{ML}}\|_a^2 &= \Big\| \sum_{i=1}^{N_L} (\hat{c}_i - c_i^{\mathrm{ML}})\hat{\psi}_i \Big\|_a^2 = \mathbf{c}_d^T \mathbf{A}_L \mathbf{c}_d = \mathbf{c}_d \mathbf{A}_L^{\mathrm{ML}} \mathbf{c}_d + \mathbf{c}_d^T \Delta_L^{\mathrm{ML}} \mathbf{c}_d \\
&\leq \Big(\|\mathbf{A}_L^{\mathrm{ML}}\|_2 + \|\Delta_L^{\mathrm{ML}}\|_2 \Big) \|\mathbf{c}_d\|_2^2 \\
&\leq \Big(\|\mathbf{A}_L^{\mathrm{ML}}\|_2 + \|\Delta_L^{\mathrm{ML}}\|_2 \Big) \sum_{\ell=1}^{L} \frac{\|\Delta_\ell\|_2^2}{\lambda_{\min}^2\Big(\mathbf{A}_{\ell\ell}^{(L)}\Big)} \|\hat{\mathbf{c}}\|_2^2 \\
&\lesssim \Big(\|\mathbf{A}_L^{\mathrm{ML}}\|_2 + \|\Delta_L^{\mathrm{ML}}\|_2 \Big) L \|\Delta_L^{\mathrm{ML}}\|_2^2 \lambda_{\min}^{-2}\Big(\mathbf{A}_L^{\mathrm{ML}}\Big) \frac{\|f\|_{L^2(D)}^2}{\lambda_{\min}(\mathbf{A}_L)}.
\end{aligned}$$

By construction, the localized hierarchical basis functions are normalized with respect to the energy norm. Consequently, for any $i, j \in \{1, \dots, N_L\}$ we have $|a(\hat{\psi}_{i,m}, \hat{\psi}_{j,m})| \leq 1$. This implies that all entries of the matrix $\mathbf{A}_L^{\mathrm{ML}}$ are uniformly bounded in absolute value. Applying Gershgorin's Circle Theorem and exploiting the finite overlap patches, we deduce that

$$\|\mathbf{A}_L^{\mathrm{ML}}\|_2 = \max\{|\lambda_{\min}\Big(\mathbf{A}_L^{\mathrm{ML}}\Big)|, |\lambda_{\max}\Big(\mathbf{A}_L^{\mathrm{ML}}\Big)|\} \lesssim m^d. \tag{4.29}$$

Since Δ_L^{ML} is symmetric as well, Gershgorin's Circle Theorem together with Theorem 4.1.1 yields that

$$\|\Delta_L^{\mathrm{ML}}\|_2 = \max\{|\lambda_{\min}\Big(\Delta_L^{\mathrm{ML}}\Big)|, |\lambda_{\max}\Big(\Delta_L^{\mathrm{ML}}\Big)|\} \lesssim H_L^{-d} m^{d/2} \zeta \sigma, \tag{4.30}$$

leading to the error estimate

$$\|\hat{u} - u_{L,m}^{\mathrm{ML}}\|_a \lesssim \Big(\frac{1 + H_L^{-d}\zeta\sigma}{\lambda_{\min}(\mathbf{A}_L)} \Big)^{1/2} H_L^{-d} \lambda_{\min}^{-1}\Big(\mathbf{A}_L^{\mathrm{ML}}\Big) \sqrt{L} m^d \zeta \sigma \|f\|_{L^2(D)}.$$

Combining this with (4.27) and (4.28) concludes the proof. □

4.4. Additional compression strategies

If the block-diagonal stiffness matrix $\mathbf{A}_L^{\mathrm{ML}}$ is well conditioned, additional compression steps to the level-wise Galerkin method introduced in (4.21) are possible. In this scenario, the inverse of $\mathbf{A}_L^{\mathrm{ML}}$ can be well approximated by a sparse matrix. Consequently, computing the approximate solution of (2.3) using the inverse approximation reduces to the computation of a matrix-vector product.

In this section, we propose two additional compression steps and quantify the resulting approximation error. The first compression step is to approximate the inverse using the Conjugate Gradient (CG) method.

4.4.1. Approximate inverse of block-diagonal stiffness matrix

The inverse of the block-diagonal matrix $\mathbf{A}_L^{\mathrm{ML}}$ is itself a block-diagonal matrix, with diagonal blocks being the inverses of the corresponding blocks of $\mathbf{A}_L^{\mathrm{ML}}$. Notably, the inverse of each block is generally a full matrix (a property derivable from the Cayley-Hamilton theorem, which relates a matrix and its characteristic polynomial). The i-th column of the inverse of the ℓ-th diagonal block of $\mathbf{A}_L^{\mathrm{ML}}$ can be computed by solving the linear system

$$\mathbf{A}_{\ell\ell}^{(L)}\mathbf{c}_\ell^{(i)} = \mathbf{e}_i,$$

where $\mathbf{A}_{\ell\ell}^{(L)}$ denotes the j-th diagonal block of $\mathbf{A}_L^{\mathrm{ML}}$ and $\mathbf{e}_i$ is the i-standard basis vector. If we solve the above linear system iteratively with CG, we obtain the following error bound

$$\left\|\mathbf{c}_\ell^{(i)} - \mathbf{c}_\ell^{(i,k)}\right\|_{\mathbf{A}_{\ell\ell}^{(L)}} \leq 2\left(\frac{\sqrt{\kappa\left(\mathbf{A}_{\ell\ell}^{(L)}\right)}-1}{\sqrt{\kappa\left(\mathbf{A}_{\ell\ell}^{(L)}\right)}+1}\right)^k \left\|\mathbf{c}_\ell^{(i)} - \mathbf{c}_\ell^{(i,0)}\right\|_{\mathbf{A}_{\ell\ell}^{(L)}},$$

where the k-th CG iterate is denoted by $\mathbf{c}_\ell^{(i,k)}$. Thus, the column $\mathbf{c}_\ell^{(i)}$ could be well approximated with a few CG iterations, provided the condition number of $\mathbf{A}_{\ell\ell}^{(L)}$ is small. Consequently, we can accurately approximate the inverse of the diagonal block $\mathbf{A}_{\ell\ell}^{(L)}$ by a cheaply computable sparse matrix $\mathbf{S}_{\ell\ell}^{(k)} \in \mathbb{R}^{N_\ell^b \times N_\ell^b}$, where

$$\mathbf{S}_{\ell\ell}^{(k)} = [\mathbf{c}_\ell^{(1,k)}, \cdots, \mathbf{c}_\ell^{(N_\ell^b,k)}].$$

The approximate inverse of $\mathbf{A}_L^{\mathrm{ML}}$ is then given by the block diagonal matrix $\mathbf{S}^{(k)} \in \mathbb{R}^{N_L \times N_L}$ with diagonal blocks $\mathbf{S}_{11}^{(k)}, \ldots, \mathbf{S}_{LL}^{(k)}$.

The following estimate quantifies the sparsity degree of the blocks of the approximate inverse $\mathbf{S}^{(k)}$, under the assumption of Cartesian meshes. If the CG iterations are initialized with $\mathbf{c}_\ell^{(i,0)} = \mathbf{0}$, the number of non-zero entries in the k-th iterate can be bounded as

$$\mathrm{nnz}\left(\mathbf{c}_\ell^{(i,k)}\right) \leq (1+4mk)^d(2^d-1), \tag{4.31}$$

where the bound is tight (i.e., attained for some $i \leq N_\ell^b$) provided k is such that the right-hand side of the inequality remains below N_ℓ^b.

Remark 4.4.1 (Non-zero entries in CG approximation)**.** The bound in (4.31) can be derived by interpreting $\mathbf{A}_{\ell\ell}^{(L)}$ as the adjacency matrix of a weighted graph $\mathcal{G}$. Then, for $k \geq 1$, the number of nonzeros in $\mathbf{c}_\ell^{(i,k)}$ equals the number of vertices in $\mathcal{G}$ that are reachable from vertex i via a path (a sequence of edges) of length at most $4mk$, considering the vertex i connected to itself.

Using this CG approximation, we set $[c_i^{\mathrm{CG}}, \dots, c_{N_L}^{\mathrm{CG}}]^T = \mathbf{c}^{\mathrm{CG}} = \mathbf{S}^{(k)}\mathbf{f}$ with $\mathbf{f} \coloneqq [(f, \hat{\psi}_1)_{L^2(D)}, \cdots, (f, \hat{\psi}_{N_L})_{L^2(D)}]^T$ and define the corresponding approximate solution to the model problem (2.3) by

$$u_{L,m}^{\mathrm{CG}} \coloneqq \sum_{i=1}^{N_L} c_i^{\mathrm{CG}} \hat{\psi}_{i,m}. \tag{4.32}$$

Theorem 4.4.2 (Error bound using CG approximation)**.** *Let $\delta^{\mathrm{CG}} > 0$ and $k \in \mathbb{N}$ be such that $\left\|(\mathbf{A}_L^{\mathrm{ML}})^{-1} - \mathbf{S}^{(k)}\right\|_2 \leq \delta^{\mathrm{CG}}$, where $\mathbf{S}^{(k)}$ denotes the approximate inverse obtained via k CG iterations. Then, for any right-hand side $f \in L^2(D)$, the additional error incurred by using the approximate solution $u_{L,m}^{\mathrm{CG}}$ from (4.32) instead of the level-wise Galerkin solution $u_{L,m}^{\mathrm{ML}}$ from (4.21) is bounded by*

$$\|u_{L,m}^{\mathrm{ML}} - u_{L,m}^{\mathrm{CG}}\|_a \lesssim \left(1 + H_L^{-d}\zeta\sigma\right)^{1/2} \sqrt{L} m^d \delta^{\mathrm{CG}} \|f\|_{L^2(D)}.$$

Proof. Using the fact that $\operatorname{supp}(\hat{\psi}_{i,m}) \subset D_i$, Friedrichs' inequality and the finite overlap of patches per level, we obtain that

$$\|\mathbf{f}\|_2^2 \leq \sum_{i=1}^{N_L} \|f\|_{L^2(D_i)}^2 \|\hat{\psi}_{i,m}\|_{L^2(D_i)}^2 \lesssim L m^d \|f\|_{L^2(D)}^2,$$

since $\|\hat{\psi}_{i,m}\|_a = 1$ by construction.

As before, we can write the level-wise Galerkin solution as

$$u_{L,m}^{\mathrm{ML}} = \sum_{i=1}^{N_L} c_i^{\mathrm{ML}} \hat{\psi}_i$$

with $[c_1^{\mathrm{ML}}, \dots, c_{N_L}^{\mathrm{ML}}]^T = \mathbf{c}^{\mathrm{ML}} = (\mathbf{A}_L^{\mathrm{ML}})^{-1}\mathbf{f}$. We set $\mathbf{c}_d = \mathbf{c}^{\mathrm{ML}} - \mathbf{c}^{\mathrm{CG}}$ and define the matrix of discarded off-block entries as $\Delta_L^{\mathrm{ML}} := \mathbf{A}_L - \mathbf{A}_L^{\mathrm{ML}}$. Using (4.29) and (4.30), we obtain that

$$\begin{aligned}
\|u_{L,m}^{\mathrm{ML}} - u_{L,m}^{\mathrm{CG}}\|_a^2 &= \left\| \sum_{i=1}^{N_L} (c_i^{\mathrm{ML}} - c_i^{\mathrm{CG}}) \hat{\psi}_i \right\|_a^2 = \mathbf{c}_d^T \left(\mathbf{A}_L^{\mathrm{ML}} + \Delta_L^{\mathrm{ML}}\right) \mathbf{c}_d \\
&\leq \left(\|\mathbf{A}_L^{\mathrm{ML}}\|_2 + \left\|\Delta_L^{\mathrm{ML}}\right\|_2\right) \|\mathbf{c}_d\|_2^2 \\
&\lesssim m^d \left(1 + H_L^{-d}\zeta\sigma\right) \left(\|(\mathbf{A}_L^{\mathrm{ML}})^{-1} - \mathbf{S}^{(k_{\delta^{\mathrm{CG}}})}\|_2 \|\mathbf{f}\|_2\right)^2 \\
&\lesssim m^d \left(1 + H_L^{-d}\zeta\sigma\right) \left(\sqrt{L} m^{d/2} \delta^{\mathrm{CG}} \|f\|_{L^2(D)}\right)^2.
\end{aligned}$$

As a direct consequence, the statement follows. □

4.4.2. Disregarding small entries in approximate inverse

In this section, we introduce the second compression stage, which consists of neglecting small entries in the approximate inverse $\mathbf{S}^{(k)}$, which is obtained via

the CG method. Let $\mathbf{S}_\epsilon \in \mathbb{R}^{N_L \times N_L}$ denote this matrix resulting from discarding all entries of $\mathbf{S}^{(k)}$ whose absolute value is smaller than a given tolerance $\epsilon > 0$. Furthermore, let N_ϵ be the maximal number of entries in any row or column of $\mathbf{S}^{(k)}$ with absolute value smaller than ϵ. Then, it follows that

$$\|\mathbf{S}_\epsilon - \mathbf{S}^{(k)}\|_2 \leq \sqrt{\|\mathbf{S}_\epsilon - \mathbf{S}^{(k)}\|_1 \|\mathbf{S}_\epsilon - \mathbf{S}^{(k)}\|_\infty} \leq N_\epsilon \epsilon. \tag{4.33}$$

We set $[c_i^{(\epsilon)}, \dots, c_{N_L}^{(\epsilon)}]^T = \mathbf{c}^{(\epsilon)} = \mathbf{S}_\epsilon \mathbf{f}$ and define the corresponding approximate solution to the model problem (2.3) by

$$u_{L,m}^{(\epsilon)} \coloneqq \sum_{i=1}^{N_L} c_i^{(\epsilon)} \hat{\psi}_i. \tag{4.34}$$

With the same procedure employed in Theorem 4.4.2, and using (4.33), we obtain the following approximation result.

Theorem 4.4.3 (Error bound using truncated approximate inverse)**.** *Let $\epsilon > 0$. Then, for any right-hand side $f \in L^2(D)$, the additional error incurred by using the truncated matrix $\mathbf{S}_\epsilon$, leading to the approximate solution $u_{L,m}^{(\epsilon)}$ from* (4.34)*, instead of the CG approximation $\mathbf{S}^{(k)}$, is bounded by*

$$\|u_{L,m}^{\mathrm{CG}} - u_{L,m}^{(\epsilon)}\|_a \lesssim \left(1 + H^{-d}\zeta\sigma\right)^{1/2} \sqrt{L} m^d N_\epsilon \epsilon \|f\|_{L^2(D)}.$$

Collecting the approximation results from Section 4.3 and the additional compression steps discussed above, we derive the following error estimate for the approximate solution incorporating all compression steps.

Corollary 4.4.4 (Overall error estimate)**.** *Let $\{g_{i,m} : i = 1, \dots, N_L\}$ be stable in the sense of Theorem 4.2.1. For any $f \in H^s(D)$ with $s \in \{0, 1\}$, the approximate solution $u_{L,m}^{(\epsilon)}$ defined in* (4.34) *satisfies*

$$\begin{aligned} \|u - u_{L,m}^{(\epsilon)}\|_a \lesssim\ & \left(H_L^{s+1} + C_{\mathrm{rb}}^{1/2} \sqrt{L} m^d \zeta\sigma\right) \|f\|_{H^s(D)} \\ & + m^d \sqrt{L(1 + H_L^{-d}\zeta\sigma)} \\ & \times \left(\frac{\zeta\sigma}{H_L^d \lambda_{\min}^{1/2}(\mathbf{A}_L) \lambda_{\min}\left(\mathbf{A}_L^{\mathrm{ML}}\right)} + \delta^{\mathrm{CG}} + N_\epsilon \epsilon\right) \|f\|_{L^2(D)}, \end{aligned}$$

where $\delta^{\mathrm{CG}} > 0$ and $\epsilon > 0$ are small parameters proportional to the prescribed accuracy.

4.5. Condition number of the hierarchical stiffness matrix

In this section, we analyze the conditioning of the diagonal blocks of the hierarchical stiffness matrix $\mathbf{A}_L^{\mathrm{ML}}$. The analysis is inspired by techniques developed

in [FP20, Lemma 6]. The resulting theorem shows that the condition numbers of these blocks are independent of the mesh size, except for the block associated with the first level. Condition (4.8) plays a crucial role in this. Additionally, this result provides further insight into the accuracy of the error estimates established in the preceding sections.

We consider the level-wise defined HSLOD basis functions $\hat{\psi}^{\mathrm{hslod}}_{\ell,i,m}$ from (4.7) and their normalized counterparts $\hat{\psi}_{\ell,i,m}$ from (4.11). We can write the L^2-orthogonal projection onto piecewise constants of those functions as

$$\Pi_\ell \hat{\psi}^{\mathrm{hslod}}_{\ell,i,m} = \sum_{K\in\mathcal{T}_\ell} p^{(i)}_K \mathbb{1}_K \quad \text{and} \quad \Pi_\ell \hat{\psi}_{\ell,i,m} = \sum_{K\in\mathcal{T}_\ell} \hat{p}^{(i)}_K \mathbb{1}_K. \tag{4.35}$$

Using the above coefficient vectors, we define the matrices $\mathbf{P}_\ell, \hat{\mathbf{P}}_\ell \in \mathbb{R}^{N_\ell \times N^b_\ell}$ with

$$(\mathbf{P}_\ell)_{ij} = p^{(j)}_{K_i} \quad \text{and} \quad (\hat{\mathbf{P}}_\ell)_{ij} = \hat{p}^{(j)}_{K_i}. \tag{4.36}$$

From (4.11), it follows that $\hat{\mathbf{P}}_\ell = \mathbf{P}_\ell \mathbf{N}_\ell$ where $\mathbf{N}_\ell \in \mathbb{R}^{N^b_\ell \times N^b_\ell}$ is the diagonal matrix such that $(\mathbf{N}_\ell)_{ii} = \|\hat{\psi}^{\mathrm{hslod}}_{\ell,i,m}\|_a^{-1}$.

In the following we want to give an estimate of the condition number and the smallest eigenvalue of the blocks $\mathbf{A}^{(L)}_{\ell\ell}$ of the hierarchical stiffness matrix. Therefore, we provide first the following two lemmas, giving an estimate for the smallest eigenvalues of the matrices $\mathbf{N}_\ell$ and $\mathbf{P}^T_\ell \mathbf{P}_\ell$, respectively.

Lemma 4.5.1 (Smallest eigenvalue of $\mathbf{N}_\ell$)**.** *For each level $1 \le \ell \le L$, the smallest eigenvalue of the diagonal matrix $\mathbf{N}_\ell \in \mathbb{R}^{N^b_\ell \times N^b_\ell}$ with $(\mathbf{N}_\ell)_{ii} = \|\hat{\psi}^{\mathrm{hslod}}_{\ell,i,m}\|_a^{-1}$ satisfies*

$$\lambda_{\min}(\mathbf{N}_\ell) \gtrsim m^{-d} H_\ell^{1-d/2}.$$

Proof. Analogous to (3.23), the SLOD basis functions used in the construction of the hierarchical basis can be obtained by applying a correction to the LOD functions; see Section 3.4.4. We denote these SLOD functions by $\tilde{\varphi}^{\mathrm{slod}}_{\ell,K,m}$, and their, with respect to the local source terms, normalized counterparts by $\hat{\varphi}^{\mathrm{slod}}_{\ell,K,m}$. According to the definition of $\hat{\psi}^{\mathrm{hslod}}_{\ell,i,m}$ in (4.7), we have

$$\hat{\psi}^{\mathrm{hslod}}_{\ell,i,m} = \sum_{K\in S^{(\ell)}_{J_i}} \tilde{d}^{(i)}_K \tilde{\varphi}^{\mathrm{slod}}_{\ell,K,m}, \tag{4.37}$$

where $\tilde{d}^{(i)}_K = d^{(i)}_K / \|\tilde{g}^{\mathrm{slod}}_{\ell,K,m}\|_{L^2(D)}$. We collect these coefficients into the vector $\tilde{\mathbf{d}}^{(i)} = (\tilde{d}^{(i)}_K)_{K\in S^{(\ell)}_{J_i}}$.

For a fixed oversampling parameter $m \in \mathbb{N}$ and a fixed level $1 \le \ell \le L$, we denote by $D_{J_i} = \mathsf{N}^m_{\ell-1}(T_{J_i})$ the patch associated to the hierarchical basis function $\hat{\psi}^{\mathrm{hslod}}_{\ell,i,m}$. Consider the SLOD function $\tilde{\varphi}^{\mathrm{slod}}_{\ell,K,m}$ for some $K \in S^{(\ell)}_{J_i}$. The L^2-orthogonal projection of $\tilde{\varphi}^{\mathrm{slod}}_{\ell,K,m}$ onto $\mathbb{P}^0(\mathcal{T}_{\ell-1,D_{J_i}})$ can be written as

$$\Pi_{\ell-1} \tilde{\varphi}^{\mathrm{slod}}_{\ell,K,m} = \sum_{T\in\mathcal{T}_{\ell-1,D_{J_i}}} q^{(K)}_T \mathbb{1}_T,$$

and the projection onto $\mathbb{P}^0(\mathcal{T}_{\ell,D_{J_i}})$ as

$$\Pi_\ell \tilde{\varphi}^{\mathrm{slod}}_{\ell,K,m} = \sum_{T\in\mathcal{T}_{\ell,D_{J_i}}} c_T^{(K)} \mathbb{1}_T. \tag{4.38}$$

Using these coefficients, we define the matrices $\mathbf{Q} \in \mathbb{R}^{N_q\times N_s}$ and $\mathbf{C} \in \mathbb{R}^{N_c\times N_s}$ by setting $\mathbf{Q}_{pj} = q_{T_p}^{(K_j)}$ and $\mathbf{C}_{pj} = c_{T_p}^{(K_j)}$, where

$$N_q = \#\mathcal{T}_{\ell-1,D_{J_i}}, \quad N_c = \#\mathcal{T}_{\ell,D_{J_i}} \quad \text{and} \quad N_s = \#S^{(\ell)}_{J_i}.$$

Finally, let $\mathbf{B} \in \mathbb{R}^{N_s\times \#\mathrm{Ker}(\mathbf{Q})}$ be the matrix whose columns form an orthonormal basis of $\mathrm{Ker}(\mathbf{Q})$.

Using condition (4.8), we deduce that $\tilde{\mathbf{d}}^{(i)} = \mathbf{B}\mathbf{y}$ for some $\mathbf{y} \in \mathbb{R}^{\#\mathrm{Ker}(\mathbf{Q})}$. To satisfy condition (4.9), we require

$$\mathbf{C}\mathbf{B}\mathbf{y} = \mathbf{e}_{K_i} - \mathbf{e}_{\widetilde{K}}, \tag{4.39}$$

where $\mathbf{e}_{K_i}, \mathbf{e}_{\widetilde{K}} \in \mathbb{R}^{N_c}$ are canonical unit vectors, with all entries zero except for those corresponding to the elements $K_i \in \widetilde{\mathrm{des}}(T_{J_i})$ and $\widetilde{K} \in \mathrm{des}(T_{J_i}) \setminus \widetilde{\mathrm{des}}(T_{J_i})$, respectively. Since $\mathbf{C}\mathbf{B}$ is, in general, a rectangular matrix, equation (4.39) can typically only be solved in the least-squares sense. The least-squares solution is given by

$$\mathbf{y} = \Big((\mathbf{C}\mathbf{B})^T\mathbf{C}\mathbf{B}\Big)^{-1}(\mathbf{C}\mathbf{B})^T(\mathbf{e}_{K_i} - \mathbf{e}_{\widetilde{K}}). \tag{4.40}$$

Note that all entries of the matrices $\mathbf{C}$, $\mathbf{B}$, and the vectors $\mathbf{e}_{K_i}$, $\mathbf{e}_{\widetilde{K}}$ are mesh-independent. Moreover, from (3.24), the absolute values of the entries of $\mathbf{C}$ are uniformly bounded by 1. Consequently, from the expression in (4.40), it follows that the entries of $\tilde{\mathbf{d}}^{(i)}$ are also mesh-independent. Additionally, according to [FP20, Equation (2.9)], the energy norm of LOD basis functions is of order $\mathcal{O}\Big(H_\ell^{d/2-1}\Big)$, which, by construction of the SLOD functions, implies

$$\|\tilde{\varphi}^{\mathrm{slod}}_{\ell,K,m}\|_a = \mathcal{O}\Big(H_\ell^{d/2-1}\Big).$$

Combining this with the representation in (4.37), we obtain

$$\|\hat{\psi}^{\mathrm{hslod}}_{\ell,i,m}\|_a \le \sum_{K\in S^{(\ell)}_{J_i}} |\tilde{d}_K^{(i)}| \|\tilde{\varphi}^{\mathrm{slod}}_{\ell,K,m}\|_a \lesssim N_s H_\ell^{d/2-1} \lesssim m^d H_\ell^{d/2-1},$$

where we used $N_s = \#S^{(\ell)}_{J_i} \lesssim m^d$. From the definition of $\mathbf{N}_\ell$, the assertion follows directly. □

Lemma 4.5.2 (Smallest eigenvalue of $\mathbf{P}_\ell^T\mathbf{P}_\ell$)**.** *The smallest eigenvalue of the matrix $\mathbf{P}_\ell^T\mathbf{P}_\ell \in \mathbb{R}^{N_\ell^b\times N_\ell^b}$, where the matrix $\mathbf{P}_\ell$ is defined in* (4.36)*, satisfies for each level $1 \le \ell \le L$ that*

$$\lambda_{\min}(\mathbf{P}_\ell^T\mathbf{P}_\ell) = \mathcal{O}(1).$$

Proof. Combining (4.35), (4.37) and (4.38), we deduce that

$$p_K^{(i)} = \sum_{T \in S_{J_i}^{(\ell)}} \tilde{d}_T^{(i)} c_K^{(T)}$$

for $K \in \mathcal{T}_{\ell, D_{J_i}}$. Since both $c_K^{(T)}$ and $\tilde{d}_T^{(i)}$ are mesh independent, it follows that $p_K^{(i)}$ is $\mathcal{O}(1)$. Furthermore, for $\ell > 1$, if conditions (4.8) and (4.9) were exactly satisfied, we would have

$$\begin{aligned}
p_{K_i}^{(i)} &= \sum_{T \in \mathcal{T}_\ell} \tilde{d}_T^{(i)} c_{K_i}^{(T)} = 1 \quad \text{for } K_i \in \widetilde{\text{des}}(T_{J_i}), \\
p_{\widetilde{K}}^{(i)} &= \sum_{T \in \mathcal{T}_\ell} \tilde{d}_T^{(i)} c_{\widetilde{K}}^{(T)} = -1 \quad \text{for } \widetilde{K} \in \text{des}(T_{J_i}) \setminus \widetilde{\text{des}}(T_{J_i}), \\
p_K^{(i)} &= \sum_{T \in \mathcal{T}_\ell} \tilde{d}_T^{(i)} c_K^{(T)} = 0 \quad \text{for all } K \notin \{K_i, \widetilde{K}\}.
\end{aligned}$$

This implies that $\mathbf{P}_\ell^T \mathbf{P}_\ell$ would be block diagonal, with each block of dimension $(2^d-1) \times (2^d-1)$, where the diagonal entries are all equal to 2 and the off-diagonal entries are all equal to 1. Thus, the smallest eigenvalue of each block would be 1 and consequently, $\lambda_{\min}(\mathbf{P}_\ell^T \mathbf{P}_\ell) = 1$. In general, however, condition (4.9) cannot be satisfied exactly but only in the least-squares-error sense. Nevertheless, if the least-squares error is sufficiently small, $\lambda_{\min}(\mathbf{P}_\ell^T \mathbf{P}_\ell)$ should remain well away from 0.

At level $\ell = 1$, the basis functions correspond to standard SLOD basis functions, and hence $\mathbf{P}_1 = \mathbf{C}$. From condition (3.24), we know that $\mathbf{C} = \mathbf{I} + \delta$, where $\mathbf{I}$ is the identity matrix and δ has zero diagonal entries and off-diagonal entries bounded by δ_s in absolute value. Therefore, $\mathbf{C}$ is a perturbed identity matrix. If δ_s from condition (3.24) is small enough, the smallest eigenvalue of $\mathbf{C}^T\mathbf{C}$ will remain far from 0, ensuring that the basis at level $\ell = 1$ is well-behaved. □

Note that the entries of the i-th column of $\mathbf{P}_\ell$ reflect the degree to which the function $\hat{\psi}_{\ell,i,m}$ is concentrated in each element of $\mathcal{T}_\ell$. Consequently, the smallest eigenvalue $\lambda_{\min}(\mathbf{P}_\ell^T \mathbf{P}_\ell)$ serves as an indicator of the linear independence of the basis set $\{\hat{\psi}_{\ell,i,m} : i = 1, \ldots, N_\ell^b\}$, and hence, of the overall basis quality. The closer this value is to 1 and the farther it is from 0, the more linearly independent (and numerically stable) the basis functions are.

We are now prepared to derive an upper bound for the condition number of the hierarchical stiffness matrix.

Theorem 4.5.3 (Condition number of the block-diagonal stiffness matrix)**.** *The condition number of the diagonal blocks $\mathbf{A}_{\ell\ell}^{(L)}$ of the hierarchical stiffness matrix $\mathbf{A}_L^{\text{ML}}$ is mesh independent for $\ell > 1$ and $\mathcal{O}(H_1^{-2})$ for $\ell = 1$. More precisely, it holds that*

$$\kappa\left(\mathbf{A}_{\ell\ell}^{(L)}\right) \lesssim \begin{cases} m^{3d} \lambda_{\min}(\mathbf{P}_\ell^T \mathbf{P}_\ell)^{-1} & \ell > 1, \\ m^{3d} H_1^{-2} \lambda_{\min}(\mathbf{P}_1^T \mathbf{P}_1)^{-1} & \ell = 1, \end{cases} \tag{4.41}$$

with $\lambda_{\min}(\mathbf{P}_\ell^T\mathbf{P}_\ell) = \mathcal{O}(1)$ *for all* $1 \leq \ell \leq L$. *Furthermore, the smallest eigenvalue of* $\mathbf{A}_{\ell\ell}^{(L)}$ *satisfies*

$$\lambda_{\min}\big(\mathbf{A}_{\ell\ell}^{(L)}\big) \gtrsim \begin{cases} m^{-2d}\lambda_{\min}(\mathbf{P}_\ell^T\mathbf{P}_\ell) & \ell > 1, \\ m^{-2d}H_1^2\lambda_{\min}(\mathbf{P}_1^T\mathbf{P}_1) & \ell = 1, \end{cases} \tag{4.42}$$

Proof. First, using the Rayleigh quotient and the definitions of the matrices $\mathbf{P}_\ell$ and $\hat{\mathbf{P}}_\ell$ from (4.36), we obtain for any level $\ell \geq 1$ and all $\mathbf{x} \in \mathbb{R}^{N_\ell^b} \setminus \{\mathbf{0}\}$ that

$$\begin{aligned} \mathbf{x}^T\hat{\mathbf{P}}_\ell^T\hat{\mathbf{P}}_\ell\mathbf{x} = \mathbf{x}^T\mathbf{N}_\ell\mathbf{P}_\ell^T\mathbf{P}_\ell\mathbf{N}_\ell\mathbf{x} &\geq \lambda_{\min}(\mathbf{P}_\ell^T\mathbf{P}_\ell)\mathbf{x}^T\mathbf{N}_\ell^2\mathbf{x} \\ &\geq \lambda_{\min}(\mathbf{P}_\ell^T\mathbf{P}_\ell)\lambda_{\min}(\mathbf{N}_\ell^2)\mathbf{x}^T\mathbf{x}. \end{aligned}$$

Consequently, using Theorem 4.5.1 yields

$$\lambda_{\min}(\hat{\mathbf{P}}_\ell^T\hat{\mathbf{P}}_\ell) \geq \lambda_{\min}(\mathbf{P}_\ell^T\mathbf{P}_\ell)\lambda_{\min}(\mathbf{N}_\ell^2) \gtrsim m^{-2d}H_\ell^{2-d}\lambda_{\min}(\mathbf{P}_\ell^T\mathbf{P}_\ell) \tag{4.43}$$

with $\lambda_{\min}(\mathbf{P}^T\mathbf{P}) = \mathcal{O}(1)$, see Theorem 4.5.2.

Using the Rayleigh quotient bound and $|K| \gtrsim H_\ell^d$ for $K \in \mathcal{T}_\ell$, we establish for an arbitrary $\mathbf{c} = (c_i)_{i\in\{1,\dots,N_\ell^b\}} \in \mathbb{R}^{N_\ell^b}$ that

$$\Big\| \sum_{i=1}^{N_\ell^b} c_i \Pi_\ell \hat{\psi}_{\ell,i,m} \Big\|_{L^2(D)}^2 \gtrsim H_\ell^d \mathbf{c}^T\hat{\mathbf{P}}_\ell^T\hat{\mathbf{P}}_\ell\mathbf{c} \geq H_\ell^d \lambda_{\min}(\hat{\mathbf{P}}_\ell^T\hat{\mathbf{P}}_\ell) \sum_{i=1}^{N_\ell^b} c_i^2.$$

On the other hand, applying the stability and approximation properties (2.6) and (2.7) of the L^2-orthogonal projection Π_ℓ, (4.8), and the fact that $H_{\ell-1} = 2H_\ell$, we obtain for $\ell > 1$ that

$$\begin{aligned} \Big\| \sum_{i=1}^{N_\ell^b} c_i \Pi_\ell \hat{\psi}_{\ell,i,m} \Big\|_{L^2(D)}^2 &\leq \Big\| \sum_{i=1}^{N_\ell^b} c_i \hat{\psi}_{\ell,i,m} \Big\|_{L^2(D)}^2 \\ &= \Big\| (1 - \Pi_{\ell-1}) \sum_{i=1}^{N_\ell^b} c_i \hat{\psi}_{\ell,i,m} \Big\|_{L^2(D)}^2 \\ &\lesssim H_{\ell-1}^2 \Big\| \sum_{i=1}^{N_\ell^b} c_i \hat{\psi}_{\ell,i,m} \Big\|_a^2 \lesssim H_\ell^2 \Big\| \sum_{i=1}^{N_\ell^b} c_i \hat{\psi}_{\ell,i,m} \Big\|_a^2. \end{aligned} \tag{4.44}$$

Combining the previous three inequalities yields

$$\Big\| \sum_{i=1}^{N_\ell^b} c_i \hat{\psi}_{\ell,i,m} \Big\|_a^2 \gtrsim m^{-2d} \lambda_{\min}(\mathbf{P}_\ell^T\mathbf{P}_\ell) \sum_{i=1}^{N_\ell^b} c_i^2.$$

Theorem 4.3.3 then implies the first line of (4.42). The case $\ell = 1$ follows almost analogously, where we use Friedrichs' inequality after the first line of (4.44).

Since $|a(\hat{\psi}_{\ell,i,m}, \hat{\psi}_{\ell,j,m})| \leq 1$ for all $i, j \in \{1, \dots, N_\ell^b\}$, the Gershgorin Circle Theorem implies that $\lambda_{\max}\big(\mathbf{A}_{\ell\ell}^{(L)}\big) \lesssim m^d$. Combining this upper bound with the lower bound from (4.42) establishes the condition number estimate stated in (4.41) for the hierarchical blocks. □

The above theorem, in combination with Theorem 4.5.2, indicates that the condition number of the diagonal blocks $\mathbf{A}_{\ell\ell}^{(L)}$, and thus of the full matrix $\mathbf{A}_L^{\mathrm{ML}}$, is influenced by the degree of linear independence of the basis functions at level ℓ. It is also worth noting that the contrast of the diffusion coefficient may affect the conditioning via the hidden constants in the stated estimates.

Moreover, by applying Weyl's inequality, we can bound the smallest eigenvalue of the full hierarchical stiffness matrix $\mathbf{A}_L$ from below in terms of the smallest eigenvalue of the block-diagonal matrix $\mathbf{A}_L^{\mathrm{ML}}$. The latter can, in turn, be estimated using Theorem 4.5.3. Let $\Delta_L^{\mathrm{ML}} := \mathbf{A}_L - \mathbf{A}_L^{\mathrm{ML}}$. Then, using the estimate (4.30), we obtain that

$$\begin{aligned}\lambda_{\min}(\mathbf{A}_L) &\geq \lambda_{\min}(\mathbf{A}_L^{\mathrm{ML}}) - \max\{|\lambda_{\min}(\Delta_L^{\mathrm{ML}})|, |\lambda_{\max}(\Delta_L^{\mathrm{ML}})|\} \\ &\gtrsim \lambda_{\min}(\mathbf{A}_L^{\mathrm{ML}}) - H^{-d} m^{d/2} \zeta \sigma.\end{aligned}$$

In the last step, we examine ζ, providing an upper bound on the Euclidean norm of the coefficient vectors from (4.12) defining the hierarchical basis functions. Using Theorem 4.3.3 and the definition of $\hat{\psi}_{\ell,i,m}$ in (4.13) yields that

$$\sum_{K \in S_{J_i}^{(\ell)}} |\hat{d}_K^{(\ell,i)}|^2 \leq \lambda_{\min}^{-1}\big(\mathbf{A}_{\ell,m}^{\mathrm{slod}}\big) \big\|\hat{\psi}_{\ell,i,m}\big\|_a^2 = \lambda_{\min}^{-1}\big(\mathbf{A}_{\ell,m}^{\mathrm{slod}}\big),$$

where $\mathbf{A}_{\ell,m}^{\mathrm{slod}} \in \mathbb{R}^{N_\ell^b \times N_\ell^b}$ denotes the stiffness matrix associated with the SLOD basis functions $\hat{\varphi}_{\ell,K,m}^{\mathrm{slod}}$ at level ℓ. According to the case $\ell = 1$ in (4.42), its smallest eigenvalue is bounded from below.

As a consequence, assuming stability and sufficient linear independence of the basis functions, we obtain an a priori error estimate. In particular, due to the exponential decay of the localization error indicator σ, the error matches that of classical SLOD or LOD methods, provided the oversampling parameter is chosen sufficiently large, i.e., $m \gtrsim |\log(H_L)|$.

4.6. Numerical Experiments

In this section, we present numerical experiments to validate our theoretical findings. For practical implementation, all infinite-dimensional problems arising in the solution of local patch problems are replaced by their $\mathbb{P}^1$-finite element discretizations on a fine mesh $\mathcal{T}_h$ with mesh size 2^{-10}, obtained through successive uniform refinements of $\mathcal{T}_L$. For stability of the SLOD basis, we employ condition (3.24) with $\delta_s = 0.5$. Additionally, we compute a reference solution u_h using the standard finite element method on $\mathcal{T}_h$ with $\mathbb{P}^1$-finite elements.

We consider two types of coefficients: a highly-heterogeneous piecewise constant one, and coefficients with high-contrast channels; see Figure 3.12 and Figure 4.5 for an example of each, respectively. In all cases, we utilize uniform Cartesian meshes over the unit square $D = (0,1)^2$ where the mesh size denotes the side length of the elements.

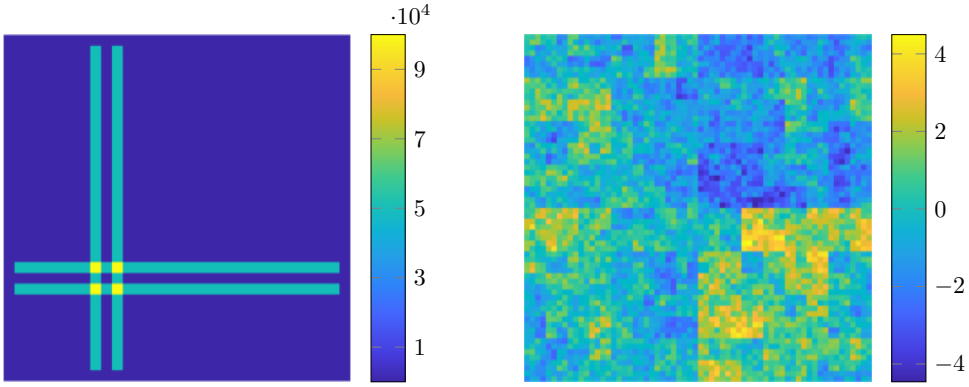

Figure 4.5.: Coefficient with high-contrast channels (left) and piecewise constant right-hand side $f \in L^2(D)$ with respect to the mesh with mesh size 2^{-6} (right).

In our numerical experiments, we consider two types of right-hand sides. First, the same smooth right-hand side $f \in H^1(D)$ as in the previous chapter, given by

$$f(x_1, x_2) = 2\pi^2 \sin(x_1) \sin(x_2). \tag{4.45}$$

Second, we employ a piecewise constant right-hand side $f \in L^2(D)$ with respect to the mesh $\mathcal{T}_f$ with mesh size 2^{-6}; see Figure 4.5. More precisely, we choose $f = \sum_{\ell=0}^{6} f_\ell$ with $f_\ell \in \mathbb{P}^0(\mathcal{T}_\ell)$ and $H_\ell = 2^{-\ell}$, where the values of each contribution f_ℓ are randomly chosen within the interval $[-1, 1]$. With this choice, we ensure that the contribution of each level to the approximate solution is non-zero.

Highly heterogeneous piecewise-constant coefficients

In our first set of experiments, we select a high-contrast coefficient A which is piecewise constant with respect to the mesh of mesh size 2^{-8}. The coefficient assumes independent and identically distributed element values ranging between $\alpha = 10^{-4}$ and $\beta = 1$. In the specific realization we consider, these boundary values are almost assumed, resulting in an actual contrast of $9.2 \cdot 10^3$.

Figure 4.6 illustrates the complete stiffness matrix associated with the HSLOD basis for different values of the patch order m. As discussed in Section 4.1, the practical hierarchical method does not yield a fully a-orthogonal basis, leading to the appearance of some non-zero off-block-diagonal entries in the stiffness matrix. However, the a-inner product between two non-orthogonal basis functions at distinct levels is small and diminishes further with increasing m. Consequently, the block-diagonal approximation, which is obtained by discarding all off-block-diagonal entries, serves as an accurate approximation to the full stiffness matrix, particularly for larger values of m.

Figure 4.7 shows the system matrix corresponding to the piecewise constant local source terms used in the collocation-type HSLOD approximation. While this matrix exhibits the same structural pattern as the full stiffness matrix, its

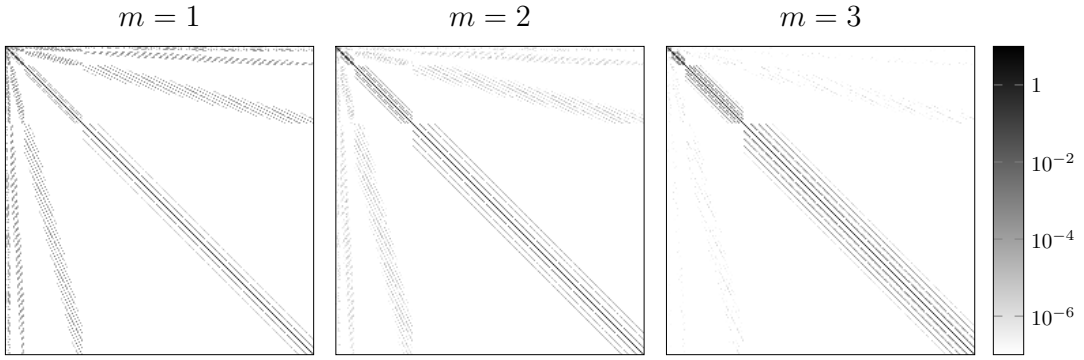

Figure 4.6.: Sparsity pattern of the complete hierarchical stiffness matrix for varying patch orders m.

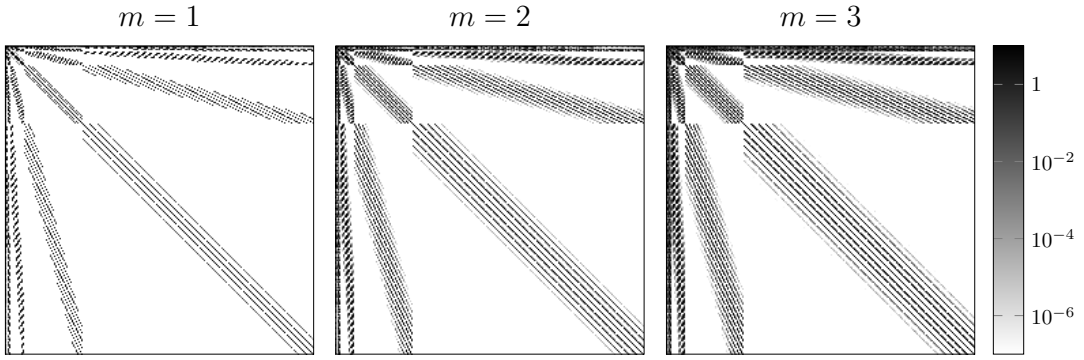

Figure 4.7.: Sparsity pattern of the system matrix associated to the local source terms for varying patch orders m.

off-block-diagonal entries remain relatively large and do not decay with increasing oversampling parameter m. As a result, the contributions from different levels in the collocation-type formulation cannot be computed independently, requiring the entire system matrix to be assembled and considered as a whole. Nonetheless, the hierarchical structure leads to a significant improvement in the conditioning of the system matrix compared to the standard SLOD approach.

Small condition numbers of the diagonal blocks of the stiffness matrix are crucial for the fast computation of their approximate inverses using the CG method. The condition numbers of the diagonal blocks are presented in Table 4.1. Consistent with Theorem 4.5.3, these blocks exhibit good conditioning, with condition numbers remaining stable across finer levels. This stability enables a reliable approximation of the inverse using only a few CG iterations.

The inverse of the block-diagonal stiffness matrix, its CG approximation, and the sparsification of this approximation according to Section 4.4.2 are illustrated in Figure 4.8. The number of non-zero entries in the sparsified CG approximation of the hierarchical stiffness matrix is reduced by more than a factor of ten compared to the complete block-diagonal inverse, and by nearly a

Table 4.1.: Properties of the diagonal blocks of the HSLOD stiffness matrix and the relative energy error of the approximate solution $u_{h,\ell,m}^{(\epsilon)}$ as defined in (4.34) for a piecewise constant coefficient with $m = 2$. The approximate solution is computed using ℓ levels of the hierarchy, with a maximum of seven CG iterations to approximate the inverse blocks of the hierarchical stiffness matrix and an entry cut-off tolerance of $\epsilon = 10^{-5}$.

ℓ	1	2	3	4	5	6
H_ℓ	2^{-1}	2^{-2}	2^{-3}	2^{-4}	2^{-5}	2^{-6}
$\mathrm{cond}(\mathbf{A}_{\ell\ell}^L)$	4	5	17	20	17	18
$\|u_h - u_{h,\ell,m}^{(\epsilon)}\|_a / \|u_h\|_a$	0.2297	0.0491	0.0117	0.0029	0.0007	0.0002

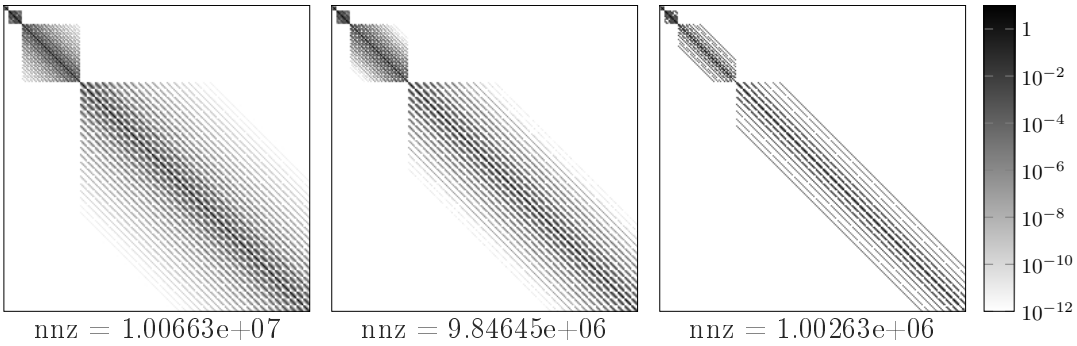

Figure 4.8.: Sparsity pattern and number of nonzeros of the inverse of the stiffness matrix after the different compression stages. Left: inverse of block-diagonal matrix; middle: CG approximation of each inverted block after seven iterations; right: discarding entries of the CG approximation with absolute value smaller than 10^{-5}. The patch order is set to $m = 2$.

factor of ten compared to the number of non-zero entries in the finite element stiffness matrix used to compute u_h. In Table 4.1, we present the relative energy error of the approximate solution for the smooth right-hand side of (4.45) using this sparsified inverse approximation.

Figure 4.9 displays the relative energy errors of the level-wise Galerkin method and the collocation-type approximation, defined in (4.21) and (4.22), respectively, for various patch orders m and coarse mesh sizes H_L applied to both types of right-hand sides f. For comparison, we also include the relative energy errors of the HLOD method, which is computed using the level-wise Galerkin approach. Since the HSLOD basis functions incorporate corrections to the standard LOD functions, the HLOD method corresponds to the case where

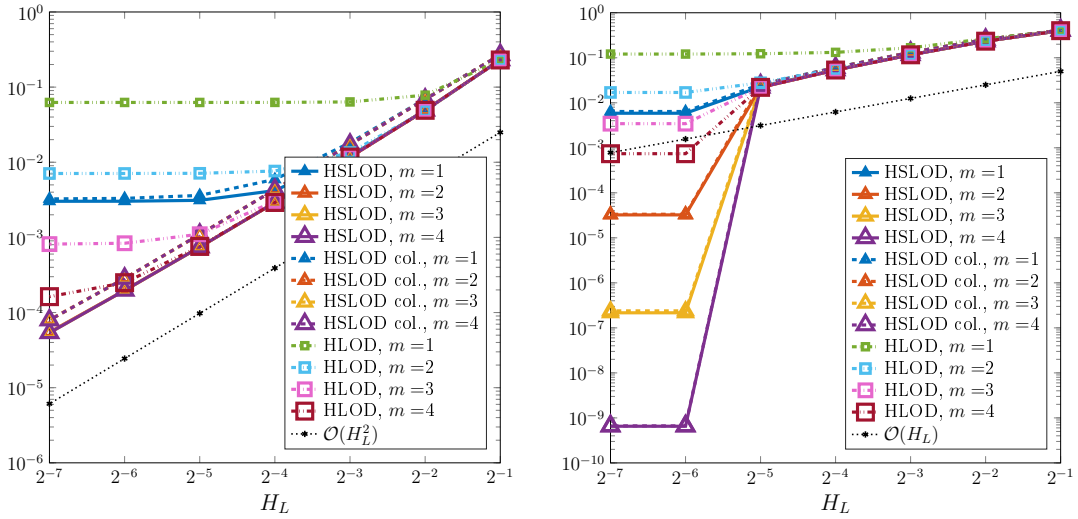

Figure 4.9.: Relative energy errors of the HSLOD and the HLOD in dependence of the mesh size H_L for the highly-heterogeneous piecewise constant coefficient. Left: errors for a smooth right-hand side, right: errors for a piecewise constant right-hand side.

these corrections are omitted. Due to condition (4.8), this version of the HLOD method exhibits a similar error behavior to the stabilized HLOD approach introduced in [HP22a], which is based on [FP20]. Furthermore, this stabilized method achieves higher accuracy than the gamblets-based approach of [Owh17], as discussed in [HP22a, Section 8.2]. Notably, both HSLOD methods consistently outperform the HLOD across all displayed parameters m, demonstrating superior accuracy.

Although the error analysis bounds the error of the level-wise Galerkin method by that of the collocation-type approximation, practical results show that, when a difference is observed, the collocation variant typically yields slightly larger errors. This suggests that the error introduced by neglecting the off-block-diagonal entries in the stiffness matrix is negligible. For a smooth right-hand side, the error in the energy norm obtained with the HSLOD methods exhibit the optimal convergence rate of $\mathcal{O}(H_L^2)$ for $m > 1$. In the case of a piecewise constant right-hand side $f \in L^2(D)$, the expected error rate of $\mathcal{O}(H_L)$ is observed, provided that no mesh in the hierarchy resolves the underlying mesh of f. However, if the finest mesh in the hierarchy does resolve $\mathcal{T}_f$, the HSLOD solution is exact up to localization error (collocation variant) plus an additional error due to omitting the off-block-diagonal entries in the stiffness matrix (level-wise Galerkin method). Both errors scale proportionally to σ (cf. Theorem 4.3.4), leading to super-exponential decay with respect to the localization parameter m and thus significantly smaller errors for the HSLOD methods compared to the HLOD. This is also illustrated in Figure 4.10, which shows the relative energy errors of the HSLOD and HLOD methods as a function of m, using six levels in the mesh

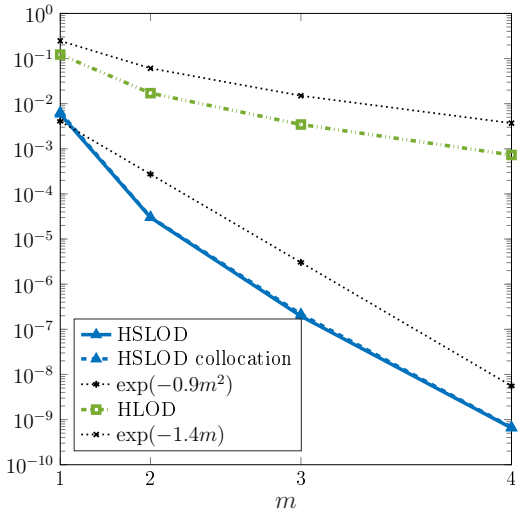

Figure 4.10.: Relative energy errors of the HSLOD and the HLOD methods as a function of the oversampling parameter m, for a highly heterogeneous piecewise constant coefficient and a piecewise constant right-hand side. The mesh hierarchy consists of six levels with $H_L = 2^{-6}$.

hierarchy with $H_L = 2^{-6}$.

Figures 4.11 to 4.13 show the relative energy errors of the HSLOD and HLOD methods, plotted against the online computing time in seconds or the number of nonzero entries in the approximate inverse of the stiffness matrix, for various numbers of compression stages. The markers indicate the hierarchy levels, with mesh sizes ranging from $H = 2^{-1}$ to $H = 2^{-7}$. The comparison between the level-wise Galerkin and the collocation-type methods is shown in Figure 4.11. After a few levels, the level-wise Galerkin method outperforms the collocation-type method in terms of online computation time because, for the collocation-type method, at each level the whole system matrix must be considered, and contributions from different levels cannot be computed independently. It is important to note, however, that the assembly of the system matrices, which is more costly for the Galerkin method, is not included in the reported online times.

The benefit of additional compression stages with respect to online performance is clearly visible. Figure 4.12 presents the energy error using the CG method with up to seven iterations, while Figure 4.13 shows results for the trimmed CG method, where entries with absolute value below 10^{-5} in the CG approximation are neglected. In this case, the reduction in the number of nonzero entries in the approximate inverse is also apparent.

It is also noteworthy that variations in the parameters α or β do not produce significant differences in the error plots or condition numbers. Hence, for this type of coefficient, the HSLOD method performs well even in the presence of

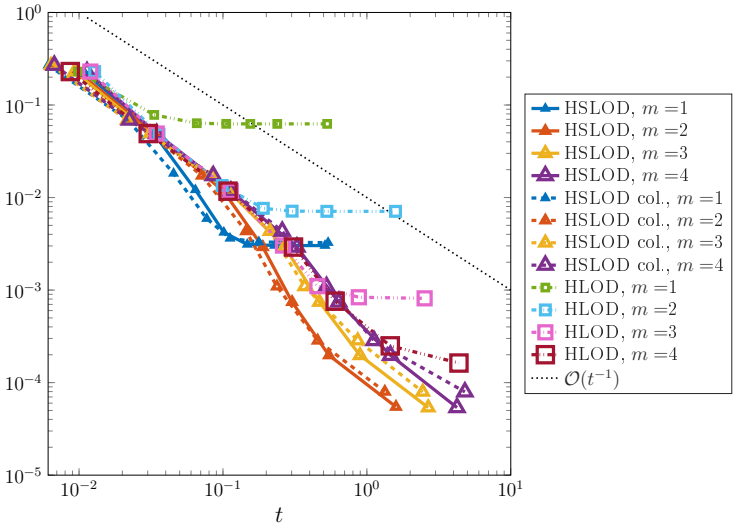

Figure 4.11.: Relative energy errors of the HSLOD and the HLOD methods as a function of the online computing time, for a highly heterogeneous piecewise constant coefficient and a smooth right-hand side.

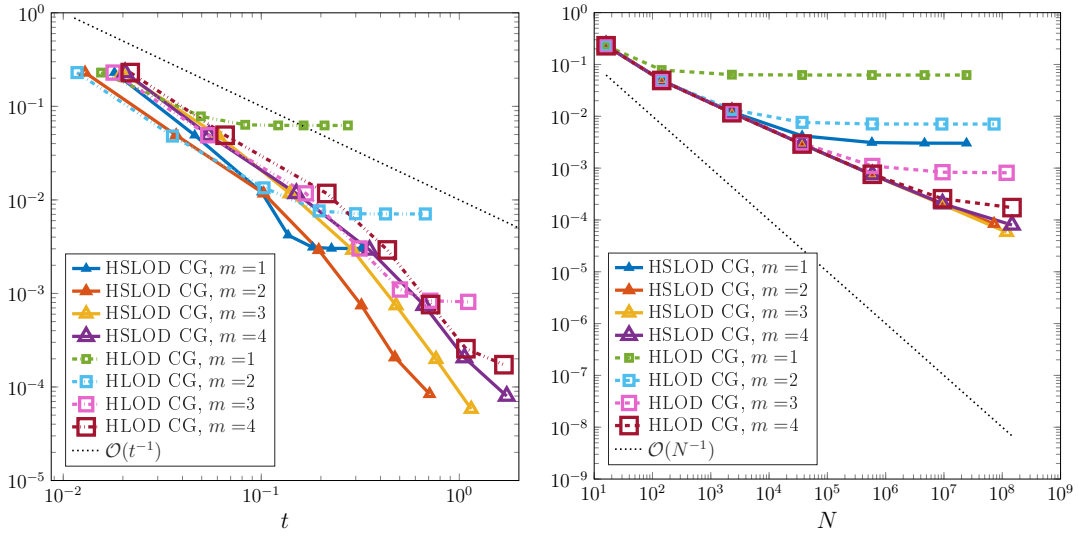

Figure 4.12.: Relative energy errors $\|u_h - u_{h,L,m}^{\mathrm{CG}}\|_a / \|u_h\|_a$ of the HSLOD and the HLOD methods, using the CG method to approximate the inverse stiffness matrix, as a function of the online computing time (left) and the number of nonzero entries in the approximate inverse (right) for a highly heterogeneous piecewise constant coefficient and a smooth right-hand side.

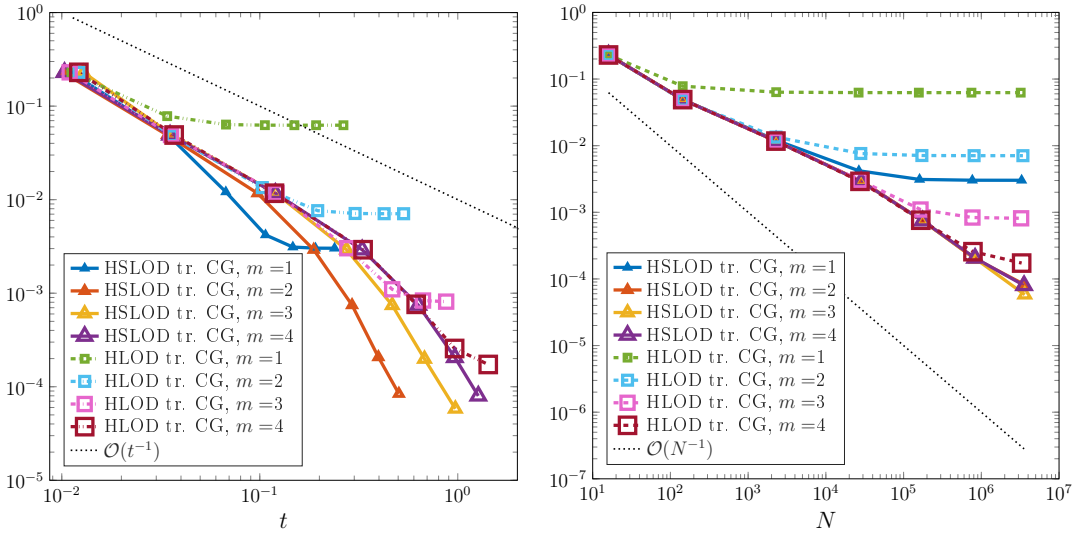

Figure 4.13.: Relative energy errors $\|u_h - u_{h,L,m}^{(\epsilon)}\|_a / \|u_h\|_a$ of the HSLOD and HLOD methods, using the trimmed CG method to approximate the inverse stiffness matrix, as a function of the online computing time (left) and the number of nonzero entries in the approximate inverse (right) for a highly heterogeneous piecewise constant coefficient and a smooth right-hand side.

high contrasts in the coefficient.

High-contrast channels

Next, we consider the coefficient from Figure 4.5, which exhibits high-contrast channels, leading to increasing difficulty in the problem. The channels are defined on a mesh with mesh size 2^{-5}. The precise definition of the coefficient is as follows:

$$A(x) = A(x_1, x_2) \coloneqq A_1(x_1, x_2) + A_1(x_2, x_1),$$

with

$$A_1(x) \coloneqq \begin{cases} \beta/2, & x \in [\frac{8}{32}, \frac{9}{32}] \times [\frac{1}{32}, \frac{31}{32}] \cup [\frac{10}{32}, \frac{11}{32}] \times [\frac{1}{32}, \frac{31}{32}] \\ 1/2, & \text{elsewhere.} \end{cases}$$

For this setup with the smooth right-hand side from (4.45), Figure 4.14 shows the relative energy errors of the HSLOD and HLOD methods for various combinations of contrast and patch order. We observed that for higher contrasts, larger values of m are necessary to achieve the optimal convergence rate of $\mathcal{O}(H_L^2)$. As in the case of the highly-heterogeneous piecewise constant coefficient, the HSLOD consistently outperforms the HLOD for all cases shown, leading to improvements over [PS16] in particular. Especially for higher contrasts, the superiority of the HSLOD is evident.

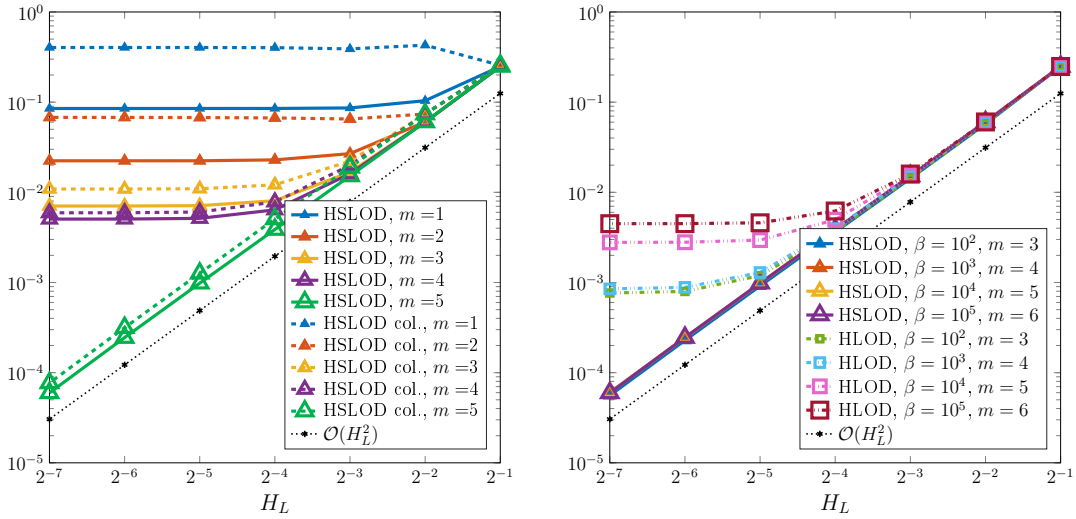

Figure 4.14.: Relative energy errors of the HSLOD and HLOD methods as a function of the mesh size H_L, for a coefficient with high-contrast channels and a smooth right-hand side. Left: results for a fixed contrast with $\beta = 10^4$; right: results for various combinations of m and β.

The condition numbers of the blocks of the HSLOD stiffness matrix for the same combinations of m and β as in the right panel of Figure 4.14 are shown in Table 4.2. For these cases, the condition numbers grow with increasing β for levels with mesh sizes close to the width of the channels. For the other levels, however, the condition numbers remain stable over different contrasts. Note that this stability is only observed when the patch order is increased for higher contrasts, leading to our choice of $m = k + 1$ for $\beta = 10^k$.

Table 4.2.: Condition numbers of the blocks of the stiffness matrix for the high-contrast channel coefficient for varying contrasts and patch orders, rounded to two significant figures.

H_ℓ	2^{-1}	2^{-2}	2^{-3}	2^{-4}	2^{-5}	2^{-6}	2^{-7}
$\beta = 10^2, m = 3$	3	8	24	110	51	17	17
$\beta = 10^3, m = 4$	3	8	370	1100	680	76	56
$\beta = 10^4, m = 5$	4	7	120	21.000	3.000	26	26
$\beta = 10^5, m = 6$	4	7	120	$1.7 \cdot 10^6$	33.000	21	21

Part II.

Random coefficients

5. Super-Localized Numerical Stochastic Homogenization

In this part of the thesis, we consider the prototypical random diffusion problem

$$-\mathrm{div}(\boldsymbol{A}\nabla \boldsymbol{u}) = f$$

subject to homogeneous Dirichlet boundary conditions, where microscopic features of the problem are encapsulated in the random diffusion coefficient $\boldsymbol{A}$. In the following, we present a computationally simple and efficient numerical stochastic homogenization method tailored for such problems, based on a collocation-type formulation of the SLOD introduced in Chapter 3.

In the deterministic case, the SLOD method constructs an almost local basis by applying the solution operator to $\mathbb{P}^0(\mathcal{T}_H)$, the space of piecewise constants on a coarse mesh $\mathcal{T}_H$. This involves selecting locally supported piecewise constant right-hand sides whose localized responses have minimal conormal derivative. The stochastic setting requires modifying this approach by choosing deterministic local source terms that minimize the expected conormal derivative of the localized responses.

A key advantage of the collocation-type formulation, in contrast to Galerkin methods, is that it eliminates the need to assemble a global stiffness matrix, which would require communication between basis functions defined on different coarse patches. Instead, only a system of linear equations on the coarse mesh corresponding to the local source terms needs to be solved. This enables each patch to be processed independently, significantly improving parallelization and accelerating the method's assembly process. Moreover, the favorable localization properties of the SLOD allow for an efficient sampling procedure.

In the case of a random diffusion coefficient with a small correlation length, and under the standard assumptions of quantitative stochastic homogenization, we provide an error estimate for the coarse-scale approximation of the presented method. This estimate incorporates certain SLOD-specific quantities in an a posteriori manner. The proof is grounded in the framework of quantitative stochastic homogenization (see, e.g., [GO11, GO12, GNO14, GNO20]). To further analyze key components of the error such as the localization error and the Riesz stability constant, we use classical LOD techniques [MP14, HP13, AHP21], and additionally conduct an a priori error analysis for the expected overall localization error. However, similar to the deterministic SLOD setting, the a priori stability of the basis functions cannot be guaranteed. Nevertheless, a practical solution to address this issue in implementation is provided.

The content and presentation of this chapter are largely based on the journal article

[HMP25] M. Hauck, H. Mohr, and D. Peterseim. A simple collocation-type approach to numerical stochastic homogenization. *Multiscale Model. Simul.*, 23(1):374–396, 2025

with significant sections taken verbatim.

5.1. Model problem

In this part of the thesis, we consider the prototypical random diffusion problem

$$\left\{\begin{aligned} -\operatorname{div}(\boldsymbol{A}(\omega)(x)\nabla \boldsymbol{u}(\omega)(x)) &= f(x), && x \in D \\ \boldsymbol{u}(\omega)(x) &= 0, && x \in \partial D \end{aligned}\right\} \quad \text{for almost all } \omega \in \Omega, \tag{5.1}$$

where $(\Omega, \mathcal{F}, \mathbb{P})$ denotes the underlying probability space, $f \in L^2(D)$ is a deterministic right-hand side and D is a d-dimensional bounded polygonal Lipschitz domain with $d \in \{1, 2, 3\}$. Without loss of generality, we assume that D is scaled to unit size. The diffusion coefficient $\boldsymbol{A}$ is an $\mathbb{R}^{d\times d}$-valued random field that is pointwise symmetric, Bochner measurable, and satisfies uniform ellipticity and boundedness conditions. Specifically, there exist constants $0 < \alpha \leq \beta < \infty$ such that, for almost all $\omega \in \Omega$, the inequality

$$\alpha\|\eta\|_2^2 \leq (\boldsymbol{A}(\omega)(x)\eta)\cdot\eta \leq \beta\|\eta\|_2^2 \tag{5.2}$$

holds for all $\eta \in \mathbb{R}^d$ and almost all $x \in \mathbb{R}^d$.

Subsequently, we introduce a shorthand notation for norms and inner products of Bochner spaces. Let X be a Hilbert space equipped with the inner product $(\cdot,\cdot)_X$. In this case, the Bochner space $L^2(\Omega; X)$, denoting the space of X-valued random fields with finite second moments, is also a Hilbert space with the inner product

$$(\boldsymbol{v}, \boldsymbol{w})_{L^2(\Omega;X)} \coloneqq \mathbb{E}\Big[(\boldsymbol{v}(\omega), \boldsymbol{w}(\omega))_X\Big].$$

We write $\|\cdot\|^2_{L^2(\Omega;X)} \coloneqq (\cdot,\cdot)_{L^2(\Omega;X)}$ for the induced norm of this inner product.

The weak formulation of the model problem (5.1) seeks an $H^1_0(D)$-valued random field $\boldsymbol{u}$ such that for almost all $\omega \in \Omega$ it holds that

$$\boldsymbol{a}_\omega(\boldsymbol{u}(\omega), v) \coloneqq \int_D (\boldsymbol{A}(\omega)\nabla\boldsymbol{u}(\omega))\cdot\nabla v \,\mathrm{d}x = (f\,,\, v)_{L^2(D)} \tag{5.3}$$

for all $v \in H^1_0(D)$. Under the given assumptions, the bilinear from $\boldsymbol{a}_\omega$ depends continuously on $\boldsymbol{A}$ and, in particular, is measurable as a function of ω. Hence, the above problem can be reformulated in the Hilbert space $L^2(\Omega; H^1_0(D))$. The

Lax–Milgram theorem then proves its well-posedness, i.e., there exists a unique solution $\boldsymbol{u} \in L^2(\Omega; H^1_0(D))$ satisfying

$$\|\nabla \boldsymbol{u}\|_{L^2(\Omega;L^2(D))} \leq \alpha^{-1} \frac{\operatorname{diam}(D)}{\pi} \|f\|_{L^2(D)}. \tag{5.4}$$

For the sake of readability, we indicate the dependence of stochastic variables from now on only by a bold symbol.

5.2. Numerical stochastic homogenization method

In the following section, we determine deterministic local source terms that minimize the expected conormal derivative of the localized responses, adapting the approach from Section 3.1 to the stochastic setting. For the derivation of basis functions, we consider a fixed element $K \in \mathcal{T}_H$ and oversampling parameter $m \in \mathbb{N}$, assuming that the patch $D_K \coloneqq \mathsf{N}^m(K)$, as defined in (2.14), does not cover the entire domain. The deterministic source term corresponding to K is denoted by $g^{\mathrm{slod}}_{K,m} \in \mathbb{P}^0(\mathcal{T}_{H,D_K})$, where the submesh $\mathcal{T}_{H,D_K}$ consists of elements $T \in \mathcal{T}_H$ contained in the patch D_K.

The global response $\boldsymbol{\varphi}^{\mathrm{slod}}_{K,m} \in L^2(\Omega; H^1_0(D))$ to $g^{\mathrm{slod}}_{K,m}$ is given for almost all $\omega \in \Omega$ by

$$\boldsymbol{a}(\boldsymbol{\varphi}^{\mathrm{slod}}_{K,m}, v) = (g^{\mathrm{slod}}_{K,m}\,,\, v)_{L^2(D)} \tag{5.5}$$

for all $v \in H^1_0(D)$. Its localized counterpart $\hat{\boldsymbol{\varphi}}^{\mathrm{slod}}_{K,m} \in L^2(\Omega; H^1_0(D_K))$ is for almost all $\omega \in \Omega$ defined by

$$\boldsymbol{a}(\hat{\boldsymbol{\varphi}}^{\mathrm{slod}}_{K,m}, v) = (g^{\mathrm{slod}}_{K,m}\,,\, v)_{L^2(D_K)} \tag{5.6}$$

for all $v \in H^1_0(D_K)$. The right choice of $g^{\mathrm{slod}}_{K,m}$ is again crucial for the approximation properties of the local version $\hat{\boldsymbol{\varphi}}^{\mathrm{slod}}_{K,m}$.

Analogous to (3.3), we denote the classical trace operator restricted to the complete subspace $H^1_\Gamma(D_K) \subset H^1(D_K)$, consisting of functions with trace zero on the boundary segment $\Gamma \coloneqq \partial D_K \cap \partial D$, by

$$\operatorname{tr} = \operatorname{tr}_{D_K} \colon H^1_\Gamma(D_K) \to X \coloneqq \operatorname{range} \operatorname{tr} \subset H^{1/2}(\partial D_K).$$

As an extension operator, we henceforth consider the $\boldsymbol{A}$-harmonic extension operator $\mathbf{tr}^{-1} \colon L^2(\Omega; X) \to L^2(\Omega; H^1_\Gamma(D_K))$ defined as follows: for almost all $\omega \in \Omega$ and for any given $\boldsymbol{b} \in L^2(\Omega; X)$, we set

$$(\operatorname{tr} \mathbf{tr}^{-1} \boldsymbol{b})(\omega) = \boldsymbol{b}(\omega)$$

and require that

$$\boldsymbol{a}(\mathbf{tr}^{-1}\boldsymbol{b}, v) = 0 \quad \text{for all } v \in H^1_0(D_K). \tag{5.7}$$

The space of locally $\boldsymbol{A}$-harmonic functions satisfying homogeneous Dirichlet boundary conditions on Γ is then given by

$$\boldsymbol{Y} \coloneqq \mathbf{tr}^{-1} L^2(\Omega; X) \subset L^2(\Omega; H^1_\Gamma(D_K)).$$

Similar to Theorem 3.1.1, we derive the identity

$$\boldsymbol{a}(\boldsymbol{\varphi}^{\mathrm{slod}}_{K,m} - \hat{\boldsymbol{\varphi}}^{\mathrm{slod}}_{K,m}, \boldsymbol{v}) = (g^{\mathrm{slod}}_{K,m}, \boldsymbol{v})_{L^2(D_K)} - \boldsymbol{a}(\hat{\boldsymbol{\varphi}}^{\mathrm{slod}}_{K,m}, \boldsymbol{v}) = (g^{\mathrm{slod}}_{K,m}, \mathbf{tr}^{-1}\mathrm{tr}\, \boldsymbol{v})_{L^2(D_K)}.$$

Taking the expectation yields, for any $\boldsymbol{v} \in L^2(\Omega; H^1_0(D))$, that

$$\mathbb{E}\Big[\boldsymbol{a}(\boldsymbol{\varphi}^{\mathrm{slod}}_{K,m} - \hat{\boldsymbol{\varphi}}^{\mathrm{slod}}_{K,m}, \boldsymbol{v})\Big] = \Big(g^{\mathrm{slod}}_{K,m}, \Pi_{H,D_K}\, \mathbb{E}[\mathbf{tr}^{-1}\mathrm{tr}\, \boldsymbol{v}]\Big)_{L^2(D_K)}. \tag{5.8}$$

As a consequence, the (almost) L^2-orthogonality of the local source term $g^{\mathrm{slod}}_{K,m}$ to the space $\mathbb{E}[\boldsymbol{Y}] \subset H^1_\Gamma(D_K)$ ensures a small expected localization error for the basis function $\hat{\boldsymbol{\varphi}}^{\mathrm{slod}}_{K,m}$.

Therefore, we can obtain an optimal choice of $g^{\mathrm{slod}}_{K,m}$ by performing an SVD of the compact operator $(\Pi_{H,D_K} \circ \mathbb{E})|_{\boldsymbol{Y}} : \boldsymbol{Y} \to \mathbb{P}^0(\mathcal{T}_{H,D_K})$ restricted to the complete subspace $\boldsymbol{Y}$. Note that the rank of $(\Pi_{H,D_K} \circ \mathbb{E})|_{\boldsymbol{Y}}$ is less than or equal to $N \coloneqq \#\mathcal{T}_{H,D_K}$. Hence, the SVD is given by

$$(\Pi_{H,D_K} \circ \mathbb{E})|_{\boldsymbol{Y}}\, \boldsymbol{v} = \sum_{k=1}^{N} \sigma_k(\boldsymbol{v}, \boldsymbol{w}_k)_{L^2(\Omega;H^1(D_K))} g_k \tag{5.9}$$

where $\sigma_1 \geq \cdots \geq \sigma_N \geq 0$ are the singular values, $g_1, \ldots, g_N$ form an orthonormal set of left singular vectors in $L^2(D_K)$, and $\boldsymbol{w}_1, \ldots, \boldsymbol{w}_N$ are the corresponding $L^2(\Omega; H^1(D_K))$-orthonormal right singular vectors.

The left singular vector g_N is an optimal choice for the local source term $g^{\mathrm{slod}}_{K,m}$ and the corresponding smallest singular value σ_N is a measure of the quasi-orthogonality between $g^{\mathrm{slod}}_{K,m}$ and $\mathbb{E}[\boldsymbol{Y}]$. Hence, we define

$$\sigma_K(H, \varepsilon, m) \coloneqq \sigma_N = \sup_{\boldsymbol{v} \in \boldsymbol{Y} \,:\, \|\boldsymbol{v}\|_{L^2(\Omega;H^1(D_K))}=1} (g_N, \mathbb{E}[\boldsymbol{v}])_{L^2(D_K)}, \tag{5.10}$$

where the parameter $\varepsilon > 0$ denotes the correlation length of the random coefficient $\boldsymbol{A}$, which will be rigorously introduced in Theorem 5.3.1 below.

We emphasize that the practical implementation of the SVD in (5.9) is challenging due to the stochasticity involved. A feasible approach based on sampling is described in Section 5.5. For the error analysis in the following section, we introduce the quantity

$$\sigma \coloneqq \sigma(H, \varepsilon, m) \coloneqq \max_{K \in \mathcal{T}_H} \sigma_K(H, \varepsilon, m), \tag{5.11}$$

which is an indicator for the overall localization error.

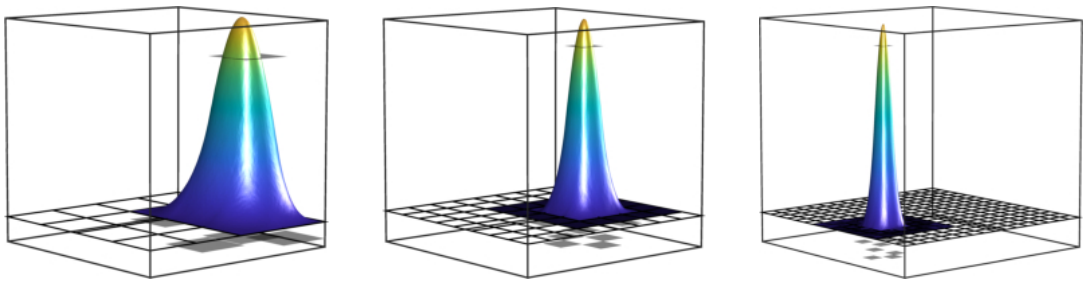

Figure 5.1.: Illustration of the localized basis functions $\mathbb{E}[\hat{\boldsymbol{\varphi}}_{K,m}^{\mathrm{slod}}]$ obtained by the presented stochastic homogenization method on successively refined meshes for a piecewise constant random coefficient with a correlation length of $\varepsilon = 2^{-7}$ in two spatial dimensions. Various values of the oversampling parameter are depicted with $m = 1$ (left), $m = 2$ (middle), and $m = 3$ (right). The corresponding L^2-normalized local source terms $g_{K,m}^{\mathrm{slod}}$ are shown in gray.

Given that, in expectation, $\hat{\boldsymbol{\varphi}}_{K,m}^{\mathrm{slod}}$ closely approximates the response of the global solution operator applied to $g_{K,m}^{\mathrm{slod}}$, it is reasonable to define the approximation of a non-Galerkin, collocation-type numerical stochastic homogenization method by

$$\bar{u}_{H,m}^{\mathrm{slod}} \coloneqq \sum_{K \in \mathcal{T}_H} c_K \Pi_H \mathbb{E}[\hat{\boldsymbol{\varphi}}_{K,m}^{\mathrm{slod}}], \tag{5.12}$$

where $(c_K)_{K \in \mathcal{T}_H}$ are the coefficients of the expansion of $\Pi_H f$ in terms of the basis functions $\{g_{K,m}^{\mathrm{slod}} : K \in \mathcal{T}_H\}$. An illustration of the deterministic basis functions $\mathbb{E}[\hat{\boldsymbol{\varphi}}_{K,m}^{\mathrm{slod}}]$ can be found in Figure 5.1.

5.3. Error analysis

In this section, we conduct an error analysis of the presented stochastic homogenization method. To do so, we first outline the necessary assumptions and lemmas, which will lead to the final error analysis at the end of the section.

We begin by specifying the structural conditions on the randomness of the coefficient field $\boldsymbol{A}$, which are required to apply results from the theory of quantitative stochastic homogenization. For simplicity, these conditions are formulated for coefficient fields defined on $\mathbb{R}^d$. Therefore, the following assumptions implicitly assume that the coefficient field is defined on the entire space $\mathbb{R}^d$, though a random field defined on the bounded domain D can be obtained by restriction.

Assumption 5.3.1 (Stationarity and decorrelation)**.** Assume that the random coefficient field $\boldsymbol{A}$ is

- *stationary*, i.e., the law of the shifted coefficient field $\boldsymbol{A}(\omega)(\cdot + x)$ coincides with the law of $\boldsymbol{A}(\omega)(\cdot)$ for all $x \in \mathbb{R}^d$,

- *quantitatively decorrelated* on scales larger than ε in the sense of the spectral gap inequality with correlation length $\varepsilon > 0$, i.e., there exists a constant $\rho > 0$ such that for any Fréchet differentiable random variable $F = F(\boldsymbol{A})$ the estimate

$$\mathbb{E}\Big[|F - \mathbb{E}[F]|^2\Big] \leq \frac{\varepsilon^d}{\rho}\,\mathbb{E}\left[\int_{\mathbb{R}^d}\left(\fint_{B_\varepsilon(x)}\left|\frac{\partial F}{\partial \boldsymbol{A}}(\tilde{x})\right|\mathrm{d}\tilde{x}\right)^2\mathrm{d}x\right] \tag{5.13}$$

  holds.

For an introduction to the notion of Fréchet derivatives, we refer the reader exemplarily to [Dei85, Chapter 2]; see also [JO22, Section 3.1] for a definition in the present context. We emphasize that the conditions in Theorem 5.3.1 on the random coefficient $\boldsymbol{A}$ are standard in the theory of quantitative stochastic homogenization; see, e.g., the work [GNO20].

The error analysis of the presented numerical stochastic homogenization method is based on the so-called Calderón–Zygmund estimates, which are a popular tool in the theory of quantitative stochastic homogenization. Such estimates were established for an equation on the full space $\mathbb{R}^d$ in [DO20], extending earlier results from [AD16, DGO20]. For annealed Calderón–Zygmund estimates we refer to [JO22, WX24], where the latter work considers the case of Lipschitz domains. Contrary to the Calderón–Zygmund estimate given below, these annealed estimates involve only a loss in stochastic integrability and not in spatial integrability. Since such annealed estimates only lead to better (hidden) constants in the final error bounds, we will henceforth stick to a suboptimal Calderón–Zygmund estimate similar to [FGP21, Lemma 4.8], where an a priori error analysis for a related numerical stochastic homogenization method in the context of LOD is performed. The proof of the following estimate, which is beyond the scope of this thesis, is analogous to the full-space case [DO20, Theorem 6.1] and uses the boundary regularity theory of [FR17, JRS24] as well as a classical regularity theory at edges and corners.

Lemma 5.3.2 (Calderón–Zygmund estimate)**.** *Let $d \in \{2, 3\}$, and let $\boldsymbol{A}$ be a random coefficient field subject to* (5.2) *and Theorem 5.3.1. Let $Q \subset \mathbb{R}^d$ be a box, let $\boldsymbol{h} \in L^2(\Omega; L^2(Q))$, and let $\boldsymbol{u} \in L^2(\Omega; H^1_0(Q))$ be a solution to the linear elliptic PDE*

$$\begin{aligned} -\nabla\cdot(\boldsymbol{A}\nabla\boldsymbol{u}) &= \nabla\cdot\boldsymbol{h} && \text{on } Q,\\ \boldsymbol{u} &\equiv 0 && \text{on } \partial Q. \end{aligned}$$

Then, for any $2 \leq p < \infty$ and any $p < q < \infty$, there holds a regularity estimate of the form

$$\fint_Q \mathbb{E}\left[\left(\fint_{B_\varepsilon(x)}|\nabla\boldsymbol{u}|^2\,\mathrm{d}\tilde{x}\right)^{p/2}\right]\mathrm{d}x \lesssim \left(\fint_Q \mathbb{E}\left[\left(\fint_{B_\varepsilon(x)}|\boldsymbol{h}|^2\,\mathrm{d}\tilde{x}\right)^{q/2}\right]\mathrm{d}x\right)^{p/q},$$

where the hidden constant depends on the bounds α, β of $\boldsymbol{A}$, the constant ρ from Theorem 5.3.1 and p and q.

To handle the stochasticity in the error analysis, we need to estimate the variance of the random variables $(\hat{\boldsymbol{\varphi}}^{\mathrm{slod}}_{K,m}, \mathbb{1}_T)_{L^2(T)}$ for any $K \in \mathcal{T}_H$ and $T \in \mathcal{T}_{H,D_K}$, where $\mathbb{1}_T$ denotes the indicator function of the element T. To achieve this, we employ the spectral gap inequality (5.13) from Theorem 5.3.1. The following lemma provides a representation of the Fréchet derivative of $(\hat{\boldsymbol{\varphi}}^{\mathrm{slod}}_{K,m}, \mathbb{1}_T)_{L^2(T)}$, a crucial element for this particular step.

Lemma 5.3.3 (L^2-representation of Fréchet derivative)**.** *Let $\boldsymbol{v} \in L^2(\Omega; H^1_0(D_K))$ for almost all $\omega \in \Omega$ be defined as the weak solution to*

$$\begin{cases} -\operatorname{div}(\boldsymbol{A}\nabla \boldsymbol{v}) &= \mathbb{1}_T \quad \text{in } D_K, \\ \boldsymbol{v} &= 0 \quad \text{on } \partial D_K. \end{cases} \tag{5.14}$$

The L^2-representation of the Fréchet derivative of $(\hat{\boldsymbol{\varphi}}^{\mathrm{slod}}_{K,m}, \mathbb{1}_T)_{L^2(T)}$ is then given by

$$\frac{\partial}{\partial \boldsymbol{A}}(\hat{\boldsymbol{\varphi}}^{\mathrm{slod}}_{K,m}, \mathbb{1}_T)_{L^2(T)} = -\nabla \hat{\boldsymbol{\varphi}}^{\mathrm{slod}}_{K,m} \otimes \nabla \boldsymbol{v},$$

where $\otimes\colon \mathbb{R}^d \times \mathbb{R}^d \to \mathbb{R}^{d\times d}$ denotes the outer product.

Proof. Let $\omega \in \Omega$ be fixed. We rewrite the Fréchet derivative of $(\hat{\boldsymbol{\varphi}}^{\mathrm{slod}}_{K,m}, \mathbb{1}_T)_{L^2(T)}$ with respect to $L^2(\mathbb{R}^d; \mathbb{R}^{d\times d})$ as

$$\begin{aligned} \frac{\partial}{\partial \boldsymbol{A}}(\hat{\boldsymbol{\varphi}}^{\mathrm{slod}}_{K,m}, \mathbb{1}_T)_{L^2(T)}(\delta \boldsymbol{A}) &= \Big(\frac{\partial \hat{\boldsymbol{\varphi}}^{\mathrm{slod}}_{K,m}}{\partial \boldsymbol{A}}(\delta \boldsymbol{A}), \mathbb{1}_T\Big)_{L^2(T)} \\ &= \int_{D_K} (\boldsymbol{A}\nabla \boldsymbol{v}) \cdot \nabla \frac{\partial \hat{\boldsymbol{\varphi}}^{\mathrm{slod}}_{K,m}}{\partial \boldsymbol{A}}(\delta \boldsymbol{A})\,\mathrm{d}x, \end{aligned}$$

where we tested the weak formulation of (5.14) with $\frac{\partial \hat{\boldsymbol{\varphi}}^{\mathrm{slod}}_{K,m}}{\partial \boldsymbol{A}}(\delta \boldsymbol{A})(\omega) \in H^1_0(D_K)$. To further simplify the expression on the right-hand side, we differentiate the local patch problems given in (5.6) with respect to $\boldsymbol{A}$ using the product rule. This gives for any $w \in H^1_0(D_K)$ that

$$\int_{D_K} \big(\delta \boldsymbol{A}\nabla \hat{\boldsymbol{\varphi}}^{\mathrm{slod}}_{K,m}\big) \cdot \nabla w\,\mathrm{d}x + \int_{D_K} \boldsymbol{A}\nabla \frac{\partial \hat{\boldsymbol{\varphi}}^{\mathrm{slod}}_{K,m}}{\partial \boldsymbol{A}}(\delta \boldsymbol{A}) \cdot \nabla w\,\mathrm{d}x = 0.$$

Using the test function $w = \boldsymbol{v}(\omega) \in H^1_0(D_K)$ and combining the previous two identities, we get

$$\frac{\partial}{\partial \boldsymbol{A}}(\hat{\boldsymbol{\varphi}}^{\mathrm{slod}}_{K,m}, \mathbb{1}_T)_{L^2(T)}(\delta \boldsymbol{A}) = -\int_{D_K} \big(\delta \boldsymbol{A}\nabla \hat{\boldsymbol{\varphi}}^{\mathrm{slod}}_{K,m}\big) \cdot \nabla \boldsymbol{v}\,\mathrm{d}x.$$

This expression directly characterizes the L^2-representation of the Fréchet derivative of $(\hat{\boldsymbol{\varphi}}^{\mathrm{slod}}_{K,m}, \mathbb{1}_T)_{L^2(T)}$, and therefore yields the assertion. □

Another ingredient in the error analysis is the following regularity result for the localized basis functions. The result is needed to further estimate the term we get after applying the spectral gap inequality. The proof of this result relies on the condition that the patches take the form of d-dimensional bricks, cf. Theorem 5.3.2. This condition can be guaranteed, for example, by considering a brick-shaped domain equipped with a Cartesian mesh.

Lemma 5.3.4 (L^4-regularity of localized basis functions)**.** *Let $\boldsymbol{A}$ be a random coefficient field subject to Theorem 5.3.1. Then, assuming that the patches D_K take the form of bricks, the localized basis functions $\hat{\boldsymbol{\varphi}}_{K,m}^{\mathrm{slod}}$ satisfy that*

$$\int_{D_K} \mathbb{E}\Big[\Big(\fint_{B_\varepsilon(x)} |\nabla \hat{\boldsymbol{\varphi}}_{K,m}^{\mathrm{slod}}|^2 \,\mathrm{d}\tilde{x}\Big)^2\Big] \,\mathrm{d}x \lesssim (mH)^{4-d}.$$

Proof. In order to apply Theorem 5.3.2, we need to construct a function h_K such that the localized basis function $\hat{\boldsymbol{\varphi}}_{K,m}^{\mathrm{slod}}$ is the weak solution to

$$\nabla \cdot (\boldsymbol{A} \nabla \hat{\boldsymbol{\varphi}}_{K,m}^{\mathrm{slod}}) = \nabla \cdot h_K \quad \text{on } D_K$$

subject to homogeneous Dirichlet boundary conditions on ∂D_K. To this end, one may choose $h_K \coloneqq \nabla r$ for r solving the Laplace problem $-\Delta r = g_{K,m}^{\mathrm{slod}}$ subject to homogeneous Dirichlet boundary conditions on ∂D_K. With Theorem 5.3.2 we then obtain that

$$\int_{D_K} \mathbb{E}\Big[\Big(\fint_{B_\varepsilon(x)} |\nabla \hat{\boldsymbol{\varphi}}_{K,m}^{\mathrm{slod}}|^2 \,\mathrm{d}\tilde{x}\Big)^2\Big] \,\mathrm{d}x \lesssim |D_K|^{1-4/q}\Big(\int_{D_K} |h_K|^q \,\mathrm{d}x\Big)^{4/q}$$

for any $4 < q < \infty$. Using standard elliptic regularity on convex domains yields that

$$\|\nabla h_K\|_{L^2(D_K)} = \|D^2 r\|_{L^2(D_K)} \lesssim \|g_{K,m}^{\mathrm{slod}}\|_{L^2(D_K)} = 1,$$

since $g_{K,m}^{\mathrm{slod}}$ is L^2-normalized. Using the Cauchy–Schwarz inequality and Friedrichs' inequality on D_K for $r \in H_0^1(D_K)$, we get that

$$\begin{aligned} \|\nabla r\|_{L^2(D_K)}^2 = (g_{K,m}^{\mathrm{slod}}, r)_{L^2(D_K)} &\leq \|g_{K,m}^{\mathrm{slod}}\|_{L^2(D_K)} \|r\|_{L^2(D_K)} \\ &\lesssim mH \|g_{K,m}^{\mathrm{slod}}\|_{L^2(D_K)} \|\nabla r\|_{L^2(D_K)}. \end{aligned} \tag{5.15}$$

With the definition of h_K it follows directly that

$$\|h_K\|_{L^2(D_K)} \lesssim mH \|g_{K,m}^{\mathrm{slod}}\|_{L^2(D_K)} = mH.$$

Applying the Sobolev embedding ($q = 6$ is the critical exponent for $d = 3$) and a scaling argument (the embedding constant scales with the diameter of D_K), we obtain that

$$\begin{aligned} \int_{D_K} |h_K|^q \,\mathrm{d}x &\lesssim (mH)^{d-qd/2} \|h_K\|_{L^2(D_K)}^q + (mH)^{d+q(2-d)/2} \|\nabla h_K\|_{L^2(D_K)}^q \\ &\lesssim (mH)^{d+q(2-d)/2}. \end{aligned}$$

Combining the previous inequalities and setting $q = 5$ gives the assertion. □

The following theorem provides an a posteriori error bound for the proposed numerical stochastic homogenization method. For the error analysis, we assume that the set $\left\{g_{K,m}^{\mathrm{slod}} : K \in \mathcal{T}_H\right\}$ is Riesz stable in the sense of Theorem 3.1.2. The error estimate involves the localization indicator σ from (5.11) and the Riesz stability constant C_{rb}, which quantifies the linear independence of the local source terms. Both constants can be computed a posteriori, as described in Section 5.5 and Theorem 3.5.1. Moreover, Section 5.4 provides a worst-case a priori upper bound for σ. In practical implementations, the Riesz stability of the local source terms can be ensured as discussed in Section 5.5.

Theorem 5.3.5 (A posteriori error bound)**.** *Let $\boldsymbol{A}$ be a random coefficient field subject to Theorem 5.3.1, and let the set $\{g_{K,m}^{\mathrm{slod}} : K \in \mathcal{T}_H\}$ be stable in the sense of Theorem 3.1.2. Then, the solution $\bar{u}_{H,m}^{\mathrm{slod}}$ of the presented numerical stochastic homogenization method, as given by* (5.12)*, satisfies, for any $f \in L^2(D)$, that*

$$\|\boldsymbol{u} - \bar{u}_{H,m}^{\mathrm{slod}}\|_{L^2(\Omega,L^2(D))} \lesssim \Big(H + C_{\mathrm{rb}}^{1/2} m^{d/2}\Big(\sigma + \varepsilon^{d/2} m^2 H^{(4-d)/2}\Big)\Big)\|f\|_{L^2(D)}$$

with the constant $C_{\mathrm{rb}}(H,m)$ from Theorem 3.1.2 and the localization indicator $\sigma(H,\varepsilon,m)$ from (5.11)*.*

Proof. For the error analysis, we introduce the function

$$\boldsymbol{u}_{H,m} \coloneqq \sum_{K\in\mathcal{T}_H} c_K \hat{\boldsymbol{\varphi}}_{K,m}^{\mathrm{slod}}, \tag{5.16}$$

where $(c_K)_{K\in\mathcal{T}_H}$ are the coefficients of the representation of $\Pi_H f$ in terms of the local source terms $\{g_{K,m}^{\mathrm{slod}} : K \in \mathcal{T}_H\}$. Using the triangle inequality, we obtain that

$$\begin{aligned}
&\|\boldsymbol{u}-\bar{u}_{H,m}^{\mathrm{slod}}\|_{L^2(\Omega,L^2(D))} \\
&\quad\le \|\boldsymbol{u} - \Pi_H\boldsymbol{u}\|_{L^2(\Omega,L^2(D))} + \|\Pi_H(\boldsymbol{u} - \boldsymbol{u}_{H,m})\|_{L^2(\Omega,L^2(D))} \\
&\qquad\quad + \|\Pi_H\boldsymbol{u}_{H,m} - \bar{u}_{H,m}^{\mathrm{slod}}\|_{L^2(\Omega,L^2(D))} \\
&\quad=: \Xi_1 + \Xi_2 + \Xi_3.
\end{aligned} \tag{5.17}$$

In the subsequent analysis, we will estimate the terms Ξ_1, Ξ_2, and Ξ_3 separately. For the term Ξ_1, we obtain using the approximation property (2.7) of the operator Π_H and the stability estimate (5.4) that

$$\Xi_1^2 = \mathbb{E}\Big[\|\boldsymbol{u} - \Pi_H\boldsymbol{u}\|_{L^2(D)}^2\Big] \lesssim H^2\,\mathbb{E}\Big[\|\nabla\boldsymbol{u}\|_{L^2(D)}^2\Big] \lesssim H^2\|f\|_{L^2(D)}^2.$$

For estimating the term Ξ_2, we first apply the L^2-stability of Π_H (cf. (2.6)) and Friedrichs' inequality. Then, following the lines of the convergence proof of the SLOD in the deterministic setting, cf. Theorem 3.2.1, we obtain that

$$\Xi_2 \lesssim \|\nabla(\boldsymbol{u} - \boldsymbol{u}_{H,m})\|_{L^2(\Omega,L^2(D))} \lesssim (H + C_{\mathrm{rb}}^{1/2} m^{d/2}\sigma)\|f\|_{L^2(D)}.$$

In order to estimate term Ξ_3, we recall definitions (5.12) and (5.16) and use the Cauchy–Schwarz inequality to obtain, setting $\boldsymbol{e} \coloneqq \Pi_H \boldsymbol{u}_{H,m} - \bar{u}_{H,m}^{\mathrm{slod}}$, that

$$\begin{aligned}\Xi_3^2 &= \sum_{K\in\mathcal{T}_H} c_K\, \mathbb{E}\Big[(\Pi_H \hat{\boldsymbol{\varphi}}_{K,m}^{\mathrm{slod}} - \Pi_H \mathbb{E}[\hat{\boldsymbol{\varphi}}_{K,m}^{\mathrm{slod}}], \boldsymbol{e})_{L^2(D_K)}\Big] \\ &\leq \sum_{K\in\mathcal{T}_H} |c_K| \|\Pi_H \hat{\boldsymbol{\varphi}}_{K,m}^{\mathrm{slod}} - \Pi_H \mathbb{E}[\hat{\boldsymbol{\varphi}}_{K,m}^{\mathrm{slod}}]\|_{L^2(\Omega,L^2(D_K))} \|\boldsymbol{e}\|_{L^2(\Omega,L^2(D_K))}.\end{aligned} \tag{5.18}$$

Algebraic manipulations then yield for the first term of each summand on the right-hand side of the previous inequality that

$$\begin{aligned}&\|\Pi_H \hat{\boldsymbol{\varphi}}_{K,m}^{\mathrm{slod}} - \Pi_H \mathbb{E}[\hat{\boldsymbol{\varphi}}_{K,m}^{\mathrm{slod}}]\|_{L^2(\Omega,L^2(D_K))}^2 \\ &\quad = \mathbb{E}\Big[\int_{D_K} \Big(\sum_{T\subset D_K} ((\hat{\boldsymbol{\varphi}}_{K,m}^{\mathrm{slod}}, \mathbb{1}_T)_{L^2(T)} - \mathbb{E}[(\hat{\boldsymbol{\varphi}}_{K,m}^{\mathrm{slod}}, \mathbb{1}_T)_{L^2(T)}])|T|^{-1}\mathbb{1}_T\Big)^2 \mathrm{d}x\Big] \\ &\quad = \sum_{T\subset D_K} |T|^{-1}\, \mathbb{E}\Big[((\hat{\boldsymbol{\varphi}}_{K,m}^{\mathrm{slod}}, \mathbb{1}_T)_{L^2(T)} - \mathbb{E}[(\hat{\boldsymbol{\varphi}}_{K,m}^{\mathrm{slod}}, \mathbb{1}_T)_{L^2(T)}])^2\Big].\end{aligned} \tag{5.19}$$

Applying the spectral gap inequality (5.13) and using the L^2-representation of the Fréchet derivative from Theorem 5.3.3, we obtain that

$$\begin{aligned}&\mathbb{E}\Big[((\hat{\boldsymbol{\varphi}}_{K,m}^{\mathrm{slod}}, \mathbb{1}_T)_{L^2(T)} - \mathbb{E}[(\hat{\boldsymbol{\varphi}}_{K,m}^{\mathrm{slod}}, \mathbb{1}_T)_{L^2(T)}])^2\Big] \\ &\quad \lesssim \varepsilon^d\, \mathbb{E}\Big[\int_{D_K} \Big(\fint_{B_\varepsilon(x)} |\nabla \hat{\boldsymbol{\varphi}}_{K,m}^{\mathrm{slod}} \otimes \nabla \boldsymbol{v}| \mathrm{d}\tilde{x}\Big)^2 \mathrm{d}x\Big] \\ &\quad \leq \varepsilon^d \Big(\int_{D_K} \mathbb{E}\Big[\Big(\fint_{B_\varepsilon(x)} |\nabla \hat{\boldsymbol{\varphi}}_{K,m}^{\mathrm{slod}}|^2 \mathrm{d}\tilde{x}\Big)^2\Big] \mathrm{d}x\Big)^{1/2} \Big(\int_{D_K} \mathbb{E}\Big[\Big(\fint_{B_\varepsilon(x)} |\nabla \boldsymbol{v}|^2 \mathrm{d}\tilde{x}\Big)^2\Big] \mathrm{d}x\Big)^{1/2},\end{aligned}$$

where we used the Cauchy–Schwarz inequality. Theorem 5.3.4 can be employed to bound the first factor on the right-hand side of the preceding inequality. For estimating the second factor, we note that problem (5.14) for $\boldsymbol{v} \in L^2(\Omega; H_0^1(D_K))$ has the same structure as problem (5.6) for the localized basis functions. Consequently, a result analogous to Theorem 5.3.4 also holds for $\boldsymbol{v}$, leading to

$$\int_{D_K} \mathbb{E}\Big[\Big(\fint_{B_\varepsilon(x)} |\nabla \boldsymbol{v}|^2 \mathrm{d}\tilde{x}\Big)^2\Big] \mathrm{d}x \lesssim (mH)^{4-d} \|\mathbb{1}_T\|_{L^2(D_K)}^4.$$

Inserting the estimates for $\hat{\boldsymbol{\varphi}}_{K,m}^{\mathrm{slod}}$ and $\boldsymbol{v}$, and using that $\|\mathbb{1}_T\|_{L^2(D_K)}^2 = |T|$, we get that

$$\mathbb{E}\Big[\Big((\hat{\boldsymbol{\varphi}}_{K,m}^{\mathrm{slod}}, \mathbb{1}_T)_{L^2(T)} - \mathbb{E}[(\hat{\boldsymbol{\varphi}}_{K,m}^{\mathrm{slod}}, \mathbb{1}_T)_{L^2(T)}]\Big)^2\Big] \lesssim \varepsilon^d (mH)^{4-d} |T|.$$

Consequently, we can bound the term in (5.19) as

$$\|\Pi_H \hat{\boldsymbol{\varphi}}_{K,m}^{\mathrm{slod}} - \Pi_H \mathbb{E}[\hat{\boldsymbol{\varphi}}_{K,m}^{\mathrm{slod}}]\|_{L^2(\Omega,L^2(D_K))}^2 \lesssim \varepsilon^d m^4 H^{4-d}. \tag{5.20}$$

Inserting this estimate into (5.18), applying the Cauchy-Schwarz inequality, recalling the finite overlap of the patches, and utilizing Theorem 3.1.2, we finally obtain for Ξ_3 that

$$\begin{aligned}\Xi_3^2 &\lesssim \varepsilon^{d/2} m^2 H^{(4-d)/2} \sqrt{\sum_{K\in\mathcal{T}_H} c_K^2} \sqrt{\sum_{K\in\mathcal{T}_H} \|\Pi_H \boldsymbol{u}_{H,m} - \bar{u}_{H,m}^{\mathrm{slod}}\|^2_{L^2(\Omega,L^2(D_K))}} \\ &\lesssim \varepsilon^{d/2} m^{2+d/2} H^{(4-d)/2} C_{\mathrm{rb}}^{1/2} \|f\|_{L^2(D)}\, \Xi_3.\end{aligned}$$

The assertion follows immediately after combining the estimates for Ξ_1, Ξ_2, and Ξ_3. □

5.4. Error analysis using LOD techniques

In this section, we apply the framework of LOD theory to derive an upper bound for the localization error indicator σ, which appears in the error estimate stated in Theorem 5.3.5. For this purpose, we consider the lowest-order LOD basis functions, see also Section 3.3.2, instead of the previously introduced basis. In addition, we further estimate the Riesz stability constant C_{rb} associated to this choice of LOD basis functions.

Analogous to (2.15), we define the space of fine-scale functions supported on D_K as

$$\mathcal{W}_{K,m} \coloneqq \{w \in H_0^1(D_K) : \Pi_{H,D_K} w = 0\}.$$

The local LOD basis function corresponding to the element $K \in \mathcal{T}_H$ is then given by

$$\hat{\boldsymbol{\varphi}}_{K,m}^{\mathrm{lod}} \coloneqq (1 - \widehat{\boldsymbol{\mathcal{C}}}_{K,m}) b_K \in L^2(\Omega; H_0^1(D_K)), \tag{5.21}$$

where $\widehat{\boldsymbol{\mathcal{C}}}_{K,m} b_K \in L^2(\Omega; \mathcal{W}_{K,m})$ denotes the fine-scale correction of the bubble function b_K defined in (2.11). For almost all $\omega \in \Omega$, the correction satisfies

$$\boldsymbol{a}(\widehat{\boldsymbol{\mathcal{C}}}_{K,m} b_K, w) = \boldsymbol{a}(b_K, w) \quad \text{for all } w \in \mathcal{W}_{K,m}. \tag{5.22}$$

Note that the well-posedness of the operator $\widehat{\boldsymbol{\mathcal{C}}}_{K,m}$ is a consequence of the Lax–Milgram theorem, recalling that $\mathcal{W}_{K,m}$ is a closed subspace of $H_0^1(D_K)$.

The upper bound on σ derived below relies on the fact that the LOD basis function $\hat{\boldsymbol{\varphi}}_{K,m}^{\mathrm{lod}}$ has (locally in D_K) a $\mathcal{T}_H$-piecewise constant source term

$$\boldsymbol{g}_{K,m}^{\mathrm{lod}} \coloneqq -\mathrm{div}\boldsymbol{A}\nabla\hat{\boldsymbol{\varphi}}_{K,m}^{\mathrm{lod}} \in L^2(\Omega; \mathbb{P}^0(\mathcal{T}_{H,D_K}));$$

see Section 3.3.2.

5.4.1. Localization error indicator

Similar to the previous section, the presence of stochasticity requires additional lemmas before deriving an upper bound on σ. In particular, the following lemma provides the L^2-representation of the Fréchet derivative of $(\boldsymbol{g}_{K,m}^{\mathrm{lod}}, \mathbb{1}_T)_{L^2(T)}$, which is essential for applying the spectral gap inequality from Theorem 5.3.1.

Lemma 5.4.1 (Fréchet derivative of LOD right-hand sides)**.** *The L^2-representation of the Fréchet derivative of $(\boldsymbol{g}_{K,m}^{\mathrm{lod}}, \mathbb{1}_T)_{L^2(T)}$ is given by*

$$\begin{aligned}&\frac{\partial}{\partial \boldsymbol{A}}(\boldsymbol{g}_{K,m}^{\mathrm{lod}}, \mathbb{1}_T)_{L^2(T)}\\ &\quad= \nabla b_K \otimes \nabla b_T - \nabla \widehat{\boldsymbol{\mathcal{C}}}_{K,m} b_K \otimes \nabla b_T - \nabla b_K \otimes \nabla \widehat{\boldsymbol{\mathcal{C}}}_{K,m} b_T + \nabla \widehat{\boldsymbol{\mathcal{C}}}_{K,m} b_K \otimes \nabla \widehat{\boldsymbol{\mathcal{C}}}_{K,m} b_T.\end{aligned}$$

Proof. Using that $\boldsymbol{g}_{K,m}^{\mathrm{lod}}$ is piecewise constant, the identity $\Pi_H b_T = \mathbb{1}_T$, and the definition of $\hat{\boldsymbol{\varphi}}_{K,m}^{\mathrm{lod}}$, we obtain that

$$(\boldsymbol{g}_{K,m}^{\mathrm{lod}}, \mathbb{1}_T)_{L^2(T)} = (\boldsymbol{g}_{K,m}^{\mathrm{lod}}, b_T)_{L^2(T)} = \boldsymbol{a}(\hat{\boldsymbol{\varphi}}_{K,m}^{\mathrm{lod}}, b_T) = \boldsymbol{a}((1 - \widehat{\boldsymbol{\mathcal{C}}}_{K,m}) b_K, b_T).$$

Hence, the Fréchet derivative of $(\boldsymbol{g}_{K,m}^{\mathrm{lod}}, \mathbb{1}_T)_{L^2(T)}$ equals

$$\frac{\partial}{\partial \boldsymbol{A}}(\boldsymbol{g}_{K,m}^{\mathrm{lod}}, \mathbb{1}_T)_{L^2(T)}(\delta \boldsymbol{A}) = \frac{\partial}{\partial \boldsymbol{A}} \boldsymbol{a}(b_K, b_T)(\delta \boldsymbol{A}) - \frac{\partial}{\partial \boldsymbol{A}} \boldsymbol{a}(\widehat{\boldsymbol{\mathcal{C}}}_{K,m} b_K, b_T)(\delta \boldsymbol{A}). \quad (5.23)$$

The first term is easily calculated, yielding

$$\frac{\partial \boldsymbol{a}(b_K, b_T)}{\partial \boldsymbol{A}}(\delta \boldsymbol{A}) = \int_{D_K} \delta \boldsymbol{A} \nabla b_K \cdot \nabla b_T \,\mathrm{d}x. \quad (5.24)$$

For the second term, we obtain with the product rule that

$$\begin{aligned}\frac{\partial \boldsymbol{a}(\widehat{\boldsymbol{\mathcal{C}}}_{K,m} b_K, b_T)}{\partial \boldsymbol{A}}(\delta \boldsymbol{A}) = &\int_{D_K} \delta \boldsymbol{A} \nabla \widehat{\boldsymbol{\mathcal{C}}}_{K,m} b_K \cdot \nabla b_T \,\mathrm{d}x\\ &+ \int_{D_K} \boldsymbol{A} \nabla \frac{\partial \widehat{\boldsymbol{\mathcal{C}}}_{K,m} b_K}{\partial \boldsymbol{A}}(\delta \boldsymbol{A}) \cdot \nabla b_T \,\mathrm{d}x.\end{aligned}$$

Using the definition of the corrections of the bubble functions from (5.22), the fact that $\frac{\partial \widehat{\boldsymbol{\mathcal{C}}}_{K,m} b_K}{\partial \boldsymbol{A}}(\delta \boldsymbol{A}) \in \mathcal{W}_{K,m}$, and the symmetry of $\boldsymbol{A}$, yields for the second term of the above inequality that

$$\int_{D_K} \boldsymbol{A} \nabla \frac{\partial \widehat{\boldsymbol{\mathcal{C}}}_{K,m} b_K}{\partial \boldsymbol{A}}(\delta \boldsymbol{A}) \cdot \nabla b_T \,\mathrm{d}x = \int_{D_K} \boldsymbol{A} \nabla \frac{\partial \widehat{\boldsymbol{\mathcal{C}}}_{K,m} b_K}{\partial \boldsymbol{A}}(\delta \boldsymbol{A}) \cdot \nabla \widehat{\boldsymbol{\mathcal{C}}}_{K,m} b_T \,\mathrm{d}x.$$

Furthermore, by differentiating (5.22), we get for any $w \in \mathcal{W}_{K,m}$ that

$$\int_{D_K} \delta \boldsymbol{A} \nabla b_K \cdot \nabla w \,\mathrm{d}x = \int_{D_K} \delta \boldsymbol{A} \nabla \widehat{\boldsymbol{\mathcal{C}}}_{K,m} b_K \cdot \nabla w \,\mathrm{d}x + \int_{D_K} \boldsymbol{A} \nabla \frac{\partial \widehat{\boldsymbol{\mathcal{C}}}_{K,m} b_K}{\partial \boldsymbol{A}}(\delta \boldsymbol{A}) \cdot \nabla w \,\mathrm{d}x.$$

Combining the three equalities above and using the test function $w = \widehat{\boldsymbol{\mathcal{C}}}_{K,m} b_T$, we obtain that

$$\begin{aligned}\frac{\partial \boldsymbol{a}(\widehat{\boldsymbol{\mathcal{C}}}_{K,m} b_K, b_T)}{\partial \boldsymbol{A}}(\delta \boldsymbol{A}) = &\int_{D_K} \delta \boldsymbol{A} \nabla \widehat{\boldsymbol{\mathcal{C}}}_{K,m} b_K \cdot \nabla b_T \,\mathrm{d}x + \int_{D_K} \delta \boldsymbol{A} \nabla b_K \cdot \nabla \widehat{\boldsymbol{\mathcal{C}}}_{K,m} b_T \,\mathrm{d}x\\ &- \int_{D_K} \delta \boldsymbol{A} \nabla \widehat{\boldsymbol{\mathcal{C}}}_{K,m} b_K \cdot \nabla \widehat{\boldsymbol{\mathcal{C}}}_{K,m} b_T \,\mathrm{d}x.\end{aligned}$$

The L^2-representation of the Fréchet derivative of $\boldsymbol{a}(\widehat{\boldsymbol{\mathcal{C}}}_{K,m}b_K, b_T)$ is therefore given by

$$\frac{\partial}{\partial \boldsymbol{A}}\boldsymbol{a}(\widehat{\boldsymbol{\mathcal{C}}}_{K,m}b_K, b_T) = \nabla\widehat{\boldsymbol{\mathcal{C}}}_{K,m}b_K \otimes \nabla b_T + \nabla b_K \otimes \nabla\widehat{\boldsymbol{\mathcal{C}}}_{K,m}b_T - \nabla\widehat{\boldsymbol{\mathcal{C}}}_{K,m}b_K \otimes \nabla\widehat{\boldsymbol{\mathcal{C}}}_{K,m}b_T.$$

The combination with (5.23) and (5.24) yields the assertion. □

The following regularity result for the LOD correction operators is needed to estimate the terms appearing after applying the spectral gap inequality in the proof of the upper bound on σ.

Lemma 5.4.2 (L^4-regularity estimate for LOD correction operators)**.** *Let $\boldsymbol{A}$ be a random coefficient field subject to Theorem 5.3.1. Then, the corrections of the bubble functions $\widehat{\boldsymbol{\mathcal{C}}}_{K,m}b_K$ satisfies the following regularity estimate*

$$\int_{D_K} \mathbb{E}\left[\left(\fint_{B_\varepsilon(x)} |\nabla\widehat{\boldsymbol{\mathcal{C}}}_{K,m}b_K|^2 \,\mathrm{d}\tilde{x}\right)^2\right] \mathrm{d}x \lesssim \left(\frac{m}{H}\right)^{4-d}.$$

Proof. First, let $\omega \in \Omega$ be arbitrary but fixed. In order to apply Theorem 5.3.2, we need to establish the appropriate right-hand side, which results in the equation for $\widehat{\boldsymbol{\mathcal{C}}}_{K,m}b_K$ taking the form as in Theorem 5.3.2. Naturally, $\widehat{\boldsymbol{\mathcal{C}}}_{K,m}b_K$ solves, together with the Lagrange multiplier $\boldsymbol{p}_{K,m} \in \mathbb{P}^0(\mathcal{T}_{H,D_K})$ the following saddle-point problem

$$\begin{pmatrix} \boldsymbol{\mathcal{A}}_{D_K} & \mathcal{P}_{D_K}^T \\ \mathcal{P}_{D_K} & 0 \end{pmatrix} \begin{pmatrix} \widehat{\boldsymbol{\mathcal{C}}}_{K,m}b_K \\ \boldsymbol{p}_{K,m} \end{pmatrix} = \begin{pmatrix} \boldsymbol{\mathcal{A}}_{D_K}\, b_K \\ 0 \end{pmatrix} \tag{5.25}$$

with the patch-local operators defined in Section 3.3.2

It is a direct consequence that $\widehat{\boldsymbol{\mathcal{C}}}_{K,m}b_K$ solves

$$\nabla \cdot (\boldsymbol{A}\nabla\widehat{\boldsymbol{\mathcal{C}}}_{K,m}b_K) = \nabla \cdot (\boldsymbol{A}\nabla b_K) + \mathcal{P}_{D_K}^T\boldsymbol{p}_{K,m},$$

which, for some $\boldsymbol{q}_{K,m} \in L^2(D_K)$, can be rewritten as

$$\nabla \cdot (\boldsymbol{A}\nabla\widehat{\boldsymbol{\mathcal{C}}}_{K,m}b_K) = \nabla \cdot (\boldsymbol{A}\nabla b_K + \boldsymbol{q}_{K,m}).$$

To see this, we set $\boldsymbol{q}_{K,m} \coloneqq \nabla v$, where v solves $-\Delta v = \boldsymbol{p}_{K,m}$ with homogeneous Dirichlet boundary conditions in a ball of radius CmH, where the constant $C > 0$ is chosen such that the ball contains D_K.

Furthermore, the local LOD source terms satisfy $\boldsymbol{g}_{K,m}^{\mathrm{lod}} = \boldsymbol{p}_{K,m}$; see [HP22b, Appendix A]. By applying the estimate

$$\|\boldsymbol{g}_{K,m}^{\mathrm{lod}}\|_{L^2(\Omega,L^2(D_K))} \lesssim H^{d/2-2}, \tag{5.26}$$

which follows from taking the expectation of the corresponding deterministic identity in [HP22b, Lemma A.2] and following the proofs in [FGP21, Lemma 4.9] and Theorem 5.3.4, we obtain that

$$\|\nabla\boldsymbol{q}_{K,m}\|_{L^2(D_K)} = \|D^2 v\|_{L^2(D_K)} \lesssim \|\boldsymbol{p}_{K,m}\|_{L^2(D_K)} \lesssim H^{d/2-2}.$$

Additionally, applying the Cauchy–Schwarz inequality and Friedrichs' inequality on D_K for $v \in H_0^1(D_K)$, we get, analogue to (5.15) the bound

$$\|\boldsymbol{q}_{K,m}\|_{L^2(D_K)} \lesssim mH\|\boldsymbol{p}_{K,m}\|_{L^2(D_K)} \lesssim mH^{d/2-1},$$

which leads to the estimate

$$\begin{aligned}\int_{D_K} |\boldsymbol{q}_{K,m}|^q \,\mathrm{d}x &\lesssim (mH)^{d-qd/2}\|\boldsymbol{q}_{K,m}\|_{L^2(D_K)}^q + (mH)^{d+q(2-d)/2}\|\nabla \boldsymbol{q}_{K,m}\|_{L^2(D_K)}^q \\ &\lesssim m^{d+q(2-d)/2}H^{d-q}.\end{aligned}$$

Moreover, using $\|\nabla b_K\|_{L^\infty} \approx H^{-1}$ we obtain that $\int_K |\boldsymbol{A}\nabla b_K|^q \,\mathrm{d}x \lesssim H^{d-q}$. Therefore, applying Theorem 5.3.2 for $Q = D_K$, $p = 4$ and $\boldsymbol{h} = \boldsymbol{A}\nabla b_K - \boldsymbol{q}_{K,m}$ yields that

$$\begin{aligned}&\int_{D_K} \mathbb{E}\left[\left(\fint_{B_\varepsilon(x)} |\nabla \widehat{\boldsymbol{\mathcal{C}}}_{K,m} b_K|^2 \,\mathrm{d}\tilde{x}\right)^2\right] \mathrm{d}x \\ &\quad\lesssim |D_K|^{(q-4)/q}\left(\mathbb{E}\left[\int_{D_K} |\boldsymbol{A}\nabla b_K|^q \,\mathrm{d}x + \int_{D_K} |\boldsymbol{q}_{K,m}|^q \,\mathrm{d}x\right]\right)^{4/q} \\ &\quad\lesssim \left(\frac{m}{H}\right)^{4-d},\end{aligned}$$

which is the assertion. □

Now, we are finally ready to present an upper bound on σ using LOD basis functions.

Lemma 5.4.3 (Upper bound on σ)**.** *Choosing an L^2-normalized version of $g_{K,m}^{\mathrm{lod}} \coloneqq \mathbb{E}[\boldsymbol{g}_{K,m}^{\mathrm{lod}}]$ in (5.10) yields the upper bound*

$$\sigma \lesssim m^2 H^{-1}\exp(-Cm) + m^4\left(\frac{\varepsilon}{H}\right)^{d/2} \tag{5.27}$$

with $C > 0$ independent of H and m, provided that ε satisfies the smallness assumption

$$\varepsilon^d \lesssim m^{-8}H^d. \tag{5.28}$$

Proof. For all $\boldsymbol{v} \in \boldsymbol{Y} \subset L^2(\Omega; H_\Gamma^1(D_K))$ it holds that $\mathbb{E}[\mathbf{tr}^{-1}\mathrm{tr}\,\boldsymbol{v}] = \mathbb{E}[\boldsymbol{v}]$. Hence, by inserting $g_{K,m}^{\mathrm{lod}} = \mathbb{E}[\boldsymbol{g}_{K,m}^{\mathrm{lod}}]$ into (5.10), we obtain that

$$\sigma_K(H,\varepsilon,m) \leq \frac{1}{\|g_{K,m}^{\mathrm{lod}}\|_{L^2(D_K)}} \sup_{\substack{\boldsymbol{v}\in L^2(\Omega;H_\Gamma^1(D_K)) \\ \|\boldsymbol{v}\|_{L^2(\Omega;H^1(D_K))}=1}} (g_{K,m}^{\mathrm{lod}}, \mathbb{E}[\mathbf{tr}^{-1}\mathrm{tr}\,\boldsymbol{v}])_{L^2(D_K)}.$$

Note that by dividing by the norm of $g_{K,m}^{\mathrm{lod}}$, we account for the fact that $g_{K,m}^{\mathrm{lod}}$ may not be normalized. We denote by $\boldsymbol{\mathcal{A}}_{D_K}^{-1}\colon L^2(\Omega; L^2(D_K)) \to L^2(\Omega; H_0^1(D_K))$

the local solution operator defined on the patch D_K, which satisfies the stability estimate

$$\|\nabla \boldsymbol{\mathcal{A}}_{D_K}^{-1} \boldsymbol{g}\|_{L^2(\Omega,L^2(D_K))} \lesssim \|\boldsymbol{g}\|_{L^2(\Omega,L^2(D_K))}, \tag{5.29}$$

for $\boldsymbol{g} \in L^2(\Omega; L^2(D_K))$.

Therefore, we obtain for any $\boldsymbol{v} \in L^2(\Omega; H^1_\Gamma(D_K))$ that

$$\begin{aligned}
&(g_{K,m}^{\mathrm{lod}}, \mathbb{E}[\mathbf{tr}^{-1}\mathrm{tr}\,\boldsymbol{v}])_{L^2(D_K)} \\
&\quad = \mathbb{E}[(\boldsymbol{g}_{K,m}^{\mathrm{lod}}, \boldsymbol{v})_{L^2(D_K)} - \boldsymbol{a}(\boldsymbol{\mathcal{A}}_{D_K}^{-1}\boldsymbol{g}_{K,m}^{\mathrm{lod}}, \boldsymbol{v})] \\
&\qquad + \mathbb{E}[(g_{K,m}^{\mathrm{lod}} - \boldsymbol{g}_{K,m}^{\mathrm{lod}}, \boldsymbol{v})_{L^2(D_K)} - \boldsymbol{a}(\boldsymbol{\mathcal{A}}_{D_K}^{-1}(g_{K,m}^{\mathrm{lod}} - \boldsymbol{g}_{K,m}^{\mathrm{lod}}), \boldsymbol{v})] \\
&\quad =: \Xi_1 + \Xi_2.
\end{aligned}$$

To estimate the term Ξ_1, we apply the deterministic result from the proof of [HP22b, Lemma 6.4] for any $\omega \in \Omega$ and use the Cauchy–Schwarz inequality to get that

$$\Xi_1 \lesssim H^{-1} \exp(-Cm) \|\boldsymbol{v}\|_{L^2(\Omega,H^1(D_K))} \|\boldsymbol{g}_{K,m}^{\mathrm{lod}}\|_{L^2(\Omega,L^2(D_K))},$$

where $C > 0$ is independent of H and m. Using the estimate (5.26) yields that

$$\Xi_1 \lesssim H^{d/2-3} \exp(-Cm)\, \|\boldsymbol{v}\|_{L^2(\Omega,H^1(D_K))}.$$

For the term Ξ_2, we obtain using (5.29) and the Cauchy–Schwarz inequality that

$$\Xi_2 \lesssim \|g_{K,m}^{\mathrm{lod}} - \boldsymbol{g}_{K,m}^{\mathrm{lod}}\|_{L^2(\Omega,L^2(D_K))} \|\boldsymbol{v}\|_{L^2(\Omega,H^1(D_K))}.$$

In order to estimate the first factor on the right-hand side, we proceed similarly as in the proof of Theorem 5.3.5 to obtain that

$$\begin{aligned}
&\|g_{K,m}^{\mathrm{lod}} - \boldsymbol{g}_{K,m}^{\mathrm{lod}}\|^2_{L^2(\Omega,L^2(D_K))} \\
&\qquad = \sum_{T \subset D_K} |T|^{-1}\, \mathbb{E}\Big[\Big((\boldsymbol{g}_{K,m}^{\mathrm{lod}}, \mathbb{1}_T)_{L^2(T)} - \mathbb{E}\left[(\boldsymbol{g}_{K,m}^{\mathrm{lod}}, \mathbb{1}_T)_{L^2(T)}\right]\Big)^2\Big].
\end{aligned}$$

Using the spectral gap inequality (5.13), we obtain for each summand that

$$\begin{aligned}
&\mathbb{E}\Big[\Big((\boldsymbol{g}_{K,m}^{\mathrm{lod}}, \mathbb{1}_T)_{L^2(T)} - \mathbb{E}[(\boldsymbol{g}_{K,m}^{\mathrm{lod}}, \mathbb{1}_T)_{L^2(T)}]\Big)^2\Big] \\
&\qquad \lesssim \varepsilon^d\, \mathbb{E}\Big[\int_{\mathbb{R}^d} \Big(\fint_{B_\varepsilon(x)} \Big|\frac{\partial (\boldsymbol{g}_{K,m}^{\mathrm{lod}}, \mathbb{1}_T)_{L^2(T)}}{\partial \boldsymbol{A}}(\tilde{x})\Big| \mathrm{d}\tilde{x}\Big)^2 \mathrm{d}x\Big].
\end{aligned} \tag{5.30}$$

The L^2-representation of the Fréchet derivative of $(\boldsymbol{g}_{K,m}^{\mathrm{lod}}, \mathbb{1}_T)_{L^2(T)}$ is derived in Theorem 5.4.1. It consists of a sum of outer products of the gradients of combinations of b_K, b_T, $\widehat{\boldsymbol{\mathcal{C}}}_{K,m} b_K$ and $\widehat{\boldsymbol{\mathcal{C}}}_{K,m} b_T$. To estimate the summands

involving bubble functions, we utilize the property (2.11) for all $T \subset D_K$ and derive the estimate

$$\int_{D_K} \Big(\fint_{B_\varepsilon(x)} |\nabla b_T|^2 \,\mathrm{d}\tilde{x} \Big)^2 \,\mathrm{d}x \lesssim H^{d-4}. \tag{5.31}$$

To proceed with the estimation of (5.30), we need to estimate the four terms resulting from the summands of the Fréchet derivative, cf. Theorem 5.4.1. In the following, we present the estimate for the second term, noting that all other estimates follow analogously. By employing the regularity result from Theorem 5.4.2 and (5.31), we obtain that

$$\begin{aligned}
&\mathbb{E}\Big[\int_{D_K} \Big(\fint_{B_\varepsilon(x)} |\nabla \widehat{\boldsymbol{\mathcal{C}}}_{K,m} b_K \otimes \nabla b_T| \,\mathrm{d}\tilde{x} \Big)^2 \,\mathrm{d}x \Big] \\
&\quad \leq \Big(\int_{D_K} \mathbb{E}\Big[\Big(\fint_{B_\varepsilon(x)} |\nabla \widehat{\boldsymbol{\mathcal{C}}}_{K,m} b_K|^2 \,\mathrm{d}\tilde{x} \Big)^2 \Big] \,\mathrm{d}x \Big)^{1/2} \Big(\int_{D_K} \Big(\fint_{B_\varepsilon(x)} |\nabla b_T|^2 \,\mathrm{d}\tilde{x} \Big)^2 \,\mathrm{d}x \Big)^{1/2} \\
&\quad \lesssim m^{2-d/2} H^{d-4},
\end{aligned}$$

where we used the Cauchy–Schwarz inequality. Note that all four terms can be majorized by $m^{4-d} H^{d-4}$, which results from estimating the last summand. The combination of the previous estimates yields that

$$\| g_{K,m}^{\mathrm{lod}} - \boldsymbol{g}_{K,m}^{\mathrm{lod}} \|_{L^2(\Omega, L^2(D_K))} \lesssim \Big(\sum_{T \subset D_K} |T|^{-1} \, \varepsilon^d m^{4-d} H^{d-4} \Big)^{1/2} \lesssim \varepsilon^{d/2} m^2 H^{-2}. \tag{5.32}$$

Using the estimate

$$\| \boldsymbol{g}_{K,m}^{\mathrm{lod}} \|_{L^2(\Omega, L^2(D_K))} \gtrsim m^{-2} H^{d/2-2},$$

which can be obtained by taking the expectation of the corresponding deterministic identity from [HP22b, Lemma A.2], we derive a lower bound for the L^2-norm of $g_{K,m}^{\mathrm{lod}}$ by computing

$$\begin{aligned}
\| g_{K,m}^{\mathrm{lod}} \|_{L^2(D_K)}^2 &= \| g_{K,m}^{\mathrm{lod}} \|_{L^2(\Omega, L^2(D_K))}^2 \\
&\geq \frac{1}{2} \| \boldsymbol{g}_{K,m}^{\mathrm{lod}} \|_{L^2(\Omega, L^2(D_K))}^2 - \| g_{K,m}^{\mathrm{lod}} - \boldsymbol{g}_{K,m}^{\mathrm{lod}} \|_{L^2(\Omega, L^2(D_K))}^2 \\
&\gtrsim \frac{1}{2} \, m^{-4} H^{d-4} - m^4 H^{-4} \varepsilon^d \gtrsim m^{-4} H^{d-4}.
\end{aligned} \tag{5.33}$$

Here, we used the reverse triangle inequality, the weighted Young's inequality for showing that for $a, b \geq 0$ it holds that $|a-b|^2 \geq \frac{a^2}{2} - b^2$, as well as the smallness assumption (5.28). Finally, combining all estimates leads to

$$\begin{aligned}
\sigma_K &\lesssim \frac{1}{\| g_{K,m}^{\mathrm{lod}} \|_{L^2(D_K)}} \Big(H^{d/2-3} \exp(-Cm) + m^2 H^{-2} \varepsilon^{d/2} \Big) \\
&\lesssim m^2 H^{-1} \exp(-Cm) + m^4 \left(\frac{\varepsilon}{H} \right)^{d/2}.
\end{aligned}$$

The assertion follows directly when taking the maximum over all $K \in \mathcal{T}_H$. □

Combining this a priori result for σ with Theorem 5.3.5 yields the error estimate given in the following corollary. The Riesz constant C_{rb} can be computed a posteriori, cf. Section 5.5.

Corollary 5.4.4 (Combined error bound)**.** *Suppose that the assumptions of Theorems 5.3.5 and 5.4.3 are fulfilled and that $m \gtrsim |\log H|$ holds. Then, the solution $\bar{u}_{H,m}^{\mathrm{slod}}$ of the proposed numerical stochastic homogenization method, as given in* (5.12)*, satisfies, for any $f \in L^2(D)$, that*

$$\|\boldsymbol{u} - \bar{u}_{H,m}^{\mathrm{slod}}\|_{L^2(\Omega,L^2(D))} \lesssim \left(H + C_{\mathrm{rb}}^{1/2} m^{4+d/2} \left(\frac{\varepsilon}{H}\right)^{d/2}\right) \|f\|_{L^2(D)}.$$

5.4.2. Riesz stability

In the next step, we show that the local source terms corresponding to the LOD basis functions are Riesz stable in the sense of Theorem 3.1.2.

Lemma 5.4.5 (Riesz stability of LOD source terms)**.** *Suppose that m is chosen such that $m \gtrsim |\log(H)|$ and that ε satisfies the smallness assumption*

$$\varepsilon^d \lesssim m^{-(8+d)} H^{4+d}. \tag{5.34}$$

Then, for the local source terms $g_{K,m}^{\mathrm{lod}} = \mathbb{E}[\boldsymbol{g}_{K,m}^{\mathrm{lod}}]$, we obtain for all $(c_K)_{K\in\mathcal{T}_H}$ that

$$H^4 \sum_{K\in\mathcal{T}_H} c_K^2 \lesssim \left\| \sum_{K\in\mathcal{T}_H} c_K \frac{g_{K,m}^{\mathrm{lod}}}{\|g_{K,m}^{\mathrm{lod}}\|_{L^2(D_K)}} \right\|_{L^2(D)}^2. \tag{5.35}$$

Proof. We begin the proof by noting that applying the weighted Young inequality twice gives the elementary estimate $|a-b-c|^2 \geq \frac{1}{4}|a|^2 - |b|^2 - |c|^2$ for any $a, b, c \geq 0$. Combining this with the inverse triangle inequality, we obtain that

$$\begin{aligned}
\left\| \sum_{K\in\mathcal{T}_H} c_K \frac{g_{K,m}^{\mathrm{lod}}}{\|g_{K,m}^{\mathrm{lod}}\|_{L^2(D_K)}} \right\|_{L^2(D)}^2 &= \left\| \sum_{K\in\mathcal{T}_H} c_K \frac{g_{K,m}^{\mathrm{lod}}}{\|g_{K,m}^{\mathrm{lod}}\|_{L^2(D_K)}} \right\|_{L^2(\Omega,L^2(D))}^2 \\
&\geq \frac{1}{4} \left\| \sum_{K\in\mathcal{T}_H} c_K \frac{\boldsymbol{g}_{K,m}^{\mathrm{lod}}}{\|\boldsymbol{g}_{K,m}^{\mathrm{lod}}\|_{L^2(D_K)}} \right\|_{L^2(\Omega,L^2(D))}^2 - \left\| \sum_{K\in\mathcal{T}_H} c_K \frac{g_{K,m}^{\mathrm{lod}} - \boldsymbol{g}_{K,m}^{\mathrm{lod}}}{\|g_{K,m}^{\mathrm{lod}}\|_{L^2(D_K)}} \right\|_{L^2(\Omega,L^2(D))}^2 \\
&\quad - \left\| \sum_{K\in\mathcal{T}_H} c_K \left(\frac{\boldsymbol{g}_{K,m}^{\mathrm{lod}}}{\|g_{K,m}^{\mathrm{lod}}\|_{L^2(D_K)}} - \frac{\boldsymbol{g}_{K,m}^{\mathrm{lod}}}{\|\boldsymbol{g}_{K,m}^{\mathrm{lod}}\|_{L^2(D_K)}} \right) \right\|_{L^2(\Omega,L^2(D))}^2 \\
&=: \frac{1}{4}\,\Xi_1 - \Xi_2 - \Xi_3.
\end{aligned}$$

For estimating the term Ξ_1 from below, we use the corresponding deterministic result from [HP22b, Lemma 6.4] and take the expectation which yields that

$$\Xi_1 \gtrsim H^4 \sum_{K\in\mathcal{T}_H} c_K^2.$$

To estimate the term Ξ_2 from above, we use the finite overlap of the patches D_K as well as estimates (5.32) and (5.33) to get that

$$\Xi_2 \lesssim m^{4+d} H^{4-d} \sum_{K \in \mathcal{T}_H} c_K^2 \, \|g_{K,m}^{\mathrm{lod}} - \boldsymbol{g}_{K,m}^{\mathrm{lod}}\|_{L^2(\Omega, L^2(D_K))}^2 \lesssim m^{8+d} \varepsilon^d H^{-d} \sum_{K \in \mathcal{T}_H} c_K^2.$$

The estimate for Ξ_3 can be derived similarly using again the finite overlap of the patches D_K, the reverse triangle inequality, (5.32) and (5.33). We obtain that

$$\begin{aligned}\Xi_3 &= \Big\| \sum_{K \in \mathcal{T}_H} c_K \frac{\boldsymbol{g}_{K,m}^{\mathrm{lod}} (\|\boldsymbol{g}_{K,m}^{\mathrm{lod}}\|_{L^2(D_K)} - \|g_{K,m}^{\mathrm{lod}}\|_{L^2(D_K)})}{\|g_{K,m}^{\mathrm{lod}}\|_{L^2(D_K)} \|\boldsymbol{g}_{K,m}^{\mathrm{lod}}\|_{L^2(D_K)}} \Big\|_{L^2(\Omega, L^2(D))}^2 \\ &\lesssim m^d \sum_{K \in \mathcal{T}_H} c_K^2 \, \mathbb{E}\left[\frac{\|g_{K,m}^{\mathrm{lod}} - \boldsymbol{g}_{K,m}^{\mathrm{lod}}\|_{L^2(D_K)}^2}{\|g_{K,m}^{\mathrm{lod}}\|_{L^2(D_K)}^2} \right] \lesssim m^{8+d} \varepsilon^d H^{-d} \sum_{K \in \mathcal{T}_H} c_K^2.\end{aligned}$$

Combining the previous estimates and using the smallness assumption (5.34) yields the assertion. □

5.5. Practical implementation

To effectively implement the presented numerical stochastic homogenization method, it is crucial to employ an efficient sampling strategy for the space $\boldsymbol{Y}$ and ensure that the local source terms $\{g_{K,m}^{\mathrm{slod}} : K \in \mathcal{T}_H\}$ form a stable basis of $\mathbb{P}^0(\mathcal{T}_H)$. These aspects will be addressed in the following two subsections.

5.5.1. Random sampling and Singular Value Decomposition

We consider an arbitrary patch D_K and denote by $N \coloneqq \#\mathcal{T}_{H,D_K}$ the number of coarse elements contained in this patch. In practical implementations, all local infinite-dimensional problems involved in the construction of the basis functions must be replaced by finite-dimensional approximations. To obtain these, we discretize using the $\mathbb{P}^1$-finite element method on the fine mesh $\mathcal{T}_{h,D_K}$, which is obtained by uniform refinement of $\mathcal{T}_{H,D_K}$. We denote by n the number of nodes in $\mathcal{T}_{h,D_K}$.

To handle the stochasticity in the definition of the space $\boldsymbol{Y}$, our implementation draws M_s samples of the random coefficient $\boldsymbol{A}$ and, for each sample, closely follows the methodology outlined in Section 3.5.1 for the deterministic case. Specifically, for each $i = 1, \dots, M_s$, we generate a matrix $\mathbf{S}_i \in \mathbb{R}^{n \times M_{bd}}$, whose columns represent the coordinate vectors of the discrete $\boldsymbol{A}(\omega_i)$-harmonic extensions of $M_{bd} \in \mathbb{N}$ samples of random boundary data on $\partial D_K \backslash \partial D$. We then compute the matrices $\mathbf{P}_i \in \mathbb{R}^{N \times M_{bd}}$ by applying the L^2-orthogonal projection onto the characteristic functions $\{\mathbb{1}_T : T \in \mathcal{T}_{H,D_K}\}$ column by column to $\mathbf{S}_i$. Finally, we compute the SVD of the matrix $\mathbf{X} \coloneqq [\mathbf{P}_1, \dots, \mathbf{P}_{M_s}]$, yielding coordinate vectors of potential right-hand sides $g_{K,m}^{\mathrm{slod}}$.

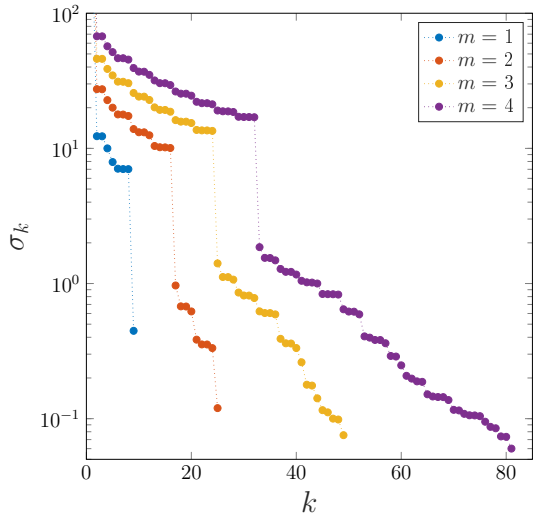

Figure 5.2.: Singular values associated to an interior patch for a $\mathcal{T}_\varepsilon$-piecewise constant random coefficient with $\varepsilon = 2^{-7}$ in two spatial dimensions. The coarse mesh size is set to $H = 2^{-4}$.

The localized deterministic basis functions are then computed as empirical means, again using M_s samples of the random coefficient, by solving discretized versions of (5.6). In the numerical experiments presented in Section 5.6, the number of random boundary samples is set to $M_{bd} = 3N$. For the number of random coefficient samples, we use $M_s = 5000$. The coefficient samples are obtained via a quasi-Monte Carlo sampling strategy based on direction numbers provided in [JK08, JK03].

5.5.2. Stable local source terms

Next, we address the practical implementation of stabilizing the local source terms $\{g_{K,m}^{\text{slod}} : K \in \mathcal{T}_H\}$. To this end, we combine two stabilization techniques discussed in Section 3.4. The first step involves using extended patches, as described in Section 3.4.3, on which we perform an SVD to identify candidate local source terms. However, due to the stochastic nature of the problem, the smallest singular value is typically less well separated from the rest compared to the deterministic setting, particularly for larger values of m, as illustrated in Figure 5.2. To address this issue, we include all candidate functions associated with singular values that lie within a specified threshold above the smallest singular value. Among these, we select the function that minimizes a weighted $L^2(D_K)$-norm, subject to a unit mass constraint. This selection follows the procedure outlined in Section 3.4.2, where we fix the parameters $r = 6$ and $p = 1.3$. Note that in the one-dimensional numerical experiments, only the second stabilization technique based on minimizing the weighted L^2-norm is used, with parameters $r = 6$ and $p = 2$.

Remark 5.5.1 (Uniform Cartesian meshes)**.** Note that in the case of uniform Cartesian meshes, the computational complexity of the method can be significantly reduced when utilizing the stationarity of the coefficient $\boldsymbol{A}$, cf. Theorem 5.3.1, similar to the case of periodic coefficients in the deterministic setting. In fact, only $\mathcal{O}(m^d)$ reference patches need to be considered for the computation of the basis functions and local source terms of the method. All other basis functions and local source terms can then be obtained by translation; see, e.g., [GP15].

5.6. Numerical experiments

The following numerical experiments are intended to demonstrate the effectiveness of the presented numerical homogenization method. In our implementation, we consider uniform Cartesian meshes of the domain $D = (0,1)^d$ with $d \in \{1,2\}$. Note that in this section, we use H to denote the side length of the elements instead of their diameter. For the solution of the local patch problems and the computation of the reference solution $\boldsymbol{u}_h$ we employ the $\mathbb{P}^1$-finite element method on the fine mesh $\mathcal{T}_h$ with $h = 2^{-12}$ for $d = 1$ and $h = 2^{-10}$ for $d = 2$. We denote by $\bar{u}^{\mathrm{slod}}_{h,H,m}$ the fully discrete numerical approximation to $\mathbb{E}[\boldsymbol{u}]$. In the following all expected values are replaced by appropriate empirical means.

The random coefficients $\boldsymbol{A}$ that are considered in the following numerical experiments are piecewise constant with respect to the uniform Cartesian meshes $\mathcal{T}_\varepsilon$ with mesh sizes $\varepsilon \in \{2^{-5}, 2^{-6}, 2^{-7}, 2^{-8}, 2^{-9}\}$. These coefficients take independent and identically distributed element values in the interval $[0.1, 1]$. We further consider the sequence of coarse meshes $\mathcal{T}_H$ with mesh sizes $H \in \{2^{-3}, 2^{-4}, 2^{-5}, 2^{-6}\}$. Note that we only consider coarse mesh sizes $H > \varepsilon$ for which the coarse mesh does not resolve the minimal length scale of the random coefficient. We also exclude combinations of H and m for which a patch coincides with the whole domain D.

To calculate the reference solution, we use $M_s = 5000$ samples of the coefficient on the whole domain D, which is consistent with the number of samples used for the local patch problems. However, in contrast to the quasi-Monte Carlo strategy employed for the local patches, these samples are generated using a standard Monte Carlo sampling approach.

Numerical investigation of σ and C_{rb}

We begin by examining the behavior of the localization error indicator σ as a function of the coarse mesh size H and the correlation length ε. To this end, we use the sequences of coarse meshes and correlation lengths introduced above. The values of σ for the numerical experiments in one and two dimensions are shown in Figures 5.3 and 5.4, respectively. The plots display the decay of σ for fixed ε and varying H (left), as well as for fixed H and varying ε (right). In both

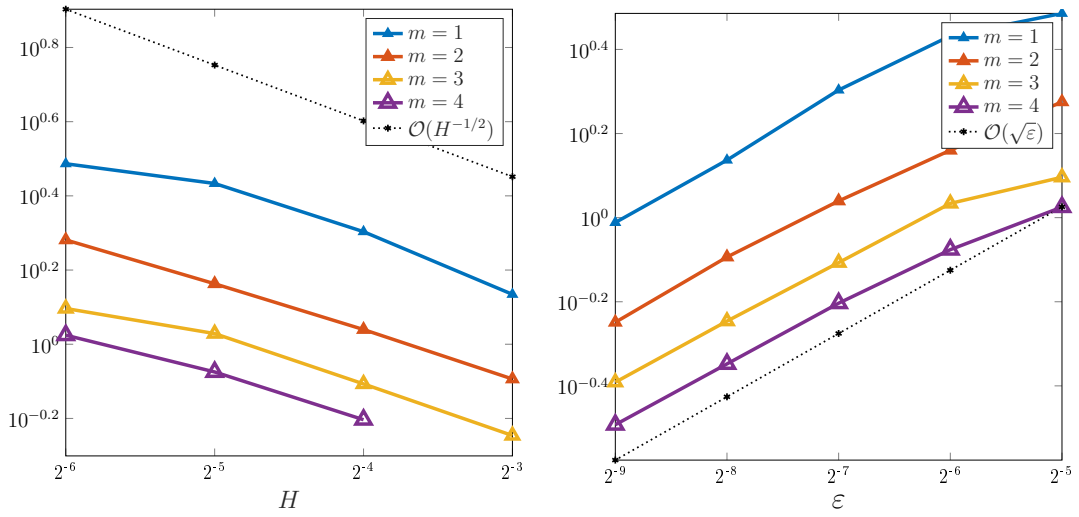

Figure 5.3.: Depiction of σ for a $\mathcal{T}_\varepsilon$-piecewise constant random coefficient in one spatial dimensions. Left: in dependence of the coarse mesh size H for $\varepsilon = 2^{-7}$; Right: in dependence of the correlation length ε for $H = 2^{-4}$.

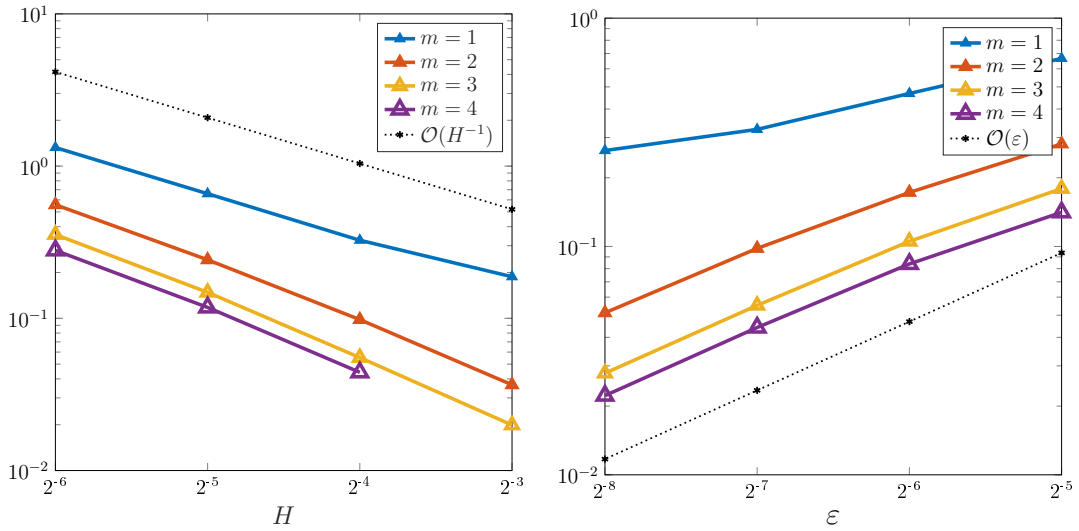

Figure 5.4.: Depiction of σ for a $\mathcal{T}_\varepsilon$-piecewise constant random coefficient in two spatial dimensions. Left: in dependence of the coarse mesh size H for $\varepsilon = 2^{-7}$; Right: in dependence of the correlation length ε for $H = 2^{-4}$.

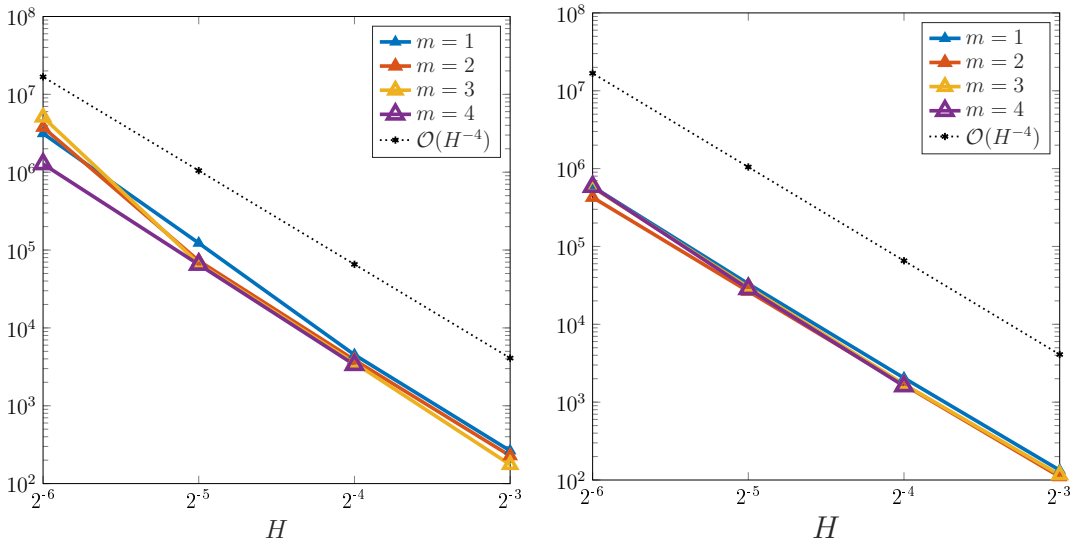

Figure 5.5.: Depiction of the Riesz stability constant C_{rb} of the stochastic SLOD as a function of the coarse mesh size H for a $\mathcal{T}_\varepsilon$-piecewise constant random coefficient with $\varepsilon = 2^{-7}$ in the 1d setting (left) and the 2d setting (right).

cases one observes a scaling like $(\varepsilon/H)^{d/2}$, which numerically validates the upper bound for σ stated in Theorem 5.4.3. It is worth noting that the stochastic component dominates the error, such that the first term in (5.27), which decays exponentially in the patch size m, is not visible in the plots. If σ were plotted as a function of m, one would observe a decay rate roughly proportional to $1/m$.

Next we examine the behavior of the Riesz stability constant C_{rb} of the local SLOD source terms $\{g_{K,m}^{\mathrm{slod}} : K \in \mathcal{T}_H\}$ as a function of H. The Riesz stability constant can be computed as outlined in Theorem 3.5.1. In Figure 5.5, we observe that C_{rb} scales like H^{-4} in both the one- and two-dimensional settings, which is consistent with the results for the stochastically averaged LOD source terms established in Theorem 5.4.5. Moreover, our numerical experiments indicate no dependency of the Riesz stability constant on either the correlation length ε or the localization parameter m, further confirming the conclusions drawn in Theorem 5.4.5.

Numerical validation of convergence

To numerically verify the convergence of the presented numerical stochastic homogenization method, we consider the source terms

$$f(x) = 2\pi^2 \sin(x), \quad f(x,y) = 2\pi^2 \sin(x)\sin(y) \tag{5.36}$$

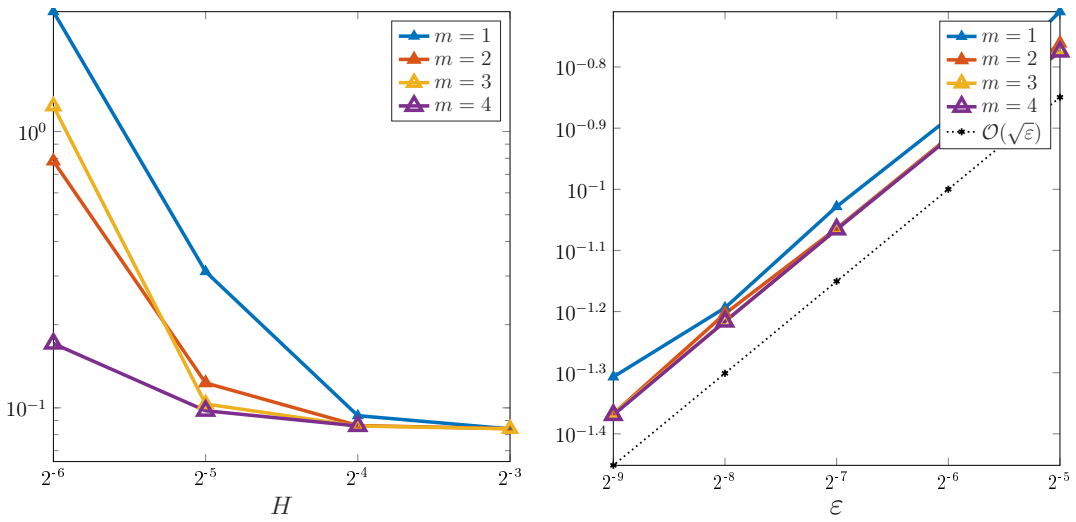

Figure 5.6.: Plot of the relative L^2-errors of the presented SLOD method for a $\mathcal{T}_\varepsilon$-piecewise constant random coefficient in one spatial dimension. Left: errors as functions of the coarse mesh size H for fixed $\varepsilon = 2^{-7}$; Right: errors in dependency of the correlation length ε for fixed $H = 2^{-4}$.

in one and two spatial dimensions, respectively. Figures 5.6 and 5.7 display the resulting relative L^2-errors

$$\|\Pi_H \boldsymbol{u}_h - \bar{u}^{\mathrm{slod}}_{h,H,m}\|_{L^2(\Omega;L^2(D))} / \|\boldsymbol{u}_h\|_{L^2(\Omega;L^2(D))},$$

which are computed using the L^2-orthogonal projection of the reference solution $\boldsymbol{u}_h$. This corresponds to the error considered in Theorem 5.3.5, where the first term Ξ_1 in the decomposition (5.17) is omitted. For fixed H and varying ε we observe the rate $\varepsilon^{d/2}$, which is in agreement with Theorem 5.4.4. In the converse setting, where ε is fixed and H is varied, the expected negative dependence on H is not observed. In the one-dimensional case, the error remains nearly constant with respect to H, provided that the coarse mesh is sufficiently coarse compared to ε. In two dimensions, a negative dependence on H is observed; however, it is significantly weaker than the theoretical rate of H^{-3} predicted by Theorem 5.4.4. Instead, the error appears to scale approximately like $H^{-0.15}$.

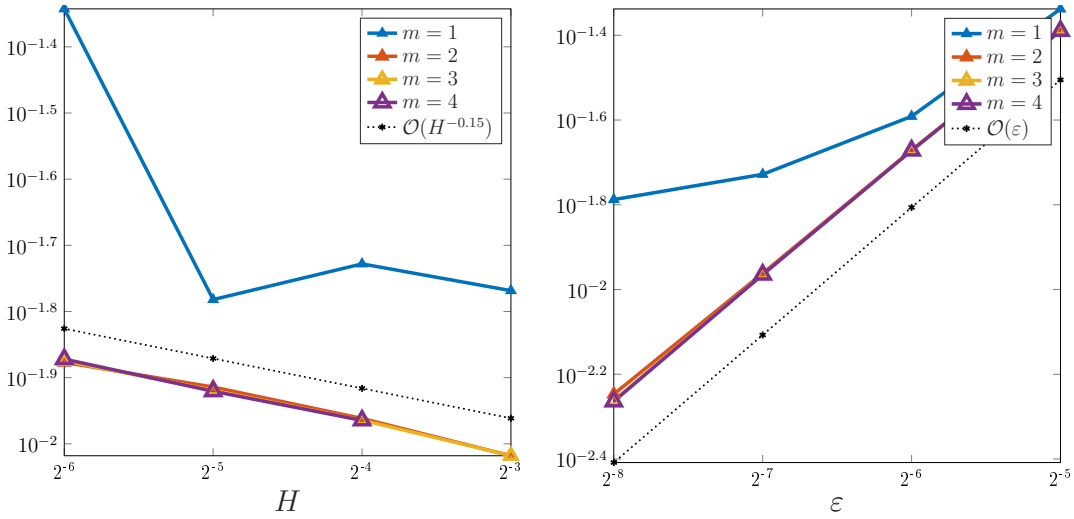

Figure 5.7.: Plot of the relative L^2-errors of the presented SLOD method for a $\mathcal{T}_\varepsilon$-piecewise constant random coefficient in two spatial dimensions. Left: errors as functions of the coarse mesh size H for fixed $\varepsilon = 2^{-7}$; Right: errors as functions of the correlation length ε for fixed $H = 2^{-4}$.

6. Hierarchical Super-Localized Numerical Stochastic Homogenization

In this chapter, we combine the methodologies developed in the previous chapters to construct a novel numerical stochastic homogenization method for elliptic PDEs with random coefficients. Specifically, we integrate the hierarchical structure introduced in Chapter 4 with the construction of super-localized basis functions in the stochastic setting from Chapter 5.

The core idea is to define a hierarchical basis composed of linear combinations of stochastic SLOD basis functions, which are associated with different levels in the mesh hierarchy. This hierarchical basis spans the approximation space at the finest level and inherits the favorable properties of the super-localized basis functions, such as rapid decay and locality.

To retain the simplicity and scalability of the stochastic SLOD method from Chapter 5, we again employ a collocation-type formulation to approximate the expected value of the solution. In doing so, we avoid the need to assemble a global stiffness matrix. As a result, the expected basis functions can be computed independently, enabling a highly parallel implementation. Instead of a global stiffness matrix, we assemble a system matrix associated with the deterministic source terms of the hierarchical basis functions to compute the coefficients in the collocation-type approximation. As confirmed by numerical experiments, the hierarchical structure significantly improves the conditioning of this system matrix compared to the standard two-level stochastic SLOD approach from Chapter 5, in which the two scales correspond to the fine-scale features of the random coefficient and the macroscopic approximation scale.

Using tools from quantitative stochastic homogenization theory, we derive an a posteriori error estimate for the coarse-scale approximation provided by the proposed hierarchical method. Furthermore, we conduct numerical experiments to validate our theoretical findings. These experiments indicate that the hierarchical formulation enhances the robustness and stability of the method, as the fine-level approximations benefit from the lower variances of the basis functions associated with coarser levels.

6.1. Numerical stochastic homogenization method

In this section, we develop a hierarchical method for the prototypical diffusion problem (5.1), building on the principles of SLOD by integrating the approaches introduced in Chapters 4 and 5. The hierarchical basis functions are constructed over a sequence of nested Cartesian meshes $\{\mathcal{T}_\ell\}_{\ell\in\{1,\dots,L\}}$ with $L \in \mathbb{N}$, covering the domain D, where each mesh $\mathcal{T}_\ell$ has mesh size H_ℓ. The refinement is uniform, with each level satisfying $H_{\ell+1} = H_\ell/2$ for $\ell \leq L-1$. We denote by $N_\ell \coloneqq \#\mathcal{T}_\ell$ the number of elements in the mesh at level ℓ.

The number of hierarchical basis functions corresponding to level ℓ, denoted by N_ℓ^b, is defined as

$$N_\ell^b \coloneqq \begin{cases} N_1, & \text{if } \ell = 1, \\ (2^d-1)N_{\ell-1}, & \text{if } \ell > 1. \end{cases}$$

At level $\ell = 1$, we use the stochastic SLOD functions $\hat{\boldsymbol{\varphi}}^{\mathrm{slod}}_{1,K,m} \in L^2(\Omega; H^1_0(D_K))$, defined in (5.6) and associated with elements $K \in \mathcal{T}_1$, as hierarchical basis functions. Hence, the stochastic HSLOD functions at this level are given by

$$\hat{\boldsymbol{\psi}}^{\mathrm{hslod}}_{1,i,m} = \hat{\boldsymbol{\varphi}}^{\mathrm{slod}}_{1,K_i,m}$$

for $i = 1, \dots, N_1$

For levels $\ell > 1$, the hierarchical basis functions are constructed as linear combinations of stochastic SLOD functions, following the approach in Section 4.1.2. These stochastic HSLOD functions are defined on patches $\mathsf{N}^m_{\ell-1}(T_{J_i})$, as introduced in (4.5), and correspond to elements $T_{J_i} \in \mathcal{T}_{\ell-1}$ from the coarser mesh level. Here, the index J_i identifies the reference element and is specified in (4.10). On each such patch, $2^d - 1$ basis functions need to be defined. To simplify notation, we fix the oversampling parameter $m \in \mathbb{N}$ and refer to the m-th order patch of $T_{J_i} \in \mathcal{T}_{\ell-1}$ on level $\ell-1$ simply as $D^{(\ell-1)}_{J_i} \coloneqq \mathsf{N}^m_{\ell-1}(T_{J_i})$.

For each $i \in \{1, \dots, N_\ell^b\}$, the hierarchical basis function $\hat{\boldsymbol{\psi}}^{\mathrm{hslod}}_{\ell,i,m}$ is constructed exclusively from stochastic SLOD functions $\hat{\boldsymbol{\varphi}}^{\mathrm{slod}}_{\ell,K,m}$, which are defined on patches composed of elements from the finer mesh $\mathcal{T}_\ell$, with their support entirely contained in the patch $D^{(\ell-1)}_{J_i}$. More precisely, for each element $T_{J_i} \in \mathcal{T}_{\ell-1}$, we define the set

$$S^{(\ell)}_{J_i} \coloneqq \{K \in \mathcal{T}_\ell : \operatorname{supp}(\hat{\boldsymbol{\varphi}}^{\mathrm{slod}}_{\ell,K,m}) \subset D^{(\ell-1)}_{J_i}\}.$$

With this notation, the HSLOD basis function $\hat{\boldsymbol{\psi}}^{\mathrm{hslod}}_{\ell,i,m} \in L^2(\Omega; H^1_0(D^{(\ell-1)}_{J_i}))$ is defined by

$$\hat{\boldsymbol{\psi}}^{\mathrm{hslod}}_{\ell,i,m} \coloneqq \sum_{K\in S^{(\ell)}_{J_i}} d_K^{(\ell,i)} \hat{\boldsymbol{\varphi}}^{\mathrm{slod}}_{\ell,K,m}, \tag{6.1}$$

where the non-trivial coefficients are chosen such that $\mathbb{E}[\hat{\boldsymbol{\psi}}^{\mathrm{hslod}}_{\ell,i,m}]$ satisfies the conditions given in (4.8) and (4.9). The corresponding deterministic local source

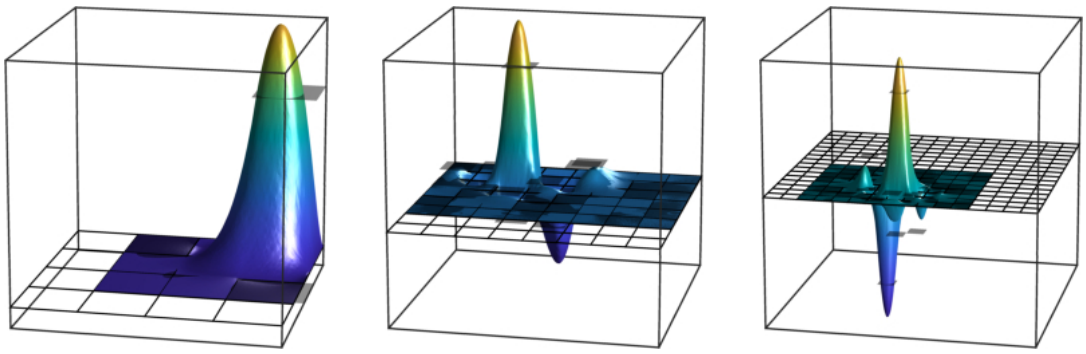

Figure 6.1.: Illustration of the localized hierarchical basis functions $\mathbb{E}[\hat{\boldsymbol{\psi}}^{\mathrm{hslod}}_{\ell,i,m}]$ on successively refined meshes for a piecewise constant random coefficient with a correlation length of $\varepsilon = 2^{-7}$ in two spatial dimensions. The oversampling parameter is set to $m = 2$. The corresponding right-hand sides $g^{\mathrm{hslod}}_{\ell,i,m}$ are shown in gray.

term $g^{\mathrm{hslod}}_{\ell,i,m}$ is defined analogously as a weighted sum of the deterministic local source terms associated with the stochastic SLOD functions $\hat{\boldsymbol{\varphi}}^{\mathrm{slod}}_{\ell,K,m}$, using the same coefficients as in (6.1). An illustration of the deterministic hierarchical basis functions $\mathbb{E}[\hat{\boldsymbol{\psi}}^{\mathrm{hslod}}_{\ell,i,m}]$ and their associated local source terms is given in Figure 6.1.

For the error analysis following in the next section, we define the quantity

$$\zeta = \zeta(H_L, m) := \max_{\ell\in\{1,\dots,L\}} \max_{i\in\{1,\dots,N^b_\ell\}} \sqrt{\sum_{K\in S^{(\ell)}_{J_i}} |d^{(\ell,i)}_K|^2}. \tag{6.2}$$

In addition, let $\sigma_{\ell,K}$ denote the expected localization error associated with the stochastic SLOD function $\hat{\boldsymbol{\varphi}}^{\mathrm{slod}}_{\ell,K,m}$, as defined in (5.10). A global measure of the localization error across all levels and elements is then given by

$$\sigma = \sigma(H_L, \varepsilon, m) := \max_{\ell\in\{1,\dots,L\}} \max_{K\in\mathcal{T}_\ell} \sigma_{\ell,K}, \tag{6.3}$$

where $\varepsilon > 0$ denotes the correlation length of the random coefficient $\boldsymbol{A}$; see Theorem 5.3.1. According to Theorem 5.4.3, where an upper bound for the localization error at each level is provided, σ satisfies

$$\sigma \lesssim m^2 H_L^{-1} \exp(-Cm) + m^4 \left(\frac{\varepsilon}{H_L}\right)^{d/2} \tag{6.4}$$

with $C > 0$ independent of H_L and m, provided that ε satisfies the smallness assumption

$$\varepsilon^d \lesssim m^{-8} H_L^d.$$

For simplicity, we refer to the hierarchical basis functions using their global indices. Thus, with

$$i = \begin{cases} j, & \text{if } \ell = 1, \\ \#\mathcal{T}_{\ell-1} + j, & \text{if } \ell > 1, \end{cases}$$

we have the relation

$$\hat{\boldsymbol{\psi}}_{i,m}^{\mathrm{hslod}} = \hat{\boldsymbol{\psi}}_{\ell,j,m}^{\mathrm{hslod}} \tag{6.5}$$

with corresponding local source term $g_{i,m}^{\mathrm{hslod}} = g_{\ell,j,m}^{\mathrm{hslod}}$. Using global indices, we refer to the patches associated with the hierarchical basis functions as $D_i = D_{J_j}^{\ell-1}$. With this notation established, we are now ready to define the novel collocation-type hierarchical method by

$$\bar{u}_{L,m}^{\mathrm{hslod}} = \sum_{i=1}^{N_L} c_i \Pi_L \mathbb{E}[\hat{\boldsymbol{\psi}}_{i,m}^{\mathrm{hslod}}], \tag{6.6}$$

where $(c_i)_{i\in\{1,\dots,N_L\}}$ are the coefficients of the expansion of $\Pi_L f$ in terms of the local source terms $g_{i,m}^{\mathrm{hslod}}$.

6.2. Error analysis

In this section, we perform an error analysis of the proposed numerical stochastic homogenization method. To this end, we assume that the local source terms $\{g_{i,m}^{\mathrm{hslod}} : i = 1,\dots,N_L\}$ are Riesz stable in the sense of Theorem 4.2.1. In addition, we impose structural assumptions on the randomness of the coefficient field $\boldsymbol{A}$, as specified in Theorem 5.3.1. The following theorem provides an a posteriori error bound for the proposed hierarchical method. The bound involves the quantity ζ, as defined in (6.2), as well as the Riesz stability constant C_{rb}. Both of these quantities can be computed a posteriori, as outlined in Section 6.3.

Theorem 6.2.1 (A posteriori error bound)**.** *Let $\boldsymbol{A}$ be a random coefficient field satisfying the conditions in Theorem 5.3.1, and assume that the set $\{g_{i,m}^{\mathrm{hslod}} : i = 1,\dots,N_L\}$ is Riesz stable in the sense of Theorem 4.2.1. Then, for any $f \in L^2(D)$, the solution $\bar{u}_{L,m}^{\mathrm{hslod}}$ of the hierarchical numerical stochastic homogenization method defined in* (6.6) *satisfies the error estimate*

$$\|\boldsymbol{u} - \bar{u}_{L,m}^{\mathrm{hslod}}\|_{L^2(\Omega,L^2(D))} \lesssim \Big(H_L + C_{\mathrm{rb}}^{1/2}\zeta m^d\sqrt{L}\Big(\sigma + m^2\Big(\frac{\varepsilon}{H_L}\Big)^{d/2}\Big)\Big)\|f\|_{L^2(D)},$$

where $C_{\mathrm{rb}}(H_L, m)$ is the stability constant from Theorem 4.2.1.

Moreover, if the additional smallness condition

$$\varepsilon^d \lesssim m^{-8} H_L^d$$

is satisfied and $m \gtrsim |\log(H_L)|$ holds, the error bound simplifies to

$$\|\boldsymbol{u} - \bar{u}_{L,m}^{\mathrm{hslod}}\|_{L^2(\Omega,L^2(D))} \lesssim \Big(H_L + C_{\mathrm{rb}}^{1/2}\zeta m^{4+d}\sqrt{L}\Big(\frac{\varepsilon}{H_L}\Big)^{d/2}\Big)\|f\|_{L^2(D)}.$$

Proof. For the error analysis, we follow the ideas of the proof of Theorem 5.3.5 and introduce the function

$$\boldsymbol{u}_{L,m} \coloneqq \sum_{i=1}^{N_L} c_i \hat{\boldsymbol{\psi}}_{i,m}^{\mathrm{hslod}}, \tag{6.7}$$

where $(c_i)_{i\in\{1,\dots,N_L\}}$ are the coefficients of the expansion of $\Pi_L f$ in terms of the local source terms $g_{i,m}^{\mathrm{hslod}}$. To simplify notation, we introduce for any subset $S \subseteq D$ the short-hand notation

$$\|\cdot\|_{\Omega,S} \coloneqq \|\cdot\|_{L^2(\Omega,L^2(S))}.$$

Using the triangle inequality yields

$$\begin{aligned}\|\boldsymbol{u} - \bar{u}_{L,m}^{\mathrm{hslod}}\|_{\Omega,D} &\\ &\leq \|\boldsymbol{u} - \Pi_L \boldsymbol{u}\|_{\Omega,D} + \|\Pi_L(\boldsymbol{u} - \boldsymbol{u}_{L,m})\|_{\Omega,D} + \|\Pi_L \boldsymbol{u}_{L,m} - \bar{u}_{L,m}^{\mathrm{hslod}}\|_{\Omega,D} \\ &=: \Xi_1 + \Xi_2 + \Xi_3.\end{aligned} \tag{6.8}$$

For the first summand Ξ_1, we obtain using the approximation property (2.7) of the operator Π_L and the stability estimate (5.4) that

$$\Xi_1^2 = \mathbb{E}\Big[\|\boldsymbol{u} - \Pi_L \boldsymbol{u}\|_{L^2(D)}^2\Big] \lesssim H_L^2\, \mathbb{E}\Big[\|\nabla \boldsymbol{u}\|_{L^2(D)}^2\Big] \lesssim H_L^2\, \|f\|_{L^2(D)}^2.$$

For estimating the term Ξ_2, we first apply the L^2-stability of Π_L, cf. (2.6), and Friedrichs' inequality. Then, following the lines of the convergence proof of the HSLOD in the deterministic setting, cf. Theorem 4.3.1, we obtain that

$$\Xi_2 \lesssim \|\nabla(\boldsymbol{u} - \boldsymbol{u}_{L,m})\|_{\Omega,D} \lesssim (H_L + C_{\mathrm{rb}}^{1/2}\sqrt{L} m^d \zeta \sigma)\|f\|_{L^2(D)}.$$

In order to estimate the term Ξ_3, we recall definitions (6.6) and (6.7) and use the Cauchy–Schwarz inequality and the fact that $\operatorname{supp}(\hat{\boldsymbol{\psi}}_{i,m}^{\mathrm{hslod}}) \subset D_i$ to obtain, setting $\boldsymbol{e} \coloneqq \Pi_L \boldsymbol{u}_{L,m} - \bar{u}_{L,m}^{\mathrm{hslod}}$, that

$$\begin{aligned}\Xi_3^2 &= \sum_{i=1}^{N_L} c_i\, \mathbb{E}\Big[\Big(\Pi_L \hat{\boldsymbol{\psi}}_{i,m}^{\mathrm{hslod}} - \Pi_L \mathbb{E}[\hat{\boldsymbol{\psi}}_{i,m}^{\mathrm{hslod}}], \boldsymbol{e}\Big)_{L^2(D_i)}\Big] \\ &\leq \sum_{i=1}^{N_L} |c_i| \|\Pi_L \hat{\boldsymbol{\psi}}_{i,m}^{\mathrm{hslod}} - \Pi_L \mathbb{E}[\hat{\boldsymbol{\psi}}_{i,m}^{\mathrm{hslod}}]\|_{\Omega,D_i} \|\boldsymbol{e}\|_{\Omega,D_i}.\end{aligned} \tag{6.9}$$

To estimate the first norm in each summand separately, we use relation (6.5), the definition (6.1), the fact that $\operatorname{supp}(\hat{\boldsymbol{\varphi}}_{\ell,K,m}^{\mathrm{slod}}) \subset D_K$, and the Cauchy–Schwarz inequality to get that

$$\begin{aligned}\|\Pi_L \hat{\boldsymbol{\psi}}_{i,m}^{\mathrm{hslod}} - \Pi_L \mathbb{E}[\hat{\boldsymbol{\psi}}_{i,m}^{\mathrm{hslod}}]\|_{\Omega,D_i}^2 &\\ &= \sum_{K\in S_{J_j}} d_K^{(\ell,j)} \mathbb{E}\Big[\big(\Pi_L \hat{\boldsymbol{\varphi}}_{\ell,K,m}^{\mathrm{slod}} - \Pi_L \mathbb{E}[\hat{\boldsymbol{\varphi}}_{\ell,K,m}^{\mathrm{slod}}], \Pi_L \hat{\boldsymbol{\psi}}_{\ell,j,m}^{\mathrm{hslod}} - \Pi_L \mathbb{E}[\hat{\boldsymbol{\psi}}_{\ell,j,m}^{\mathrm{hslod}}]\big)_{L^2(D_K)}\Big] \\ &\leq \sum_{K\in S_{J_j}} |d_K^{(\ell,j)}| \|\Pi_L \hat{\boldsymbol{\varphi}}_{\ell,K,m}^{\mathrm{slod}} - \Pi_L \mathbb{E}[\hat{\boldsymbol{\varphi}}_{\ell,K,m}^{\mathrm{slod}}]\|_{\Omega,D_K} \|\Pi_L \hat{\boldsymbol{\psi}}_{\ell,j,m}^{\mathrm{hslod}} - \Pi_L \mathbb{E}[\hat{\boldsymbol{\psi}}_{\ell,j,m}^{\mathrm{hslod}}]\|_{\Omega,D_K}.\end{aligned}$$

Following the steps leading to estimate (5.20) in the proof of Theorem 5.3.5 yields

$$\begin{aligned}
&\|\Pi_L \hat{\boldsymbol{\varphi}}^{\mathrm{slod}}_{\ell,K,m} - \Pi_L \mathbb{E}[\hat{\boldsymbol{\varphi}}^{\mathrm{slod}}_{\ell,K,m}]\|^2_{\Omega,D_K} \\
&\quad = \sum_{T\in\mathcal{T}_{L,D_K}} |T|^{-1}\mathbb{E}\Big[\big((\hat{\boldsymbol{\varphi}}^{\mathrm{slod}}_{\ell,K,m}, \mathbb{1}_T)_{L^2(T)} - \mathbb{E}[(\hat{\boldsymbol{\varphi}}^{\mathrm{slod}}_{\ell,K,m}, \mathbb{1}_T)_{L^2(T)}]\big)^2\Big] \\
&\quad \lesssim (mH_\ell)^{4-d}\varepsilon^d |\{T\in\mathcal{T}_L : T\subset D_K\}| \lesssim m^4\Big(\frac{\varepsilon}{H_L}\Big)^d,
\end{aligned}$$

where we used that $H_\ell = H_L 2^{L-\ell}$. The combination of the previous two estimates, the Cauchy–Schwarz inequality, and the finite overlap of patches gives

$$\begin{aligned}
&\|\Pi_L \hat{\boldsymbol{\psi}}^{\mathrm{hslod}}_{i,m} - \Pi_L \mathbb{E}[\hat{\boldsymbol{\psi}}^{\mathrm{hslod}}_{i,m}]\|^2_{\Omega,D_i} \\
&\quad \lesssim m^2\varepsilon^{d/2}H_L^{-d/2}\sqrt{\sum_{K\in S_{J_j}} |d_K^{(\ell,j)}|^2}\sqrt{\sum_{K\in S_{J_j}} \|\Pi_L \hat{\boldsymbol{\psi}}^{\mathrm{hslod}}_{i,m} - \Pi_L \mathbb{E}[\hat{\boldsymbol{\psi}}^{\mathrm{hslod}}_{i,m}]\|^2_{\Omega,D_K}} \\
&\quad \lesssim m^{2+d/2}\varepsilon^{d/2}H_L^{-d/2}\zeta \|\Pi_L \hat{\boldsymbol{\psi}}^{\mathrm{hslod}}_{i,m} - \Pi_L \mathbb{E}[\hat{\boldsymbol{\psi}}^{\mathrm{hslod}}_{i,m}]\|_{\Omega,D_i}.
\end{aligned}$$

Inserting into (6.9), applying the Cauchy–Schwarz inequality once more, using Theorem 4.2.1, and employing the finite overlap of patches per level, we obtain that

$$\begin{aligned}
\Xi_3^2 &\lesssim m^{2+d/2}\varepsilon^{d/2}H_L^{-d/2}\zeta\sqrt{\sum_{i=1}^{N_L}|c_i|^2}\sqrt{\sum_{i=1}^{N_L}\|\Pi_L \boldsymbol{u}_{L,m} - \bar{u}^{\mathrm{hslod}}_{L,m}\|^2_{\Omega,D_i}} \\
&\lesssim C_{\mathrm{rb}}^{1/2}\sqrt{L}m^{2+d}\zeta\varepsilon^{d/2}H_L^{-d/2}\|f\|_{L^2(D)}\,\Xi_3.
\end{aligned}$$

By combining the estimates for Ξ_1, Ξ_2, and Ξ_3, we obtain the first error bound stated in the theorem. Additionally, incorporating Theorem 5.4.3 and adapting it to the hierarchical setting (cf. (6.4)), results in the second error estimate. □

6.3. Numerical Experiments

In the following, we present a series of numerical experiments to illustrate the effectiveness of the proposed hierarchical numerical homogenization method. To this end, we compare its performance with the two-level stochastic SLOD method introduced in Chapter 5. We consider uniform Cartesian meshes of the domain $D = (0,1)^d$ with spatial dimension $d \in \{1,2\}$. From this point on, we use H to denote the side length of the mesh elements, rather than their diameter. The random coefficients $\boldsymbol{A}$ are piecewise constant with respect to uniform Cartesian meshes $\mathcal{T}_\varepsilon$ with mesh sizes $\varepsilon \in \{2^{-6}, 2^{-7}, 2^{-8}, 2^{-9}\}$. The values of $\boldsymbol{A}$ are independently and identically distributed on each element, taking values uniformly in the interval $[0.1, 1]$.

The SLOD basis functions are computed according to the procedure outlined in Section 5.5, using the $\mathbb{P}^1$-finite element method on the fine mesh $\mathcal{T}_h$, which is

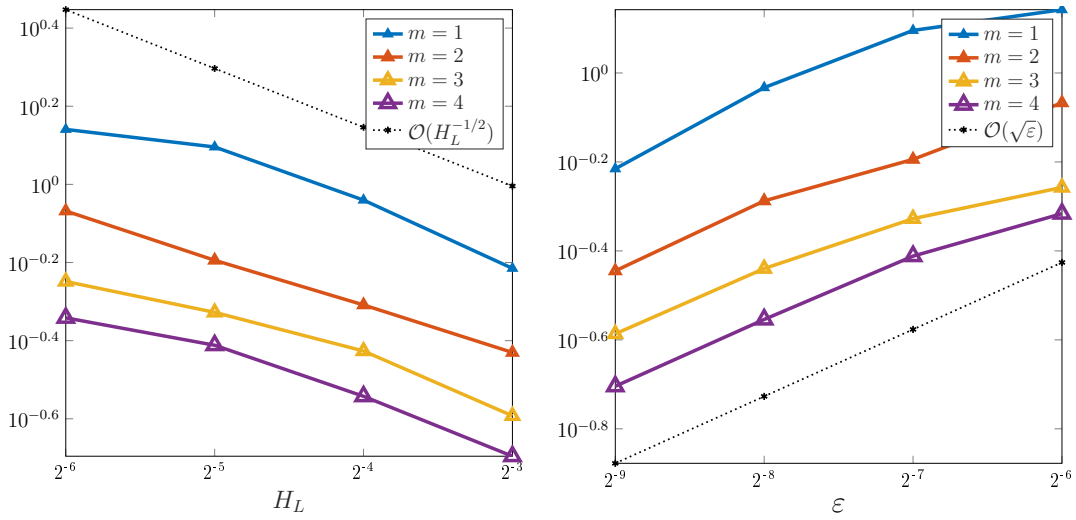

Figure 6.2.: Depiction of σ for a $\mathcal{T}_\varepsilon$-piecewise constant random coefficient in one spatial dimensions. Left: in dependence of the coarse mesh size H_L for $\varepsilon = 2^{-7}$; Right: in dependence of the correlation length ε for $H_L = 2^{-5}$.

generated by successive uniform refinements of the coarse mesh. Specifically, we set $h = 2^{-12}$ for $d = 1$ and $h = 2^{-10}$ for $d = 2$. The hierarchical basis functions are then obtained as a linear combination of the SLOD functions, where the coefficients are chosen such that the conditions given in (4.8) and (4.9) hold. The resulting fully discrete numerical approximation of $\mathbb{E}[\boldsymbol{u}]$ is denoted by $\bar{u}^{\text{hslod}}_{h,L,m}$. In the experiments, all expectations are approximated by empirical means.

To compute the reference solution, we use $M_s = 1000$ samples of the coefficient field on the entire domain D, generated via standard Monte Carlo sampling. For the local patch problems, we use $M_s = 1000$ quasi-Monte Carlo samples of the coefficient.

Numerical investigation of σ, ζ and C_{rb}

Numerical experiments, illustrated in Figures 6.2 and 6.3, show that σ decays proportionally to $(\varepsilon/H_L)^{d/2}$, consistent with the theoretical upper bound derived in (6.4) and the observations discussed in Section 5.6.

The quantity ζ is defined as the maximum Euclidean norm of the coefficient vectors used in the basis construction and can therefore be computed easily. However, to enhance the numerical linear independence of the $2^d - 1$ hierarchical basis functions associated with each patch, we incorporate an additional orthonormalization step with respect to the Euclidean inner product after enforcing conditions (4.8) and (4.9). As a result of this procedure, we obtain $\zeta = 1$ in all numerical experiments.

In the hierarchical setting, the Riesz stability constant C_{rb} remains essentially

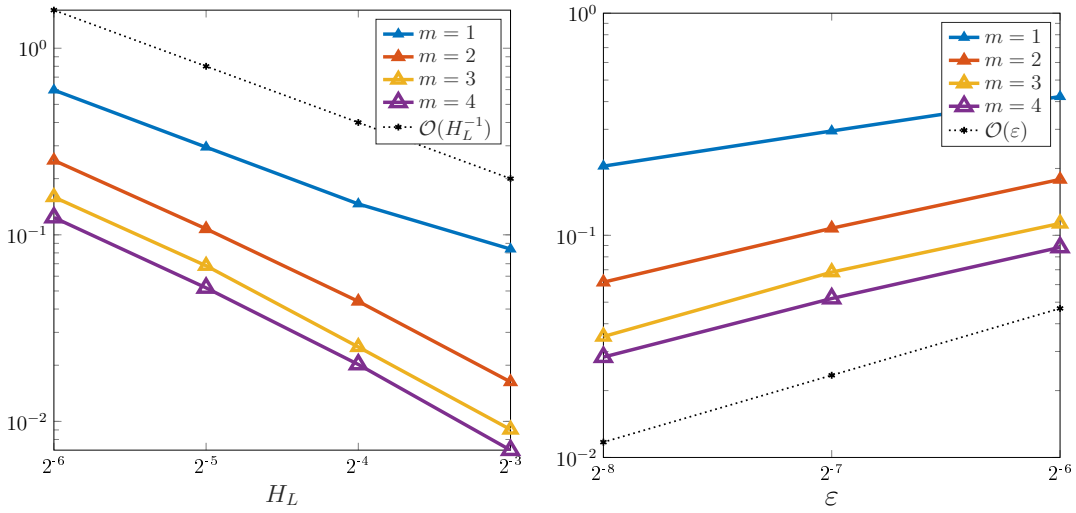

Figure 6.3.: Depiction of σ for a $\mathcal{T}_\varepsilon$-piecewise constant random coefficient in two spatial dimensions. Left: in dependence of the coarse mesh size H_L for $\varepsilon = 2^{-7}$; Right: in dependence of the correlation length ε for $H_L = 2^{-5}$.

unchanged with the addition of refinement levels. Consequently, no dependence on the parameter H_L is observed in either one- or two-dimensional cases. Similar to the two-level stochastic SLOD setting, the constant C_{rb} is also largely independent of the correlation length ε, and no significant dependence on the oversampling parameter m is evident.

Numerical validation of convergence

To numerically verify the convergence of the proposed stochastic homogenization method, we consider the smooth right-hand sides introduced in (5.36), as in the previous section. The hierarchy employs successively refined meshes, with the mesh size of the coarsest level generally set to $H_1 = 2^{-3}$. However, for small values of ε and larger oversampling parameters m, this choice does not yield good approximations in two dimensions. Therefore, for $\varepsilon = 2^{-8}$ in 2D, we instead use $H_1 = 2^{-4}$.

The relative L^2-errors

$$\frac{\|\boldsymbol{u}_h - \bar{u}^{\mathrm{hslod}}_{h,L,m}\|_{L^2(\Omega;L^2(D))}}{\|\boldsymbol{u}_h\|_{L^2(\Omega;L^2(D))}}, \tag{6.10}$$

considered in Theorem 6.2.1 are shown in Figures 6.4 and 6.6 for the one- and two-dimensional settings, respectively. In addition, Figures 6.5 and 6.7 display the relative L^2-errors

$$\frac{\|\Pi_L \boldsymbol{u}_h - \bar{u}^{\mathrm{hslod}}_{h,L,m}\|_{L^2(\Omega;L^2(D))}}{\|\boldsymbol{u}_h\|_{L^2(\Omega;L^2(D))}}, \tag{6.11}$$

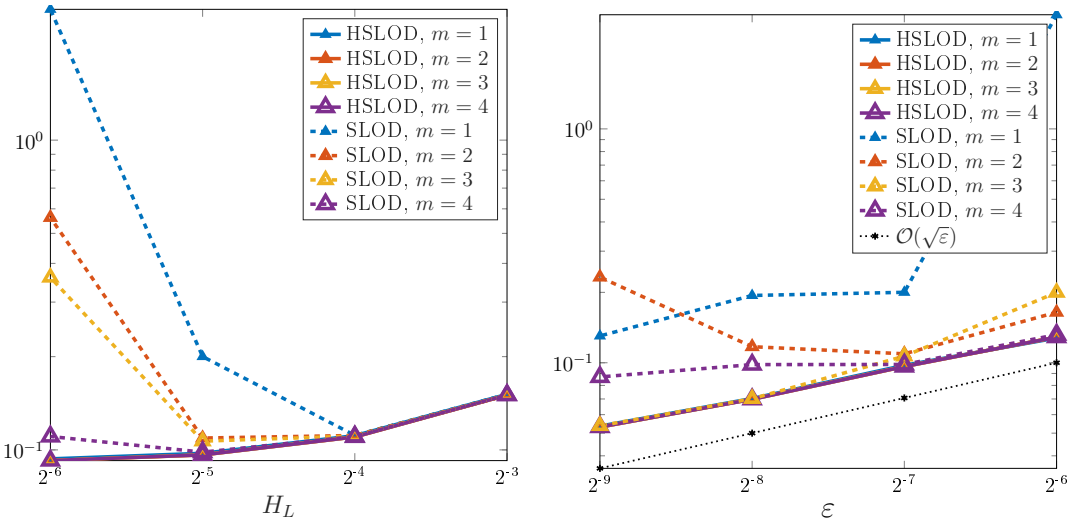

Figure 6.4.: Relative L^2-errors $\|\boldsymbol{u}_h - \bar{u}^{\text{hslod}}_{h,L,m}\|_{L^2(\Omega;L^2(D))}/\|\boldsymbol{u}_h\|_{L^2(\Omega;L^2(D))}$ of the proposed HSLOD method for a $\mathcal{T}_\varepsilon$-piecewise constant random coefficient in one spatial dimension. Left: errors as functions of the coarse mesh size H_L for fixed $\varepsilon = 2^{-7}$; Right: errors in dependency of the correlation length ε for fixed $H_L = 2^{-5}$.

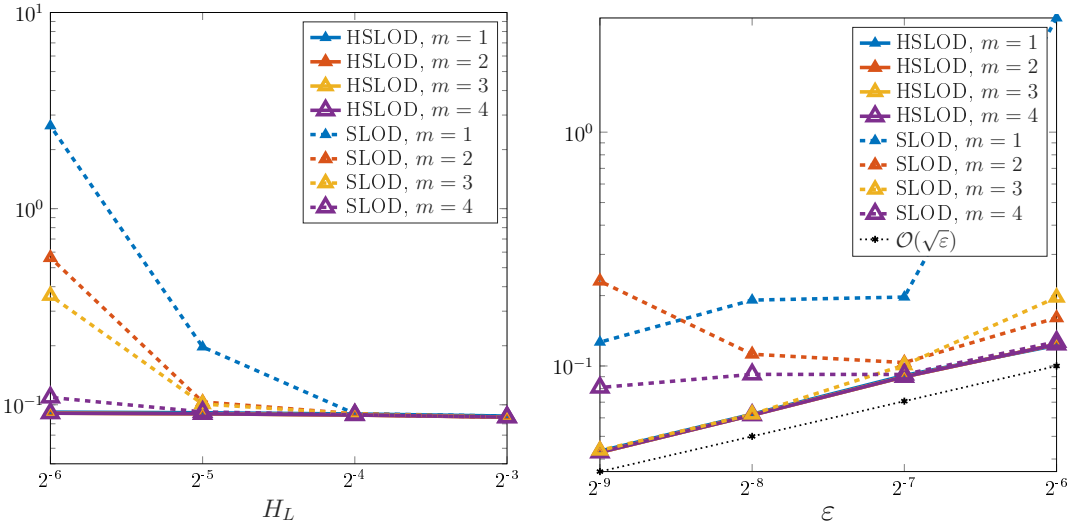

Figure 6.5.: Relative L^2-errors $\|\Pi_L \boldsymbol{u}_h - \bar{u}^{\text{hslod}}_{h,L,m}\|_{L^2(\Omega;L^2(D))}/\|\boldsymbol{u}_h\|_{L^2(\Omega;L^2(D))}$ of the proposed HSLOD method for a $\mathcal{T}_\varepsilon$-piecewise constant random coefficient in one spatial dimension. Left: errors as functions of the coarse mesh size H_L for fixed $\varepsilon = 2^{-7}$; Right: errors in dependency of the correlation length ε for fixed $H_L = 2^{-5}$.

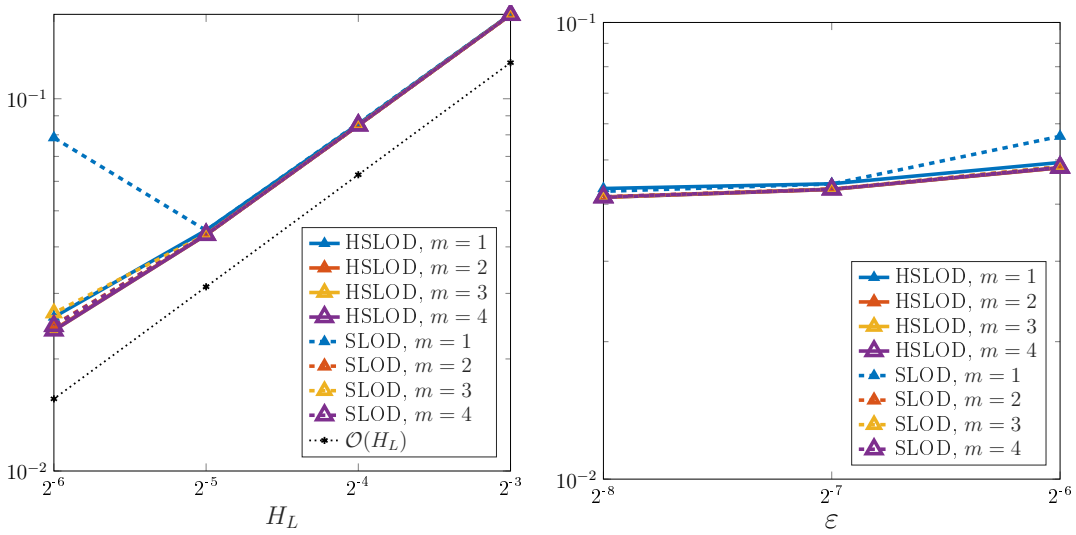

Figure 6.6.: Relative L^2-errors $\|\boldsymbol{u}_h - \bar{u}^{\text{hslod}}_{h,L,m}\|_{L^2(\Omega;L^2(D))}/\|\boldsymbol{u}_h\|_{L^2(\Omega;L^2(D))}$ of the proposed HSLOD method for a $\mathcal{T}_\varepsilon$-piecewise constant random coefficient in two spatial dimensions. Left: errors as functions of the coarse mesh size H_L for fixed $\varepsilon = 2^{-7}$; Right: errors as functions of the correlation length ε for fixed $H_L = 2^{-5}$.

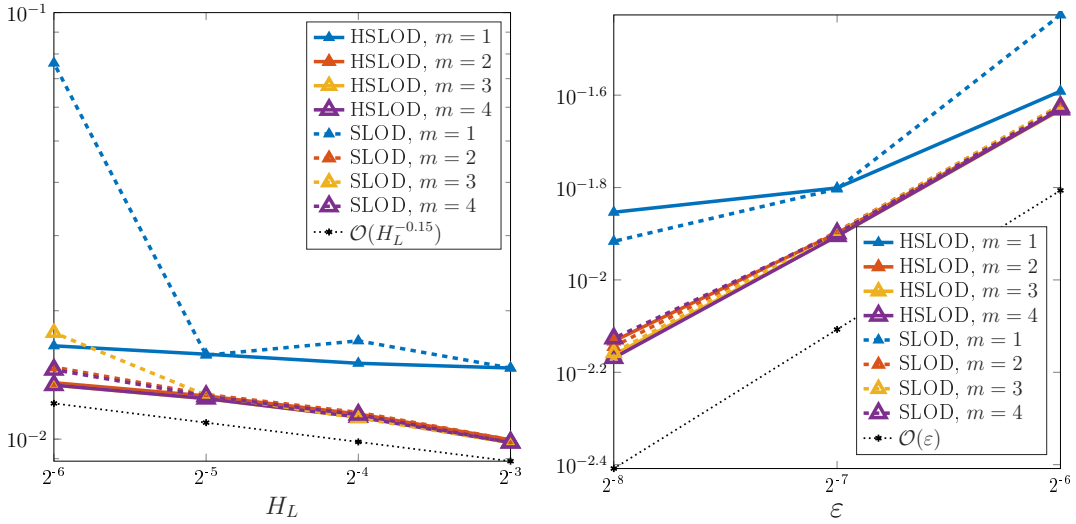

Figure 6.7.: Relative L^2-errors $\|\Pi_L \boldsymbol{u}_h - \bar{u}^{\text{hslod}}_{h,L,m}\|_{L^2(\Omega;L^2(D))}/\|\boldsymbol{u}_h\|_{L^2(\Omega;L^2(D))}$ of the proposed HSLOD method for a $\mathcal{T}_\varepsilon$-piecewise constant random coefficient in two spatial dimensions. Left: errors as functions of the coarse mesh size H_L for fixed $\varepsilon = 2^{-7}$; Right: errors as functions of the correlation length ε for fixed $H_L = 2^{-5}$.

Table 6.1.: Condition numbers of the full system matrix associated with the local source terms for different numbers of hierarchy levels in two dimensions, rounded to two significant figures. The correlation length is set to $\varepsilon = 2^{-7}$ and the oversampling parameter to $m = 2$.

H_L	2^{-3}	2^{-4}	2^{-5}	2^{-6}
stochastic SLOD	510	$7.2 \cdot 10^3$	$1.1 \cdot 10^5$	$1.9 \cdot 10^6$
stochastic HSLOD	510	$1.1 \cdot 10^3$	$1.6 \cdot 10^3$	$2.6 \cdot 10^3$

computed using the L^2-orthogonal projection $\Pi_L \boldsymbol{u}_h$ of the reference solution. This corresponds to the error reported in Theorem 6.2.1 with the first term Ξ_1 from the decomposition in (6.8) omitted. It also matches the error metric considered in Section 5.6.

When considering the full error from (6.10), the first term is dominant, particularly in the two-dimensional case. This results in an overall error decay rate of $\mathcal{O}(H_L)$. The one-dimensional case also shows a dependence on H_L, though this decay is much weaker. For the complementary setting, where the number of hierarchy levels is fixed and the correlation length ε is varied, the decay in ε is approximately $\mathcal{O}(\sqrt{\varepsilon})$ in one dimension and remains nearly constant in two dimensions.

When excluding the first term of the error, i.e., when considering the truncated error (6.11), the observed behavior aligns well with the results presented in Section 5.6. Notably, the hierarchical construction appears to produce more stable approximations, particularly in the one-dimensional case or when finer levels are included in the hierarchy, compared to the two-level stochastic SLOD method, which is highly sensitive to the correct parameter choice (especially in 1D) within the stabilization procedure described in Section 5.5. Furthermore, the hierarchical method already yields good approximations with the minimal choice $m = 1$.

Another advantage of the proposed hierarchical method is the significantly improved conditioning of the system matrix associated with the deterministic local source terms of the hierarchical basis functions, compared to the two-level stochastic SLOD. This system matrix is used to compute the coefficients in the collocation-type approximation. The improvement is demonstrated in Table 6.1, which presents the condition numbers of the full system matrices for both the stochastic SLOD and stochastic HSLOD methods in two dimensions, considering a coefficient with correlation length $\varepsilon = 2^{-7}$ and an oversampling parameter $m = 2$. The lowest level in the hierarchy has a mesh size of 2^{-3}, and the condition numbers are shown for different numbers of hierarchy levels. Note that variations in ε or m do not significantly affect the conditioning.

7. Conclusion and Outlook

This thesis has explored the development and analysis of advanced numerical multiscale methods for solving elliptic diffusion problems with highly heterogeneous and, in some cases, random coefficients. Central to this work are several extensions of the SLOD method, originally introduced in [HP22b].

We began by identifying the key challenges posed by classical FEMs when applied to problems with fine-scale heterogeneities. In particular, the failure of traditional approaches to capture multiscale features efficiently motivated the need for more sophisticated discretization schemes. The concept of multiscale approximation spaces derived from global solution operators was introduced as a theoretical ideal. Although such spaces offer excellent approximation properties, their global nature renders them impractical for computation. The LOD method was introduced as a viable alternative, using localization strategies to construct exponentially decaying basis functions, thus enabling a practical and scalable multiscale method.

The SLOD method, introduced in the subsequent chapter, improves upon LOD by achieving super-exponential decay of localized basis functions in practice. This enhancement is accomplished through a refined localization strategy based on minimizing conormal derivatives on patch boundaries. We rigorously established this decay property in the case of a constant diffusion coefficient in Theorem 3.3.2. Furthermore, we proposed new stabilization techniques which are also effective in the stochastic or hierarchical settings in Sections 3.4.3 and 3.4.4.

In extending the SLOD framework to hierarchical settings, we developed the HSLOD method. Starting from an existing SLOD approximation, this hierarchical approach enables systematic accuracy improvement by incorporating additional discretization levels. The hierarchical construction produces a sparse and quasi-orthogonal basis, which facilitates an efficient multiresolution decomposition of the solution space. The resulting stiffness matrix is block-diagonal, with mesh-independent condition numbers for all but the first block (see Theorem 4.5.3). Assuming stability and linear independence of the basis functions, conditions that are practically ensured by the criterion in (4.9), we derived an error estimate that matches those of the classical SLOD and LOD methods.

The final part of this thesis addressed stochastic settings, where the diffusion coefficients are modeled as random fields. Building on the SLOD framework, we developed a stochastic homogenization method tailored to such problems. By exploiting the super-exponential decay of the localized basis functions, the method enables efficient sampling and achieves significant computational savings. Its collocation-type formulation eliminates the need to assemble a global stiff-

ness matrix, thereby greatly enhancing parallelization and reducing the overall assembly cost. A rigorous error analysis, grounded in the theory of quantitative stochastic homogenization, is provided in Theorem 5.3.5. Additionally, leveraging LOD techniques, we derived an a priori estimate for the localization error indicator, as presented in Theorem 5.4.3.

Building on the concepts developed in the preceding chapters, we introduced a novel hierarchical stochastic homogenization method. The hierarchical design improves the conditioning of the system matrix associated with the local source terms, enhancing both stability and computational efficiency. A rigorous error analysis is presented in Theorem 6.2.1, and the theoretical results are supported by numerical experiments.

Looking ahead, several promising directions and open questions emerge from this work. A particularly challenging problem is the extension of the super-localization results for SLOD basis functions to more general settings. While the current result relies on the assumption $A \equiv 1$, it remains an open question whether similar decay properties hold under more general, possibly rough, coefficients or in domains with irregular boundaries. One potential avenue involves tools from spectral geometry; however, this typically requires strong regularity assumptions on both the coefficient field and the domain boundary (cf. [HL01, PST15, GT16]), limiting its general applicability. Closely related is the open problem of designing a stabilization technique for SLOD basis functions that a priori guarantees both super-exponential decay and stability of the basis.

Another natural extension lies in adapting the HSLOD and stochastic homogenization methods to Helmholtz-type problems. Given the encouraging performance of SLOD-based approaches in deterministic Helmholtz settings (see [FHP24]), it is reasonable to expect that these hierarchical and stochastic variants could also provide significant benefits for modeling wave propagation in heterogeneous media.

Bibliography

[AB96] G. Allaire and M. Briane. Multiscale convergence and reiterated homogenisation. *Proc. Roy. Soc. Edinburgh Sect. A*, 126(2):297–342, 1996.

[Abd05] A. Abdulle. On a priori error analysis of fully discrete heterogeneous multiscale FEM. *Multiscale Model. Simul.*, 4(2):447–459, 2005.

[AC18] S. Armstrong and P. Cardaliaguet. Stochastic homogenization of quasilinear Hamilton-Jacobi equations and geometric motions. *J. Eur. Math. Soc.*, 20:797–864, 2018.

[ACB+11] A. Anantharaman, R. Costaouec, C. L. Bris, F. Legoll, and F. Thomines. Introduction to numerical stochastic homogenization and the related computational challenges: some recent developments. In: *Multiscale Modeling and Analysis for Materials Simulation*, volume 22 of *Lect. Notes Ser. Inst. Math. Sci. Natl. Univ. Singap.*, pp. 197–272. World Scientific, 2011.

[ACS14] S. Armstrong, P. Cardaliaguet, and P. Souganidis. Error estimates and convergence rates for the stochastic homogenization of Hamilton-Jacobi equations. *J. Amer. Math. Soc.*, 27:479–540, 2014.

[AD16] S. Armstrong and J.-P. Daniel. Calderón–Zygmund estimates for stochastic homogenization. *J. Funct. Anal.*, 270(1):312–329, 2016.

[AEEVE12] A. Abdulle, W. E, B. Engquist, and E. Vanden-Eijnden. The heterogeneous multiscale method. *Acta Numer.*, 21:1–87, 2012.

[AFK20] S. Armstrong, S. Ferguson, and T. Kuusi. Higher-order linearization and regularity in nonlinear homogenization. *Arch. Rational Mech. Anal.*, 237:631–741, 2020.

[AH12] K. Atkinson and W. Han. *Sperical harmonics and approximations on the unit sphere: an introduction*, volume 2044. Springer Science & Business Media, 2012.

[AHKM21] S. Armstrong, A. Hannukainen, T. Kuusi, and J.-C. Mourrat. An iterative method for elliptic problems with rapidly oscillating coefficients. *ESAIM: M2AN*, 50(1):37–55, 2021.

[AHP21] R. Altmann, P. Henning, and D. Peterseim. Numerical homogenization beyond scale separation. *Acta Numer.*, 30:1–86, 2021.

[AKM17] S. Armstrong, T. Kuusi, and J.-C. Mourrat. The additive structure of elliptic homogenization. *Invent. Math.*, 208:999–1154, 2017.

[AKM19] S. Armstrong, T. Kuusi, and J.-C. Mourrat. *Quantitative Stochastic Homogenization and Large-Scale Regularity*. Grundlehren der mathematischen Wissenschaften. Springer, Cham, 2019.

[All92] G. Allaire. Homogenization and two-scale convergence. *SIAM J. Math. Anal.*, 23(6):1482–1518, 1992.

[AMS25] C. Alber, C. Ma, and R. Scheichl. A mixed multiscale spectral generalized finite element method. *Numer. Math.*, 157:1–40, 2025.

[AS16] S. Armstrong and C. Smart. Quantitative stochastic homogenization of convex integral functionals . *Ann. Sci. Eć. Norm. Supeŕ. (4)*, 49:423–481, 2016.

[Auc05] G. Auchmuty. Steklov eigenproblems and the representation of solutions of elliptic boundary value problems. *Numer. Funct. Anal. Optim.*, 25(3-4):321–348, 2005.

[BCO94] I. Babuška, G. Caloz, and J. E. Osborn. Special finite element methods for a class of second order elliptic problems with rough coefficients. *SIAM J. Numer. Anal.*, 31:945–981, 1994.

[Beb03] M. Bebendorf. A note on the Poincaré inequality for convex domains. *Z. Anal. Anwendungen*, 22(4):751–756, 2003.

[BFHR97] F. Brezzi, L. P. Franca, T. J. R. Hughes, and A. Russo. $b = \int g$. *Comput. Methods Appl. Mech. Engrg.*, 145(3-4):329–339, 1997.

[BFP24] F. Bonizzoni, P. Freese, and D. Peterseim. Super-localized orthogonal decomposition for convection-dominated diffusion problems. *Bit Numer. Math.*, 64:33, 2024.

[BHP24] F. Bonizzoni, M. Hauck, and D. Peterseim. A reduced basis super-localized orthogonal decomposition for reaction–convection–diffusion problems. *J. Comput. Phys.*, 499:112698, 2024.

[BJ11] G. Bal and W. Jing. Corrector theory for MsFEM and HMM in random media. *Multiscale Model. Simul.*, 9(4):1549–1587, 2011.

[BL11] I. Babuška and R. Lipton. Optimal local approximation spaces for generalized finite element methods with application to multiscale problems. *Multiscale Model. Simul.*, 9:373–406, 2011.

[BLB23] X. Blanc and C. Le Bris. *Homogenization Theory for Multiscale Problems*. Springer, Cham, 2023.

[BLBL16] C. Blanc, C. Le Bris, and F. Legoll. Some variance reduction methods for numerical stochastic homogenization. *Philos. Trans. A*, 374:20150168, 2016.

[BLSS20] I. Babuška, R. Lipton, P. Sinz, and M. Stuebner. Multiscale-spectral GFEM and optimal oversampling. *Comput. Methods Appl. Mech. Engrg.*, 364:112960, 2020.

[BLT14] C. L. Bris, F. Legoll, and F. Thomines. Multiscale finite element approach for "weakly" random problems and related issuesa. *ESAIM: M2AN*, 48(3):815–858, 2014.

[BO83] I. Babuška and J. E. Osborn. Generalized finite element methods: their performance and their relation to mixed methods. *SIAM J. Numer. Anal.*, 20:510–536, 1983.

[BO00] I. Babuška and J. E. Osborn. Can a finite element method perform arbitrarily badly? *Math. Comp.*, 69(230):443–462, 2000.

[BP04] A. Bourgeat and A. Piatnitski. Approximations of effective coefficients in stochastic homogenization. *Ann. Inst. Henri Poincaré Probab. Stat.*, 40(2):153–165, 2004.

[Bre94] S. C. Brenner. Two-level additive Schwarz preconditioners for nonconforming finite elements. In: *Domain decomposition methods in scientific and engineering computing (University Park, PA, 1993)*, volume 180 of *Contemp. Math.*, pp. 9–14. Amer. Math. Soc., Providence, RI, 1994.

[BS07] N. Bantia and M. Sappakittipakorn. Toughness enhancement in steel fiber reinforced concrete through fiber hybridization. *Cem. Concr. Res*, 37(9):1366–1372, 2007.

[BS08] S. C. Brenner and L. R. Scott. *The mathematical theory of finite element methods*, volume 15 of *Texts in Applied Mathematics*. Springer, New York, third edition, 2008.

[BS18] A. Buhr and K. Smetana. Randomized local model order reduction. *SIAM J. Sci. Comput.*, 40(4):A2120–A2151, 2018.

[CCE+20] S. W. Cheung, E. T. Chung, Y. Efendiev, W. T. Leung, and M. Vasilyeva. Constraint energy minimizing generalized multiscale finite element method for dual continuum model. *Commun. Math. Sci.*, 18(3):663–685, 2020.

[CEGL16] V. M. Calo, Y. Efendiev, J. Galvis, and G. Li. Randomized oversampling for generalized multiscale finite element methods. *Multiscale Model. Simul.*, 14(1):482–501, 2016.

[CEH23] E. Chung, Y. Efendiev, and T. Y. Hou. *Multiscale model reduction—multiscale finite element methods and their generalizations*, volume 212 of *Applied Mathematical Sciences*. Springer, Cham, 2023.

[CEL19] E. Chung, Y. Efendiev, and W. T. Leung. Generalized multiscale finite element methods with energy minimizing oversampling. *Internat. J. Numer. Methods Engrg.*, 117(3):316–343, 2019.

[CELS15] E. Cancès, V. Ehrlacher, F. Legoll, and B. Stamm. An embedded corrector problem to approximate the homogenized coefficients of an elliptic equation. *C. R. Math. Acad. Sci. Paris*, 353(9):801–806, 2015.

[CELZ18] E. T. Chung, Y. Efendiev, W. T. Leung, and Z. Zhang. Cluster-based generalized multiscale finite element method for elliptic PDEs with random coefficients. *J. Comput. Phys.*, 371:606–617, 2018.

[CH18] V. T. Chu and V. H. Hoang. High-dimensional finite elements for multiscale Maxwell-type equations. *IMA J. Numer. Anal.*, 38(1):227–270, 2018.

[CHW24] Y. Chen, T. Hou, and Y. Wang. Exponentially convergent multiscale finite element method. *Commun. Appl. Math. Comput.*, 6:8862–878, 2024.

[Cia78] P. G. Ciarlet. *The finite element method for elliptic problems*, volume 4 of *Studies in Mathematics and its Applications*. North-Holland, 1978.

[CL18] L. Chamoin and F. Legoll. A posteriori error estimation and adaptive strategy for the control of MsFEM computations. *Comput. Methods Appl. Mech. Engrg.*, 336:1–38, 2018.

[CLLW20] K. Chen, Q. Li, J. Lu, and S. J. Wright. Randomized sampling for basis function construction in generalized finite element methods. *Multiscale Model. Simul.*, 18(2):1153–1177, 2020.

[CS08] Z. Chen and T. Y. Savchuk. Analysis of the multiscale finite element method for nonlinear and random homogenization problems. *SIAM J. Numer. Anal.*, 46(1):260–279, 2008.

[Dei85] K. Deimling. *Nonlinear Functional Analysis*. Springer Berlin Heidelberg, 1985.

[DGO20] M. Duerinckx, A. Gloria, and F. Otto. The structure of fluctuations in stochastic homogenization. *Commun. Math. Phys.*, 377:259–306, 2020.

[DHM23] Z. Dong, M. Hauck, and R. Maier. An improved high-order method for elliptic multiscale problems. *SIAM J. Numer. Anal.*, 61(4):1918–1937, 2023.

[DO20] M. Duerinckx and F. Otto. Higher-order pathwise theory of fluctuations in stochastic homogenization. *Stoch. PDE: Anal. Comp.*, 8:625–692, 2020.

[EE03] W. E and B. Engquist. The heterogeneous multiscale methods. *Commun. Math. Sci.*, 1(1):87–132, 2003.

[EG04] A. Ern and J.-L. Guermond. *Theory and practice of finite elements*, volume 159 of *Applied Mathematical Sciences*. Springer-Verlag, New York, 2004.

[EG17] A. Ern and J.-L. Guermond. Finite element quasi-interpolation and best approximation. *ESAIM: M2AN*, 51(4):1367–1385, 2017.

[EGH13] Y. Efendiev, J. Galvis, and T. Y. Hou. Generalized multiscale finite element methods (GMsFEM). *J. Comput. Physics*, 251:116–135, 2013.

[EGMP13] D. Elfverson, E. H. Georgoulis, A. Målqvist, and D. Peterseim. Convergence of a discontinuous Galerkin multiscale method. *SIAM J. Numer. Anal.*, 51(6):3351–3372, 2013.

[EH09] Y. Efendiev and T. Y. Hou. *Multiscale Finite Element Methods: Theory and Applications*. Surveys and Tutorials in the Applied Mathematical Sciences. Springer New York, NY, New York, 2009.

[EHW00] Y. Efendiev, T. Y. Hou, and X.-H. Wu. Convergence of a nonconforming multiscale finite element method. *SIAM J. Numer. Anal.*, 37(3):888–910, 2000.

[EMZ05] W. E, P. Ming, and P. Zhang. Analysis of the heterogeneous multiscale method for elliptic homogenization problems. *J. Amer. Math. Soc.*, 18(1):121–156, 2005.

[FGP21] J. Fischer, D. Gallistl, and D. Peterseim. A priori error analysis of a numerical stochastic homogenization method. *SIAM J. Numer. Anal.*, 59(2):660–674, 2021.

[FHKP23] P. Freese, M. Hauck, T. Keil, and D. Peterseim. A super-localized generalized finite element method. *Numer. Math.*, 156(1):205–235, 2023.

[FHP24] P. Freese, M. Hauck, and D. Peterseim. Super-localized orthogonal decomposition for high-frequency Helmholtz problems. *SIAM J. Sci. Comput.*, 46(4):A2377–A2397, 2024.

[FL96] S.-Y. Fu and B. Lauke. Effects of fiber length and fiber orientation distributions on the tensile strength of short-fiber-reinforced polymers. *Compos. Sci. Technol.*, 53(10):1179–1190, 1996.

[FP20] M. Feischl and D. Peterseim. Sparse compression of expected solution operators. *SIAM J. Numer. Anal.*, 58(6):3144–3164, 2020.

[FR17] J. Fischer and C. Raithel. Liouville principles and a large-scale regularity theory for random elliptic operators on the half-space. *SIAM J. Math. Anal.*, 49(1):82–114, 2017.

[Glo06] A. Gloria. An analytical framework for the numerical homogenization of monotone elliptic operators and quasiconvex energies. *Multiscale Model. Simul.*, 5(3):996–1043, 2006.

[Glo08] A. Gloria. An analytical framework for numerical homogenization. II. Windowing and oversampling. *Multiscale Model. Simul.*, 7(1):274–293, 2008.

[Glo12] A. Gloria. Numerical homogenization: survey, new results, and perspectives. *ESAIM: Proc.*, 37:50–116, 2012.

[GMP10] V. Ginting, A. Målqvist, and M. Presho. A novel method for solving multiscale elliptic problems with randomly perturbed data. *Multiscale Model. Simul.*, 8(3):977–996, 2010.

[GMPZ24] J. C. Garay, H. Mohr, D. Peterseim, and C. Zimmer. Hierarchical super-localized orthogonal decomposition method. *arXiv preprint 2407.18671*, 2024.

[GNO14] A. Gloria, S. Neukamm, and F. Otto. Quantification of ergodicity in stochastic homogenization: optimal bounds via spectral gap on glauber dynamics. *Invent. Math.*, 199(2):455–515, 2014.

[GNO20] A. Gloria, S. Neukamm, and F. Otto. A regularity theory for random elliptic operators. *Milan J. Math.*, 88(1):99–170, 2020.

[GO11] A. Gloria and F. Otto. An optimal variance estimate in stochastic homogenization of discrete elliptic equations. *Ann. of Prob.*, 39(3):779–856, 2011.

[GO12] A. Gloria and F. Otto. An optimal error estimate in stochastic homogenization of discrete elliptic equations. *Ann. Appl. Probab.*, 22(1), 2012.

[GO17] A. Gloria and F. Otto. Quantitative results on the corrector equation in stochastic homogenization. *J. Eur. Math. Soc.*, 19:3489–3548, 2017.

[GP15] D. Gallistl and D. Peterseim. Stable multiscale Petrov-Galerkin finite element method for high frequency acoustic scattering. *Comput. Methods Appl. Mech. Eng.*, 295:1–17, 2015.

[GP17] D. Gallistl and D. Peterseim. Computation of quasi-local effective diffusion tensors and connections to the mathematical theory of homogenization. *Multiscale Model. Simul.*, 15(4):1530–1552, 2017.

[GP19] D. Gallistl and D. Peterseim. Numerical stochastic homogenization by quasilocal effective diffusion tensors. *Commun. Math. Sci.*, 17(3):637–651, 2019.

[GT16] J. Galkowski and J. Toth. Pointwise bounds for Steklov eigenfunctions. *J. Geom. Anal.*, 29, 2016.

[GWZ14] M. D. Gunzburger, C. G. Webster, and G. Zhang. Stochastic finite element methods for partial differential equations with random input data. *Acta Numer.*, 23:521–650, 2014.

[Hau23] M. Hauck. *Numerical Homogenization: Multi-resolution and Super-localization Approaches*. Ph.D. thesis, University of Augsburg, Augsburg, 2023.

[Hel97] R. Helmig. *Multiphase flow and transport processes in the subsurface: A contribution to the modeling of hydrosystems*. Springer Berlin Heidelberg, 1997.

[HFMQ98] T. J. R. Hughes, G. R. Feijóo, L. Mazzei, and J.-B. Quincy. The variational multiscale method—a paradigm for computational mechanics. *Comput. Methods Appl. Mech. Engrg.*, 166(1-2):3–24, 1998.

[HL01] P. Hislop and C. Lutzer. Spectral asymptotics of the Dirichlet-to-Neumann map on multiply connected domains in $\mathbb{R}^d$. *Inverse Probl.*, 17:1717–1741, 2001.

[HM14] P. Henning and A. Målqvist. Localized orthogonal decomposition techniques for boundary value problems. *SIAM J. Sci. Comput.*, 36(4):A1609–A1634, 2014.

[HMP15] P. Henning, P. Morgenstern, and D. Peterseim. Multiscale partition of unity. In: M. Griebel and M. A. Schweitzer (eds.), *Meshfree Methods for Partial Differential Equations VII*, volume 100 of Lecture Notes in Computational Science and Engineering, pp. 185–204. Springer, 2015.

[HMP25] M. Hauck, H. Mohr, and D. Peterseim. A simple collocation-type approach to numerical stochastic homogenization. *Multiscale Model. Simul.*, 23(1):374–396, 2025.

[HMS21] A. Hannukainen, J.-C. Mourrat, and H. Stoppels. Computing homogenized coefficients via multiscale representation and hierarchical hybrid grids. *ESAIM: M2AN*, 55:149–185, 2021.

[HMZ19] T. Hou, D. Ma, and Z. Zhang. A model reduction method for multiscale elliptic PDEs with random coefficients using an optimization approach. *Multiscale Model. Simul.*, 17(2):826–853, 2019.

[Hoa08] V. H. Hoang. Sparse finite element method for periodic multiscale nonlinear monotone problems. *Multiscale Model. Simul.*, 7(3):1042–1072, 2008.

[HOS14] P. Henning, M. Ohlberger, and B. Schweizer. An Adaptive Multiscale Finite Element Method. *SIAM Multiscale Model. Simul.*, 12(3):1078–1107, 2014.

[HP13] P. Henning and D. Peterseim. Oversampling for the multiscale finite element method. *Multiscale Model. Simul.*, 11(4):1149–1175, 2013.

[HP22a] M. Hauck and D. Peterseim. Multi-resolution localized orthogonal decomposition for Helmholtz problems. *Multiscale Model. Simul.*, 20(2):657–684, 2022.

[HP22b] M. Hauck and D. Peterseim. Super-localization of elliptic multiscale problems. *Math. Comp.*, 92(342):981–1003, 2022.

[HS05] V. H. Hoang and C. Schwab. High-dimensional finite elements for elliptic problems with multiple scales. *Multiscale Model. Simul.*, 3(1):168–194, 2005.

[HS07] T. J. R. Hughes and G. Sangalli. Variational multiscale analysis: the fine-scale Green's function, projection, optimization, localization, and stabilized methods. *SIAM J. Numer. Anal.*, 45(2):539–557, 2007.

[HS11] H. Harbrecht and C. Schwab. Sparse tensor finite elements for elliptic multiple scale problems. *Comput. Methods Appl. Mech. Engrg.*, 200(45-46):3100–3110, 2011.

[Hug95] T. J. R. Hughes. Multiscale phenomena: Green's functions, the Dirichlet-to-Neumann formulation, subgrid scale models, bubbles and the origins of stabilized methods. *Comput. Methods Appl. Mech. Engrg.*, 127(1–4):387–401, 1995.

[HW97] T. Y. Hou and X.-H. Wu. A multiscale finite element method for elliptic problems in composite materials and porous media. *J. Comput. Phys.*, 134(1):169–189, 1997.

[HWC99] T. Y. Hou, X.-H. Wu, and Z. Cai. Convergence of a multiscale finite element method for elliptic problems with rapidly oscillating coefficients. *Math. Comp.*, 68(227):913–943, 1999.

[HWZ04] T. Y. Hou, X.-H. Wu, and Y. Zhang. Removing the cell resonance error in the multiscale finite element method via a Petrov-Galerkin formulation. *Commun. Math. Sci.*, 2(2):185–205, 2004.

[JK03] S. Joe and F. Y. Kuo. Remark on algorithm 659: Implementing sobol's quasirandom sequence generator. *ACM Trans. Math. Softw.*, 29(1):49–57, 2003.

[JK08] S. Joe and F. Y. Kuo. Constructing sobol sequences with better two-dimensional projections. *SIAM Journal on Scientific Computing*, 30(5):2635–2654, 2008.

[JKO94] V. V. Jikov, S. M. Kozlov, and O. A. Oleinik. *Homogenization of differential operators and integral functionals*. Springer-Verlag, 1994.

[JMSDO14] J. Jagalur Mohan, O. Sahni, A. Doostan, and A. A. Oberai. Variational multiscale analysis: The fine-scale green's function for

stochastic partial differential equations. *SIAM/ASA J. Uncertain. Quantif.*, 2(1):397–422, 2014.

[JO22] M. Josien and F. Otto. The annealed Calderón-Zygmund estimate as convenient tool in quantitative stochastic homogenization. *J. Funct. Anal.*, 283(7):109594, 2022.

[JRS24] M. Josien, C. Raithel, and M. Schäffner. Stochastic homogenization and geometric singularities: A study on corners. *SIAM J. Math. Anal.*, 56(2):2395–2455, 2024.

[KKO20] V. Khoromskaia, B. N. Khoromskij, and F. Otto. Numerical study in stochastic homogenization for elliptic partial differential equations: Convergence rate in the size of representative volume elements. *Numer. Linear Algebra Appl.*, 27(3), 2020.

[KMM+18] G. Kettil, A. Mark, A. Målqvist, F. Edelvik, M. Fredlund, and K. Wester. A multiscale methodology for simulation of mechanical properties of paper. In: *Proceedings of the 6th European Conference on Computational Mechanics*. Glasgow, UK, 06, 2018.

[Koz79] S. M. Kozlov. The averaging of random operators. *Mat. Sb. (N.S.)*, 109(151)(2):188–202, 327, 1979.

[KPY18] R. Kornhuber, D. Peterseim, and H. Yserentant. An analysis of a class of variational multiscale methods based on subspace decomposition. *Math. Comp.*, 87(314):2765–2774, 2018.

[KV25] D. Kolombage and B. Verfürth. Offline-online approximation of multiscale eigenvalue problems with random defects. *ESAIM: M2AN*, to appear, online first, 2025. Preprint available as arXiv:2411.19614.

[KY16] R. Kornhuber and H. Yserentant. Numerical homogenization of elliptic multiscale problems by subspace decomposition. *Multiscale Model. Simul.*, 14(3):1017–1036, 2016.

[LBLM16] C. Le Bris, F. Legoll, and W. Minvielle. Special quasirandom structures: A selection approach for stochastic homogenization. *Monte Carlo Methods Appl.*, 22:25–54, 2016.

[LM72] J.-L. Lions and E. Magenes. *Non-homogeneous boundary value problems and applications. Vol. I.* Die Grundlehren der mathematischen Wissenschaften, Band 181. Springer-Verlag, New York-Heidelberg, 1972.

[LM05] M. G. Larson and A. Målqvist. Adaptive variational multiscale methods based on a posteriori error estimation: duality techniques for elliptic problems. In: *Multiscale methods in science and engineering*, volume 44 of *Lect. Notes Comput. Sci. Eng.*, pp. 181–193. Springer, Berlin, 2005.

[LM07] M. G. Larson and A. Målqvist. Adaptive variational multiscale methods based on a posteriori error estimation: energy norm estimates for elliptic problems. *Comput. Methods Appl. Mech. Engrg.*, 196(21-24):2313–2324, 2007.

[LM09] M. G. Larson and A. Målqvist. An adaptive variational multiscale method for convection-diffusion problems. *Comm. Numer. Methods Engrg.*, 25(1):65–79, 2009.

[LOW24] J. Lu, F. Otto, and L. Wang. Optimal artificial boundary conditions based on second-order correctors for three dimensional random elliptic media. *Commun. Partial Differ. Equ.*, 49(7-8):609–670, 2024.

[LPR+21] P. Lauff, P. Pugacheva, M. Rutzen, U. Weiss, O. Fischer, D. Volkmer, M. A. Peter, and C. U. Grosse. Evaluation of the behavior of carbon short fiber reinforced concrete (CSFRC) based on a multi-sensory experimental investigation and a numerical multiscale approach. *Materials*, 14(22), 2021.

[LRLBH22] F. Legoll, P.-L. Rothé, C. Le Bris, and U. Hetmaniuk. An MsFEM approach enriched using Legendre polynomials. *Multiscale Model. Simul.*, 20(2):798–834, 2022.

[Ma25] C. Ma. A unified framework for multiscale spectral generalized FEMs and low-rank approximations to multiscale PDEs. *Found. Comput. Math.*, 2025.

[Mai20] R. Maier. *Computational Multiscale Methods in Unstructured Heterogeneous Media*. Ph.D. thesis, University of Augsburg, Augsburg, 2020.

[Mai21] R. Maier. A high-order approach to elliptic multiscale problems with general unstructured coefficients. *SIAM J. Numer. Anal.*, 59(2):1067–1089, 2021.

[Mål05] A. Målqvist. *Adaptive variational multiscale methods*. Ph.D. thesis, Chalmers University of Technology, 2005.

[Mål11] A. Målqvist. Multiscale methods for elliptic problems. *Multiscale Model. Simul.*, 9(3):1064–1086, 2011.

[MAS23] C. Ma, C. Alber, and R. Scheichl. Wavenumber explicit convergence of a multiscale generalized finite element method for heterogeneous helmholtz problems. *SIAM J. Numer. Anal.*, 61(3):1546–1584, 2023.

[MM24] C. Ma and J. M. Melenk. Exponential convergence of a generalized FEM for heterogeneous reaction-diffusion equations. *Multiscale Model. Simul.*, 22(1):256–282, 2024.

[Mou18] J.-C. Mourrat. Efficient methods for the estimation of homogenized coefficients. *Found. Comput. Math.*, 19(2):435–483, 2018.

[MP14] A. Målqvist and D. Peterseim. Localization of elliptic multiscale problems. *Math. Comp.*, 83(290):2583–2603, 2014.

[MP20] A. Målqvist and D. Peterseim. *Numerical Homogenization by Localized Orthogonal Decomposition*. Society for Industrial and Applied Mathematics (SIAM), 2020.

[MS02] A.-M. Matache and C. Schwab. Two-scale FEM for homogenization problems. *ESAIM: M2AN*, 36(4):537–572, 2002.

[MSD22] C. Ma, R. Scheichl, and T. Dodwell. Novel design and analysis of generalized finite element methods based on locally optimal spectral approximations. *SIAM J. Numer. Anal.*, 60(1):244–273, 2022.

[MV22] A. Målqvist and B. Verfürth. An offline-online strategy for multiscale problems with random defects. *ESAIM: M2AN*, 56(1):237–260, 2022.

[Ngu89] G. Nguetseng. A general convergence result for a functional related to the theory of homogenization. *SIAM J. Math. Anal.*, 20(3):608–623, 1989.

[NH06] J. Niessner and R. Helmig. Multi-scale modelling of two-phase—two-component processes in heterogeneous porous media. *Numer. Linear Algebra Appl.*, 13(9):699–715, 2006.

[NPP08] J. Nolen, G. Papanicolaou, and O. Pironneau. A framework for adaptive multiscale methods for elliptic problems. *Multiscale Model. Simul.*, 7(1):171–196, 2008.

[Ohl05] M. Ohlberger. A posteriori error estimates for the heterogeneous multiscale finite element method for elliptic homogenization problems. *Multiscale Model. Simul.*, 4(1):88–114, 2005.

[OS19] H. Owhadi and C. Scovel. *Operator-Adapted Wavelets, Fast Solvers, and Numerical Homogenization*, volume 35 of *Cambridge Monographs on Applied and Computational Mathematics*. Cambridge University Press, Cambridge, 2019.

[Osw93] P. Oswald. On a BPX-preconditioner for P1 elements. *Computing*, 51(2):125–133, 1993.

[Owh15] H. Owhadi. Bayesian numerical homogenization. *Multiscale Model. Simul.*, 13(3):812–828, 2015.

[Owh17] H. Owhadi. Multigrid with rough coefficients and multiresolution operator decomposition from hierarchical information games. *SIAM Rev.*, 59(1):99–149, 2017.

[OZB14] H. Owhadi, L. Zhang, and L. Berlyand. Polyharmonic homogenization, rough polyharmonic splines and sparse super-localization. *ESAIM: M2AN*, 48(2):517–552, 2014.

[Pet16] D. Peterseim. Variational multiscale stabilization and the exponential decay of fine-scale correctors. In: *Building Bridges: Connections and Challenges in Modern Approaches to Numerical Partial Differential Equations*, pp. 341–367. Springer, 2016.

[PS16] D. Peterseim and R. Scheichl. Robust numerical upscaling of elliptic multiscale problems at high contrast. *Comput. Methods Appl. Math.*, 16(4):579–603, 2016.

[PST15] I. Polterovich, D. Sher, and J. Toth. Nodal length of Steklov eigenfunctions on real-analytic Riemannian surfaces. *J. für die Reine und Angew. Math.*, 2019:17–47, 2015.

[PT95] L. Piegl and W. Tiller. *The NURBS Book*. Springer-Verlag, Berlin, Heidelberg, 1995.

[PV79] G. C. Papanicolaou and S. R. S. Varadhan. Boundary value problems with rapidly oscillating random coefficients. *Random fields*, 1:835–873, 1979.

[PW60] L. E. Payne and H. F. Weinberger. An optimal Poincaré inequality for convex domains. *Arch. Rational Mech. Anal.*, 5:286–292 (1960), 1960.

[PWZ24] D. Peterseim, J. Wärnegård, and C. Zimmer. Super-localised wave function approximation of Bose-Einstein condensates. *J. Comput. Phys.*, 510:113097, 2024.

[SAK23] N. Schroeder, W. Alhejaili, and C.-Y. Kao. Steklov eigenvalue problems on nearly spherical and nearly annular domains. *arXiv preprint 2310.19585*, 2023.

[Tar09] L. Tartar. *The general theory of homogenization*, volume 7 of *Lecture Notes of the Unione Matematica Italiana*. Springer-Verlag, Berlin; UMI, Bologna, 2009. A personalized introduction.

[TH19] W. C. Tan and V. H. Hoang. High dimensional finite element method for multiscale nonlinear monotone parabolic equations. *J. Comput. Appl. Math.*, 345:471–500, 2019.

[TH20] W. C. Tan and V. H. Hoang. Sparse tensor product finite element method for nonlinear multiscale variational inequalities of monotone type. *IMA J. Numer. Anal.*, 40(3):1875–1907, 2020.

[WX24] L. Wang and Q. Xu. Calderon-Zygmund estimates for stochastic elliptic systems on bounded Lipschitz domains. *arXiv preprint 2211.04940*, 2024.

[XH14] B. Xia and V. H. Hoang. High dimensional finite elements for multiscale wave equations. *Multiscale Model. Simul.*, 12(4):1622–1666, 2014.

[Yur86] V. V. Yurinskiĭ. Averaging of symmetric diffusion in a random medium. *Sibirsk. Mat. Zh.*, 27(4):167–180, 215, 1986.

[ZCH15] Z. Zhang, M. Ci, and T. Y. Hou. A multiscale data-driven stochastic method for elliptic PDEs with random coefficients. *Multiscale Model. Simul.*, 13(1):173–204, 2015.